ANALYSIS OF LAMINATED GLASS ARCHES AND CYLINDRICAL SHELLS

A THESIS SUBMITTED TO
THE GRADUATE SCHOOL OF NATURAL AND APPLIED SCIENCES
OF
MIDDLE EAST TECHNICAL UNIVERSITY

BY

EBRU DURAL

IN PARTIAL FULFILLMENT OF THE REQUIREMENTS
FOR
THE DEGREE OF DOCTOR OF PHILOSOPHY
IN
ENGINEERING SCIENCES

JANUARY 2011

Approval of the thesis:

ANALYSIS OF LAMINATED GLASS ARCHES AND CYLINDRICAL SHELLS

Submitted by **EBRU DURAL** in partial fulfillment of the requirements for the degree of **doctor of philosophy in Engineering Sciences Department, Middle East Technical University** by,

Prof. Dr. Canan Özgen _____
Dean, Graduate School of **Natural and Applied Sciences**

Prof. Dr. Turgut Tokdemir _____
Head of Department, **Engineering Sciences**

Prof. Dr. M. Zülfü Aşık _____
Supervisor, **Engineering Sciences Dept., METU**

Examining Committee Members:

Prof. Dr. Gülin Ayşe Birlik _____
Engineering Sciences Dept., METU

Prof. Dr. M. Zülfü Aşık _____
Engineering Sciences Dept., METU

Prof. Dr. Uğurhan Akyüz _____
Civil Engineering Dept., METU

Assoc. Prof. Dr. Hakan I. Tarman _____
Engineering Sciences Dept., METU

Assist. Prof. Dr. Mehmet Yetmez _____
Mechanical Engineering Dept., ZKU

Date: 12.01.2011

I hereby declare that all information in this document has been obtained and presented in accordance with academic rules and ethical conduct. I also declare that, as required by these rules and conduct, I have fully cited and referenced all material and results that are not original to this work.

Name, Last Name : Ebru DURAL
Signature :

ABSTRACT

ANALYSIS OF LAMINATED GLASS ARCHES AND CYLINDRICAL SHELLS

DURAL, Ebru
Ph. D, Department of Engineering Sciences
Supervisor: Prof. Dr. M. Zülfü AŞIK

January 2011, 244 pages

In this study, a laminated glass unit which consists of two glass sheets bonded together by PVB is analyzed as a curved beam and as a cylindrical shell. Laminated glass curved beams and shells are used in architecture, aerospace, automobile and aircraft industries. Curved beam and shell structures differ from straight structures because of their initial curvature. Because of mathematical complexity most of the studies are about linear behavior rather than nonlinear behavior of curved beam and shell units. Therefore it is necessary to develop a mathematical model considering large deflection theory to analyze the behavior of curved beams and shells. Mechanical behavior of laminated glass structures are complicated because they can easily perform large displacement since they are very thin and the materials with the elastic modulus have order difference. To be more precise modulus of elasticity of glass is about $7*10^4$ times greater than the modulus of elasticity of PVB interlayer. Because of the nonlinearity, analysis of the laminated glass has to be performed by considering large deflection effects. The mathematical model is developed for curved beams and shells by applying both the variational and the minimum potential energy principles to obtain nonlinear governing differential equations. The iterative technique is employed to obtain the deflections. Computer programs are developed

to analyze the behavior of cylindrical shell and curved beam. For the verification of the results obtained from the developed model, the results from finite element models and experiments are used. Results used for verification of the model and the explanation of the bahavior of the laminated glass curved beams and shells are presented in figures.

Keywords: Laminated Glass, large deflection, curved beam, shell, nonlinear behavior.

ÖZ

LAMİNA CAM EĞRİSEL KİRİŞ VE SİLİNDİRİK KABUKLARIN ÇÖZÜMLEMESİ

DURAL, Ebru
Doktora., Mühendislik Bilimleri Bölümü
Tez yöneticisi: Prof. Dr. M. Zülfü AŞIK

Ocak 2011, 244 sayfa

Bu çalışmada PVB ile birbirine bağlanmış iki cam levhadan oluşan lamina cam eğrisel kiriş ve silindirik kabuk yapının çözümlenmesi yapılmıştır. Lamina cam eğrisel kiriş ve kabuklar mimari, havacılık, otomobil ve uçak endüstrisinde kullanılırlar. Eğrisel kirişler ve kabuk yapılar eğrilikleri nedeniyle düzlemsel yapılardan farklıdırlar. Matematiksel karmaşıklıkları nedeniyle yapılan çalışmaların bir çoğu eğrisel kiriş ve kabuk elemanların doğrusal olmayan davranışlarından ziyade doğrusal olan davranışları ile ilgilidir. Dolayısıyla eğrisel kiriş ve kabukların davranışını çözümlemek için büyük yerdeğiştirmeler kuramını dikkate alan bir matematiksel model geliştirilmesi gerekmektedir. Lamina cam yapılar ince olmaları nedeniyle kolayca büyük yerdeğiştirmeler gösterdiklerinden ve malzemelerin elastisite modülleri arasındaki büyük farktan dolayı mekanik davranışları karmaşıktır. Daha açıklayıcı şekilde ifade edilirse camın elastisite modülü PVB aratabakanın elastisite modülünden yaklaşık $7*10^4$ kez daha büyüktür. Doğrusal olamayan davranışları nedeniyle lamina camların gerçekçi çözümlemesi büyük yerdeğiştirmelerin etkisi gözönüne alınarak yapılması gerektiğinden eğrisel kiriş ve

kabukların doğrusal olmayan hakim denklemlerini elde etmek için değişim ve minimum potensiyel enerji ilkeleri kullanılarak matematiksel model geliştirilmiştir. Yerdeğiştirmeleri elde etmek için tekrarlamalı çözüm yöntemi kullanılmıştır. Türetilen doğrusal olmayan denklemleri sayısal çözmek için bilgisayar programı geliştirilmiştir ve elde edilen sayısal sonuçları doğrulamak için yapılan deneylerden ve sonlu elemanlar yönteminden elde edilen sonuçlar kullanılmıştır. Eğrisel kiriş ve kabukların davranışını açıklayan ve geliştirilen modelleri doğrulayan sonuçlar grafikler halinde verilmiştir.

Anahtar Kelimeler: Lamina cam, büyük yer değiştirme, eğrisel kiriş, kabuk, doğrusal olmayan davranış.

To My Family,

For your endless support and love

ACKNOWLEDGEMENTS

I wish to express his deepest gratitude to his supervisor Prof. Dr. Mehmet Zülfü AŞIK for his guidance, advice, criticism, encouragements and insight throughout the research.

I would also like to appreciate to my friends, especially Volkan İşbuğa, Serap Güngör Geridönmez, Pınar Demirci, Yasemin Kaya, Hakan Bayrak, Alper Akın, Semih Erhan, for their friendship and encouragement during my thesis.

I owe appreciate to my husband Onur Dural for his boundless moral support giving me joy of living.

Words cannot describe my gratitude towards the people dearest to me Nevra, Şeref, Serap and Eren my family; my mother, my father, my sister and my brothers. Their belief in me, although at times irrational, has been vital for this work. I dedicate this thesis to them.

TABLE OF CONTENTS

ABSTRACT……..……..iv

ÖZ…….…..……..vi

ACKNOWLEDGEMENTS…….…….…….……...ix

TABLE OF CONTENTS…….……..……....x

LIST OF FIGURES……..…….……...……...xiii

LIST OF TABLES……...xxxii

LIST OF SYMBOLS……...xxxiii

CHAPTERS

1.INTRODUCTION……...……...…….....……....1

1.1 Laminated Glass……..……..1

1.2 Previous Research…….3

1.2.1 Hooper's analytical and experimental studies…….3

1.2.2 Mathematical Model developed by Vallabhan……5

1.2.3 Experimental studies conducted by Behr……...8

1.2.4 Norville developed a theoretical model……12

1.2.5 Van Duser developed finite element model……13

1.2.6 Minor conducted experiments about failure strength…….....14

1.2.7 Studies about shell structures……..14

1.2.8 Studies about curved beam …….15

1.3 Object and scope of the thesis…….18

2. BEHAVIOR OF LAMINATED CURVED GLASS BEAMS……..…..……...21

2.1 Introduction to theory of curved beams……..21

2.2 Mathematical modelling……..……...22

2.3 Numerical tests for the optimized number divisions and tolerance……31

2.4 Experimental technique and verification of the model for curved beam.....33

2.4.1 Finite element investigation……..33

2.4.2 Experimental investigation……38

2.5 Numerical results……..……..41

2.5.1 Simply supported curved beam…….....41

2.5.2 Fixed supported curved beam……...54

2.5.3 Simple-fixed supported curved beam…….....63

2.6 Summary and Conclusion……...72

3. BEHAVIOUR OF LAMINATED GLASS CYLINDRICAL SHELL…….....74

3.1 Introduction to theory of shells……...74

3.2 Nonlinear behavior of shells……..…….75

3.3 Mathematical model for laminated glass shell unit……..……..76

3.4 Finite difference expressions for field and boundary equations and the iterative solution technique…..…….……..…..…….…….88

3.4.1 Application of Finite Difference Method……..…….....88

3.4.2 Solution algorithm……..……..……...101

3.5 Verification of model……..…….....103

3.6 Numerical solution and results……...……..…….107

3.6.1 Numerical results for fixed supported cylindrical shell subjected to uniform distributed load towards out of the top shell surface…….107

3.6.2 Strength factor analysis of laminated glass unit…….…...……155

3.6.3 Numerical results for fixed supported cylindrical shell subjected to uniform distributed load towards the top shell surface....…….……..156

3.6.4 Numerical results for hinged supported cylindrical shell subjected to uniform distributed load towards out of the top shell surface…….....189

4. SUMMARY AND CONCLUSIONS……..…….…….……...236

4.1 Recommendations for future work……..…….238

REFERENCES……239

CURRICULUM VITAE……243

LIST OF FIGURES

FIGURES

Figure 1.1	Laminated glass	1
Figure 2.1	Laminated Circular Glass Beam with an Interlayer PVB	23
Figure 2.2	Deformed and undeformed sections of laminated glass unit	25
Figure 2.3	Deflection versus load for laminated glass curved beam	32
Figure 2.4	Displacement versus load for laminated glass curved beam for different tolerances	32
Figure 2.5	Displacement versus load for laminated glass straight beam for different tolerances	32
Figure 2.6	Central deflection values in the fixed supported laminated glass curved beam	34
Figure 2.7	Maximum stress values in the fixed supported laminated glass curved beam	35
Figure 2.8	Central deflection values in the monolithic simply supported curved beam	35
Figure 2.9	Central deflection values in the laminated simply supported curved beam	36
Figure 2.10	Maximum stress values in the laminated simply supported curved beam	37
Figure 2.11	Deformed and undeformed shapes of the beam	37
Figure 2.12	A view of meshed finite element model	38
Figure 2.13	Laminated glass beam (Dimensions in mm)	39
Figure 2.14	Comparison of the stresses at center and on the bottom surface of the laminated glass curved beam. (Strain gage 4)	40

Figure 2.15	Pictorial presentation of boundary conditions for the simply supported curved beam	41
Figure 2.16	Normalized maximum deflection versus load for simply supported beam	42
Figure 2.17	Maximum deflection versus load	43
Figure 2.18	Maximum stresses versus load	43
Figure 2.19	Circumferential displacement (u1) of the top glass along the arc length of the beam	44
Figure 2.20	Circumferential displacement (u2) of the bottom glass along the arc length of the beam	44
Figure 2.21	Radial deflections for different load values	45
Figure 2.22	Deflections along the arc length of simply supported beam at load P=2 kN	45
Figure 2.23	Variation of shear stress along the arc length of the beam	46
Figure 2.24	Membrane and bending stresses for the top surface of the top ply	47
Figure 2.25	Membrane and bending stresses for the bottom surface of the top ply	47
Figure 2.26	Membrane and bending stresses for the top surface of the bottom ply	48
Figure 2.27	Membrane and bending stresses for the bottom surface of the bottom ply	48
Figure 2.28	Stress on bottom surface of the top glass along the arc length of the simply supported beam	49
Figure 2.29	Stress on top surface of the top glass along the arc length of the simply supported beam	49
Figure 2.30	Stress on bottom surface of the bottom glass along the arc length of the simply supported beam	50

Figure 2.31	Stress on top surface of the bottom glass along the arc length of the simply supported beam	50
Figure 2.32	Maximum stresses versus load of the laminated glass	51
Figure 2.33	Stress on the top surface along the arc length of the simply supported beam at load P=2 kN	52
Figure 2.34	Stress on the bottom surface along the arc length of the simply supported beam at load P=2kN	52
Figure 2.35	Variation of strength factor of simply supported curved beam	53
Figure 2.36	Pictorial presentation of boundary conditions for the fixed supported curved beam	54
Figure 2.37	Normalized maximum deflection versus load for fixed supported beam	55
Figure 2.38	Maximum deflections versus load	56
Figure 2.39	Maximum stress versus load	56
Figure 2.40	Circumferential displacement (u1)of the top glass along the arc length of the beam	57
Figure 2.41	Circumferential displacement (u2) of the bottom glass along the arc length of the beam	57
Figure 2.42	Radial deflection for different load values	58
Figure 2.43	Comparison of deflections along the arc length of the fixed supported beam at load P=2 kN	58
Figure 2.44	Variation of shear stress along the arc length of the beam	59
Figure 2.45	Stress on the bottom surface of the bottom glass along the arc length of the fixed supported beam	60
Figure 2.46	Stress on the top surface of the bottom glass along the arc length of the fixed supported beam	60
Figure 2.47	Stress on the bottom surface of the top glass along the arc length of the fixed supported beam	61

Figure 2.48	Stress on the top surface of the top glass along the arc length of the fixed supported beam	61
Figure 2.49	Maximum stresses versus load of the laminated glass	62
Figure 2.50	Stress on the top surface along the arc length of fixed supported beam at load P=2 kN	62
Figure 2.51	Stress on the bottom surface along the arc length of the fixed supported beam at load P=2kN	62
Figure 2.52	Variation of strength factor with load in a curved beam	63
Figure 2.53	Pictorial presentation of boundary conditions for fixed and simply supported curved beam	64
Figure 2.54	Maximum deflection versus load for fixed and simply supported beam	64
Figure 2.55	Maximum stress versus load for fixed and simply supported beam	65
Figure 2.56	Radial deflections along the beam fixed at one end and simply supported at the other end for different load values	65
Figure 2.57	Circumferential deflection (u1) of the top glass along the arc length of the beam	66
Figure 2.58	Circumferential deflection (u2) of the bottom glass along the arc length of the beam	66
Figure 2.59	Stress on the top surface of top glass along the arc length of the fixed at one end and simply supported at the other end beam	67
Figure 2.60	Stress on the bottom surface of top glass along the arc length of the fixed at one end and simple supported at the other end beam	67
Figure 2.61	Stress on the top surface of bottom glass along the arc length of the fixed at one end and simple supported at the other end beam	68
Figure 2.62	Stress on the bottom surface of bottom glass along the arc length of the fixed at one end and simple supported at the other end beam	68

Figure 2.63	Variation of strength factor with load of the laminated curved beam fixed at one end and simply supported at the other end	69
Figure 2.64	Comparison of maximum displacements for different boundary conditions	69
Figure 2.65	Comparison of maximum stresses for different boundary conditions	70
Figure 2.66	Comparison of radial deflections along the arc length of the beam	70
Figure 2.67	Comparison of maximum stresses on the top surface along the arclength of the beam	71
Figure 2.68	Comparison of maximum stresses on the bottom surface along the arc length of the beam	71
Figure 2.69	Comparison of strength factor	71
Figure 3.1	Laminated glass cylindrical shell	77
Figure 3.2	Pictorial presentation of boundary conditions for the fixed supported laminated cylindrical glass shell	87
Figure 3.3	Comparison of central deflection values for monolithic case	104
Figure 3.4	Comparison of central deflection values for the laminated cylindrical glass shell	106
Figure 3.5	Comparison of the stress values for the laminated cylindrical glass shell	106
Figure 3.6	A view of contours of radial deflection obtained from ABAQUS	107
Figure 3.7	Normalized maximum deflection versus load for clamped cylindrical shell	108
Figure 3.8	Stress versus load for clamped cylindrical shell	109
Figure 3.9	Maximum deflection versus load	110
Figure 3.10	Maximum stress versus load	110

Figure 3.11	Circumferential displacement of the top glass unit along the center line at y=0	111
Figure 3.12	Circumferential displacement of the bottom glass unit along the centerline at y=0	111
Figure 3.13	Axial displacement of the top glass unit along the center line at θ=0	112
Figure 3.14	Axial displacement of the bottom glass unit along the center line at θ=0	113
Figure 3.15	Radial deflection of the unit along the the centerline at y=0	113
Figure 3.16	Radial deflection of the shell along the diagonal	114
Figure 3.17	Circumferential displacement of the top glass shell along the diagonal	114
Figure 3.18	Circumferential displacement of the bottom glass shell along the diagonal	115
Figure 3.19	Axial displacement of the top glass shell along the diagonal	115
Figure 3.20	Axial displacement of the bottom glass shell along the diagonal	115
Figure 3.21	Maximum stress on the top surface of the top glass along the center line at y=0	116
Figure 3.22	Minimum stress on the top surface of the top glass along the center line at y=0	117
Figure 3.23	Maximum stress on the bottom surface of the bottom glass along the center line at y=0	117
Figure 3.24	Minimum stress on the bottom surface of the bottom glass along the center line at y=0	117
Figure 3.25	Maximum stress on the bottom surface of top shell along the center line at y=0	118
Figure 3.26	Maximum stress on the top surface of bottom shell along center line at y=0	119

Figure 3.27 Minimum stress on the bottom surface of top shell along center line at y=0 119

Figure 3.28 Minimum stress on the top surface of bottom shell along center line at y=0 120

Figure 3.29 Maximum stress on the top surface of the top glass along the center line at θ=0 121

Figure 3.30 Minimum stress on the top surface of the top glass along the center line at θ=0 121

Figure 3.31 Maximum stress on the bottom surface of the bottom shell along the center line at θ=0 122

Figure 3.32 Minimum stress on the bottom surface of the bottom shell along the center line at θ=0 122

Figure 3.33 Maximum stress on the top surface of the top shell along the diagonal 122

Figure 3.34 Minimum stress on the top surface of the top shell along the diagonal 123

Figure 3.35 Maximum stress on the bottom surface of the bottom shell along the diagonal 123

Figure 3.36 Minimum stress on the bottom surface of the bottom shell along the diagonal 123

Figure 3.37 Shear stress along θ direction 124

Figure 3.38 Shear stress along y direction 124

Figure 3.39 Contours of radial displacement (mm) for q=10 kPa 125

Figure 3.40 Contours of radial displacement (mm) for q=20 kPa 125

Figure 3.41 Contours of radial displacement (mm) for q=30 kPa 126

Figure 3.42 Contours of radial displacement (mm) for q=40 kPa 126

Figure 3.43 Contours of radial displacement (mm) for q=50 kPa 127

Figure 3.44 Contours of maximum principal stresses (*10^4 kPa) on the top surface of the top shell for q= 10 kPa 128

Figure 3.45 Contours of maximum principal stresses (*10^4 kPa) on the top surface of the top shell for q= 30 kPa 128

Figure 3.46 Contours of maximum principal stresses (*10^4 kPa) on the top surface of the top shell for q= 50 kPa 129

Figure 3.47 Contours of maximum principal stresses (*10^4 kPa) on the top surface of the top shell for q= 70 kPa 129

Figure 3.48 Contours of maximum principal stresses (*10^4 kPa) on the top surface of the top shell for q= 90 kPa 130

Figure 3.49 Contours of maximum principal stresses (*10^4 kPa) on the top surface of the top shell for q= 100 kPa 130

Figure 3.50 Contours of minimum principal stresses (*10^4 kPa) on the top surface of the top shell for q= 10 kPa 131

Figure 3.51 Contours of minimum principal stresses (*10^4 kPa) on the top surface of the top shell for q= 30 kPa 131

Figure 3.52 Contours of minimum principal stresses (*10^4 kPa) on the top surface of the top shell for q= 50 kPa 132

Figure 3.53 Contours of minimum principal stresses (*10^4 kPa) on the top surface of the top shell for q= 70 kPa 132

Figure 3.54 Contours of minimum principal stresses (*10^4 kPa) on the top surface of the top shell for q= 90 kPa 133

Figure 3.55 Contours of minimum principal stresses (*10^4 kPa) on the top surface of the top shell for q= 100 kPa 133

Figure 3.56 Contours of maximum principal stresses (*10^4 kPa) on the bottom surface of the bottom shell for q= 5 kPa 134

Figure 3.57 Contours of maximum principal stresses (*10^4 kPa) on the bottom surface of the bottom shell for q= 20 kPa 135

Figure 3.58	Contours of maximum principal stresses (*10^4 kPa) on the bottom surface of the bottom shell for q= 30 kPa	135
Figure 3.59	Contours of maximum principal stresses (*10^4 kPa) on the bottom surface of the bottom shell for q= 50 kPa	136
Figure 3.60	Contours of maximum principal stresses (*10^4 kPa) on the bottom surface of the bottom shell for q= 70 kPa	136
Figure 3.61	Contours of maximum principal stresses (*10^4 kPa) on the bottom surface of the bottom shell for q= 90 kPa	137
Figure 3.62	Contours of maximum principal stresses (*10^4 kPa) on the bottom surface of the bottom shell for q= 100 kPa	137
Figure 3.63	Contours of minimum principal stresses (*10^4 kPa) on the bottom surface of the bottom shell for q= 10 kPa	138
Figure 3.64	Contours of minimum principal stresses (*10^4 kPa) on the bottom surface of the bottom shell for q= 30 kPa	139
Figure 3.65	Contours of minimum principal stresses (*10^4 kPa) on the bottom surface of the bottom shell for q= 50 kPa	139
Figure 3.66	Contours of minimum principal stresses (*10^4 kPa) on the bottom surface of the bottom shell for q= 70 kPa	140
Figure 3.67	Contours of minimum principal stresses (*10^4 kPa) on the bottom surface of the bottom shell for q= 90 kPa	140
Figure 3.68	Contours of minimum principal stresses (*10^4 kPa) on the bottom surface of the bottom shell for q= 100 kPa	141
Figure 3.69	Contours of maximum principal stresses (*10^4 kPa) on the bottom surface of the top shell for q= 10 kPa	142
Figure 3.70	Contours of maximum principal stresses (*10^4 kPa) on the bottom surface of the top shell for q= 30 kPa	143
Figure 3.71	Contours of maximum principal stresses (*10^4 kPa) on the bottom surface of the top shell for q= 50 kPa	143

Figure 3.72	Contours of maximum principal stresses (*10^4 kPa) on the bottom surface of the top shell for q= 70 kPa	144
Figure 3.73	Contours of maximum principal stresses (*10^4 kPa) on the bottom surface of the top shell for q= 90 kPa	144
Figure 3.74	Contours of maximum principal stresses (*10^4 kPa) on the bottom surface of the top shell for q= 100 kPa	145
Figure 3.75	Contours of maximum principal stresses (*10^4 kPa) on the top surface of the bottom shell for q= 10 kPa	145
Figure 3.76	Contours of maximum principal stresses (*10^4 kPa) on the top surface of the bottom shell for q= 20 kPa	146
Figure 3.77	Contours of maximum principal stresses (*10^4 kPa) on the top surface of the bottom shell for q= 30 kPa	146
Figure 3.78	Contours of maximum principal stresses (*10^4 kPa) on the top surface of the bottom shell for q= 50 kPa	147
Figure 3.79	Contours of maximum principal stresses (*10^4 kPa) on the top surface of the bottom shell for q= 70 kPa	147
Figure 3.80	Contours of maximum principal stresses (*10^4 kPa) on the top surface of the bottom shell for q= 90 kPa	148
Figure 3.81	Contours of maximum principal stresses (*10^4 kPa) on the top surface of the bottom shell for q= 100 kPa	148
Figure 3.82	Contours of minimum principal stresses (*10^4 kPa) on the bottom surface of the top shell for q= 10 kPa	149
Figure 3.83	Contours of minimum principal stresses (*10^4 kPa) on the bottom surface of the top shell for q= 30 kPa	149
Figure 3.84	Contours of minimum principal stresses (*10^4 kPa) on the bottom surface of the top shell for q= 50 kPa	150
Figure 3.85	Contours of minimum principal stresses (*10^4 kPa) on the bottom surface of the top shell for q= 70 kPa	150

Figure 3.86	Contours of minimum principal stresses (*10^4 kPa) on the bottom surface of the top shell for q= 90 kPa	151
Figure 3.87	Contours of minimum principal stresses (*10^4 kPa) on the bottom surface of the top shell for q= 100 kPa	151
Figure 3.88	Contours of minimum principal stresses (*10^4 kPa) on the top surface of the bottom shell for q= 10 kPa	152
Figure 3.89	Contours of minimum principal stresses (*10^4 kPa) on the top surface of the bottom shell for q= 30 kPa	152
Figure 3.90	Contours of minimum principal stresses (*10^4 kPa) on the top surface of the bottom shell for q= 50 kPa	153
Figure 3.91	Contours of minimum principal stresses (*10^4 kPa) on the top surface of the bottom shell for q= 70 kPa	153
Figure 3.92	Contours of minimum principal stresses (*10^4 kPa) on the top surface of the bottom shell for q= 90 kPa	154
Figure 3.93	Contours of minimum principal stresses (*10^4 kPa) on the top surface of the bottom shell for q= 100 kPa	154
Figure 3.94	Strength factor for the fixed supported laminated cylindrical shell	156
Figure 3.95	Comparison of central deflection values for laminated glass shell	158
Figure 3.96	Comparison of stress values for laminated glass shell	158
Figure 3.97	A view of radial deflection contours obtained from ABAQUS	159
Figure 3.98	Comparison of displacement of the laminated glass subjected to uniform tension and compressive load	159
Figure 3.99	Maximum deflection versus load	160
Figure 3.100	Maximum stress versus load	160
Figure 3.101	Circumferential displacement of the top glass unit along the center line at y=0	161

Figure 3.102 Circumferential displacement of the bottom glass unit along the center line at y=0 161

Figure 3.103 Axial displacement of the top glass unit along the center line at θ=0 162

Figure 3.104 Axial displacement of the bottom glass unit along the center line at θ=0 163

Figure 3.105 Radial deflection of the unit at the center along the center line at y=0 163

Figure 3.106 Radial deflection of the unit along the diagonal of shell 164

Figure 3.107 Circumferential displacement of the top glass shell along the diagonal 164

Figure 3.108 Circumferential displacement of the bottom glass shell along the diagonal 164

Figure 3.109 Axial displacement of the top glass shell along the diagonal 165

Figure 3.110 Axial displacement of the bottom glass shell along the diagonal 165

Figure 3.111 Maximum stress on the top surface of the top glass along the center line at y=0 166

Figure 3.112 Maximum stress on the bottom surface of the bottom glass along the center line at y=0 166

Figure 3.113 Minimum stress on the top surface of the top glass along the center line at y=0 167

Figure 3.114 Minimum stress on the bottom surface of the bottom glass along the center line at y=0 167

Figure 3.115 Maximum stress at the bottom surface of the top shell along the center line at y=0 168

Figure 3.116 Maximum stress at the top surface of the bottom shell along the center line at y=0 169

Figure 3.117 Minimum stress at the bottom surface of the top shell along the center line at y=0 169

Figure 3.118 Minimum Stress at the top surface of the bottom shell along the center line at y=0 169

Figure 3.119 Maximum stress on the top surface of the top glass along the center line at θ=0 170

Figure 3.120 Maximum stress on the bottom surface of the bottom glass along the center line at θ=0 171

Figure 3.121 Minimum stress on the top surface of the top glass along the center line at θ=0 171

Figure 3.122 Minimum stress on the bottom surface of the bottom glass along the center line at θ=0 171

Figure 3.123 Contours of radial displacement (mm) for q=10 kPa 172

Figure 3.124 Contours of radial displacement (mm) for q=20 kPa 173

Figure 3.125 Contours of radial displacement (mm) for q=30 kPa 173

Figure 3.126 Contours of radial displacement (mm) for q=40 kPa 174

Figure 3.127 Contours of radial displacement (mm) for q=50 kPa 174

Figure 3.128 Contours of maximum principal stresses (*10^4 kPa) on the top surface of the top shell for q= 10 kPa 175

Figure 3.129 Contours of maximum principal stresses (*10^4 kPa) on the top surface of the top shell for q= 30 kPa 176

Figure 3.130 Contours of maximum principal stresses (*10^4 kPa) on the top surface of the top shell for q= 40 kPa 176

Figure 3.131 Contours of maximum principal stresses (*10^4 kPa) on the top surface of the top shell for q= 50 kPa 177

Figure 3.132 Contours of maximum principal stresses (*10^4 kPa) on the top surface of the top shell for q= 70 kPa 177

Figure 3.133 Contours of maximum principal stresses (*10^4 kPa) on the top surface of the top shell for q= 90 kPa 178

Figure 3.134 Contours of maximum principal stresses (*10^4 kPa) on the top surface of the top shell for q= 100 kPa 178

Figure 3.135 Contours of maximum principal stresses (*10^4 kPa) on the bottom surface of the bottom shell for q= 10 kPa 179

Figure 3.136 Contours of maximum principal stresses (*10^4 kPa) on the bottom surface of the bottom shell for q= 30 kPa 179

Figure 3.137 Contours of maximum principal stresses (*10^4 kPa) on the bottom surface of the bottom shell for q= 40 kPa 180

Figure 3.138 Contours of maximum principal stresses (*10^4 kPa) on the bottom surface of the bottom shell for q= 50 kPa 180

Figure 3.139 Contours of maximum principal stresses (*10^4 kPa) on the bottom surface of the bottom shell for q= 70 kPa 181

Figure 3.140 Contours of maximum principal stresses (*10^4 kPa) on the bottom surface of the bottom shell for q= 90 kPa 181

Figure 3.141 Contours of maximum principal stresses (*10^4 kPa) on the bottom surface of the bottom shell for q= 100 kPa 182

Figure 3.142 Contours of minimum principal stresses (*10^4 kPa) on the top surface of the top shell for q= 10 kPa 182

Figure 3.143 Contours of minimum principal stresses (*10^4 kPa) on the top surface of the top shell for q= 30 kPa 183

Figure 3.144 Contours of minimum principal stresses (*10^4 kPa) on the top surface of the top shell for q= 40 kPa 183

Figure 3.145 Contours of minimum principal stresses (*10^4 kPa) on the top surface of the top shell for q= 50 kPa 184

Figure 3.146 Contours of minimum principal stresses (*10^4 kPa) on the top surface of the top shell for q= 70 kPa 184

Figure 3.147 Contours of minimum principal stresses (*10^4 kPa) on the top surface of the top shell for q= 90 kPa 185

Figure 3.148 Contours of minimum principal stresses (*10^4 kPa) on the top surface of the top shell for q= 100 kPa 185

Figure 3.149	Contours of minimum principal stresses (*10^4 kPa) on the bottom surface of the bottom shell for q= 10 kPa	186
Figure 3.150	Contours of minimum principal stresses (*10^4 kPa) on the bottom surface of the bottom shell for q= 30 kPa	186
Figure 3.151	Contours of minimum principal stresses (*10^4 kPa) on the bottom surface of the bottom shell for q= 40 kPa	187
Figure 3.152	Contours of minimum principal stresses (*10^4 kPa) on the bottom surface of the bottom shell for q= 50 kPa	187
Figure 3.153	Contours of minimum principal stresses (*10^4 kPa) on the bottom surface of the bottom shell for q= 70 kPa	188
Figure 3.154	Contours of minimum principal stresses (*10^4 kPa) on the bottom surface of the bottom shell for q= 90 kPa	188
Figure 3.155	Contours of minimum principal stresses (*10^4 kPa) on the bottom surface of the bottom shell for q= 100 kPa	189
Figure 3.156	Pictorial presentation of boundary conditions for the hinged supported laminated cylindrical glass shell	190
Figure 3.157	Central deflection values for hinged cylindrical shell	199
Figure 3.158	Central stress values for hinged cylindrical shell	199
Figure 3.159	A view of radial deflection contour for hinged supported shell	200
Figure 3.160	Normalized maximum deflection versus load for hinged supported shell	201
Figure 3.161	Stress versus load for hinged supported shell	201
Figure 3.162	Maximum deflection versus load	202
Figure 3.163	Maximum stress versus load	202
Figure 3.164	Circumferential displacement of the top glass unit along the center line at y=0	203
Figure 3.165	Circumferential displacement of the bottom glass unit along the center line at y=0	203

Figure 3.166 Radial deflection along the center line at y=0 204

Figure 3.167 Axial displacement of the top glass along the center line at θ=0 204

Figure 3.168 Axial displacement of the top glass unit at the center along the center line at θ=0 205

Figure 3.169 Radial deflection along the diagonal 205

Figure 3.170 Circumferential displacement of the top glass shell along the diagonal 206

Figure 3.171 Circumferential displacement of the bottom glass shell along the diagonal 206

Figure 3.172 Axial displacement of the top glass shell along the diagonal 206

Figure 3.173 Axial displacement of the bottom glass shell along the diagonal 207

Figure 3.174 Maximum stress at the top surface of the top glass along the θ direction of hinged supported shell 208

Figure 3.175 Minimum stress at the top surface of the top glass along the θ direction of hinged supported shell 208

Figure 3.176 Maximum stress at the bottom surface of the bottom glass along the θ direction of hinged supported shell 208

Figure 3.177 Minimum stress at the bottom surface of the bottom glass along the θ direction of hinged supported shell 209

Figure 3.178 Maximum stress at the bottom surface of the top glass shell along the centerline at y=0 210

Figure 3.179 Minimum stress at the bottom surface of the top glass shell along the centerline at y=0 210

Figure 3.180 Maximum stress at the top surface of the bottom glass shell along the centerline at y=0 210

Figure 3.181 Minimum stress at the top surface of the bottom glass shell along the centerline at y=0 211

Figure 3.182 Maximum stress at the top surface of the top glass along the center line at θ=0 212

Figure 3.183 Minimum stress at the top surface of the top glass along the center line at θ=0 212

Figure 3.184 Maximum stress at the bottom surface of the bottom glass along the center line at θ=0 212

Figure 3.185 Minimum stress at the bottom surface of the bottom glass along the center line at θ=0 213

Figure 3.186 Maximum stress at the top surface of the top glass shell along the diagonal 213

Figure 3.187 Minimum stress at the top surface of the top glass shell along the diagonal 213

Figure 3.188 Maximum stress at the bottom surface of the bottom glass shell along the diagonal 214

Figure 3.189 Minimum stress at the bottom surface of bottom glass shell along the diagonal 214

Figure 3.190 Shear stress of the interlayer along the center line at y=0 215

Figure 3.191 Shear stress of the interlayer along along the center line at θ=0 215

Figure 3.192 Membrane stress along the center line at y=0 for 10 kPa 216

Figure 3.193 Bending stress along the center line at y=0 for 10 kPa 216

Figure 3.194 Membrane stress along the center line at θ=0 for 10 kPa 216

Figure 3.195 Bending stress along the center line at θ=0 for 10 kPa 217

Figure 3.196 Strength factor versus load for hinged supported shell 217

Figure 3.197 Contours of radial displacement (mm) for q=10 kPa 218

Figure 3.198 Contours of d radial displacement (mm) for q=20 kPa 219

Figure 3.199 Contours of radial displacement (mm) for q=30 kPa 219

Figure 3.200 Contours of radial displacement (mm) for q=40 kPa 220

Figure 3.201 Contours of radial displacement (mm) for q=50 kPa 220

Figure 3.202 Contours of maximum principal stresses (*10^4 kPa) on the top surface of the top shell for q= 10 kPa 221

Figure 3.203 Contours of maximum principal stresses (*10^4 kPa) on the top surface of the top shell for q= 30 kPa 222

Figure 3.204 Contours of maximum principal stresses (*10^4 kPa) on the top surface of the top shell for q= 40 kPa 222

Figure 3.205 Contours of maximum principal stresses (*10^4 kPa) on the top surface of the top shell for q= 50 kPa 223

Figure 3.206 Contours of maximum principal stresses (*10^4 kPa) on the top surface of the top shell for q= 70 kPa 223

Figure 3.207 Contours of maximum principal stresses (*10^4 kPa) on the top surface of the top shell for q= 90 kPa 224

Figure 3.208 Contours of maximum principal stresses (*10^4 kPa) on the top surface of the top shell for q= 100 kPa 224

Figure 3.209 Contours of maximum principal stresses (*10^4 kPa) on the bottom surface of the bottom shell for q= 10 kPa 225

Figure 3.210 Contours of maximum principal stresses (*10^4 kPa) on the bottom surface of the bottom shell for q= 30 kPa 225

Figure 3.211 Contours of maximum principal stresses (*10^4 kPa) on the bottom surface of the bottom shell for q= 40 kPa 226

Figure 3.212 Contours of maximum principal stresses (*10^4 kPa) on the bottom surface of the bottom shell for q= 50 kPa 226

Figure 3.213 Contours of maximum principal stresses (*10^4 kPa) on the bottom surface of the bottom shell for q= 70 kPa 227

Figure 3.214 Contours of maximum principal stresses (*10^4 kPa) on the bottom surface of the bottom shell for q= 90 kPa 227

Figure 3.215 Contours of maximum principal stresses (*10^4 kPa) on the bottom surface of the bottom shell for q= 100 kPa 228

Figure 3.216 Contours of minimum principal stresses (*10^4 kPa) on the top surface of the top shell for q= 10 kPa 228

Figure 3.217 Contours of minimum principal stresses (*10^4 kPa) on the top surface of the top shell for q= 30 kPa 229

Figure 3.218 Contours of minimum principal stresses (*10^4 kPa) on the top surface of the top shell for q= 40 kPa 229

Figure 3.219 Contours of minimum principal stresses (*10^4 kPa) on the top surface of the top shell for q= 50 kPa 230

Figure 3.220 Contours of minimum principal stresses (*10^4 kPa) on the top surface of the top shell for q= 70 kPa 230

Figure 3.221 Contours of minimum principal stresses (*10^4 kPa) on the top surface of the top shell for q= 90 kPa 231

Figure 3.222 Contours of minimum principal stresses (*10^4 kPa) on the top surface of the top shell for q= 100 kPa 231

Figure 3.223 Contours of minimum principal stresses (*10^4 kPa) on the bottom surface of the bottom shell for q= 10 kPa 232

Figure 3.224 Contours of minimum principal stresses (*10^4 kPa) on the bottom surface of the bottom shell for q= 30 kPa 232

Figure 3.225 Contours of minimum principal stresses (*10^4 kPa) on the bottom surface of the bottom shell for q= 40 kPa 233

Figure 3.226 Contours of minimum principal stresses (*10^4 kPa) on the bottom surface of the bottom shell for q= 50 kPa 233

Figure 3.227 Contours of minimum principal stresses (*10^4 kPa) on the bottom surface of the bottom shell for q= 70 kPa 234

Figure 3.228 Contours of minimum principal stresses (*10^4 kPa) on the bottom surface of the bottom shell for q= 90 kPa 234

Figure 3.229 Contours of minimum principal stresses (*10^4 kPa) on the bottom surface of the bottom shell for q= 100 kPa 235

LIST OF TABLES

TABLES

Table 2.1	Physical properties of laminated glass curved beam	31
Table 2.2	Comparison of results for the fixed supported laminated curved beam	34
Table 2.3	Comparison of results for the simply supported laminated curved beam	36
Table 2.4	Physical properties of laminated glass curved beam	39
Table 2.5	Comparison of central maximum stresses for experimental and mathematical model results	40
Table 3.1	Comparison of deflections for the monolithic cylindrical shell	101
Table 3.2	Physical properties of laminated glass shell unit	105
Table 3.3	Comparison of the results for the fixed supported laminated cylindrical shell	105
Table 3.4	Strength Factor values in building codes	155
Table 3.5	Comparison of the results for the fixed supported laminated cylindrical shell	157

LIST OF SYMBOLS

h_1, h_2	Thickness of top and bottom glass ply
t	Thickness of the interlayer
b	Width of beam
h	Distance between the midpoints of the top and bottom plies
$N1$, $N2$	Cross sectional force at the top and bottom glass ply
$u1$, $u2$	Circumferential displacement for the top and bottom ply in the θ direction
$v1$, $v2$	Axial displacement for the top and bottom ply in the y direction
r_1, r_2	Radius of the top and bottom ply
A_1, A_2	Cross sectional area of top and bottom glass ply
w	Lateral deflection of the top and bottom plies
E	Modulus of elasticity of glass
G	Shear modulus of interlayer
θ, r	polar coordinates
P	Point load applied at the middle of beam
q	Uniformly distributed load applied over the length of beam
U	Total strain energy
V	Potential energy of applied loads
Π	Total potential energy of the system
I_1, I_2	Cross sectional moment of inertia of the top ply
I	Cross sectional moment of inertia of the laminated glass section

γ_I	Shear strain in the interlayer for curved beam
$\gamma_{\theta r}$, γ_{yr}	Shear strain in the interlayer
τ	Shear stress in the interlayer
U^i_m	Membrane strain energy for the top and bottom ply
U^i_b	Bending strain energy for the top and bottom ply
U_I	Shear strain energy for the interlayer
$U^i_{yr}, U^i_{\theta r}$	Shear strain energy of the interlayer in the radial and circumferential directions, respectively
$\kappa_\theta, \kappa_y, \kappa_{\theta y}$	Bending strains
$\varepsilon_\theta, \varepsilon_y, \varepsilon_{\theta y}$	Membrane strains
Ω	Load potential function
ρ	Poisson ratio of the interlayer
ε^i_m	Membrane strain energy for the top and bottom ply
ε^i_b	Bending strain energy for the top and bottom ply
top-top	Top surface of the top glass
top-bot	Bottom surface of the top glass
bot-top	Top surface of the bottom glass
bot-bot	Bottom surface of the bottom glass

CHAPTER 1

INTRODUCTION

1.1 Laminated Glass

Laminated glass is an architectural unit which is a combination of two or more thin glass sheets and a soft interlayer PVB (Polyvinyl Butyral) or resin which bonds them together. Polyvinyl Butyral can be produced with varying plasticizer contents by different manufacturers.

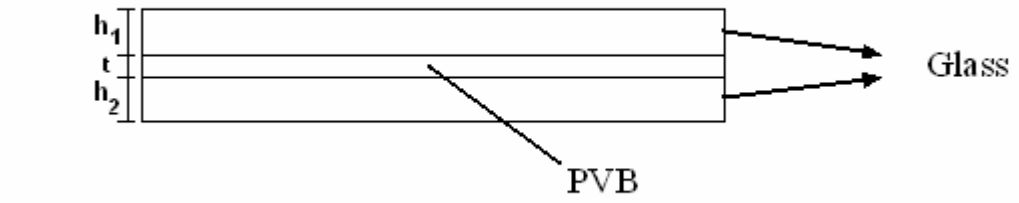

Figure 1.1 Laminated glass

Laminated glasses have long been used in the manufacturing of aircraft and automobile windscreens and nowadays they are widely used in the architectural components of the buildings.

Laminated glass is used in architectural glazing industry because of its properties like safety, security, sound control, ultraviolet screening, solar energy control, durability, protection from bomb blast and natural disasters like hurricane, earthquake, etc.

Laminated glass can help to provide protection from injury, and prevents property damage from man made and natural disasters by keeping the glass intact within the frame. When laminated glass is broken, the polyvinyl butyral interlayer keeps the

glass shards together. The interlayer is also advantageous in other respects. Because of shear damping performance of the PVB, laminated glass is an effective sound control product. The ability of interlayer to reflect and/or absorb and re-radiate much of the solar UV radiation, solar control can also be accomplished.

Laminated glass has some disadvantages: it has relatively low bending strength compared with monolithic glass of the same overall thickness due to the presence of the plastic interlayer.

Laminated glass units are used in architectural glazing products such as overhead glazing, safety glazing and insulating glass because of their resistance to a wide range of loading and environmental conditions. Laminated glass units have the advantage of withstanding blast pressures, high wind pressures or missile impact rather than ordinary glass units such as tempered, annealed or heat-strengthened laminated glass.

Behavior of laminated glass unit is highly complicated because of two different types of materials, glass and PVB. The modulus of elasticity of glass about 10^4 times greater than the elasticity modulus of polyvinyl butyral and laminated glass unit is very thin, and can easily show large displacement. Therefore, the equilibrium equations governing their behavior are based on large deflection theory.

Glass unit used as a structural member could be layered, laminated or monolithic.

Layered glass consists of two glass sheets with no friction between them. Stress distribution of each ply is symmetric with respect to their individual neutral axis. The glass sheets share the load equally. ‘Plane sections before deformation remain plane after deformation’ assumption is not valid for layered glass units because centers of curvature of two plies are different.

Monolithic glass consists of one glass sheet. Stress distribution of monolithic glasses is symmetric around the neutral axis of the glass unit. Because of single center of curvature, 'plane sections remain plane' assumption is valid for monolithic glass units.

Laminated glass consists of two or more glass sheets connected with an interlayer. Stress distribution in the cross section of laminated glass is formed as constant coupling stress of interlayer and the two triangular stress distribution of a layered glass, which is symmetrical about the neutral axes of each ply. The size of coupling stress depends on the shear modulus of the interlayer. While coupling stress is compressive at the top ply, it is tensile at the bottom ply when pressure is applied towards top ply.

1.2 Previous Research

In literature, there are many studies concerned with behavior of laminated glass unit. A brief summary of the studies is listed below.

1.2.1 Hooper's Analytical and Experimental Studies

Hooper (1973) conducted the first study about laminated glass beams. In his study, a mathematical model for the bending of laminated glass beams under four point loading was derived. The relevant differential equation in terms of applied bending moment and the axial force in one of the plies were solved using Laplace transform.

Hooper plotted three influence factors K_1, K_2 and K_3 respectively proportional to the axial force in one of the plies, shear strain in the interlayer and central deflection. He noted that shear modulus of PVB can be written as a function of time which approaches zero as time increases, since PVB is a viscoelastic material.

Hooper carried out two types of experiments. At first, tests on laminated glass beam with soft and hard PVB interlayer under short and long loading durations was conducted. For short-term loading tests, he bonded strain gages with thin lead wires to inner and outer glass sheets of laminated glass beam. Then he placed the plastic

interlayer between the gaged glass layers and laminated them. He loaded the beams via universal testing machine at an ambient temperature of 21^{o}C. Gage readings were taken at several loads. Short-term loading tests took about 3 minutes. Bending stresses across the laminated glass section and central deflections were obtained. The changes in shear modulus versus temperature were plotted for soft and hard interlayer cases.

While load deformation curves were linear and creep deformation was negligible for beams containing a soft interlayer they were slightly nonlinear and creep deformation occurred for beams containing a hard interlayer. Results of strain gage readings were in good agreement with the results of computed strains. Hooper found that shear strain of the unit was increasing as the interlayer thickness was decreasing. Another phenomenon observed was the modulus of hard interlayer being ten times higher than that of soft interlayer.

In addition to above experiments Hooper also conducted creep experiments. In creep experiments, the applied loads were in the form of dead weights and located at the quarter points of small laminated glass beams at various temperatures. The experiment duration was 80 days and measurements of central deflection and ambient temperature were taken at intervals throughout this period. As results of creep experiments Hooper plotted shear modulus- temperature graphs and he noted that the severe degradation of shear modulus of soft interlayer began between 10-20 degrees Celsius whereas it began between 30-40 degrees Celsius for hard interlayer. Hooper concluded that response of architectural laminated glass unit subjected to sustained loading for long-term was the same for all types of PVB interlayer. If a short-term load was applied to the already loaded section, then the stress field could be calculated by using the combination of sustained and transient loading stresses. Shear modulus of the soft and hard interlayer at different temperatures were calculated and shear modulus-temperature graphs were plotted.

The results Hooper (1973) deduced from these studies were that bending resistance of laminated glasses principally depend upon the thickness and shear modulus of the interlayer. Creep deformation took place within the plastic interlayer if the applied loads were sustained except at relatively low temperatures, which allowed the glass

layers to deflect as layered glass. But laminated glass would respond as a composite member having an interlayer shear modulus appropriate to its temperature if it was undergoing sustained loading.

Hooper advised that for the structural design, architectural laminates, which were subjected to sustained loads like snow or self-weight loading, should be considered as layered glass. For short term loading like wind loading, glass bending stresses might be estimated on the basis of interlayer shear modulus corresponding to the maximum temperature at which such loading was likely to occur, remembering that solar radiation might well raise the temperature of glazed laminate to well above that of surrounding atmosphere. If laminates were subjected to both sustained and transient loading, the resulting stresses might be calculated by superposition method.

1.2.2 Mathematical Model Developed by Vallabhan

Vallabhan et al. (1983) determined that Von Karman plate theory assumptions were acceptable for the nonlinear behavior of thin glass plates. Boundary conditions were prescribed as simply supported. A computer model was developed by Vallabhan et al. to analyze the nonlinear behavior of monolithic glass plates using finite difference method. They compared nonlinear behavior of monolithic and layered glass using the finite difference solution incorporating Von Karman plate theory.

Vallabhan et al. (1987) developed a nonlinear model for two plates placed without an interlayer to determine the limits of laminated glass units.

Strength factor of glass unit/plate geometries for a wide range of pressures were considered by them. Nonlinear theory of thin rectangular plates was used for strength factor analysis. The ratio of maximum principal tensile stress in monolithic glass system to the maximum principal tensile stress in layered glass system was defined as the strength factor.

In analysis, they used nondimensional parameters of load, deflection, stress and aspect ratio. They found that strength factor began to increase nonlinearly, starting from the linear value of 0.5 to approach and exceed 1, when the pressure increased.

In 1993 Vallabhan et al. developed a new mathematical model for the nonlinear analysis of laminated glass units using the principle of minimum potential energy and variational calculus. Because of symmetry with respect to x and y axes only a quarter of plate was considered. Five nonlinear governing differential equations and boundary conditions were obtained via variational and energy methods. Von Karman nonlinear plate theory was used for modelling the glass plates. The glass plies were assumed to have both bending and membrane strain energies while the interlayer has only shear strain energy. Finite difference method was used to solve the nonlinear differential equations. All the nonlinear terms were collected on the right hand side of the differential equation so the left hand side was obtained as linear. To verify the results obtained from the mathematical model, detailed full-scale exp
eriments were conducted in the Glass Research and Testing Laboratory at Texas Tech University. They conducted a series of tests on a special laminated unit size (152.4×152.4 cm.). The thicknesses of glass plies and interlayer are 0.47625 cm. and 0.1524 cm., respectively. To provide simply supported boundary conditions they used round teflon fasteners. The results of mathematical model and experiments were quite close.

Asik and Vallabhan (1995) studied the convergence of nonlinear plate solutions. They solved nonlinear plate equations by using two methods. For both of the methods they used classical Von Karman assumptions and finite difference method. In the first method they used ϕ (Airy stress function) and w (lateral displacement) of the plate to convert the plate equations. In the second method the same equations were converted into displacements (u, v, w) of the middle surface of the plate. Although the above two methods have the same assumptions, convergence characteristics of them were different. As a conclusion they observed that both methods yielded the same solution but first method's convergence was faster than the second one. They also observed that second model not only converged slowly but also could diverge after a particular load. For coarser mesh as the displacement diverged from the actual path the method stopped even at low pressures. However, when they made fine mesh they could not observe this behavior.

Asik (2003) improved Vallabhan's et al. model (1993) by using modified strongly implicit (MSI) procedure to avoid the storage of full matrix that needed large memory and to provide less calculation time. Minimizing the total potential energy of the laminated glass unit with respect to five displacement parameters, the in-plane displacements in x and y directions of the two plates and the common lateral displacement, five nonlinear partial differential equations were obtained as in the study of Vallabhan et al. (1993).

To write these governing differential equations in discrete form central finite difference method was used. The discrete form of these equations was written in matrix form. While symmetric banded coefficient matrix was obtained for lateral displacement, full coefficient matrices were obtained for each one of in plane displacements.

He used variable underrelaxation parameter for lateral displacement w while overrelaxation factor was used for in plane displacements to overcome the convergence difficulties and to decrease the number of iterations to reach the solution.

Asik used modified strongly implicit (MSI) procedure for in-plane displacements. Instead of full coefficient matrix with $2*(n_x+1)^2*(n_y+1)^2$ elements, the coefficients of finite difference equations were stored as vectors with totally $2*5*(n_x+1)*(n_y+1)$ elements.

As a conclusion, he applied special solvers that provide advantage in storage and computation time for nonlinear governing differential equations of a laminated glass. The results of his study dictated that nonlinearity have to be considered for the analysis of the behavior of laminated glass units. He observed that location of maximum stress started to travel at the center and moved towards the corner of the plate when the nonlinear terms in governing equations start to be affected under increasing pressure.

1.2.3 Experimental Studies conducted by Behr

Behr et al. conducted a series of experiments in 1985 on layered, monolithic and laminated glass units, to verify the theoretical model for a laterally loaded, thin plates developed by Vallabhan and Wang (1983).

The experiments were conducted using laminated glass units having dimensions of 152.4×243.84 cm. To obtain uniformly distributed load, air was evacuated from the chamber using vacuum control. To represent the ideal support conditions in the theoretical model round teflon beads which permit rotation and in-plane displacement were used. To evaluate the structural behavior of laminated glass unit tests were performed at temperatures between $0°$ C and $77°$ C. As a result of the experiments, it is concluded that:

1-Stresses in the layered glass unit were larger near the corner and smaller near the center than comparable stresses in the monolithic glass plate.

2-The maximum principle tensile stress near the corner of laminated glass unit at room temperature and below were smaller than theoretically predicted stress in a monolithic glass.

3-At levels above the room temperature, corner stress in laminated glass increased when temperature was increasing. On the contrary, maximum principle tensile stress at the center of laminated glass decreased with increasing temperature.

4-Larger principal stresses in layered and laminated glass unit at $77°$ C were %50 larger than the largest principal stresses of monolithic glass.

Finally, it was observed that stresses in layered glass were larger near the corner and smaller near the center than monolithic glass plates. It was also observed that at room temperature and below maximum principal stresses near the corner of laminated unit were slightly smaller than the theoretically predicted stresses at the same location in a monolithic glass plate.

It can be said that at room temperature laminated glass unit behaved like a monolithic glass plate, whereas at higher temperatures it behaved like a layered glass unit. So the behavior of laminated glass unit was bounded by these two limiting

cases. His test results also verified the accuracy of the Vallabhan's et al. theoretical model (1983).

Behr et al. (1986) conducted some experiments to consider laminated glass unit structural behavior for different interlayer thickness and load durations. They performed multiphased theoretical and experimental research program to develop and verify analytical models, which define the behavior of laminated glass units used in building application. Their research included the analysis of laminated glass unit for a wide range of geometries, failure criteria definition of glass and the effects of temperature, load duration, chemical and mechanical abrasion and ultraviolet radiation to the failure criteria and analyze method.

To consider the effect of the interlayer thickness laminated glass unit with two interlayer thicknesses 0.0762 cm and 0.1524 cm were tested for simply supported boundary conditions and uniform lateral pressure.

It was concluded that the glass unit with a thicker interlayer have reduced flexural stiffness. Interlayer thickness affected magnitude of the maximum stress by less than %10 while the maximum difference in these two deflections was %5. As a result, it is concluded that the effect of interlayer thickness on laminated glass unit did not appear to be significant.

To consider the effect of long duration loading on laminated glass units a $152.4 \times 243.8 \times 0.71$ cm unit was subjected to a lateral pressure of 1.4 kPa for 3500 seconds or 1 hour. The tests were performed at $22°C$, $49°C$ and $77°C$.

As a result of long duration loading tests at different temperatures they concluded that, for all three test temperatures there was 20 % increase for corner stress, while maximum lateral deflection at the center of the unit increased by 10 %. Conversely, principal stresses at the center of laminated glass unit decreased slightly.

Behr et al. (1993) reported the results of theoretical and experimental studies conducted over a 20-year time period by several researchers. Their objectives were to review and assess information about the structural behavior of architectural laminated glass and to provide a compendium of research results. They considered the major structural characteristics of laminated glass like load deflection behavior,

load stress relationships, temperature effects, duration of loading, interlayer thickness and aspect ratio.

They noted that temperature effect was significant for the behavior of laminated glass units at 77 ^{o}C, but were not significant at room temperatures. Conversely, Hooper's test (1973) showed a severe degradation in effective shear modulus of interlayer below the room temperature. Differences in PVB chemistry and differences between the experiment procedures could explain the differences between the results of Hooper and Behr.

They also considered the relationship of surface stress to lateral pressure in the structural behavior of laminated, layered and monolithic glass. They concluded that similarities existed between monolithic and laminated glass stresses at room temperature and below but at elevated temperatures stresses of laminated glass moved towards layered glass stresses.

The effect of duration of loading on the structural behavior of laminated glass was considered by Behr et al. While dead loads and snow loads produce long duration loading, wind loads produce load durations measured in seconds. Hooper (1973) performed creep tests on small scale laminated glass beams under four point loading of 49 ^{o} C, 25 ^{o} C and 14 ^{o} C. They observed very small amount of creep over the 80 day loading period and the behavior of laminated glass was nearly layered at 25 ^{o} C while they observed no creep and layered behavior at 49^{o} C. At 14 ^{o} C the behavior of laminated glass unit was completely monolithic and substantial creep was observed at 80 days load duration. So Hooper concluded that substantial creep was observed at low temperatures.

Behr (1986) performed full scale creep tests under 1 hour on a laminated glass at temperatures 22 ^{o} C, 49 ^{o} C and 77 ^{o} C. They made the following observations as a result of their test:

1. The increase in corner stress was 22 % at 77^{o} C and 49^{o} C while it was 18% at 22^{o} C.

2. There was a decrease at the center principal stresses of laminated glass unit for all three test temperatures over the 1 hour loading duration.

3. The increase in maximum lateral deflection at the corner of laminated glass unit was 10% for all three test temperatures over the 1 hour load duration.

The results of Behr's full scale laminated glass plate tests were different from the Hooper's small scale test results. The creep was pronounced for small scale laminated glass beams. This difference was attributable to the difference in PVB chemistry.

Behr noted that the impact resistance of laminated glass units increased when the thickness of PVB interlayer increased.

Hooper (1973) observed a reduction in effective shear modulus of hard PVB as the result of small scale beam tests. As the interlayer thickness increased from 0.38 mm to 1.02 mm the shear modulus decreased from 15.2 MPa to 11.7 MPa. They did not investigate the effect of interlayer thickness for soft PVB interlayer.

Behr et al. (1986) conducted tests on laminated glass unit with interlayer thicknesses of 0.76 mm and 1.52 mm. They observed small differences in the stress and deformation responses of the units. Laminated glass unit with 1.52 mm interlayer thickness had higher stresses and deflections than laminated glass unit with 0.76 mm interlayer thickness. The differences in maximum stresses were less than 10% while they were below 5% for deflections.

In order to examine the structural behavior of laminated glass unit with large aspect ratios, experiments were conducted at 0^{o} C, 23^{o} C and 49^{o} C.

While center deflections of laminated glass beam specimens tested at 0^{o} C were lower than those in monolithic beams, they were almost equal at 23^{o} C. At 49^{o} C the central deflections of laminated units were higher than the deflections of monolithic beams but significantly less than those in layered beams. They sustained the maximum load for 1 minute and they observed 11%, 18% and 9% increases for the central deflections of laminated glass beams tested at 49^{o} C, 23^{o} C and 0^{o} C, respectively.

They observed that at room temperature and below, the stresses in laminated units were equal to or lower than those in monolithic glass beams; While they were higher than the stresses of monolithic glass beam at 49^{o} C. Increase of stresses were observed as 8%, 6% and 4% at 49^{o} C, 23^{o} C and 0^{o} C, respectively when the constant

2.8 kPa load was held constant for sixty seconds. It was concluded that even at high aspect ratios, under short term loading and below room temperature laminated glass appeared to behave like monolithic glass.

1.2.4 Norville developed a theoretical model

Norville et al. (1999) developed a theoretical model, which explained the behavior of laminated glass. The model was based on mechanics of materials and indicated that the interlayer in laminated glass provided an increase in effective section modulus with respect to monolithic glass beam having the same nominal thickness. The increase in effective shear modulus resulted in lower flexural stresses and higher fracture strengths. PVB's function in laminated glass unit was assumed to maintain spacing between the glass plies and transferring a fraction of the horizontal shear force between the glass plies. Effective section modulus for laminated glass under uniform loading as a function of the fraction of horizontal shear force transferred by the PVB interlayer could be computed by using this model. The horizontal shear force transferred by the interlayer between the glass plies was expressed as the product of a shear force transfer parameter and the horizontal shear force of middle fiber of monolithic glass beam. The laminated glass beam acted as a layered glass beam when this parameter was zero. It behaved as a monolithic glass beam when the parameter was 1.

Norville et al. performed laminated glass beam test to verify measurements of center deflection reported by Behr (1993). The results were in close agreement and deflections predicted by this model strongly supported the model's validity. They also performed laminated glass lite tests and observed that laminated glass series with varying thickness, dimension and loading displayed mean fracture stress ranging from 98% to 230% that of monolithic series of the same dimensions.

As a conclusion, they developed a theoretical model to investigate the behavior of laminated glass under uniform loading. PVB was assumed to transfer a horizontal shear force between the glass plies. They observed that, for the laminated glass, to

produce equivalent or greater section modulus than monolithic glass, the fraction of shear force transfer was less than 1, and at 49^{o}C behavior of the laminated glass was far below the layered glass model. At room temperature, under short duration (<60 sec.) uniform loading, laminated glass constructions indicated lower stresses. In addition, laminated glass units had equivalent or higher fracture strengths than monolithic glass units with the same dimensions and thickness.

1.2.5 Van Duser developed a finite element model

Van Duser et al. (1999) presented a three dimensional finite element model based on large deformation for stress analysis of laminated units. The analysis had capability to predict the stress generated during biaxial flexure. They solved a laminated glass subjected to uniform pressure using the commercial finite element model ABAQUS (1997) to demonstrate the accuracy of their approach. They solved the models tested by Vallabhan et al. (1993) to be able to compare their results. They also combined stress analysis with a Weibull statistical probability of failure, to describe the load bearing capacity of laminates of arbitrary shape and size under specific loading conditions. As a result of their study they concluded that laminated glass polymer units behaved in a complex manner due to large difference between stiffness of materials, nonlinearity, large deflection, polymer viscoelasticity and additional stiffening effect of polymer thickness. They also observed that stress development might fall outside of the monolithic and layered limit because of the membrane stresses of plate. The other finding of their study was that stress development was influenced by temperature. At higher temperatures and loads principal stresses shifted systematically towards the corner. They concluded that under almost all conditions Weibull effective stress was lower for laminated plates than for the equivalent monolithic one.

1.2.6 Minor conducted experiments about failure strength

Minor et al. (1990) conducted some tests to make comparisons between failure strengths of monolithic and laminated glass units. They selected three sizes of annealed monolithic glass samples: $152.4 \times 243.84 \times 0.635$ cm; $96.52 \times 193.04 \times 0.635$ cm and $167.64 \times 167.64 \times 0.635$ cm. These samples were used to evaluate the failure strengths as function of several variables like; temperature, glass type (heat treatment) and surface conditions. Laminated glass samples were selected as heat strengthened and fully tempered. To apply uniform pressure to test specimens, an accumulator was used to evacuate air from vacuum chamber. As a result, failure strengths of laminated glass and annealed monolithic glass samples were compared. At room temperature laminated glass strengths and monolithic glass strengths were found to be equal whereas the strength of laminated glass decreased when temperature were elevated. It is also observed that fully tempered and heat strengthened laminated glass samples were 3 or 5 times stronger than annealed laminated and monolithic glass samples.

1.2.7 Studies about Shell Structures

There are no studies about nonlinear behavior of laminated glass shell structures. But some of the studies about shell structures are summarized below.

Turkmen (1999) studied cylindrically curved laminated composite panels subjected to the blast shock wave. He obtained numerical and theoretical results for this problem and considered the effect of curvature and fiber orientation angle. Love's theory for thin elastic shells was used for mathematical modeling. The resulting equations were solved by using Runga-Kutta method. In addition to the numerical analysis (Runge–Kutta Method), finite element program ANSYS was used to obtain results for cylindrically curved shell. The results were compared and a good agreement was found. Turkmen concluded that the central deflection of the clamped cylindrical laminated shell decreased and response frequency of the panel increased while the stiffness of the panel was increasing. Also the effect of damping and loading conditions considered for this composite panel.

Schimmels and Plazatto (1994) analyzed nonlinear geometric behavior of laminated shell geometry by using orthogonal curvilinear coordinates. They applied transformation between Cauchy and Lagrangian coordinate system for isotropic and composite shells. Using nonlinear strain displacement relations and minimum potential energy theory nonlinear algebraic equations were obtained for displacements. To solve the nonlinear equations they were converted to linear equations and finite element method was used to solve these equations.
They verified their model by using the results of Sabir (1972). It is observed that the fiber rotations became large enough to affect the material transformation matrix when the shell displacement reached three times of the shell thickness.

Aksogan and Sofiyev (2001) considered the dynamic stability of a laminated truncated conical shell with variable modulus of elasticity and densities in the thickness direction subject to a uniform external pressure, which is a power function of time. Analytical solutions were obtained for the critical dynamic and static loads and pertinent wave numbers. To verify the results, the critical dynamic loads for a truncated conical shell with a single layer, found analytically in the present study were compared with those found experimentally by Sachenkov and Klementev (1980). They also considered nonlinear free vibration of laminated non- homogenous orthotropic cylindrical shells. The equations and basic relations were based on the Donnel-Musthari shell equations. By using Galerkin method frequency of the cylindrical shell was obtained from Donnel-Musthari shell equations as a function of shell displacement and compared with the results in literature. It was observed that the number and ordering of the layers affect the values of vibration frequencies both in the homogenous and non-homogenous cases.

1.2.8 Studies about curved beam

D. J. Dawe (1974) presented finite element model for the solution of a circular arch with radius R and thickness t. The strain energy of the system was written in terms of

tangential and normal components of displacements. To obtain the differential equations which govern the behavior of the arch, the first variation of the energy was used. By solving two differential equations, tangential and radial displacements were obtained. Five circular arch models, which are given below where numerically solved. Those models were:

i) Quintic-quintic model with twelve independent coefficients in the expressions of displacement. Six of them were for normal displacement u and six for tangential displacement w.

ii) Cubic-quintic model with ten independent coefficients in the expressions of displacements (6 independent coefficients four u and 4 for w).

iii) Quintic-cubic model with 4 independent coefficients for tangential displacement and 6 independent coefficients for normal displacement.

iv) Cubic-cubic model with 4 independent coefficients for tangential displacement and normal displacement.

v) A constant strain, linear curvature element based on the coupled displacement field.

To apply the described models a computer program which double precision arithmetic throughout was used to solve arch problems. He obtained the displacements, moments, force distribution of a deep clamped arc carrying a point load. As a result of study he improved an independently interpolated model by increasing the order of assumed displacement from cubic to quintic.

Rajasekaran and Padmanabhan (1989) derived the governing equations for curved beams by employing large displacement theory. To obtain the governing equations they ignored shear strains due to shear stress and shear strains in the planes normal to middle surface. In the solution procedure, the large displacements and the small strains were also assumed, and the length of the member was much larger than the depth. To start the derivation they used three-dimensional small strain large displacement relations in cylindrical coordinate system by ignoring the nonlinear terms associated with displacement in z direction (w), since it was much smaller compared to the displacement in x and y directions. They wrote the equilibrium

equations and boundary conditions by integrating the principle of virtual displacement as the product of Kirchhoff stress tensor and Green's strain tensor.
Palani and Rajasekaran (1992) presented a model for static and stability analysis of thin walled curved beams made of composites by using straight beam element. In the study, they used Euler-Lagrange equilibrium equations and the associated boundary conditions derived by Rajasekaran and Padmanabhan (1989). To derive flexural stiffness matrix they used straight beam element by employing suitable transformations. While lateral displacement and angle of twist were represented by first order Hermitian polynomial, axial displacement was represented by zeroth order Hermitian polynomial for static analysis. The new curved beam model, which was obtained by using straight beam, required less computational effort, and the results were accurate and could be implemented in the programs like SAP. To verify the model they compared their results obtained for curved beam subjected to uniformly distributed radial loads with the results of Timoshenko and Gere (1961) and Rajasekaran and Padmanabhan (1989).

Kang and Yoo (1994) presented a consistent formulation for thin walled curved beams. They derived equilibrium equations governing the linear, large displacement and buckling behavior using the principle of minimum potential energy. In their study, it is assumed that:

1. Cross sections retained their original shapes.
2. The displacements were finite.
3. The shear stresses and strains were negligibly small.
4. The shear stress strains along the middle surface were negligibly small.
5. The length of beam was much larger than the other dimensions of the beam.
6. The radius of curvature was large.

To obtain the governing differential equations the total potential energy of the system was defined as the summation of strain energy and potential energy due to applied

loads. By neglecting the nonlinear term of the equations, they obtained the equations for linear behavior of a curved beam. The governing coupled differential equations of displacement (i.e. longitudinal, radial and vertical displacement) and boundary conditions of the curved beam were obtained via the first variation of total potential energy. In their derivation, the curvature effect was included. Analytical solution to the coupled equations obtained was not easy: In order to solve the equations an approximation based on the binomial series was adopted by ignoring the higher order terms. The derivation was more reliable than the previous derivation because of the following three advantages: First, they preferred energy method instead of free body method because free body method involved possibility of omitting some significant terms. Secondly, their interpretations were appropriate for thin walled curved beam. Lastly, their approximation was explicit and consistent.

Lin and Heish (2006) developed a closed form analytical solution for in plane laminated curved beam of variable curvatures. Before their study there were only a few paper devoted to laminated composite materials. Most of the studies were about the isotropic beam. To analyze curved beams numerically and analytically, approximate methods were applied for the displacement field by the previous researchers. They obtained the set of equations, which were the general solutions of axial force, shear force, moment, rotation angle and displacement field for laminated curved beam in terms of angle of tangential slope.
To show the validity of the model they compared the results of their study with the results of published articles for isotropic material. Also they solved various curved laminated beams such as cycloid, exponential spiral, catenary, parabola and elliptic under various loading cases.

1.3 Object and Scope of Thesis

Because of the high difference between the elasticity modulus of glass sheets and interlayer, the classic assumption that ‘plane section for the whole system before deformation remains plane after deformation’ is not realistic for laminated glass

units. Therefore, the existing theories in the literature cannot be employed for the analysis of laminated curved glass beam and shell structures.

The aim of the present study is to investigate the behavior of laminated curved glass beams and cylindrical shells. To develop a more realistic model it is assumed that plane section before bending remains plane after bending for each individual sheet and the interlayer translate a certain amount of shear between the glass sheets. Deflection and stress resultant values, the level of nonlinearity on the bending behavior and the effect of boundary conditions, strength factor of laminated curved glass beams and shells are obtained. Mathematical model and computer program are developed to analyze the nonlinear behavior of curved beams and shells. The model is based on minimum potential energy principle and variational approach. To verify the results of developed model nonlinear finite element analyses are performed for curved beam and shell structures. Besides, results of curved beam experiments previously conducted by Uzhan (2010) are used to verify the developed model.

Chapter 1, provides an introduction to the thesis and gives information about laminated glass units and background for the studies of laminated glass unit.

Chapter 2, Laminated curved glass beams are analyzed. The total potential energy of curved beam is expressed in terms of radial and circumferential displacement. Minimum potential energy principle and variational approach are used to obtain three nonlinear governing differential equations and boundary conditions. The equations are converted into matrix form by using finite difference method. Using iterative solution technique, the equations are solved. The results are verified by using finite element method and by comparing with the results obtained from experiments conducted in Experimental Mechanics Laboratory in the Department of Engineering Sciences at Middle East Technical University by Uzhan (2010). The results of study are given in graphs and interpreted in conclusion.

Chapter 3, Laminated glass shell structures are analyzed. The total potential energy of shell is expressed in terms of radial and circumferential displacement. Minimum potential energy principle and variational approach are used to obtain the five nonlinear governing differential equations and boundary conditions. The equations are converted into matrix form by using finite difference method. Using iterative

solution technique, the equations are solved. The results are verified by using finite element method. The results of the study are given in graphs and interpreted in conclusion.

Chapter 4, conclusions and recommendations obtained as result of study are given

CHAPTER 2

BEHAVIOR OF LAMINATED CURVED GLASS BEAMS

2.1 Introduction to Theory of Curved Beams

It has been quite a time since laminated glasses are in use. First laminated glasses with flat shapes were used as their production was easy, and design parameters were available. Nowadays, curved laminated glasses are also used in many modern buildings. Also curved elements can be used for spring design, electrical machinery blades, aerospace structures, design of arch bridges and highway constructions.

Curved beams are two dimensional structures which span the spaces. They are used to support loads from above. Because of the downward pressure, curved beams can carry much greater load than a straight beam. According to their structural behavior, curved beams are classified as fixed, hinged, two-hinged or tree-hinged. To satisfy fixed boundary conditions at the supports rotation is prevented. Fixed ended curved beams are more suitable for large spans than hinged ended curved beams because of their greater stiffness.

Because of lack of information about structural behavior of curved beams, they have not been employed much in practice. A curved beam differs from a straight beam due to its initial curvature. Because of mathematical complexity, most of the studies are about the linear behavior rather than the nonlinear behavior of curved beams.

Therefore, it is necessary to develop a mathematical model considering large deflection theory to predict the strength and behavior of curved beams.

In the present study, the behavior of the laminated glass curved beams is investigated since the curved glass units are being used in modern buildings nowadays and to author's knowledge, there is not any significant research on the laminated glass curved beams. Mathematical model is developed to predict the deflections and stresses developing in the unit in polar coordinates. Minimum potential energy principle is used to minimize the total potential energy which is the summation of the bending and membrane energies in glasses and the energy due to the shear deformation in the soft interlayer and force potential. Three nonlinear coupled differential equations are derived through variational principles. Numerical model is developed to solve the continuous form of the governing equations. Finite difference method is employed for the discretization of the nonlinear partial differential equations, and then those equations are solved iteratively. The model is verified by using the data obtained from the finite element model and using previously done experimental results by Uzhan [27]. Results are presented by the figures for the verification of the model and the prediction of the behavior. Moreover, the behavior of laminated glass beams is presented in comparison to the behavior of the monolithic and layered glass beams as limiting cases since the design charts are available only for monolithic glasses.

2.2 Mathematical Modeling

Behavior of the laminated curved beam- shown in Figure 2.1-, which contains two thin glass sheets and an interlayer PVB placed in between the glass sheets, can be represented by three nonlinear partial differential equations obtained for three displacement components. Two of these equations are used to represent circumferential displacements and the third one is for the radial displacement of the unit.

Therefore, total potential energy of the unit, shown in Figure 2.1, is written as the summation of bending, membrane, shear and force potential energies to obtain the governing differential equations in terms of displacements. Because of the nature of the problem, the bending and membrane strain energies of the glass layers and the shear strain energy of the PVB interlayer are only considered. Then the first variation of the total potential energy of the unit with respect to the circumferential and radial displacements gives the governing differential equations.

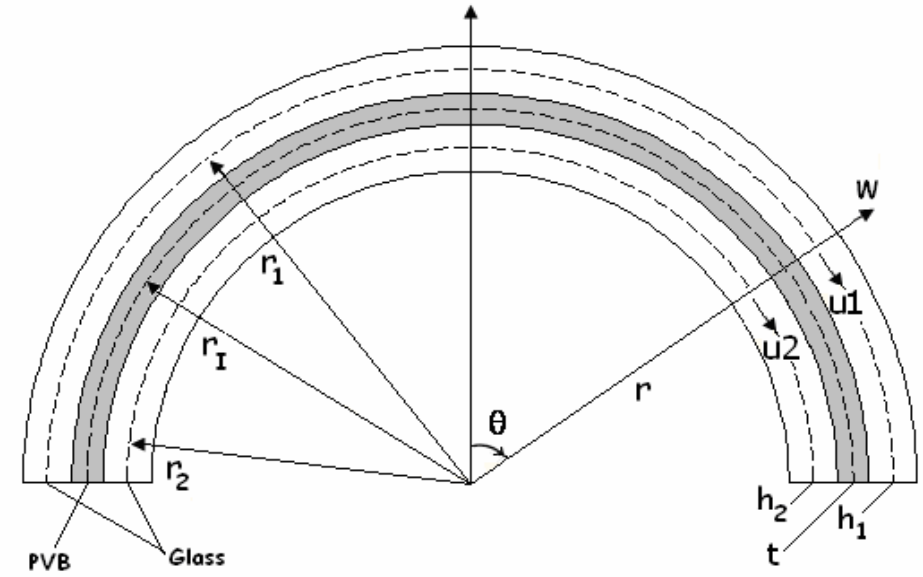

Figure 2.1 Laminated glass curved beam with an interlayer PVB

For mathematical modeling of glass sheets, the following assumptions are made:

1. The beam material is completely homogenous and isotropic.

2. The beam material is elastic and obeys Hooke's law.

3. Because of the small thicknesses of the glass beams, shear deformation is ignored.

4. Plane sections initially normal to the mid surface remain plane and normal to the mid surface during bending for each glass ply but not for a unit.

5. For nonlinear behavior, because of in-plane displacement derivatives are so small, the higher powers of the in-plane displacement derivatives and their products are ignored.

6. For the laminated glass unit, it is assumed that radial deflection does not change in the cross section since the layers are thin.

For the interlayer the following assumptions are made:

1. Plane section before deformation remains plane after deformation.

2. Material is homogenous and isotropic.

3. Material is elastic and obeys Hooke's law.

4. Linear shear strains are assumed instead of finite strains to introduce a simplification

5. No slip occurs between the adjacent faces of the plies and interlayer.

6. PVB interlayer only transfers shear and has a negligible compression in transverse direction.

Using the above assumptions, which are given for interlayer and glass layers, the total potential energy of the system can be written as:

$$\Pi = U_m^1 + U_b^1 + U_m^2 + U_b^2 + U_I + \Omega \tag{2.1}$$

where U_m^1, U_m^2 are the membrane strain energies and U_b^1, U_b^2 are the bending strain energies for the inner and outer glass arches, respectively; U_I is the shear strain energy of the PVB interlayer, and Ω is the potential energy due to the applied loads. Here, Π is written in terms of the radial displacement w, and circumferential displacements u_1 and u_2 as follows

$$\Pi = \sum_{i=1}^{2} \left\{ \int_V \frac{1}{2} E (\varepsilon_m^i)^2 \, dV + \int_V \frac{1}{2} E (\varepsilon_b^i)^2 \, dV \right\} \quad (2.2)$$

$$+ \int_V \frac{1}{2} G (\gamma_I)^2 \, dV - \int_0^s qwds$$

where

$$\varepsilon_m^1 = \frac{u1_\theta + w}{r_1} + \frac{1}{2}\left(\frac{w_\theta}{r_1}\right)^2 \qquad \varepsilon_m^2 = \frac{u2_\theta + w}{r_2} + \frac{1}{2}\left(\frac{w_\theta}{r_2}\right)^2$$

$$\varepsilon_b^1 = -z\frac{w_{\theta\theta}}{r_1^2} \qquad \varepsilon_b^2 = -z\frac{w_{\theta\theta}}{r_2^2}$$

Shear strain of the unit is obtained from deformed and undeformed geometry as seen in Figure 2.2.

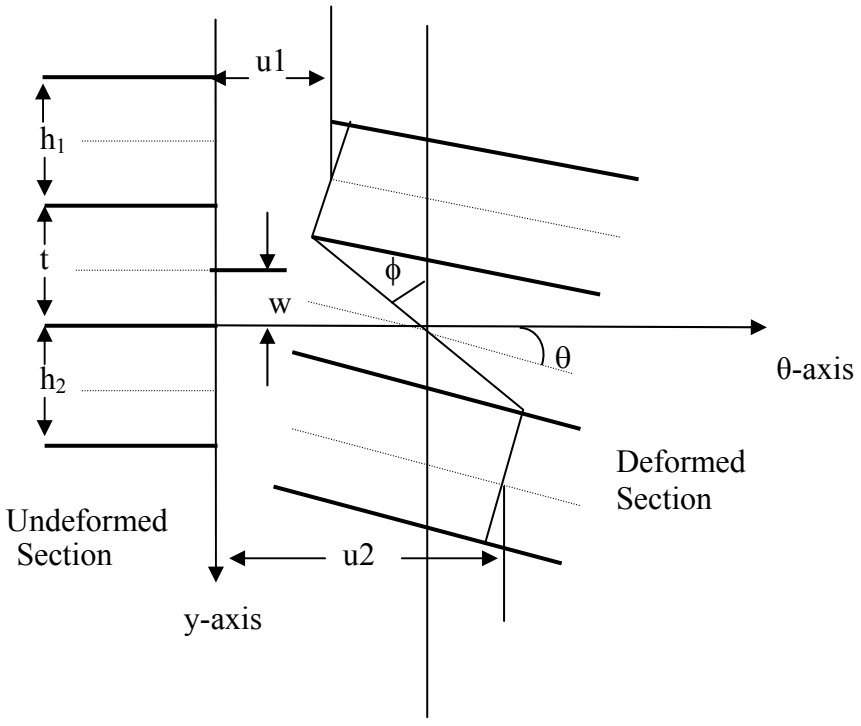

Figure 2.2 Deformed and undeformed sections of laminated glass unit

Shear strain for the interlayer is:

$$\gamma_I = \frac{u1 - u2 - \left(\frac{1}{r_1}\frac{h_1}{2} + \frac{1}{r_2}\frac{h_2}{2} + \frac{t}{r_1}\right)\frac{dw}{d\theta}}{t}$$

Therefore the total potential energy of the system in extended form is:

$$\Pi = \sum_{i=1}^{2} \left\{ \int_V \tfrac{1}{2} E\left(\frac{ui_\theta + w}{r_i} + \frac{1}{2}\left(\frac{w_\theta}{r_i} \right)^2 \right)^2 dV + \int_V \tfrac{1}{2} E\left(-z \frac{w_{\theta\theta}}{r_i^2} \right)^2 dV \right\}$$
$$+ \int_V \tfrac{1}{2} G\left(\frac{u1 - u2 - \left(\frac{1}{r_1}\frac{h_1}{2} + \frac{1}{r_2}\frac{h_2}{2} + \frac{t}{r_1} \right)\frac{dw}{d\theta}}{t} \right)^2 dV - \int_0^s qwds \tag{2.3}$$

Variation of total potential energy Π with respect to radial displacement, w, and circumferential displacements, u_1 and u_2, gives following stationary equations.

$$\delta\Pi[u1] = 0$$

$$\delta\Pi[u2] = 0$$

$$\delta\Pi[w] = 0$$

Therefore, three nonlinear coupled differential equations and boundary conditions for a laminated glass curved beam are obtained:

$$\frac{d}{d\theta^2}\left(EI\frac{d^2w}{d\theta^2} \right) - \frac{d}{d\theta}\left(\left(\frac{N1}{r_1} + \frac{N2}{r_2} \right)\frac{dw}{d\theta} \right) + (N1 + N2) +$$
$$Gbr_1\left(\frac{1}{r_1}\frac{h_1}{2} + \frac{1}{r_2}\frac{h_2}{2} + \frac{t}{r_1} \right)\frac{d\gamma_1}{d\theta} - qr_1 = 0 \tag{2.4}$$

$$\frac{dN1}{d\theta} - Gbr_1\gamma_1 = 0 \tag{2.5}$$

$$\frac{dN2}{d\theta} + Gbr_1\gamma_1 = 0 \tag{2.6}$$

in which

$$N1 = EA_1\left(\frac{u1_\theta + w}{r_1} + \frac{1}{2r_1^2} w_\theta^{\,2}\right) \tag{2.7}$$

$$N2 = EA_2\left(\frac{u2_\theta + w}{r_2} + \frac{1}{2r_2^2} w_\theta^{2}\right) \tag{2.8}$$

$I = I_1 + I_2$ in which $I_1 = \frac{bh_1^3}{12r_1^3}$, $I_2 = \frac{bh_2^3}{12r_2^3}$;

where N_1 and N_2 are the outer and inner circumferential forces in glass arches, respectively. γ_1 is the shear strain in the interlayer; G is the shear modulus of interlayer; E is the elasticity modulus of glass; h_1 and h_2 are the thicknesses of outer and inner glass arches; A_1 and A_2 are the cross section areas of outer and inner glass arches, respectively; b is the width of the unit; q is a uniformly distributed load; and I is the moment of inertia of the glass arches.

The governing equations (2.4) to (2.6) in terms of displacements are:

$$\begin{aligned}
&EI\frac{d^4 w}{d\theta^4} - \frac{Gbr_1}{t}\left(\frac{1}{r_1}\frac{h_1}{2} + \frac{1}{r_2}\frac{h_2}{2} + \frac{t}{r_1}\right)^2 (w_{\theta\theta}) = qr_1 + \\
&\frac{EA_1}{r_1}\left(\frac{u1_{\theta\theta} + w_\theta}{r_1} + \frac{w_{\theta\theta} w_\theta}{r_1^2}\right) w_\theta + \frac{EA_1}{r_1}\left(\frac{u1_\theta + w}{r_1} + \frac{w_\theta^2}{2r_1^2}\right)(w_{\theta\theta} - 1) \\
&+ \frac{EA_2}{r_2}\left(\frac{u2_{\theta\theta} + w_\theta}{r_2} + \frac{w_{\theta\theta} w_\theta}{r_2^2}\right) w_\theta + \frac{EA_2}{r_2}\left(\frac{u2_\theta + w}{r_2} + \frac{w_\theta^2}{2r_2^2}\right)(w_{\theta\theta} - 1) \\
&- \frac{Gbr_1}{t}\left(\frac{1}{r_1}\frac{h_1}{2} + \frac{1}{r_2}\frac{h_2}{2} + \frac{t}{r_1}\right)\left(\frac{du1}{d\theta} - \frac{du2}{d\theta}\right)
\end{aligned} \tag{2.9}$$

$$\begin{aligned}
&\frac{EA_1}{r_1}(u1_{\theta\theta}) - \frac{Gbr_1}{t} u1 = \frac{EA_1}{r_1}(w_\theta)(1 + \frac{1}{r_1} w_{\theta\theta}) \\
&+ \frac{Gbr_1}{t}\left(-u2 - \left(\frac{1}{r_1}\frac{h_1}{2} + \frac{1}{r_2}\frac{h_2}{2} + \frac{t}{r_1}\right)\frac{dw}{d\theta}\right)
\end{aligned} \tag{2.10}$$

$$\frac{EA_2}{r_2}(u1_{\theta\theta}) - \frac{Gbr_1}{t}u2 = \frac{EA_2}{r_2}(w_\theta)(1 + \frac{1}{r_2}w_{\theta\theta})$$
$$-\frac{Gbr_1}{t}\left(u1 - \left(\frac{1}{r_1}\frac{h_1}{2} + \frac{1}{r_2}\frac{h_2}{2} + \frac{t}{r_1}\right)\frac{dw}{d\theta}\right) \quad (2.11)$$

Boundary equations of curved beam could be obtained as follows:

At $\theta = \theta_1$ and $\theta = \theta_2$ (at supports of curved unit) for Equation (2.4)

$$-\frac{d}{d\theta}\left(EI\frac{d^2w}{d\theta^2}\right) + (N1 + N2)\frac{dw}{d\theta}$$
$$-\frac{Gbr_1}{t}\left(\frac{1}{r_1}\frac{h_1}{2} + \frac{1}{r_2}\frac{h_2}{2} + \frac{t}{r_1}\right)\left[u1 - u2 - \left(\frac{1}{r_1}\frac{h_1}{2} + \frac{1}{r_2}\frac{h_2}{2} + \frac{t}{r_1}\right)\frac{dw}{d\theta}\right] = \tilde{V}$$

or radial deflection w is prescribed,

$-EI\frac{d^2w}{d\theta^2} = \tilde{M}$ or $\frac{dw}{d\theta}$ is prescribed,

for Eqs. (2.5) and (2.6)

$\frac{EA_1}{r_1}\left(\frac{u1_\theta + w}{r_1} + \frac{w_\theta^2}{2r_1^2}\right) = \tilde{N1}$ or $u1$ is prescribed and

$\frac{EA_2}{r_2}\left(\frac{u2_\theta + w}{r_2} + \frac{w_\theta^2}{2r_2^2}\right) = \tilde{N2}$ or $u2$ is prescribed;

where $\tilde{V}$ is the applied shear force, $\tilde{M}$ is the applied moment and $\tilde{N1}$, $\tilde{N2}$ are the applied axial forces for outer and inner glass arches, respectively.

For a simply supported laminated curved glass beam without applied forces at the ends, as a special case, boundary conditions take the following form:

at $\theta = \theta_1$ and $\theta = \theta_2$ (at the supports): $w = 0$ and $\frac{d^2w}{d\theta^2} = 0$

$u1 = 0$ and $u2 = 0$

For a fixed supported laminated curved glass beam without applied forces at the ends, as a special case, boundary conditions take the following form:

at $\theta = \theta_1$ and $\theta = \theta_2$ (at the supports): $w = 0$ and $\frac{dw}{d\theta} = 0$

$u1 = 0$ and $u2 = 0$

Analytic solution of three governing nonlinear differential equations (2.9)-(2.11) is difficult. Therefore, the numerical Finite Difference Method (FDM) is used to solve the governing equations (2.9)-(2.11). The solution procedure given by Asik [24] is modified for a curved beam. The nonlinear differential equations are converted into algebraic equations by using central finite difference method and written in matrix form. All nonlinear terms in the equations are placed on the right hand side. Then, governing equations become:

$$[\mathrm{A}]\{\mathrm{w}\} = \underline{\mathrm{R}} \tag{2.12}$$

where $\underline{\mathrm{A}}$ is a qui-diagonal matrix, and only the elements belonging to five diagonals are stored as vectors. The right hand side vector, $\underline{R}$ includes applied load and other terms are calculated at every discrete point on the right hand side of Equation (2.9). Iterative procedure is employed since the equations are coupled and nonlinear. The equations are modified at the boundaries of the unit. Applied load is considered in small increments for convergence, where:

$\{w\}$ = the radial displacement vector,

[A]=coefficient matrice for radial displacement.

For the radial deflection, the finite difference mesh size is chosen to be $\Delta\theta$, n is the number of subdivisions in the θ directions. In order to reduce the total number of equations the radial deflection values at the fixed supported edges which are zero, are not incorporated. Central finite difference expression of the field equation for the radial deflection in the domain is:

$$Aw_{i-2} + Bw_{i-1} + Cw_{i} + Dw_{i+1} + Ew_{i+2} = RHS_{i}, \tag{2.14}$$

for i=1, 2,…, n-1.

where

$A=E=1,$

$$B = D = -4 - \frac{Gbr_1}{EIt}\left(\frac{1}{r_1}\frac{h_1}{2} + \frac{1}{r_2}\frac{h_2}{2} + \frac{t}{r_1}\right)^2 (\Delta\theta)^2 ,$$

$$C = 6 + \frac{(\Delta\theta)^4}{EI}\left(\frac{Ebh_1}{r_1} + \frac{Ebh_1}{r_1}\right) + 2\frac{Gbr_1}{EIt}\left(\frac{1}{r_1}\frac{h_1}{2} + \frac{1}{r_2}\frac{h_2}{2} + \frac{t}{r_1}\right)^2 (\Delta\theta)^2 ,$$

$$RHS = \frac{EA_2}{r_1} w_\theta \left(\frac{u1_{\theta\theta} + w_\theta}{r_1} + \frac{w_{\theta\theta} w_\theta}{r_1^2}\right) + \frac{EA_1}{r_1}\left(\frac{u1_\theta + w}{r_1} + \frac{w_\theta^2}{2r_1^2}\right)(w_{\theta\theta} - 1)$$

$$+ \frac{EA_2}{r_2} w_\theta \left(\frac{u2_{\theta\theta} + w_\theta}{r_2} + \frac{w_{\theta\theta} w_\theta}{r_2^2}\right) + \frac{EA_2}{r_2}\left(\frac{u2_\theta + w}{r_2} + \frac{w_\theta^2}{2r_2^2}\right)(w_{\theta\theta} - 1)$$

$$- \frac{Gbr_1}{t}\left(\frac{1}{r_1}\frac{h_1}{2} + \frac{1}{r_2}\frac{h_2}{2} + \frac{t}{r_1}\right)\left(\frac{du1}{d\theta} - \frac{du2}{d\theta}\right) + qr_1$$

Steps of iterative solution procedure for every load increment can be written as:

1) assume $\underline{w}$, $\underline{u1}$, $\underline{u2}$,

2) calculate $\underline{R}$,

3) obtain w(i) from Eq. (2.14),

4) w(i)= α w(i)+(1- α)wo(i),

5) if $\dfrac{\sum_i |w(i) - wo(i)|}{(num * w_{\max})} \le tol$ then stop,

6) calculate the right hand side of the Eq. (2.10) and obtain $u1$,

7) calculate the right hand side of the Eq. (2.11) and obtain $u2$,

8) go to step 2,

In this iterative procedure α is the variable under relaxation parameter. It is calculated by interpolation regarding the nondimensional maximum deflection 2*w(max)/(h_1+h_2) as a result of numerical experiment, and wo(i) is the radial deflection calculated in the previous step.

2.3 Numerical tests for the optimized number of divisions and tolerance

In the solution procedure, number of divisions and tolerance are very important. For this reason, first numerical test is carried out to determine the number of divisions n along the unit and tolerance which gives good approximation. Laminated glass model, shown in Figure 2.1 with the physical properties given in Table 2.1, is used to analyze number of divisions and tolerance. Results are presented in Figures 2.3 and 2.4. It is observed from Figure 2.3 that there is a big difference between the results of different tolerance values. The displacement value, which is obtained for 1E-4 tolerance value, is more than 3 times of that 1E-3 tolerance value. Displacements are getting closer to each other while the tolerance values are getting smaller. From the figures, it is observed that results obtained with 5000 and 10000 divisions and results obtained with 1E-6 and 1E-7 tolerances are very close to each other. It is decided that 5000 divisions and 1E-7 tolerance are sufficient to obtain a good approximation. Therefore, 5000 divisions and 1E-7 tolerance are used in all calculations. As shown in Figure 2.5 unlike curved beam the displacements for different tolerance values are almost the same for straight laminated glass beam.

Table 2.1 Physical properties of laminated glass curved beam

	Dimensions (mm)				Modulus	
	Thickness	Width	Radius	Arc Length	E	G
Glass 1	5	100	1000	3140	72 GPa	28.8 GPa
PVB	0.76	100	997.12	3140	3000 kPa	1000 kPa
Glass 2	5	100	994.24	3140	72 GPa	28.8 GPa

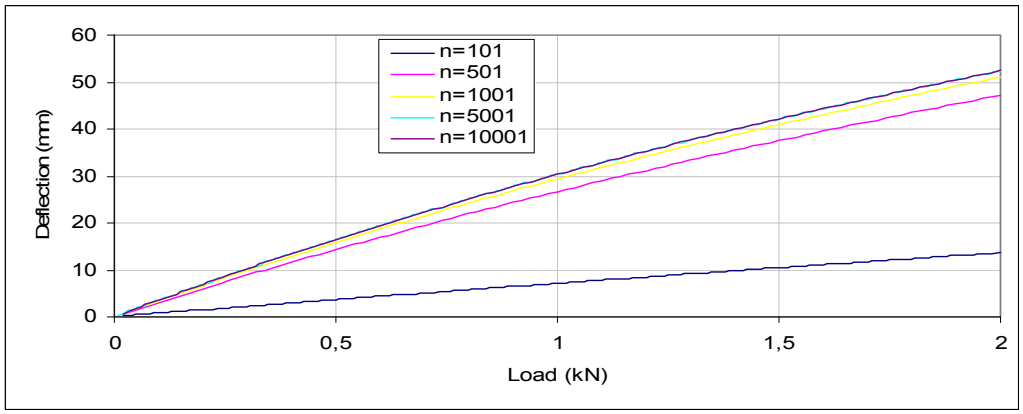

Figure 2.3 Deflection versus load for laminated glass curved beam

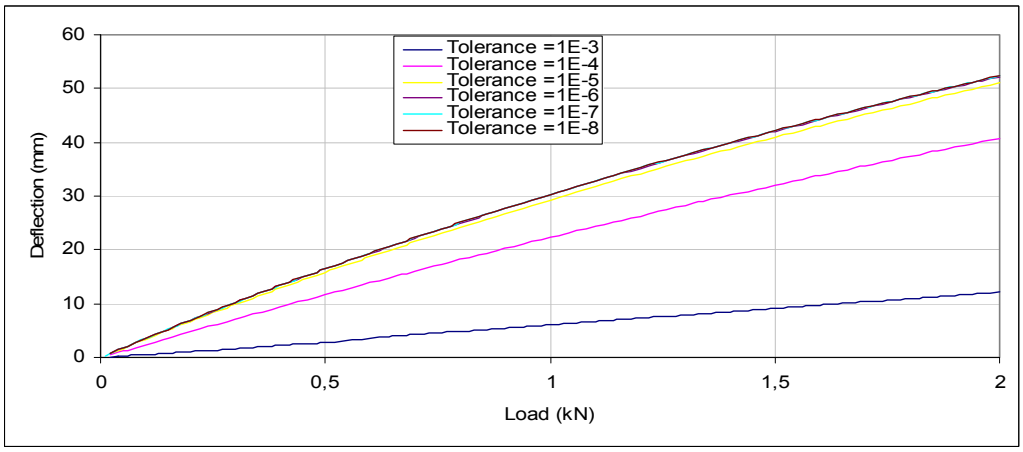

Figure 2.4 Displacement versus load for laminated glass curved beam for different tolerances

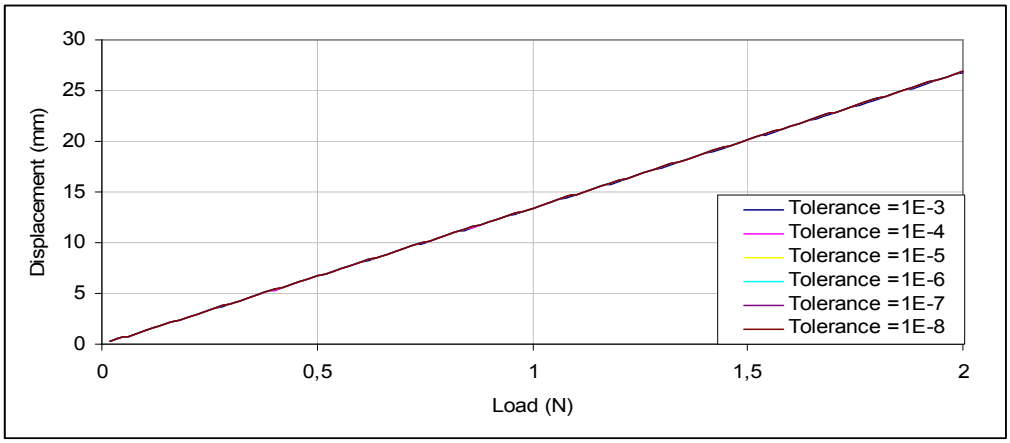

Figure 2.5 Displacement versus load for laminated glass straight beam for different tolerances

2.4 Experimental technique and verification of the model for the curved beam

2.4.1 Finite Element Investigation

In order to verify the developed mathematical model, results are compared with those of the finite element model for fixed end conditions. The two-dimensional model developed for the finite element method is developed and solved with ABAQUS version 6.7-1. Load is concentrated at midspan. Eight node plane stress element (CPS8R) is used in meshing since it gives more accurate results where large deformations are involved and leads to faster convergence. The dimensions of the laminated glass model are 1m outer glass radius, 100 mm width and 5+0.76+5 mm thickness. The physical properties of laminated glass curved beam are given in Table 2.1. To achieve perfect bound between the layers the surfaces constrained to each other by using tie option. The Young's modulus and Poisson's ratio of glass are taken to be 72 GPa and 0.25, respectively; but the shear modulus and Poisson's ratio of the interlayer are taken as 1000 kPa and 0.29, respectively. To achieve the fixed end boundary condition for the model, vertical and horizontal degrees of freedom of all the nodes at both ends of the beams are set to zero. Large deformation analysis is performed by using nonlinear geometry.

A comparison of the deflections and stresses for laminated fixed supported beam are presented in Table 2.2 and Figures 2.6 and 2.7. It is observed from Figure 2.6 that there is almost no difference between the central deflections of the present and finite element model; maximum error (difference) is about 4.68 %. Comparison of stresses is presented in Figure 2.7. It is observed Figure 2.7 that the stresses in the finite element model are higher than those in the model; however, this difference is 3.77% at most. Therefore, the model developed to analyze the laminated glass beams gives reliable results for the fixed supported laminated glass curved beams showing nonlinear behavior.

Table 2.2 Comparison of the results for the fixed supported laminated curved beam

	Displacement (mm)			Maximum Stress (MPa)		
Point Load (N)	FEM	Model	% Error	FEM	Model	% Error
0	0.00	0.00	0.00	0.00	0.00	0.00
100	3.06	2.94	3.79	12.86	12.64	1.74
200	6.02	5.78	3.88	25.92	25.07	3.28
300	8.89	8.54	3.95	38.07	37.31	2.00
400	11.67	11.20	4.05	50.44	49.36	2.14
500	14.36	13.78	4.06	62.66	61.23	2.28
600	16.98	16.28	4.15	74.73	72.93	2.41
700	19.52	18.70	4.21	86.66	84.46	2.54
800	21.99	21.05	4.28	98.40	95.83	2.61
900	24.38	23.33	4.31	110.10	107.04	2.78
1000	26.71	25.54	4.36	121.60	118.11	2.87
1100	28.97	27.70	4.40	133.00	129.02	2.99
1200	31.17	29.79	4.44	144.30	139.80	3.12
1300	33.31	31.82	4.47	155.40	150.44	3.19
1400	35.40	33.80	4.52	166.40	160.95	3.28
1500	37.43	35.72	4.56	177.30	171.33	3.37
1600	39.40	37.60	4.58	188.10	181.58	3.47
1700	41.33	39.42	4.62	198.80	191.71	3.56
1800	43.20	41.20	4.63	209.40	201.73	3.66
1900	45.03	42.93	4.66	219.90	211.63	3.76
2000	46.81	44.62	4.68	230.10	221.43	3.77

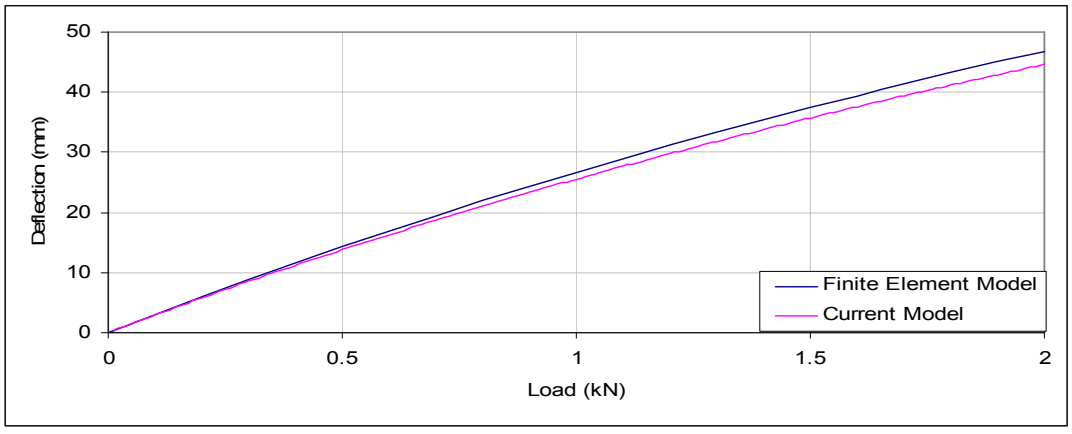

Figure 2.6 Central deflection values in the fixed supported laminated glass curved beam

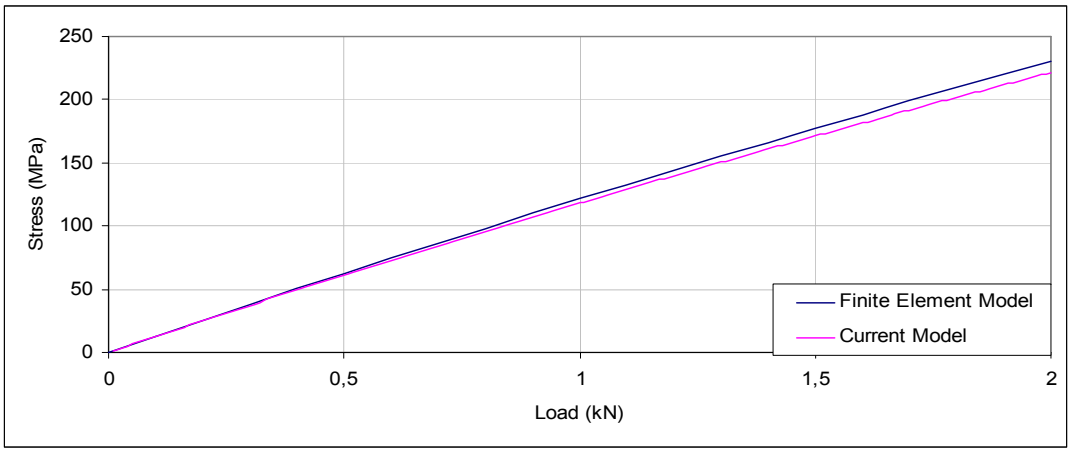

Figure 2.7 Maximum stress values in the fixed supported laminated glass curved beam

While comparison of deflection values for monolithic simply supported beam are presented in Figure 2.8, comparison of the resulting deflections and stresses for laminated simply supported beam, which are obtained by finite element method and current model, are presented in Table 2.3, Figures 2.9 and 2.10. It is observed from Figure 2.9 that there is almost no difference between the central deflections; maximum error (difference) is about 2.18 %. Comparison of stresses is presented in Figure 2.10 and the error percentage is about 6.26% at most. Therefore, the model developed to analyze the curved laminated glass beams gives reliable results for the simply supported laminated case, too. It is observed from figures that behavior of laminated curved beam is not linear.

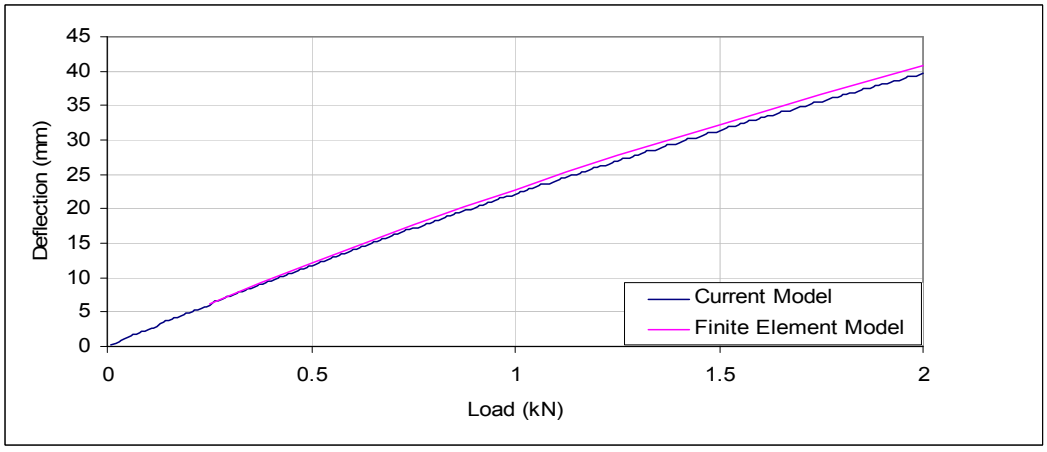

Figure 2.8 Central deflection values in the monolithic simply supported curved beam

Table 2.3 Comparison of results for the laminated simply supported curved beam

	Displacement (mm)			Maximum Stress (MPa)		
Point Load (N)	FEM	Model	% Error	FEM	Model	% Error
0	0.00	0.00	0.00	0.00	0.00	0.00
100	3.48	3.53	-1.66	14.08	13.40	4.81
200	6.83	6.94	-1.55	27.94	26.58	4.88
400	13.52	13.40	0.92	55.04	52.28	5.01
500	16.32	16.46	-0.84	68.30	64.83	5.09
600	19.29	19.42	-0.65	81.38	77.18	5.16
800	24.98	25.04	-0.26	107.00	101.33	5.30
1000	30.37	30.32	0.17	132.00	124.78	5.47
1200	35.48	35.27	0.60	156.40	147.59	5.63
1400	40.33	39.92	1.01	180.20	169.79	5.78
1500	42.66	42.15	1.20	191.90	180.68	5.85
1600	44.94	44.31	1.40	203.50	191.43	5.93
1800	49.34	48.45	1.80	226.30	212.53	6.08
2000	53.53	52.36	2.18	248.70	233.13	6.26

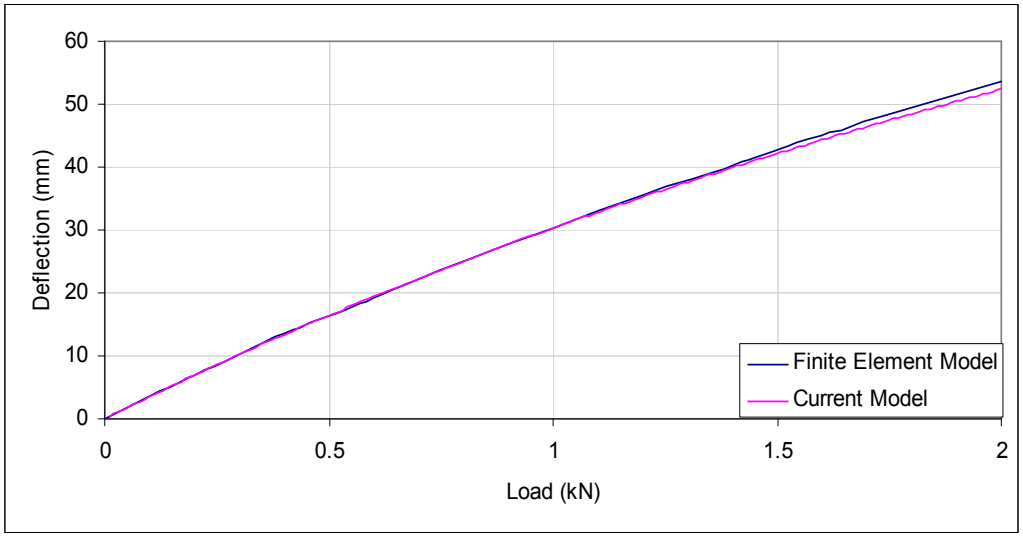

Figure 2.9 Central deflection values in the laminated simply supported curved beam

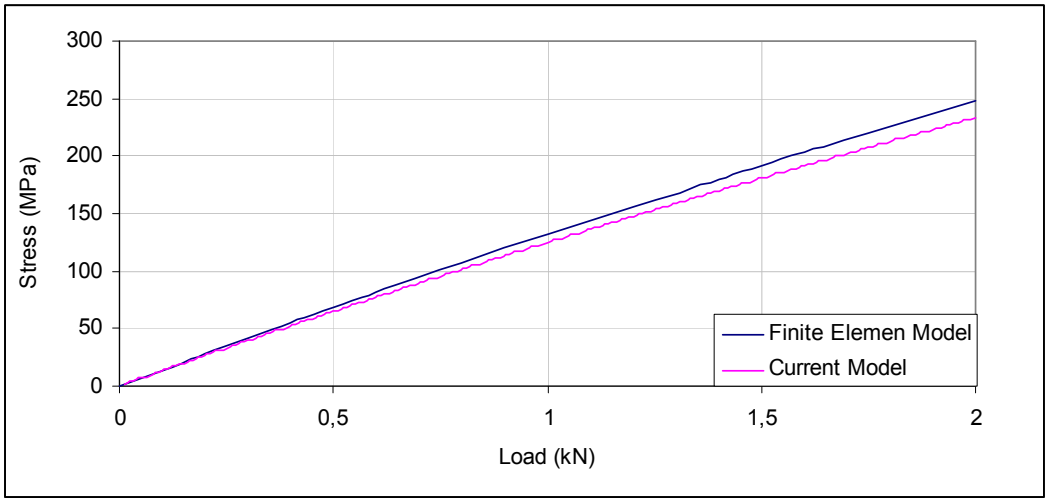

Figure 2.10 Maximum stress values in the laminated simply supported curved beam

Deformed and undeformed shapes of ABAQUS model are illustrated in Figure 2.11. While the radial displacements are stretching out near the center, they are stretching in near the boundaries of the beam. A view of meshed model is illustrated in Figure 2.12. The effect of shear is observable for PVB interlayer from Figure 2.12.

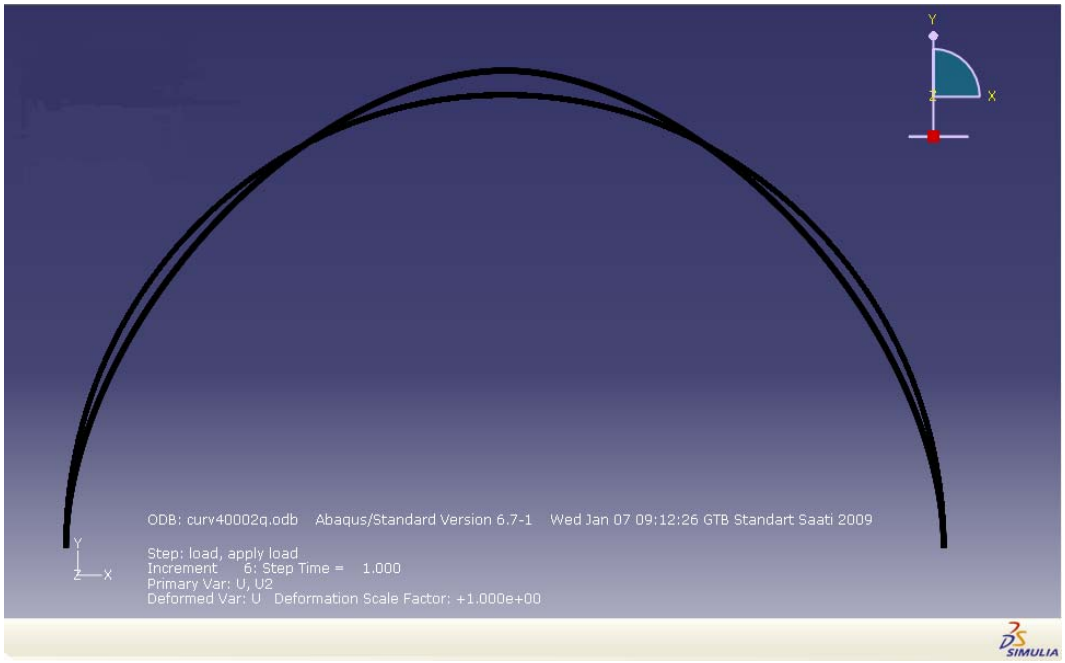

Figure 2.11 Deformed and undeformed shapes of the beam

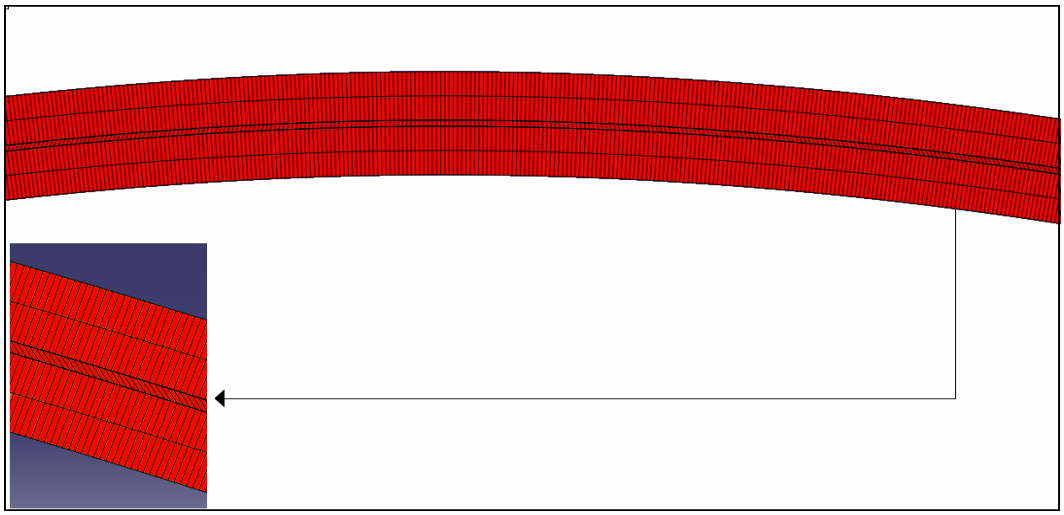

Figure 2.12 A view of meshed finite element model

2.4.2 Experimental Investigation

Uzhan (2010) conducted experiments on curved laminated glass with glass thickness 5+5 mm, PVB thickness of 1.52 mm, outer glass radius of 1000 mm, inner glass radius of 993.48 mm and interlayer radius of 996.74 mm. He conducted experiments on 7 test specimens with physical properties given in Table 2.4. The dimensions of test specimen shown in Figure 2.13 are 680 mm in length with 700 mm arc length, 10 cm width. He applied different forces to the specimens. The experiments were conducted at 22-23 degrees Celsius. The Young's modulus of glass and shear modulus of interlayer PVB are taken to be 70 GPa and 1000 kPa, respectively. To collect data for every load value he used strain gages, material testing machine and data logger. To apply quasi simply supported boundary conditions he left 6 cm from both sides free. Radial degrees of freedom of all nodes of the boundaries are set as zero while circumferential deflection and rotation are set to free at the boundaries. So the boundary conditions can be expressed as:

Table 2.4 Physical properties of laminated glass unit

	Dimensions (mm)				Modulus	
	Thickness	Width	Radius	Arc Length	E	G
Glass 1	5	100	1000	700	70 GPa	28.8 GPa
PVB	1.52	100	996.74	700	3000 kPa	1000 kPa
Glass 2	5	100	993.48	700	70 GPa	28.8 GPa

at $\theta = \theta_1$ and $\theta = \theta_2$ (at the supports): $w = 0$ and $\dfrac{d^2 w}{d\theta^2} = 0$

$$\tilde{N}1 = 0 \text{ and } \tilde{N}2 = 0$$

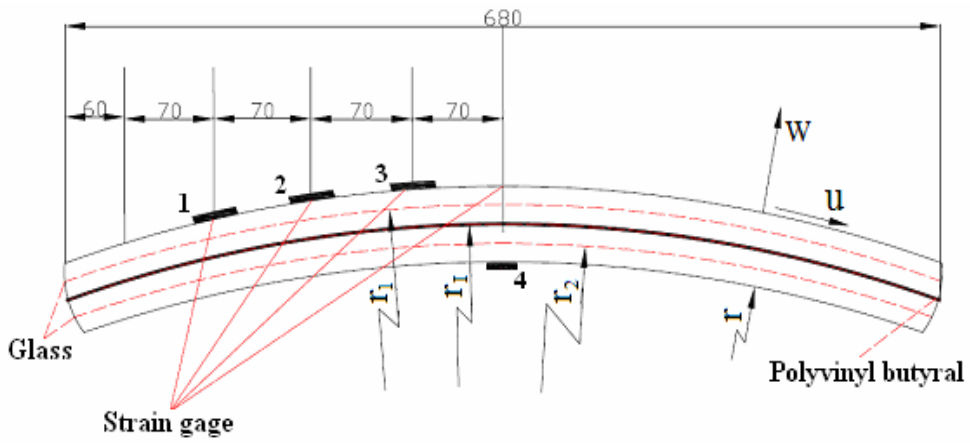

Figure 2.13 Laminated glass beam (Dimensions in mm)

To verify the performance of current model the results are compared with the experimental results conducted by Uzhan at the Experimental Mechanics Laboratory in the Department of Engineering Sciences at Middle East Technical University. Comparison of the maximum stress, which are obtained from the experiment and current model, are presented in Table 2.5 and Figure 2.14. It is observed from Table 2.5 and Figure 2.14 that the differences in stress values between the experiment and mathematical model are not more than 2%.

Table 2.5 Comparison of central maximum stresses for experimental and mathematical model results

Load (N)	Maximum Stress(MPa)			
	Experiment	Model	Std. Dev.	Error (%)
0	0	0	0	0
50	7.37	7.27	0.04	1.36
100	14.84	14.55	0.31	1.95
150	22.17	21.82	0.2	1.58
200	29.45	29.11	0.36	1.15
250	36.33	36.39	0.99	-0.17
300	44.03	43.68	0.62	0.79
350	50.33	50.97	1.92	-1.27
400	59.8	58.27	0.89	2.56
450	66.62	65.56	1.03	1.59
500	73.9	72.87	0.95	1.39

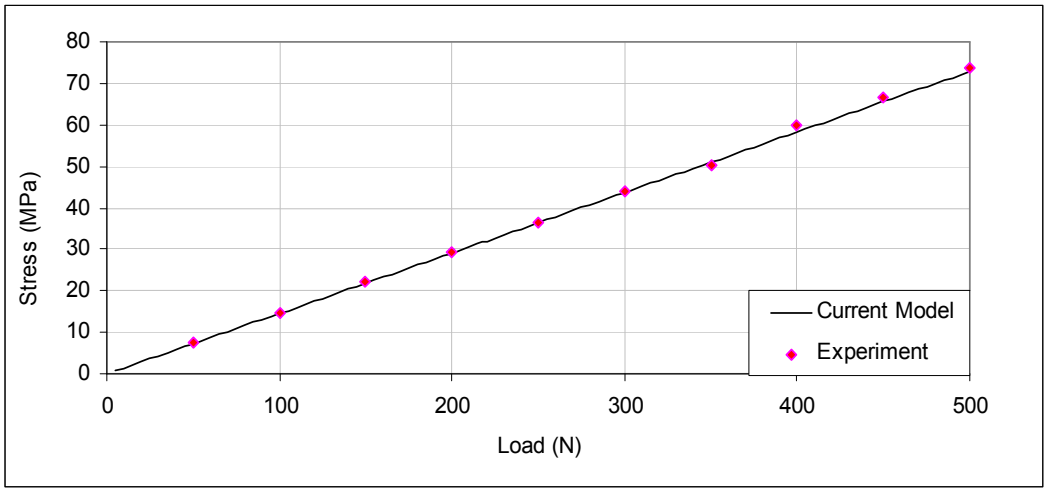

Figure 2.14 Comparison of the stresses at the center and on the bottom surface of the laminated glass curved beam. (Strain gage 4)

2.5 Numerical Results

Geometric and material properties of the unit shown in Figure 2.1 are given as r_1=1 m, θ=3.14, width of unit b=0.1 m, h_1=h_2=5 mm, interlayer thickness t=0.76 mm, E=72x10^6 kPa, G=500 and 1000 kPa. Concentrated load P=2 kN is assumed at the mid point of the outer glass arch. Load is applied in increments of 0.002 kN to have a convergent sequence. Variable SOR parameter is very helpful to have a convergent solution. Radial displacement w is interpolated by using SOR parameter α which changes with the ratio of $\frac{w_{max}}{h}$.

2.5.1 Simply Supported Curved Beam

Boundary conditions of a simply supported curved beam are given as follows. Figure 2.15 presents the pictorial presentation of simply supported curved beam.

At $\theta = \theta_1$ and $\theta = \theta_2$ (at the supports): $w = 0$ and $\frac{d^2w}{d\theta^2} = 0$

$u1 = 0$ and $u2 = 0$

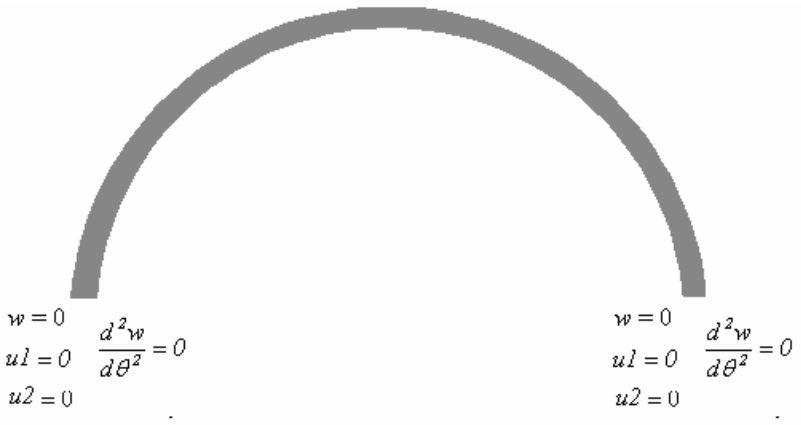

Figure 2.15 Pictorial presentation of boundary conditions for the simply supported curved beam

Figure 2.16 shows the comparison of linear and nonlinear approach to predict the behavior of the simply supported laminated glass beam. Linear and nonlinear

solution results are plotted as normalized deflection versus load. The level of nonlinearity may be defined as the $\frac{w_{max}}{h}$ ratio, where w_{max} is the deflection at the center of a beam, and h is the thickness of the single glass beam. Separation between linear and nonlinear solutions starts when $\frac{w_{max}}{h}$ is about 2.0. It can be said that nonlinear solution should be considered when the ratio of maximum deflection to thickness of a single glass beam is greater than 2.0. It is observed that this ratio (the level of nonlinearity) is about 10.4 for a load P=2 kN in Figure 2.16. The central deflection obtained from linear approach is almost one and a half times of the deflection obtained by nonlinear approach at load P=2 kN.

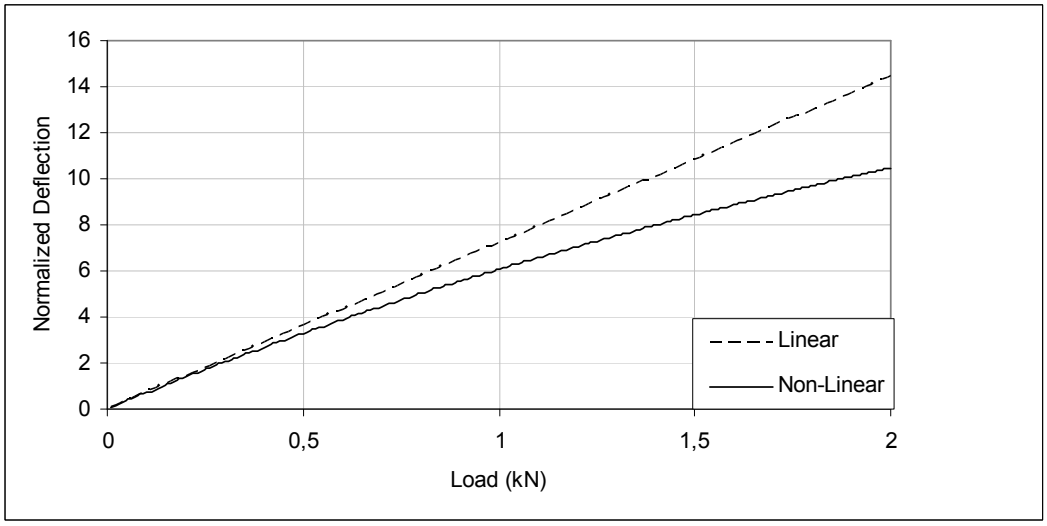

Figure 2.16 Normalized maximum deflection ($\frac{w_{max}}{h}$) versus load for the simply supported beam

Figures 2.17 and 2.18 are plotted to compare the behavior of simply supported laminated glass curved beam with those of monolithic glass arch having thickness of 10 mm and layered glass curved beam consisting of two glass layers with the thickness of 5 mm each and having no bonding between the glass layers. The developed model is able to predict the behavior of monolithic, layered and laminated curved glass beams. Two laminated glass units with the PVB having shear modulus

of 500 and 1000 kPa are considered to have an idea about PVB's effect on the behavior of laminated glass unit. Figures 2.17 and 2.18 are showing deflection and maximum stress versus load, respectively. The behavior of laminated glass beam is close to the behavior of monolithic glass beam as can be seen in Figures 2.17 and 2.18. Their behavior is bounded by two limiting cases, which are monolithic and layered behavior. As the shear modulus of PVB interlayer gets smaller, the behavior of laminated glass gets closer to the behavior of layered glass unit. Deflection of curved laminated glass, which has 1000 kPa interlayer shear modulus, is nearly half of that layered unit.

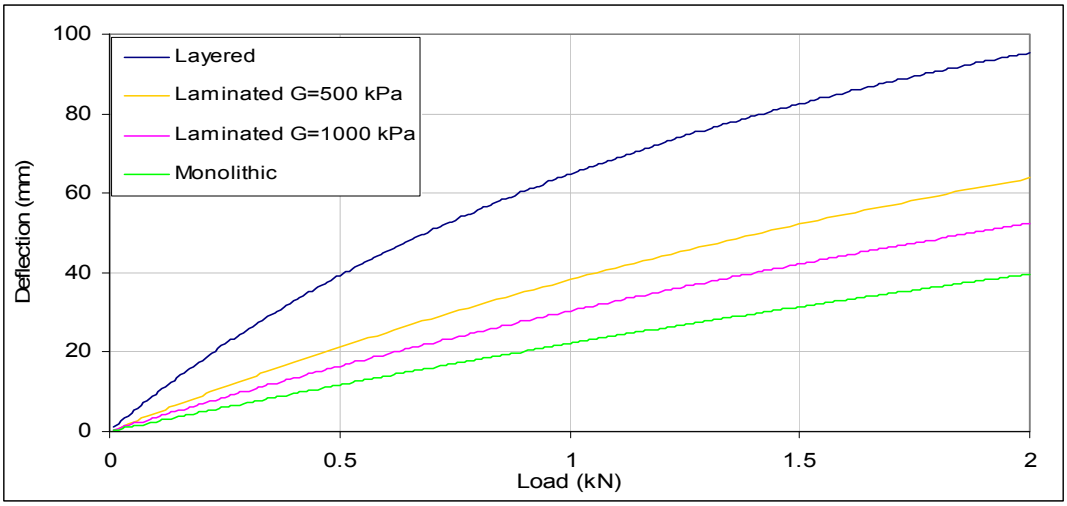

Figure 2.17 Maximum displacement versus load

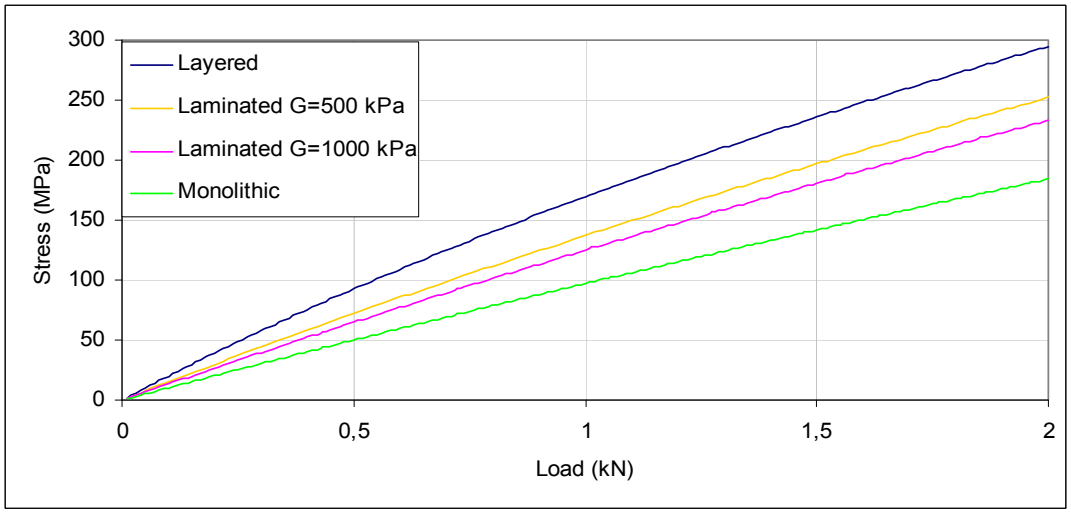

Figure 2.18 Maximum stresses versus load

Figures 2.19 to 2.22 are plotted to observe the behavior along the arc length of the laminated glass curved beam. While circumferential displacements of the top and bottom glass unit along the arc length of the beam for different load values are given in Figure 2.19 and 2.20, respectively, radial displacements along the beam for different load values are presented in Figure 2.21. From Figures 2.19 and 2.20 it is observed that circumferential deflections at the center and at the ends of the arch are zero. While circumferential deflections are in positive direction at the left hand side of the beam, they are in negative direction at the right hand side of the arch. As expected, maximum radial deflection is at the center of the unit and at the boundaries of the unit radial deflection is zero because of the boundary conditions.

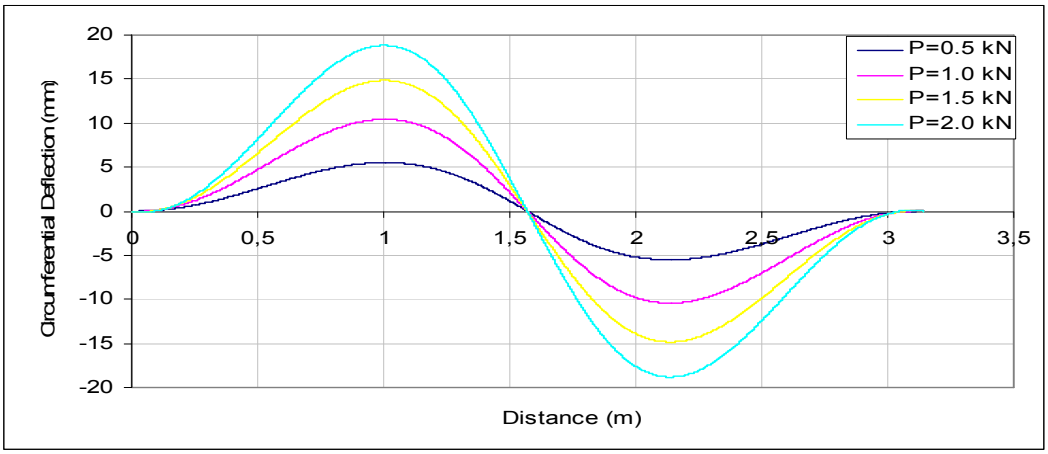

Figure 2.19 Circumferential displacement (u1) of the top glass along the arc length of the beam

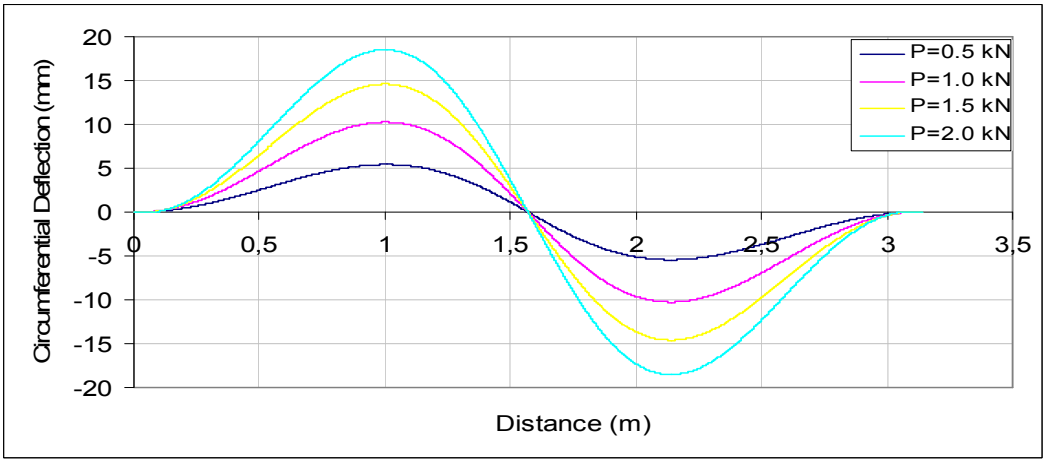

Figure 2.20 Circumferential displacement (u2) of the bottom glass along the arc length of the beam

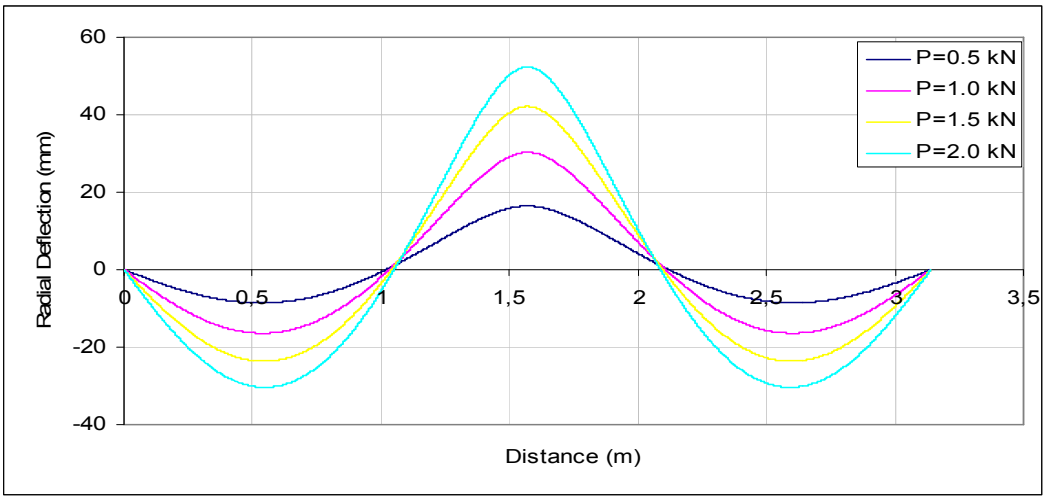

Figure 2.21 Radial displacements for different load values

Figure 2.22 is plotted to compare the radial displacement of laminated, monolithic and layered glass unit at load P=2 kN. Behavior of laminated glass is close to the behavior of monolithic unit. The maximum value of radial deflection of layered glass unit is 1.82 times of deflection of laminated glass unit. The sign of circumferential and radial deflections along the arc length of beam are changing as seen in figures because of double curvature occurrence when load is applied since beam has initial curvature.

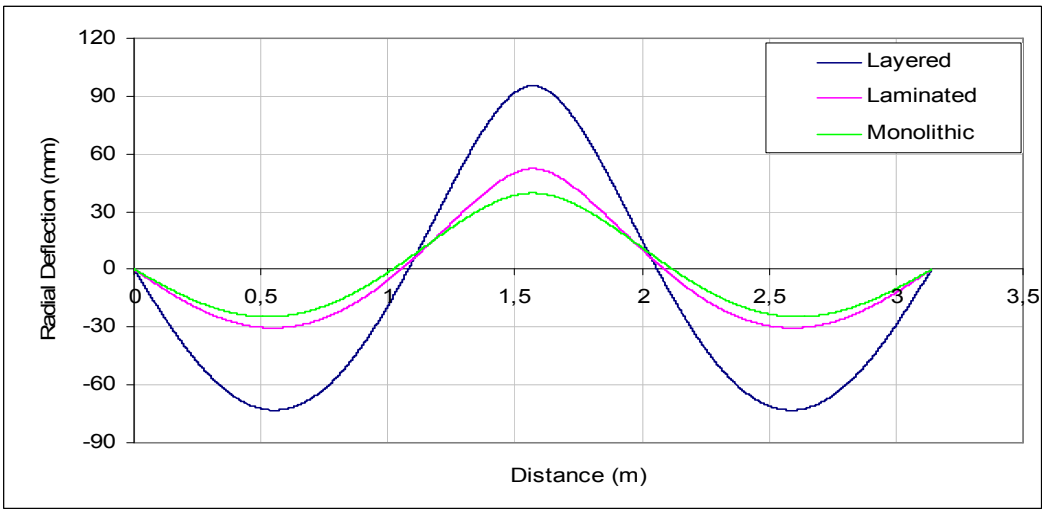

Figure 2.22 Displacements along the arc length of simply supported beam at load P=2 kN

The term $Gbr_I\gamma$ in Equations 2.5 and 2.6 represents the distributed load between the two plies in circumferential direction. The shear strain is contributed by the PVB interlayer. Because of the applied shear strain relative rotation and motion in plane direction occurs in glass plies. When shear strain is applied to the interlayer, between the glass plies, a distributed force is transmitted to the top and bottom glass plies in opposite directions.

If we integrate Equation 2.5

$$\frac{dN1}{d\theta} - Gbr_I\gamma_I = 0$$

$$N1 = \int Gbr_I\gamma(\theta)d\theta = \int G\gamma(\theta)dA = \int \tau dA$$

Thus, the in-plane force of glass plies obtained by integrating shear stress along the area. Function of shear stress along the arc length of the simply supported curved beam beam is plotted in Figure 2.23 for the applied loads. Shear stresses take their maximum value at the supports and zero at the middle of the beam as observed from the figure. Shear stresses change their sign at every quarter of the beam arc length.

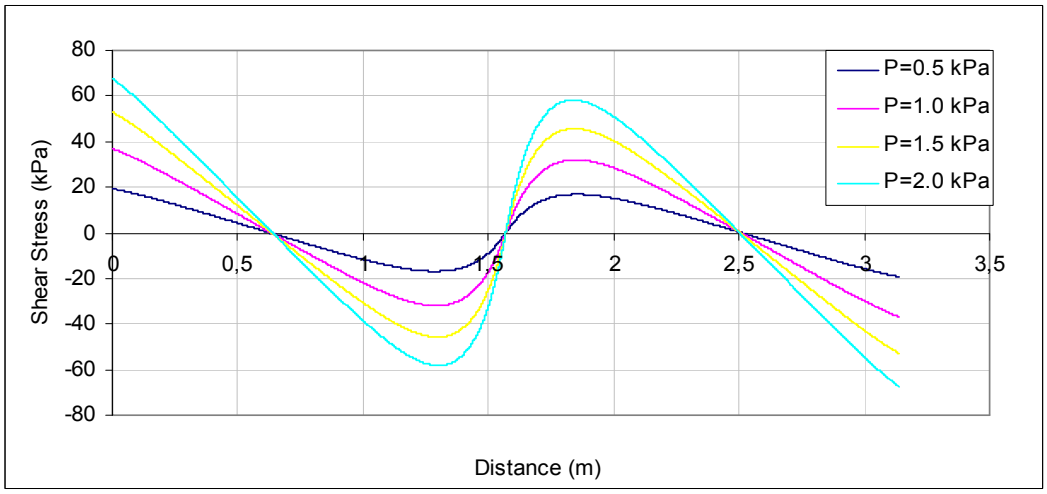

Figure 2.23 Variation of shear stress along the arc length of the beam

The stresses at surfaces of the plies are obtained by combination of membrane and bending stresses.

$$\sigma_I^{top} = \frac{M}{I}\frac{h_I}{2} + \frac{N1}{A_I}$$

$$\sigma_1^{bot} = -\frac{M}{I}\frac{h_1}{2} + \frac{N1}{A_1}$$

$$\sigma_2^{top} = \frac{M}{I}\frac{h_2}{2} + \frac{N2}{A_2}$$

$$\sigma_2^{bot} = -\frac{M}{I}\frac{h_2}{2} + \frac{N2}{A_2}$$

Bending and membrane stresses at the center of curved beam on each surface of glass plies are illustrated in Figures 2.24-2.27. Membrane stress is smaller than bending stress as seen in the following figures. While membrane and bending stress on the top surface of the top glass are tension, they are compression on the bottom surface of the bottom glass.

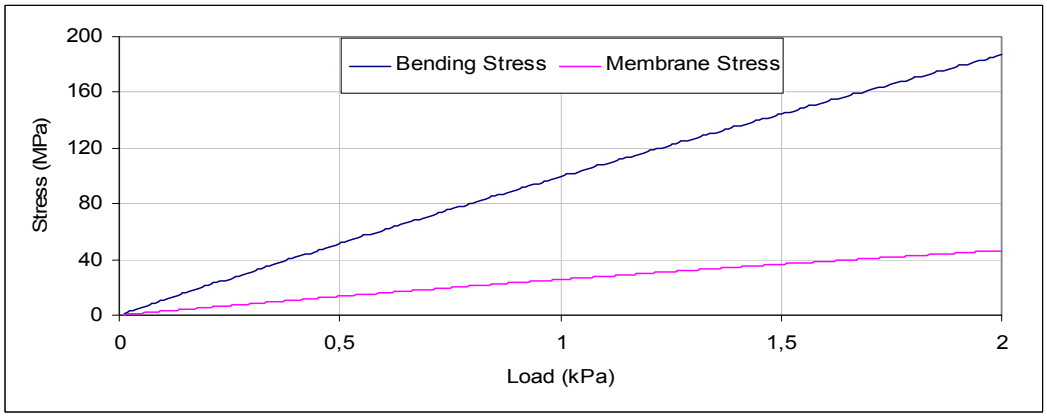

Figure 2.24 Membrane and bending stresses at the center of curved beam for the top surface of the top ply

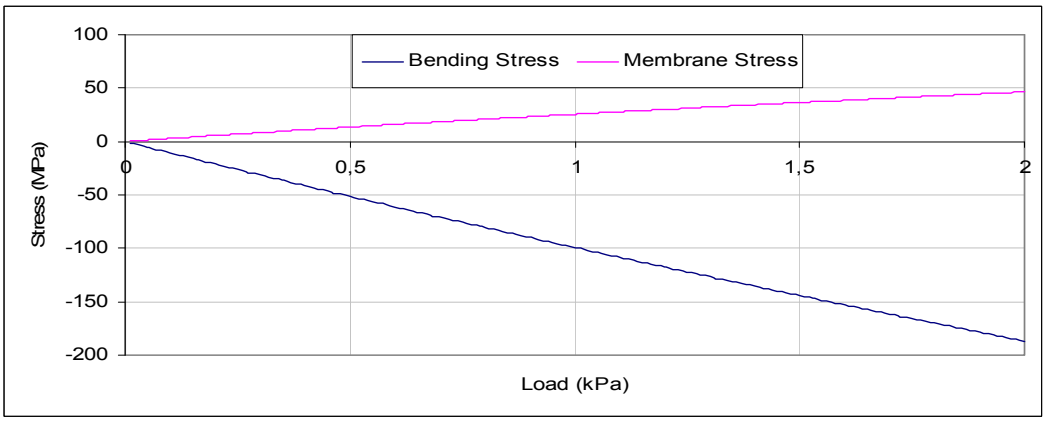

Figure 2.25 Membrane and bending stresses at the center of curved beam for the bottom surface of the top ply

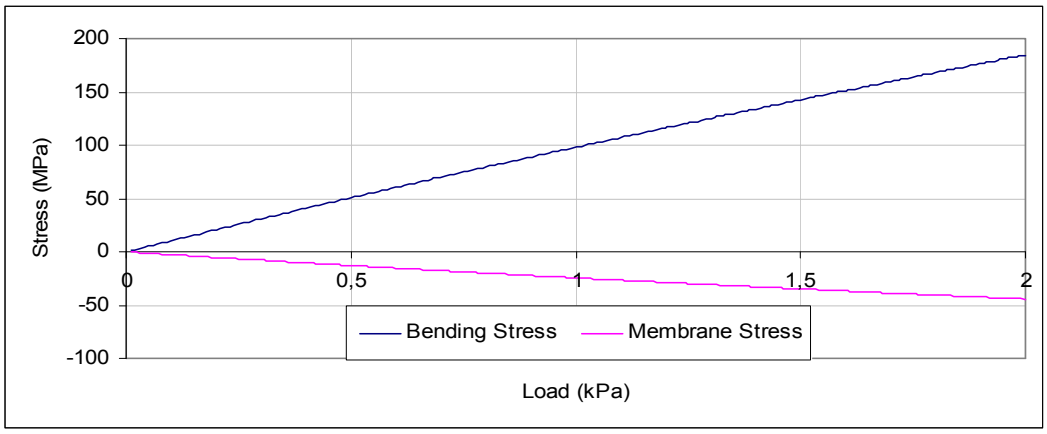

Figure 2.26 Membrane and bending stresses at the center of curved beam for the top surface of the bottom ply

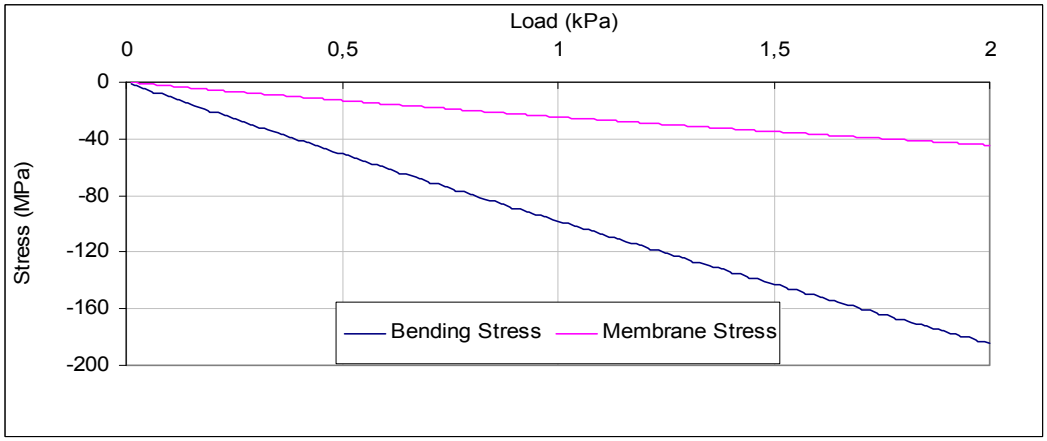

Figure 2.27 Membrane and bending stresses at the center of curved beam for the bottom surface of the bottom ply

Figures 2.28-2.31 illustrate how maximum stress changes along the θ direction of curved beam for different load levels. Maximum stress from Figures 2.28 and 2.30 are observed as compression at the bottom surfaces of the top and bottom glasses. The value of maximum compression stress at bottom surface of the unit is nearly 230 MPa for applied 2 kN load. Stress curves are getting closer to each other when pressure is decreased. From the Figures 2.29 and 2.31, maximum stresses at the top surfaces of top and bottom glass units are observed as tension. The maximum value of tension stress at top surface for applied 2 kN load is 230 MPa. Because of the perfect bound between the glass sheets and interlayer, the stresses at bottom surface

of top glass and the stresses at top surface of bottom glass are equal to the top and bottom surface stresses of PVB interlayer, respectively. The maximum stress value for 2 kN load is nearly 140 MPa. The maximum stresses along θ direction change their sign at two points as observed in Figures 2.28-2.31. Because of the membrane stresses at the boundaries of unit, it is observed that the stresses at the boundaries of unit are not zero.

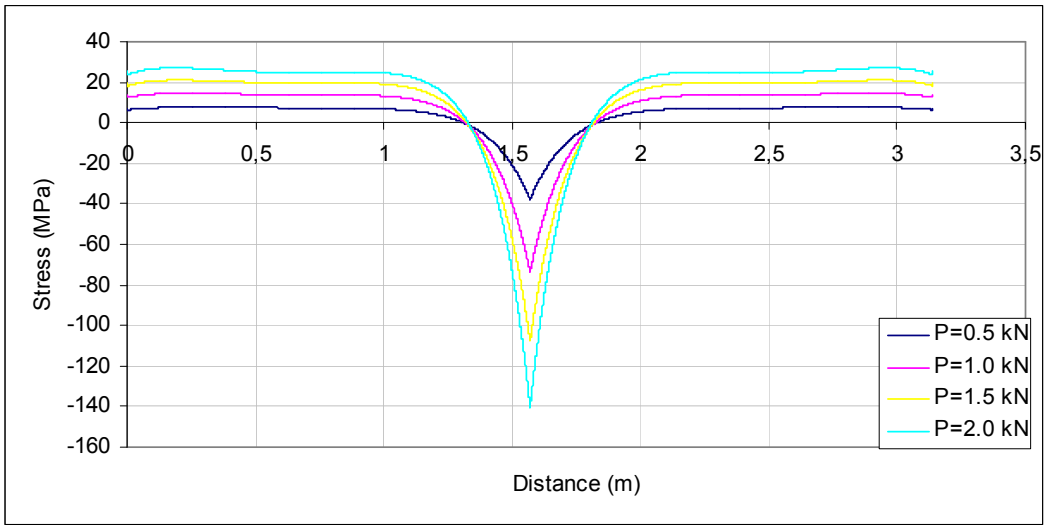

Figure 2.28 Stresses on the bottom surface of the top glass along the arc length of the simply supported beam

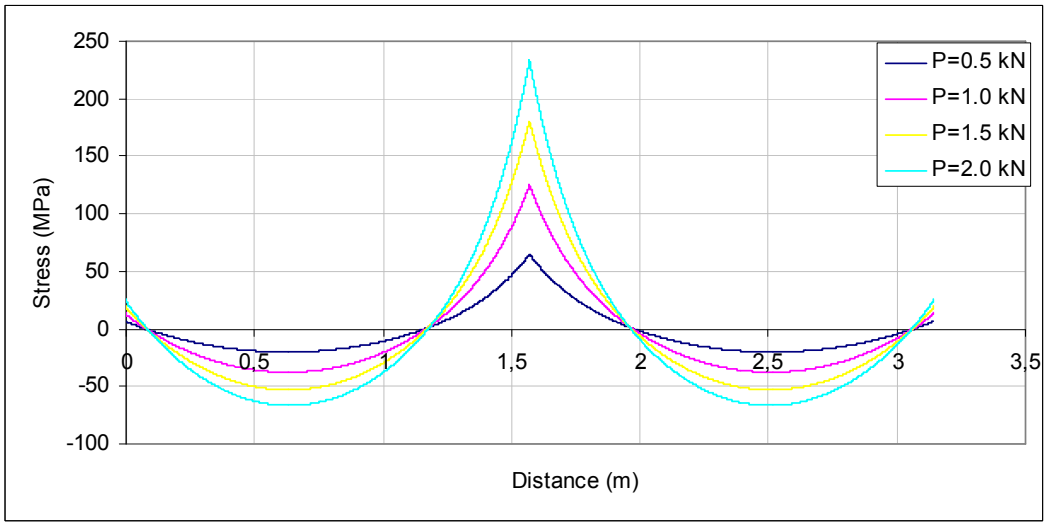

Figure 2.29 Stresses on the top surface of the top glass along the arc length of the simply supported beam

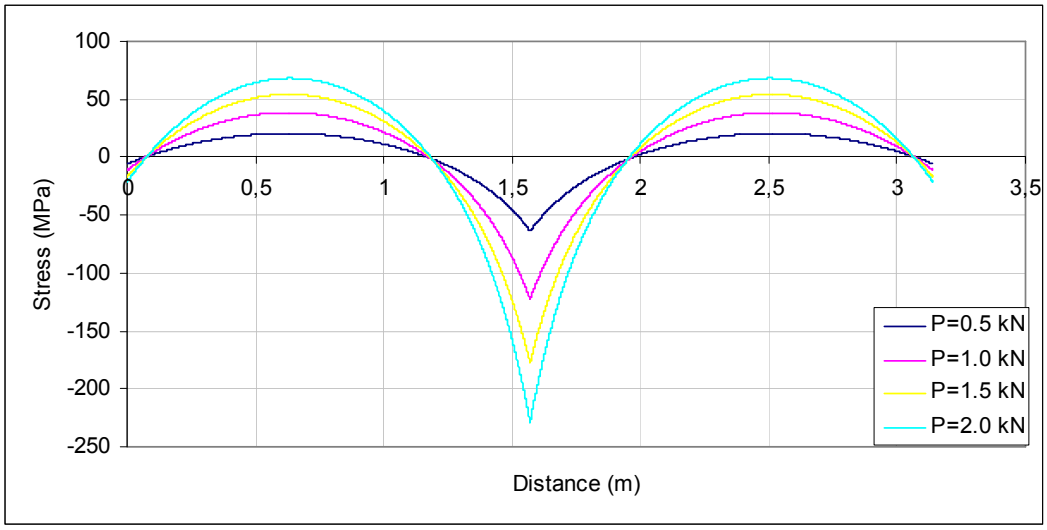

Figure 2.30 Stresses on the bottom surface of the bottom glass along the arc length of the simply supported beam

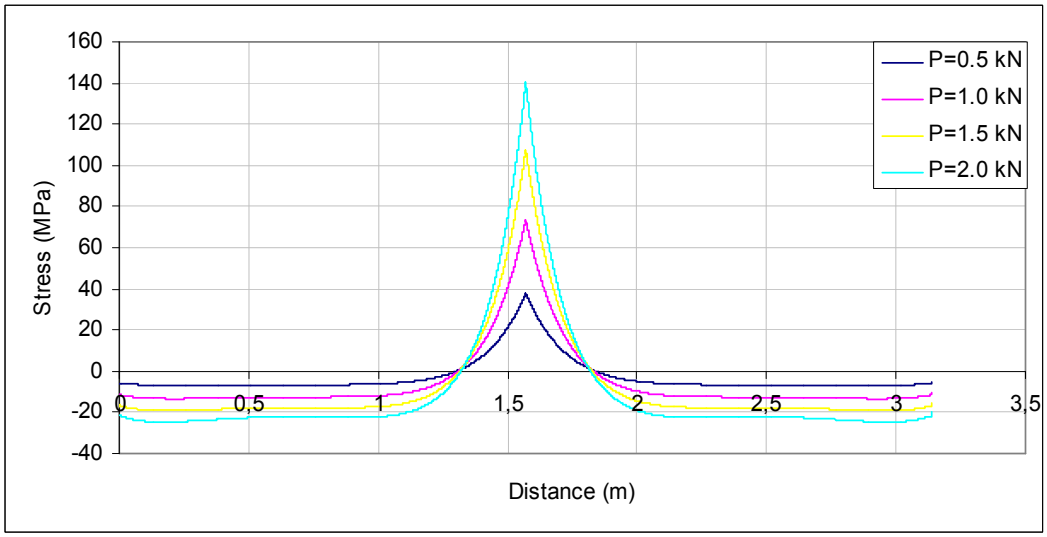

Figure 2.31 Stresses on the top surface of the bottom glass along the arc length of the simply supported beam

Figure 2.32 gives the relationship between the applied radial force and the maximum stress at the surfaces of glass sheets. While maximum stress on the top surface of the top glass (top-top) and on the top surface of the bottom glass units (bot-top) are tension, maximum stress on the bottom surface of the top glass (top-bot) and on the bottom surface of the bottom glass units (bot-bot) are compression. From Figure 2.32 it is observed that the maximum stress on the top and bottom surfaces of interlayer is

nearly half of the stresses of top surface of the top glass and bottom surface of bottom glass.

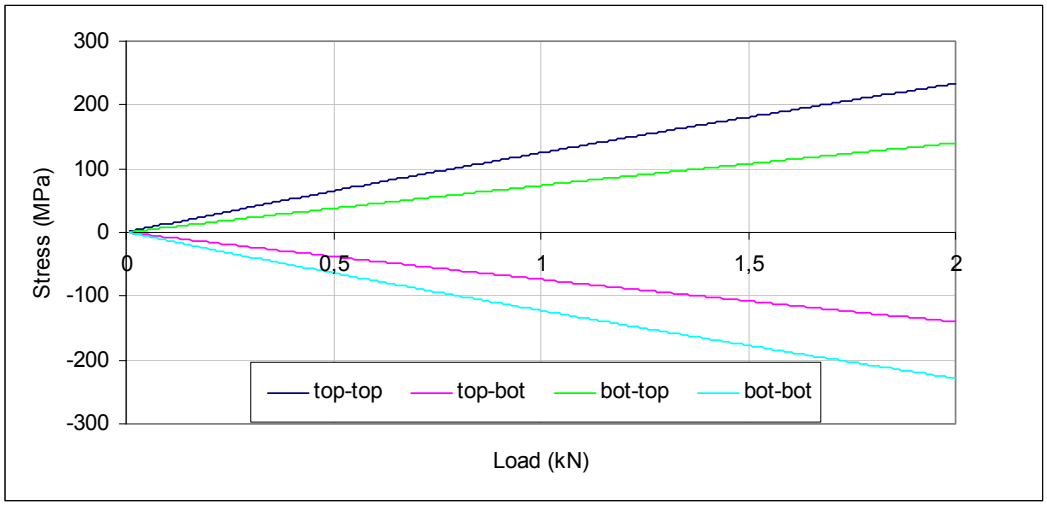

Figure 2.32 Maximum stresses versus load of the laminated glass

Maximum stresses on the top and bottom surfaces of the glass unit at load 2 kN are given in Figures 2.33 and 2.34. Compression stresses are developing at the bottom surface while tension stresses are developing at the top surface of the curved beam as expected. Stresses in monolithic and laminated curved glass beam are close to each other while the stresses in layered glass beam are moving away from their stress curves. Stresses reach their maximum values at the midpoint of the laminated glass unit. Stresses change their sign at two points along θ direction. The points, which the stresses change their sign, are the same for layered and laminated units at the top and bottom surfaces. The stresses near the boundary are compression at top surface. On the other hand, stresses near the boundary are tension at the bottom surface of the unit. The sign of stresses along the arc length are changing as seen in the figures because of double curvature occurrence when load is applied since beam has initial curvature. Therefore compression and tension stresses are taking place along the laminated glass curved beam at the top and bottom surfaces. Stresses along the beam for top and bottom surfaces have absolutely same shape. It is interesting that the behavior of laminated glass beam is close to the behavior of monolithic glass beam along the arc length but its behavior along the arc length also lies between the

monolithic and layered cases as seen in Figures 2.33 and 2.34. Because of PVB interlayer membrane stresses of laminated glass unit are higher than the membrane stresses of layered and monolithic glass units. For this reason, the stresses at the boundaries of layered and monolithic curved laminated glass beam is very small with respect to boundary stresses of laminated glass unit.

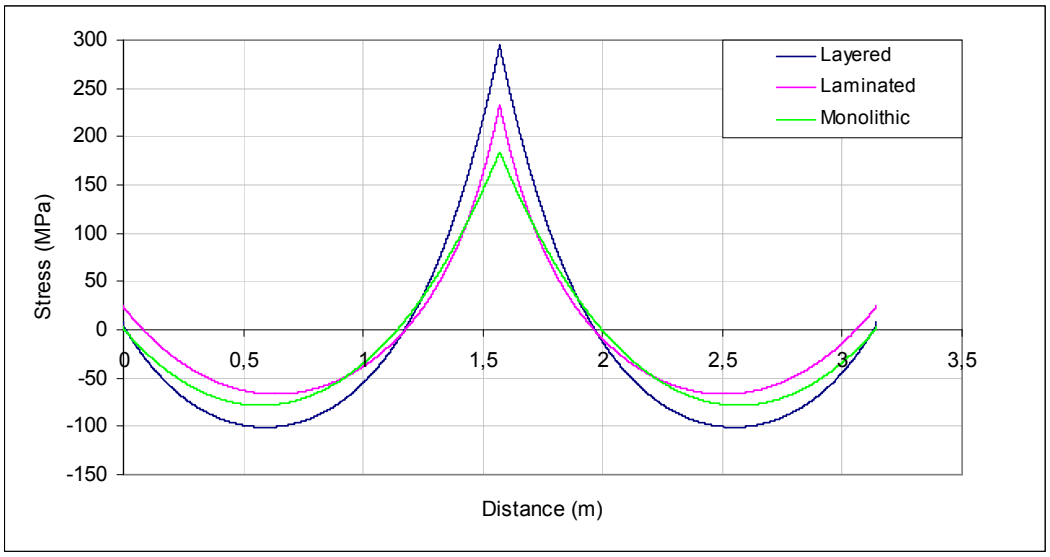

Figure 2.33 Stresses on the top surface of the top glass along the arc length of the simply supported beam at load P=2 kN

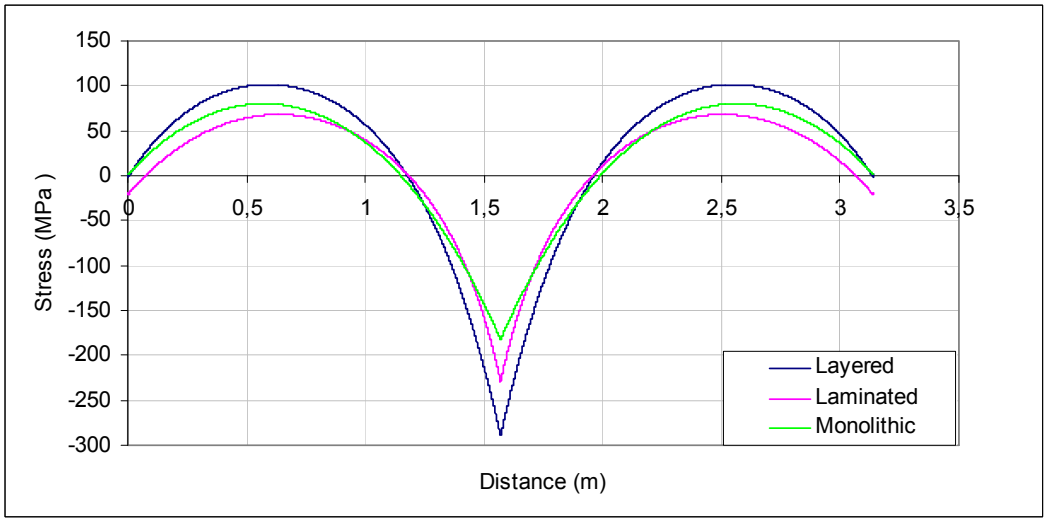

Figure 2.34 Stresses on thebottom surface of the bottom glass along the arc length of the simply supported beam at load P=2kN

The ratio of maximum principal tensile stress in monolithic glass system to the maximum principal tensile stress in laminated glass system is defined as strength factor. Strength factor analyses are made to establish the limits of laminated glass behavior. Strength factor of simply supported curved beam is nearly 0.8. Strength factor for laminated glass arch is presented in Figure 2.35.

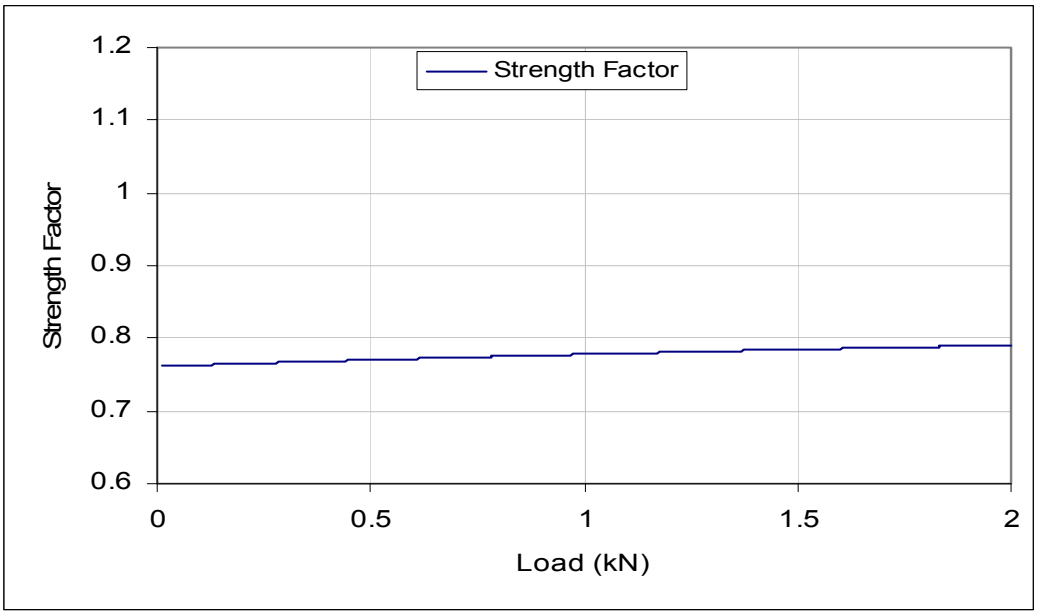

Figure 2.35 Variation of strength factor of simply supported curved beam

2.5.2 Fixed Supported Curved Beam

To consider the effect of boundary conditions the glass arch with the physical properties given in Table 2.1 is solved for different boundary conditions. Nonlinear coupled differential equations derived for laminated glass beams by using large deflection theory are used to predict the behavior of a fixed supported laminated glass curved beam. The pictorial presentation of fixed supported curved beam is presented in Figure 2.36. Boundary conditions for a fixed supported unit are as follows:

At $\theta = \theta_1$ and $\theta = \theta_2$ (at the supports): $w = 0$ and $\frac{dw}{dx} = 0$

$u1 = 0$ and $u2 = 0$

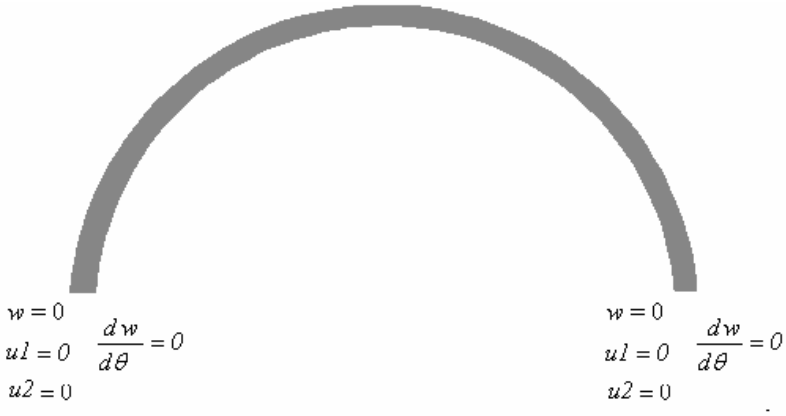

Figure 2.36 Pictorial presentation of boundary conditions for the fixed supported curved beam

Hereafter the laminated glass unit considered as an example has the radius of 1 m and θ=3.14. The thickness of each glass beam is $h_1 = h_2 = h$ = 5 mm. and the width of the unit is 0.1 m. Modulus of elasticity of the glass is given as E = 72 GPa. Shear modulus of elasticity and the thickness of interlayer PVB are taken as 1000 kPa and 0.76 mm, respectively. Point load P is applied at the midpoint of a beam as tension.

Figure 2.37 shows the comparison of linear and nonlinear approach to predict the behavior of the fixed supported laminated glass beam. Linear and nonlinear solution results are plotted as normalized deflection versus load. Separation between linear

and nonlinear solutions starts when $\frac{w_{max}}{h}$ about 1.85. It can be said that nonlinear solution should be considered when the ratio of maximum deflection to thickness of a single glass beam is greater than 1.85. It is observed that this ratio (the level of nonlinearity) is about 8.92 for a load P=2 kN in Figure 2.37. The central deflection obtained from linear approach is almost 1.3 times of the deflection obtained by nonlinear approach at load P=2 kN.

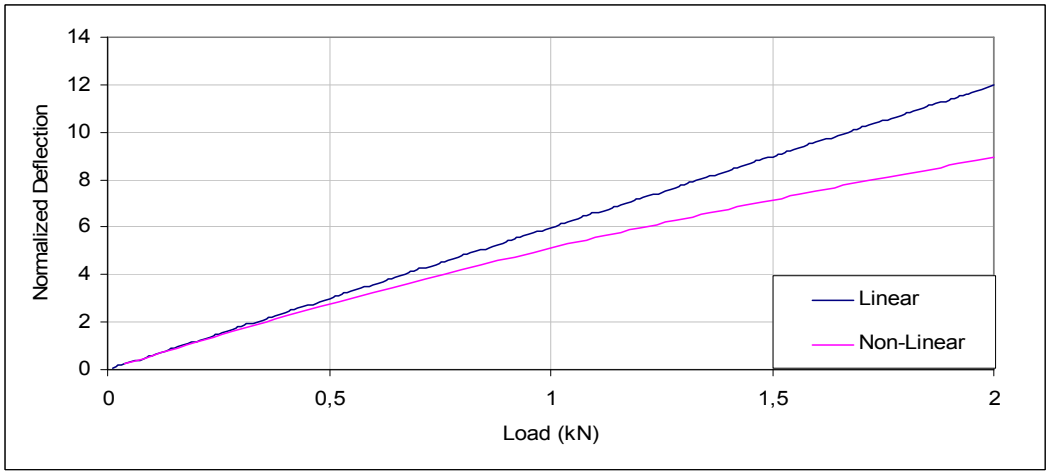

Figure 2.37 Normalized maximum deflection ($\frac{w_{max}}{h}$) versus load for fixed supported beam

Figures 2.38-2.39 are plotted in a comparative approach. Results of monolithic, layered and laminated glass beams with interlayer shear modulus of 500 and 1000 kPa, are presented together. It may be concluded that the behavior of simply supported laminated glass beam presented in Figures 2.17 and 2.18 is closer to that of layered glass beam which is contrary to the behavior of fixed supported laminated curved glass beam presented in Figures 2.38 and 2.39. Figures 2.40, 2.41 and 2.42 are plotted to investigate the circumferential and radial deflections along the arc length of the fixed supported beam. Circumferential displacements of top and bottom glass sheets are zero at the boundaries and at the center of the unit because of the geometry and boundary conditions of glass unit. While they are positive at the left hand side of the center, they take negative values at the right hand side of the center of the unit. The absolute values of circumferential deflection at left hand side and

right hand side are equal in accordance with symmetry of unit. Because of the effect of geometric nonlinearity displacement curves are getting closer to each other for increasing load levels. Radial deflections of laminated layered and monolithic curved glass beams for applied 2 kN load are shown in Figure 2.43. While the difference between maximum radial displacement of monolithic and laminated glass unit for simply supported beam is nearly 12 mm, it is nearly 20 mm for fixed supported beam. Therefore, it can be concluded that behavior of simply supported laminated and monolithic curved glass beams are closer to each other than that of the behavior fixed supported units.

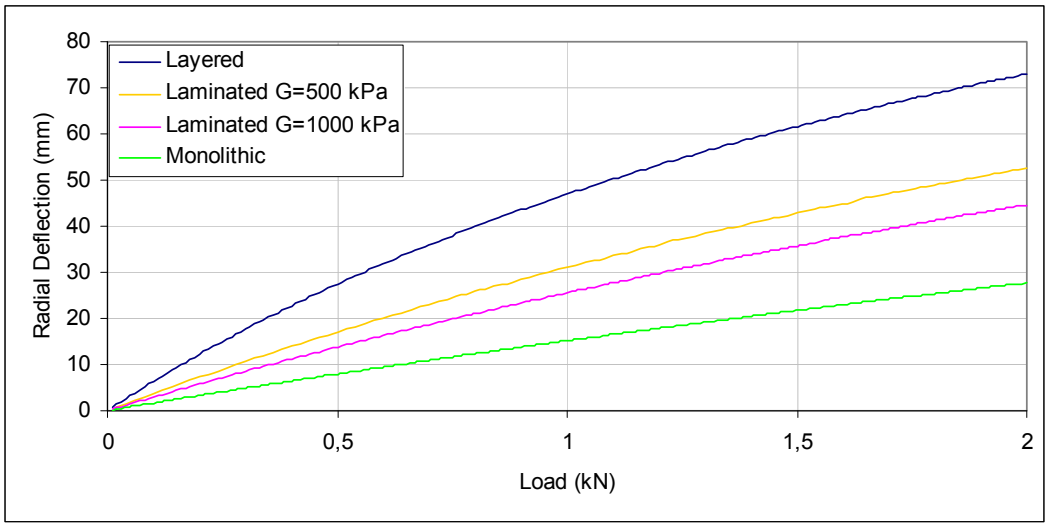

Figure 2.38 Maximum displacements versus load

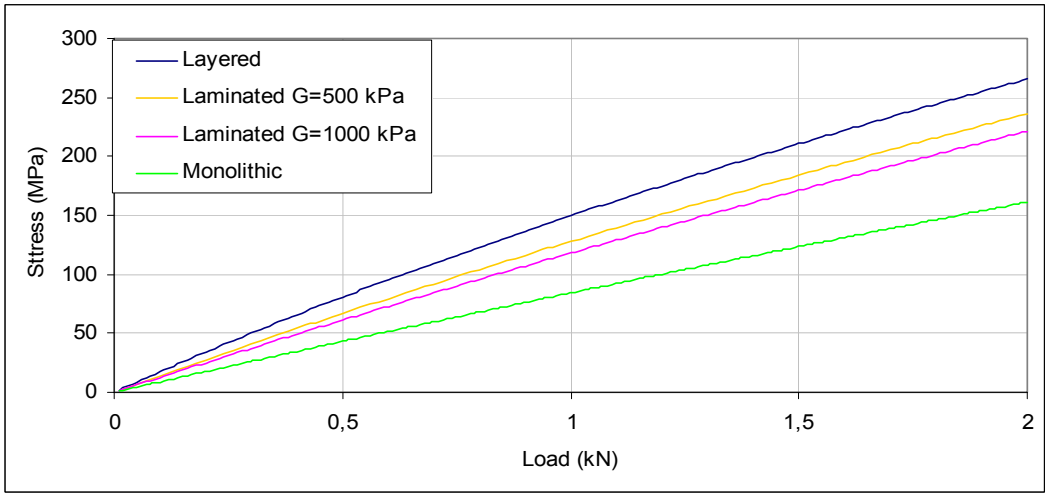

Figure 2.39 Maximum stress versus load

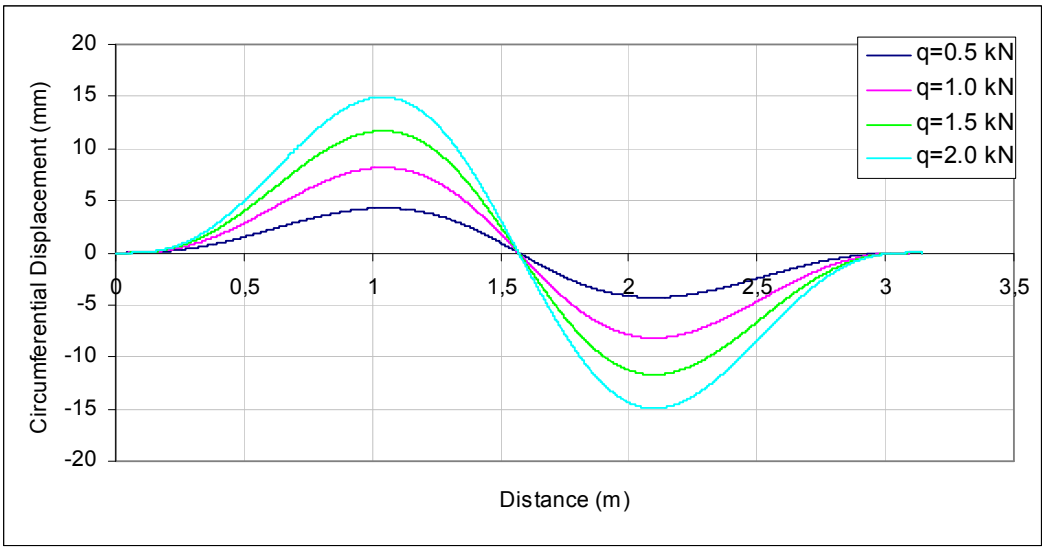

Figure 2.40 Circumferential displacement (u1) of the top glass along the arc length of the beam

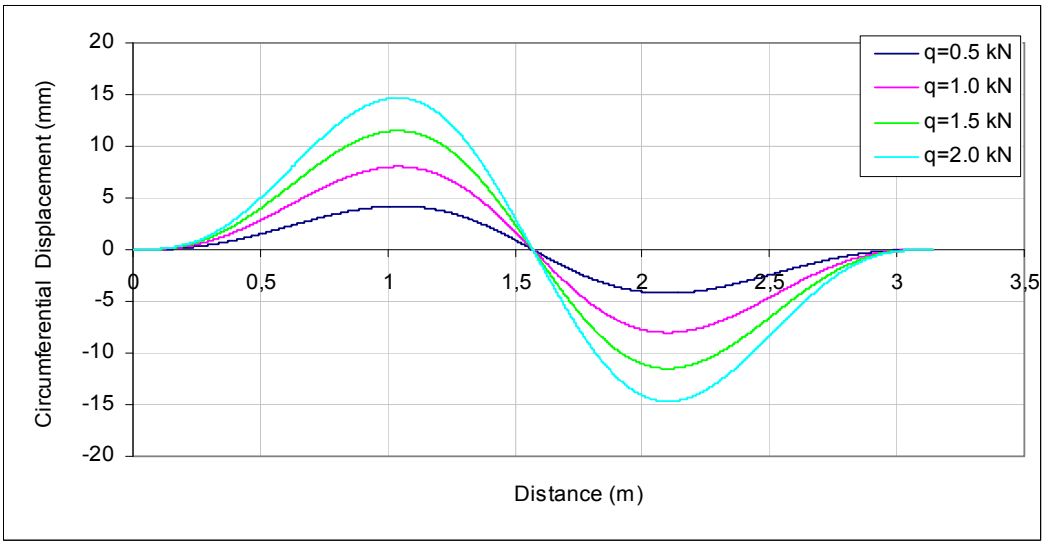

Figure 2.41 Circumferential displacement (u2) of the bottom glass along the arc length of the beam

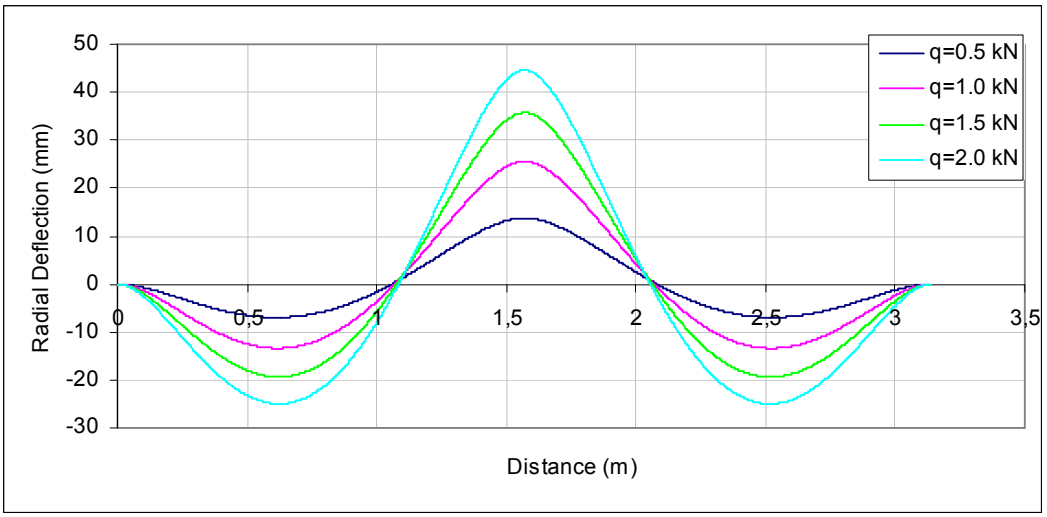

Figure 2.42 Radial Displacement for different load values

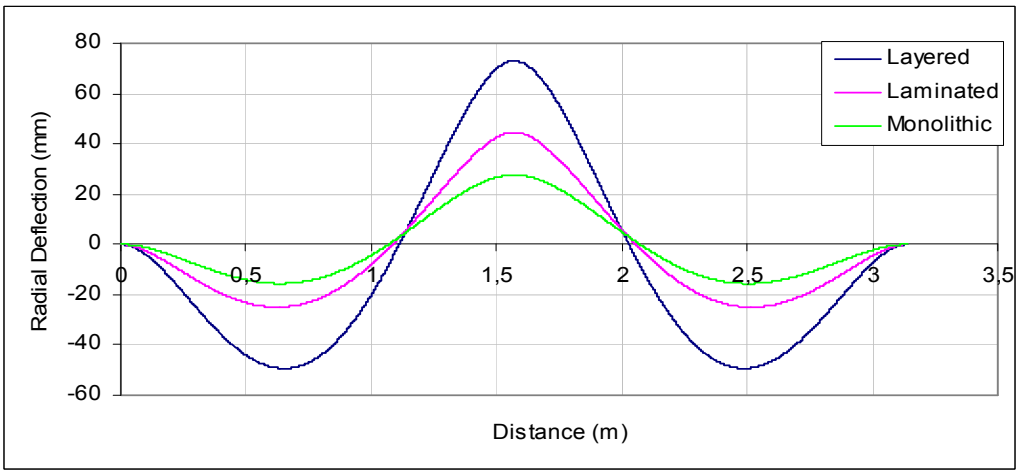

Figure 2.43 Comparison of displacements along the arc length of the fixed supported beam at load P=2 kN

Function of shear stress along θ direction from the left boundary to the right boundary of fixed supported curved beam is plotted in Figure 2.44 for the applied pressure levels. Shear stresses are zero at the boundaries and at every quarter of the beam. While shear stresses take their maximum value at the left and right hand side of center for fixed supported beam, they take their maximum value at the boundaries for simply supported beam. The maximum value of shear stress is nearly 70 kPa for simply supported beam, while it is nearly 55 kPa for fixed supported beam.

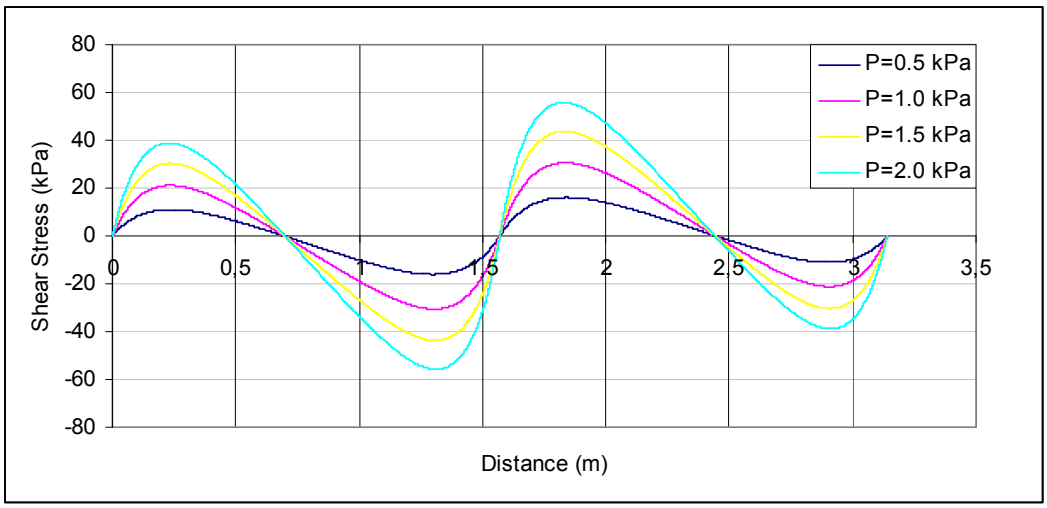

Figure 2.44 Variation of shear stress along the arc length of the beam

Stresses along the arc length at the surfaces curved beam for different load values are given in Figures 2.45-2.48. While the maximum stresses at the bottom surface of the top and bottom glass units are in compression, stresses on the top surface of the top and bottom glass units are tension. The boundary stresses of fixed supported beam are greater than that of simply supported beam. The stress curves are getting closer to each other when load is increased. Figure 2.49 is plotted for the maximum stress (which is at the center) versus load P at the center at every surface of glass layers. While maximum stress on the top surface of the top glass (top-top) and on the top surface of the bottom glass units (bot-top) are tension, maximum stress on the bottom surface of the top glass (top-bot) and on the bottom surface of the bottom glass units (bot-bot) are compression. Figures 2.50 and 2.51 are plotted for the comparison of stress distribution along the arc length on the top and bottom surfaces of the curved beam. Stresses on the top surface of the top glass beam are in tension at midpoint and at support of the beam. Stresses at the bottom surface of the bottom glass beam show a reverse pattern, i.e. stress patterns on top and bottom surfaces show an anti-symmetric distribution. From Figures 2.50 and 2.51 it is observed that for the bottom surface of the bottom glass beam, it is interesting to note that the stress curve for the laminated glass beam starts with a stress value almost equal to the stress value of the layered glass beam at midpoint and ends with a stress value almost equal to a stress

value of monolithic glass beam at support. For the top surface of the top glass beam, the stress curve for the laminated glass beam shows a reverse pattern.

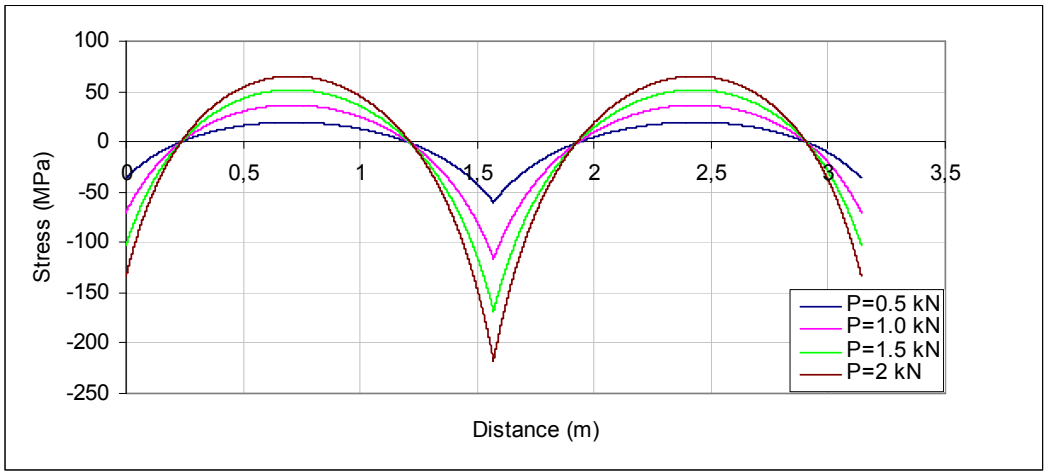

Figure 2.45 Stresses on the bottom surface of the bottom glass along the arc length of the fixed supported beam

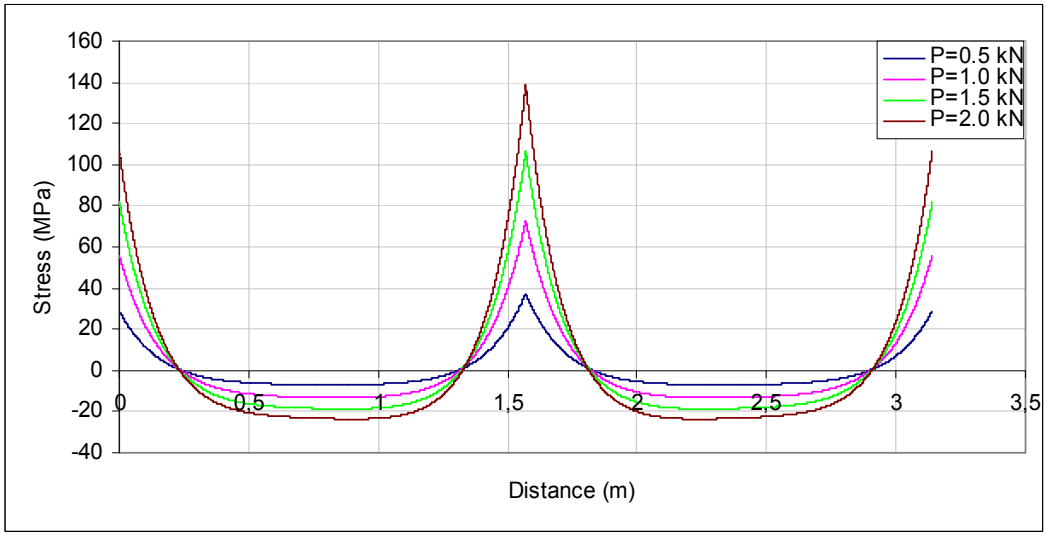

Figure 2.46 Stresses on the top surface of the bottom glass along the arc length of the fixed supported beam

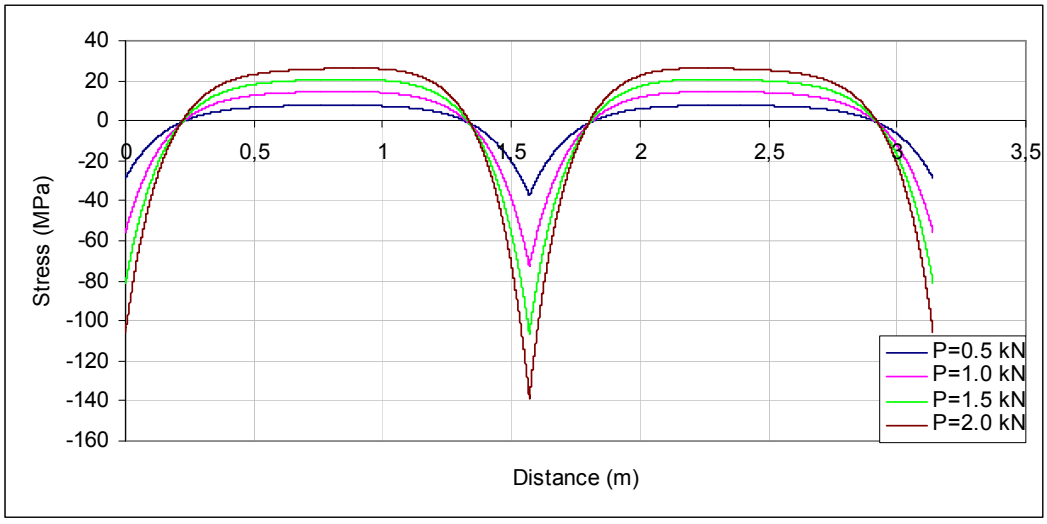

Figure 2.47 Stresses on the bottom surface of the top glass along the arc length of the fixed supported beam

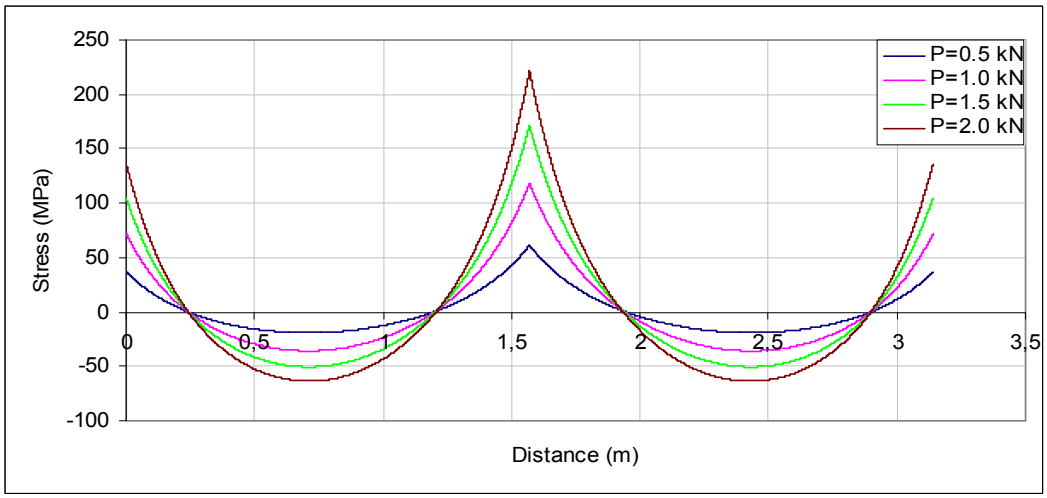

Figure 2.48 Stresses on the top surface of the top glass along the arc length of the fixed supported beam

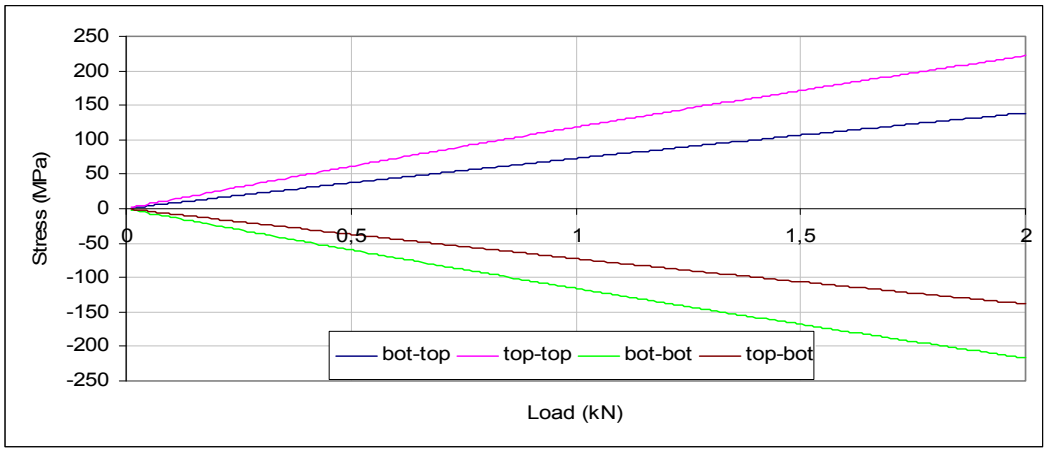

Figure 2.49 Maximum stresses versus load of the laminated glass

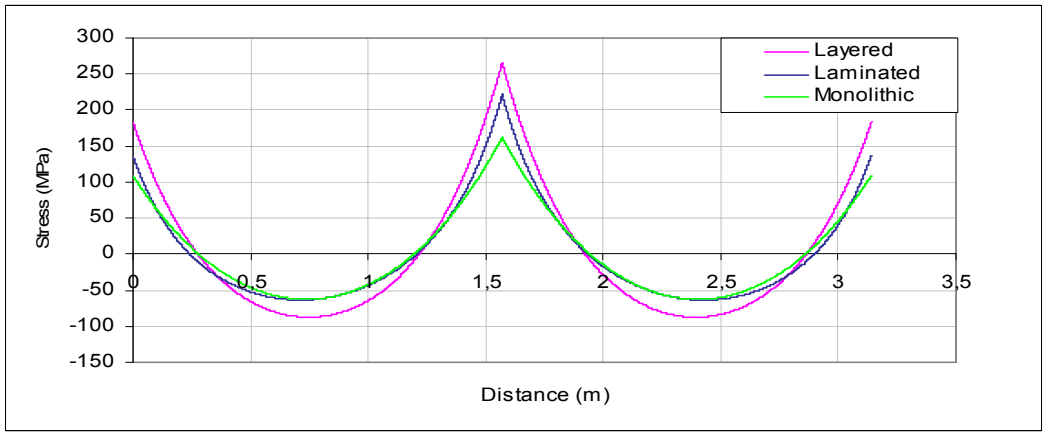

Figure 2.50 Stresses on the top surface of the top glass along the arc length of fixed supported beam at load P=2 kN

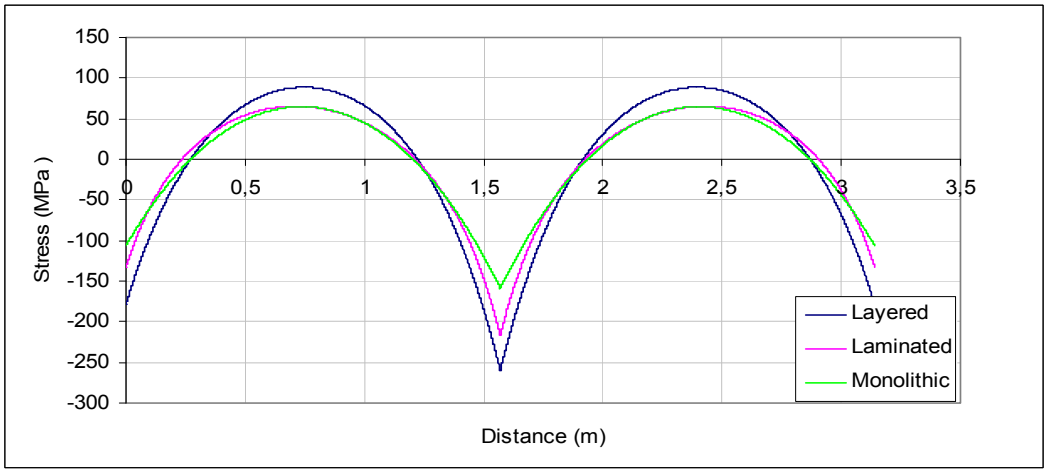

Figure 2.51 Stresses on the bottom surface of the bottom glass along the arc length of the fixed supported beam at load P=2kN

Strength factor of fixed supported curved beam is nearly 0.7 as seen in Figure 2.52, while it is nearly 0.8 for simply supported curved beam.

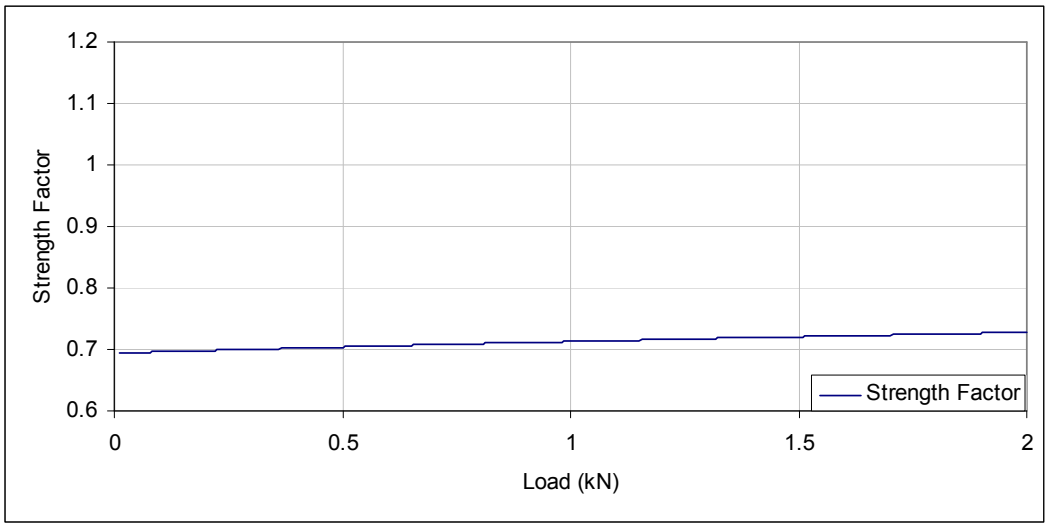

Figure 2.52 Variation of strength factor for fixed supported curved beam

2.5.3 Fixed-Simply Supported Curved Beam

Boundary conditions of fixed simply supported curved beam with the physical properties given in Table 2.1 are given as follows and the pictorial presentation of them is given in Figure 2.53.

At $\theta = \theta_1$ and (at the left support): $w = 0$ and $\frac{dw}{d\theta} = 0$

$u1 = 0$ and $u2 = 0$

At $\theta = \theta_2$ (at the right support): $w = 0$ and $\frac{d^2w}{d\theta^2} = 0$

$u1 = 0$ and $u2 = 0$

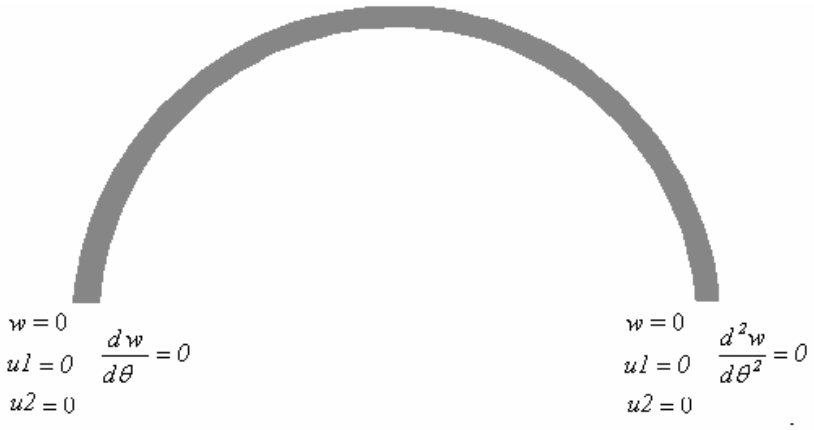

Figure 2.53 Pictorial presentation of boundary conditions for fixed and simply supported curved beam

The same beam is solved as, fixed at one end and simply supported at the other end, to consider the effect different boundary conditions to the behavior of curved beam. Figures 2.54 and 2.55 are plotted to compare the behavior of laminated, layered and monolithic beams. Circumferential and radial displacement and stresses along the glass surface of laminated beam are seen in Figures 2.56-2.62. Strength factor of the beam is 0.75 as shown in Figure 2.63.

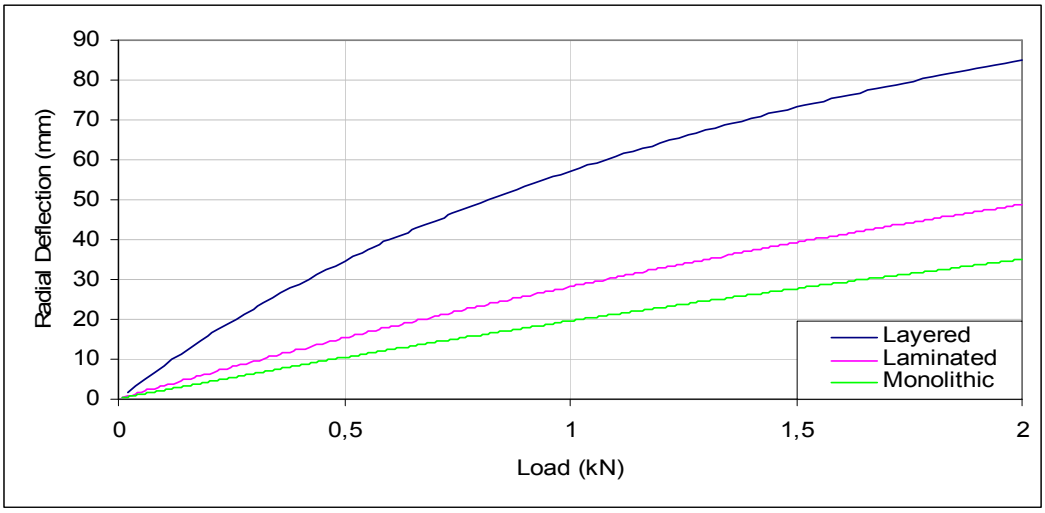

Figure 2.54 Maximum displacements versus load for fixed and simply supported beam

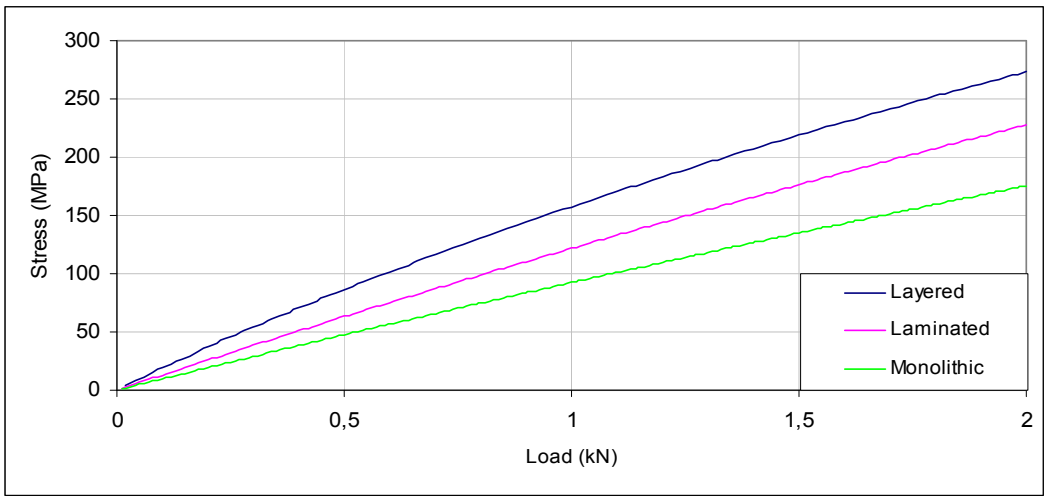

Figure 2.55 Maximum displacements versus load for fixed and simply supported beam

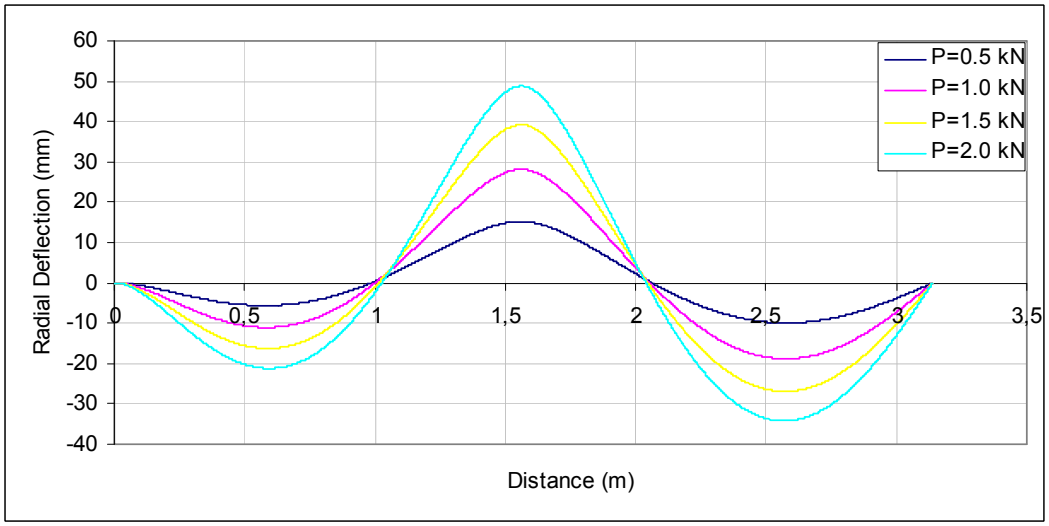

Figure 2.56 Radial displacements along the arc length of the beam fixed at one end and simply supported at the other end for different load values

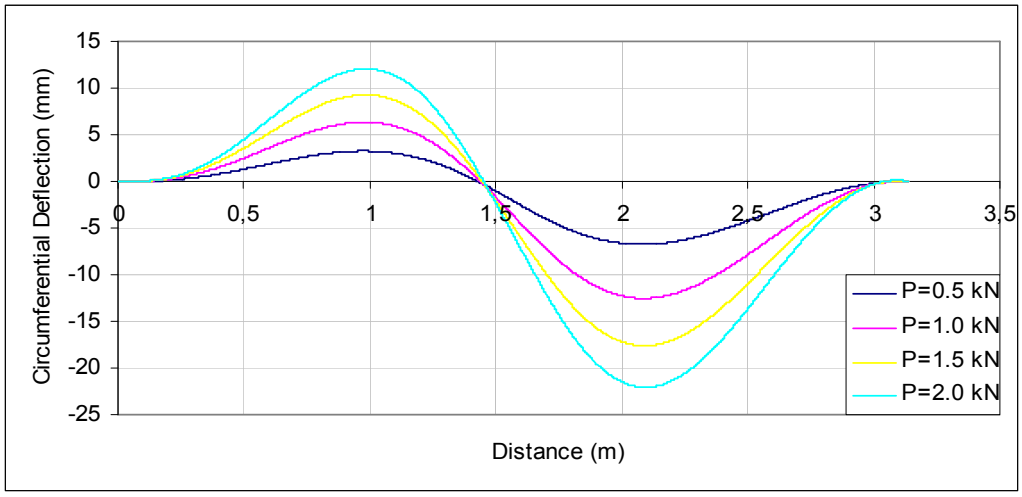

Figure 2.57 Circumferential displacement (u1) of the top glass along the arc length of the beam

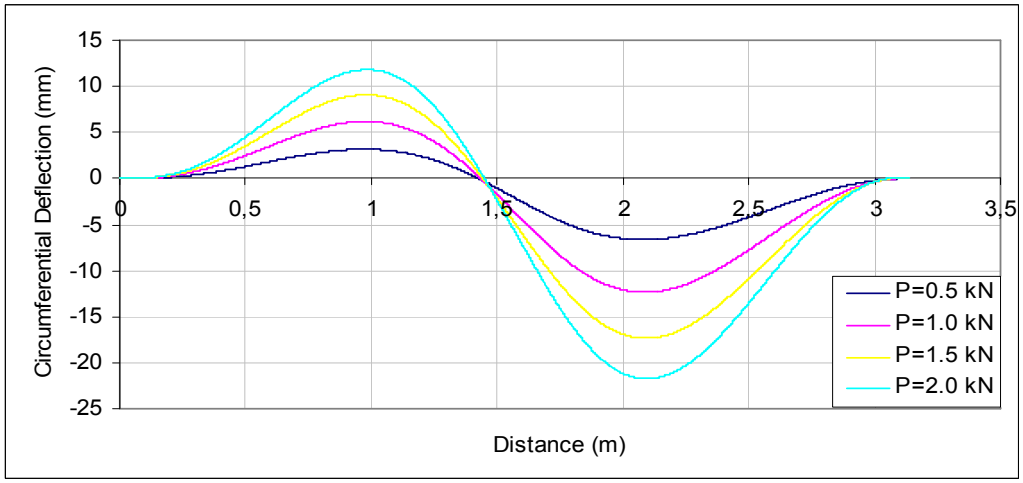

Figure 2.58 Circumferential displacement (u2) of the bottom glass along the arc length of the beam

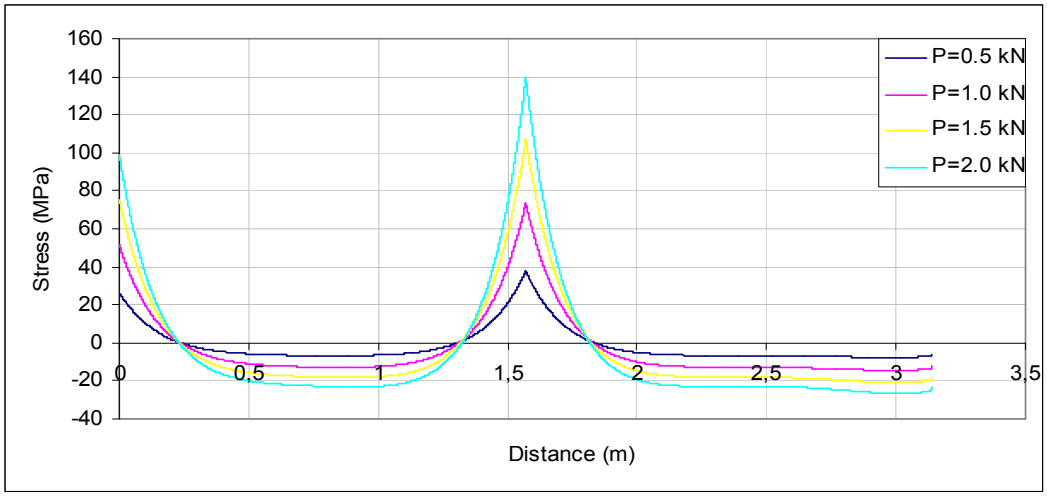

Figure 2.59 Stresses on the top surface of the top glass along the arc length of the fixed at one end and simply supported at the other end beam

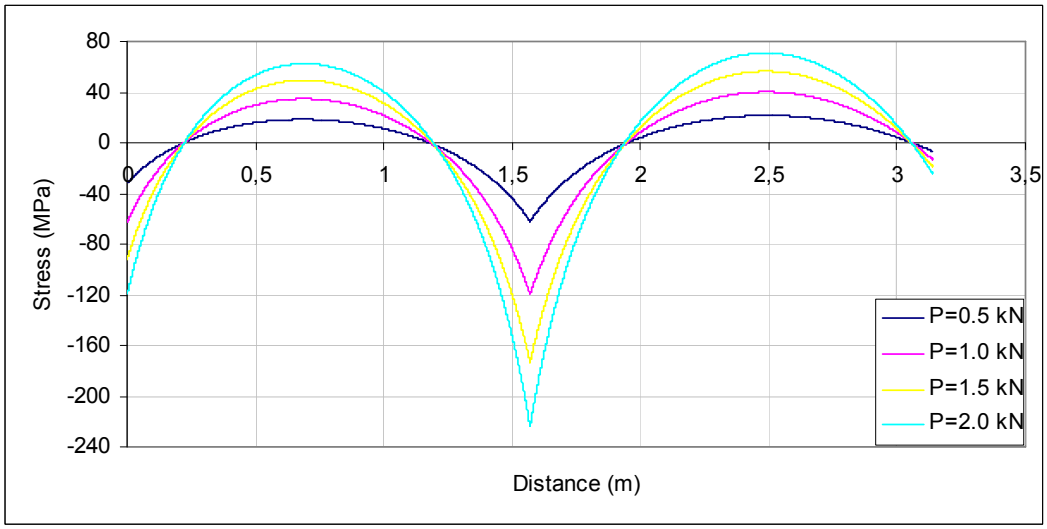

Figure 2.60 Stresses on the bottom surface of the top glass along the arc length of the fixed at one end and simple supported at the other end beam

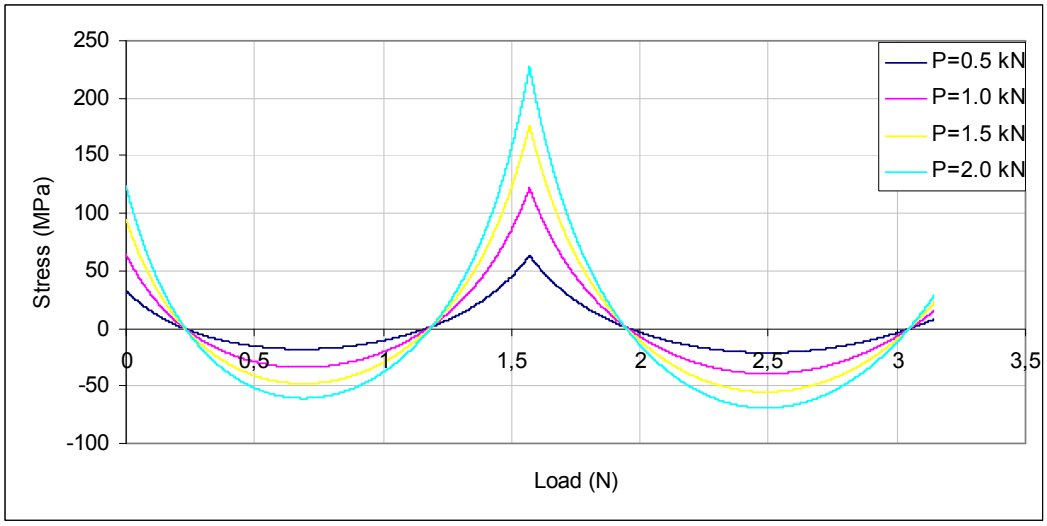

Figure 2.61 Stresses on the top surface of the bottom glass along the arc length of the fixed at one end and simple supported at the other end beam

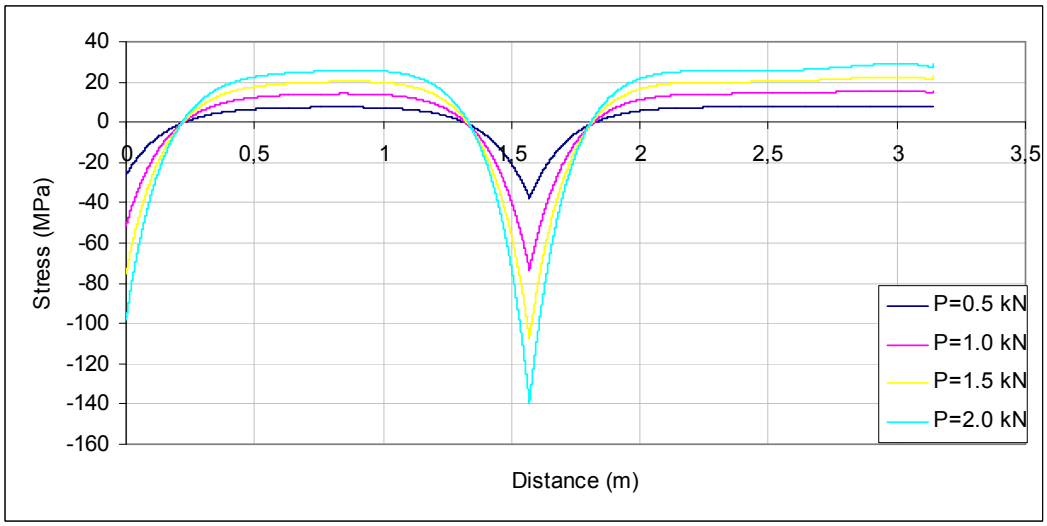

Figure 2.62 Stresses on the bottom surface of the bottom glass along the arc length of the fixed at one end and simple supported at the other end beam

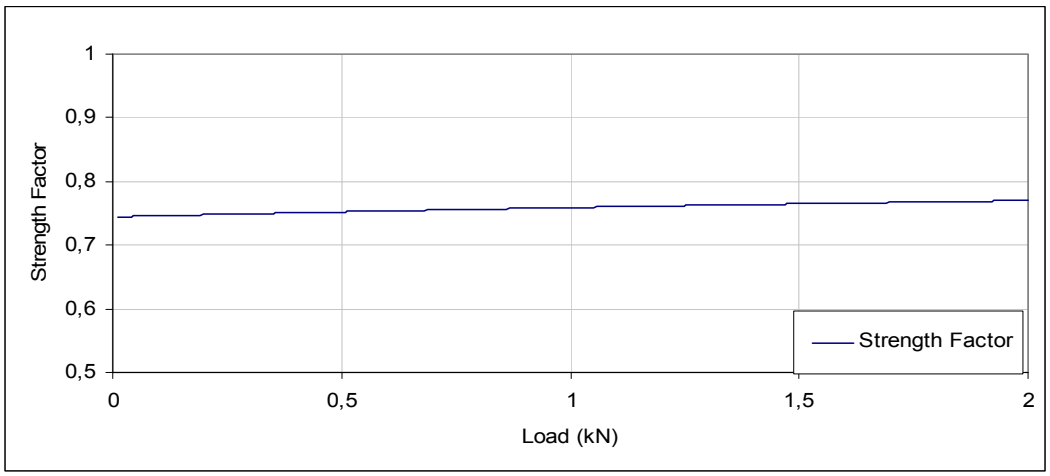

Figure 2.63 Variation of strength factor with load of the laminated curved beam fixed at one end and simply supported at the other end

Comparisons of boundary conditions are given below. Comparison of deflection and stress values for different boundary conditions are presented in Figures 2.64 and 2.65. Deflection and stress of simply supported beam is higher than those of fixed and simple-fixed beams. The behavior of fixed- simple supported beam is bounded by the behaviors of simple-simple and fixed-fixed supported beams. While the behavior of fixed-simple supported beam is close to the behavior of fixed supported beam at left hand side of the beam, it is close to the behavior of simple supported beam on the right hand side of the beam, as expected.

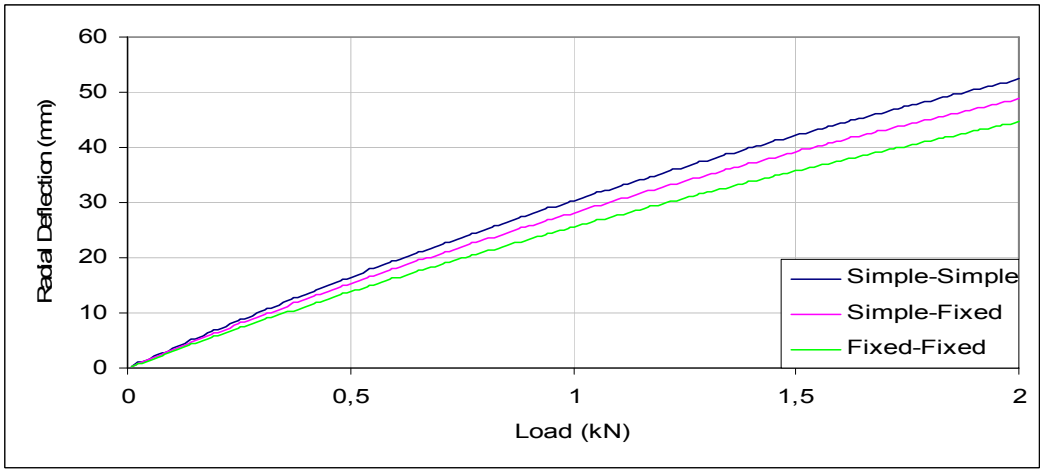

Figure 2.64 Comparison of maximum displacements for different boundary conditions

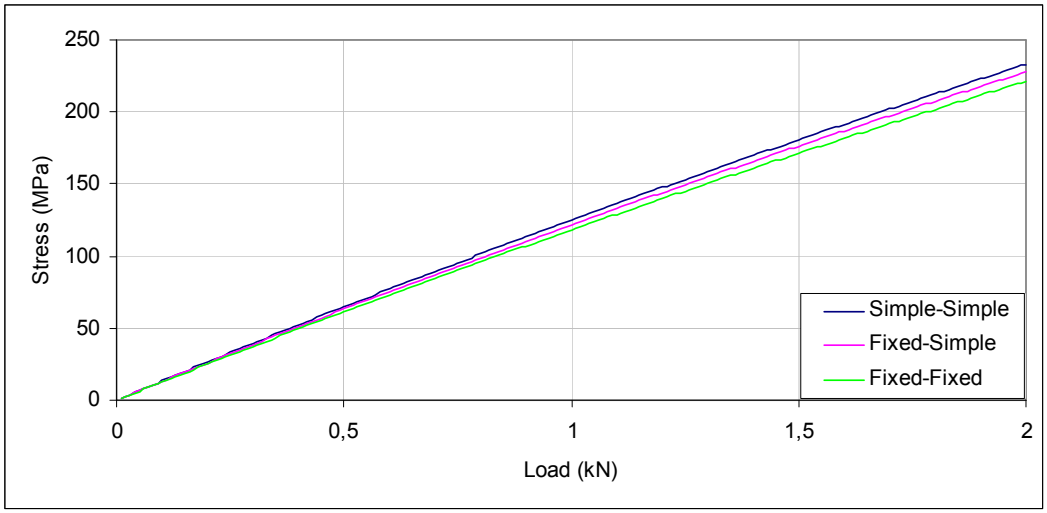

Figure 2.65 Comparison of maximum stresses for different boundary conditions

Comparison of radial deflections, top and bottom surface stresses for 2 kN load along the arc length of curved beam are given in Figures 2.66, 2.67 and 2.68, respectively. Strength factor values for different boundary conditions are given in Figure 2.69.

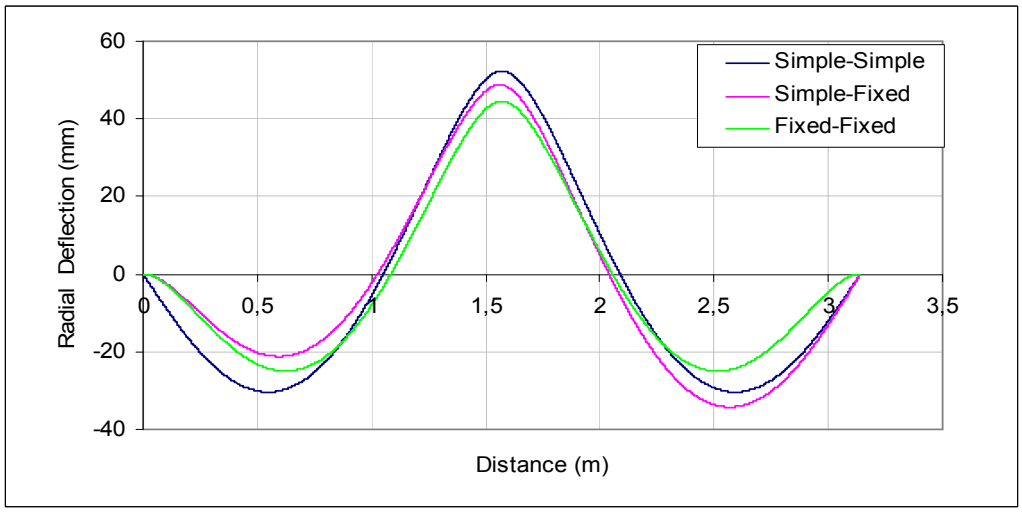

Figure 2.66 Comparison of radial deflections along the arc length of the beam

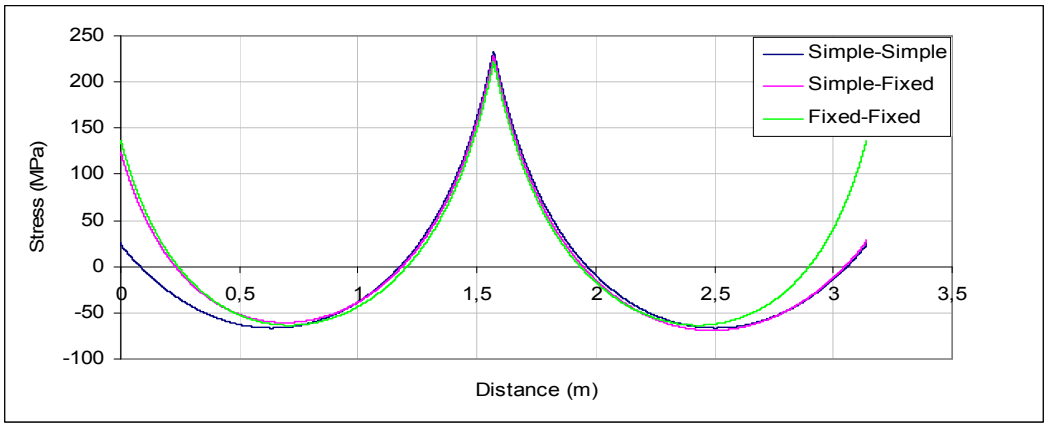

Figure 2.67 Comparison of maximum stresses on the top surface of the top glass along the arc length of the beam

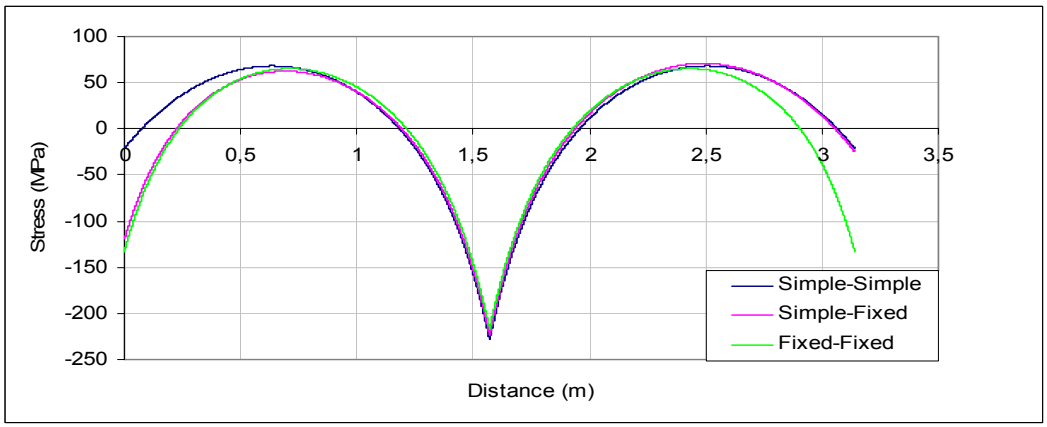

Figure 2.68 Comparison of maximum stresses on the bottom surface of the bottom glass along the arc length of the beam

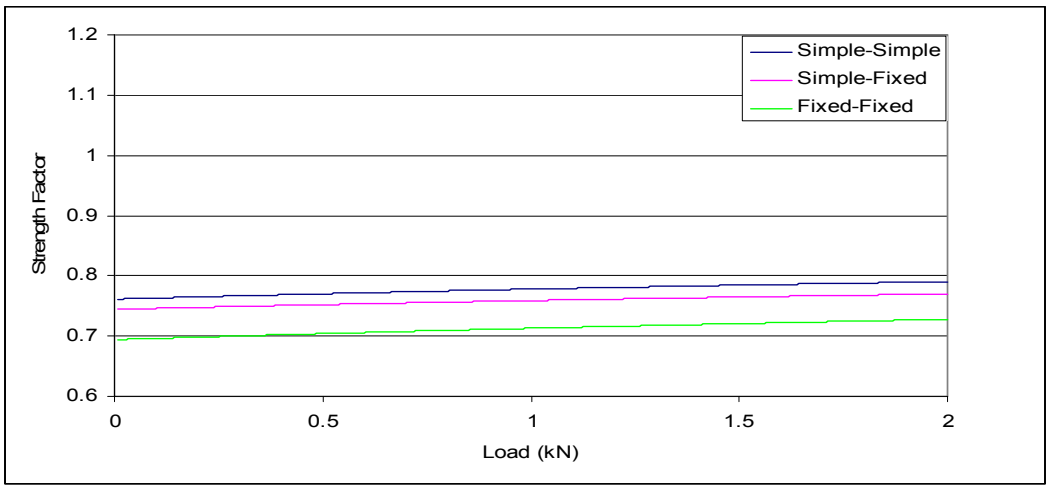

Figure 2.69 Comparison of strength factor

2.6 Summary and Conclusion

A mathematical model with nonlinear partial differential equations and a numerical solution technique are developed to predict the linear and nonlinear behavior of a laminated glass curved beam. Governing nonlinear coupled differential equations involving circumferential displacements u_1 and u_2 and radial displacement w are derived by using minimum potential energy theorem and variational approach. To develop nonlinear model and to obtain field and boundary equations large deflection theory is used. In the numerical solution of the nonlinear partial differential equations convergence difficulties are faced and to overcome these convergence difficulties variable SOR (here is named as SUR: Successive Under Relaxation) parameter is used. It also needs higher number of divisions and tolerance value than those for straight beams. Model is verified by test results conducted by Uzhan [27] in the mechanics laboratory of the Department of Engineering Sciences and by generating and solving a commercial finite element program. The comparison of results obtained from the current theoretical model, finite element model and experiments on laminated glass curved beam are matching quite well.

The developed model simulates the layered and monolithic glass cases successfully. Although the behavior of a laminated glass curved beam is bounded by the behavior of monolithic and layered curved glass beams these bounds are violated at some parts of the beam along its arc length, which is not the case in the behavior of straight beams. On the other hand, the behavior of a curved laminated glass beam depends on the shear modulus of interlayer PVB. It is possible to make the laminated glass arch stronger than the monolithic glass arch by increasing the shear modulus of interlayer. The present model provides valuable insight to the general behavior of laminated glass curved beam. The effect of PVB's shear modulus, the level of nonlinearity, displacement, moment and stress functions are observed. To consider the effect of boundary conditions to the behavior of curved beam the model is solved for different boundary conditions. The results are compared in figures. Nonlinearity level of simply supported beam is found to be higher than that of fixed supported beam.

Strength factor, which is employed to adjust laminated strengths by using available design charts, is obtained for curved beams. Strength factor of fixed supported laminated curved beam is found to be higher than that of simply supported beam. While strength factor of simply supported curved beam is nearly 0.8, strength factor of fixed supported curved beam is nearly 0.7.

CHAPTER 3

BEHAVIOR OF LAMINATED GLASS CYLINDRICAL SHELLS

3.1 Introduction to Theory of Shells

Shell structures are load carrying elements which have a great importance in engineering and in particular, in civil, mechanical, architectural and marine engineering. Large span roofs, water tanks, concrete arch domes, liquid retaining structures are examples of shell structures. A shell is said to be a curved structural element whose thickness is small when compared with the other dimensions of shell and with its radius of the curvature. Examples of the shell structures include pipes, pressure vessels, roofs, dooms, sheds, airplane wings, car sheds, turbine disks and bulkheads. Mid surface of the shell can be defined as the plane bisecting the shell thickness. To describe the shape of the shell we specify the geometry of middle surface and the thickness of the shell at each point.

When thickness of the shell is one-twentieth of radius of curvature or less they are defined as thin otherwise they are defined as thick shells.

To analyze the shell structures, equations of elasticity, membrane and bending theory are applied. Membrane forces are obtained for the given loading and then superimposed on the bending theory for edge loads. The solution procedure of shell is based on the following Love shell theory assumptions:

1- the shell is thin,

2- the displacement and rotations are small,

3- the normal shell datum surface before deformation remains normal after deformation,

4- the transverse normal stress is negligible.

The above assumptions are often called Kirchhoff-Love shell theory, which is an extension of Kirchhoff flat-plate theory.

3.2 Nonlinear Behavior of Shells

In the general case, nonlinearities are present when describing the response of a solid body. There are two types of nonlinearities due to material and geometry. Material nonlinearity is a result of changing material properties with the applied loads or force-displacement or stress-strain law, which is not linear.

Geometric nonlinearity is a result of nonlinear kinematic quantities such as the strain- displacement relations. Large strains, large displacements and large rotations can cause geometric nonlinearity.

The lateral deflection of the shell is not small when compared with the thickness of the shell. For this reason the mid-plane of the shell, develop stresses and the differential equations become nonlinear.

The geometry of a cylindrical glass shell unit may be layered, laminated or monolithic.

Layered glass consists of two glass sheets with no friction between them. Stress distribution of each ply is symmetric with respect to their individual neutral axis. The glass sheets share the load equally. ‘Plane sections before deformation remain plane after deformation’ assumption is not valid for layered glass units because curvature centers of plies are different.

Monolithic glass consists of one glass sheet. Stress distribution of monolithic glasses is symmetric around the neutral axis of the glass unit. Because of single center of curvature, ‘plane sections remain plane’ assumption is valid for monolithic glass units.

Laminated glass consists of two or more glass sheets connected with an interlayer. Stress distribution of laminated glass is the summation of constant coupling stress of interlayer and the two triangular stress distribution of a layered beam, which is

symmetrical about the neutral axes of each ply. The size of coupling stress is depending on the shear modulus of the interlayer. While coupling stress is compressive at the top ply, it is tensile at the bottom ply.

3.3 Mathematical Model for Laminated Glass Shell Unit

Laminated glass unit consists of two thin glass shells and an interlayer placed in between the glass sheets. The behavior of laminated glass unit which is subjected to the radial pressures is highly nonlinear since the maximum value of radial displacement in the units becomes larger than the thickness of it and shear modulus of the interlayer is very small when compared with that of the glass shell. The effect of nonlinear behavior is considered in the derivation of the field equations and boundary conditions. Because of nonlinearity, the classic assumption that 'plane section before deformation remains plane after deformation' is no longer valid. For this reason, the existing theories can not be employed satisfactorily and a more realistic new model is needed. Therefore, a new nonlinear shell theory has been developed for the analysis of laminated glass shells by using minimum potential energy theorem. The minimum potential energy theorem is a possible tool to obtain the field equations and boundary conditions for the considered problem.

For mathematical modeling of glass shells, the following assumptions are made:

1. The shell material is completely homogenous and isotropic.

2. The material of the shell is elastic and obeys Hooke 's law.

3. Because of small thickness of the shell shear deformation is ignored.

4. Normal to the mid-plane of the shell before deformation remains normal after deformation.

5. For nonlinear behavior, in-plane displacement derivatives are so small that the higher powers of the in-plane displacement derivatives and values of their product are ignored.

6. For nonlinear behavior, membrane stresses are developed in the mid-plane, but are still small when compared with the other shell dimensions. This causes the mid-plane to be stretched under the effect of radial loads.

For the interlayer the following assumptions were made:

1. Plane section before deformation remains plane after deformation.

2. Material is homogenous and isotropic.

3. Material is elastic and obeys Hooke's law and the interlayer shear modulus is constant.

4. Linear shear strains are assumed instead of finite strains to introduce a simplification. The radial deflection of the top ply is considered as that of the bottom ply, because when the radial deflection of the whole system is compared, the interlayer thickness is very small and the compressibility of the interlayer is disregarded.

5. No slip occurs between the adjacent faces of the plies and interlayer.

6. The energy that is stored in the interlayer due to the normal stresses is disregarded as compared to the shear strain energy.

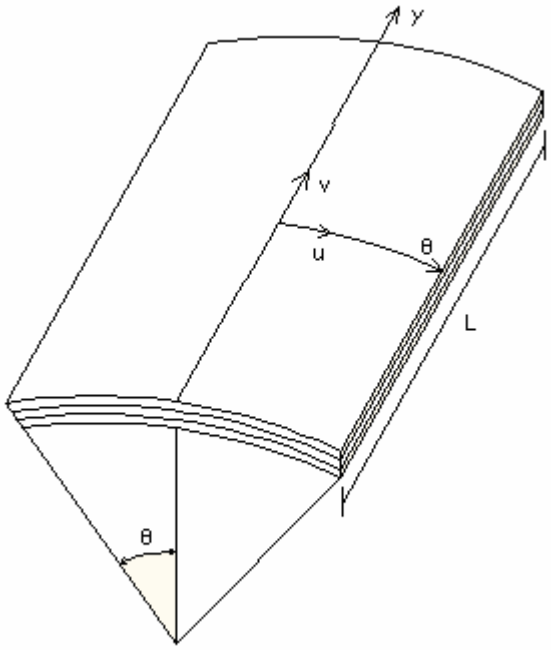

Figure 3.1 Laminated glass cylindrical shell

Laminated cylindrical shell unit and reference axes that are considered in this study are shown in Figure 3.1. Because of symmetry only a quarter part of this shell is taken into consideration.

Using the above assumptions, which are given for glass layers and interlayer, the total potential energy Π of the system, can be written as:

$$\Pi = U + V$$

$$\Pi = U_m^1 + U_m^2 + U_b^1 + U_b^2 + U_{yr}^I + U_{\theta r}^I + \Omega \tag{3.1}$$

where,

U_m^1, U_m^2 = membrane strain energy for the top and bottom shells, respectively,

U_b^1, U_b^2 = bending strain energy for the top and bottom shells, respectively,

U_{yr}^I,$U_{\theta r}^I$ = shear strain energy of the interlayer in y-r and r-θ planes, respectively,

Ω = potential energy function due to applied loads.

According to Langhaar (1962), the bending strain energy functions are given as:

$$U_b^1 = \frac{Eh_1^3 r_1}{24(1-\nu^2)} \int_{-\theta_1}^{\theta_1} \int_{-a}^{a} (\kappa_{1\theta})^2 + (\kappa_{1y})^2 + 2\nu(\kappa_{1\theta})(\kappa_{1y}) + (\frac{1-\nu}{2})(\kappa_{1\theta y})^2)d\theta dy \tag{3.2}$$

$$U_b^2 = \frac{Eh_2^3 r_2}{24(1-\nu^2)} \int_{-\theta_1}^{\theta_1} \int_{-a}^{a} (\kappa_{2\theta})^2 + (\kappa_{2y})^2 + 2\nu(\kappa_{2\theta})(\kappa_{2y}) + (\frac{1-\nu}{2})(\kappa_{2\theta y})^2)d\theta dy \tag{3.3}$$

In the above equation $\kappa_{1\theta}, \kappa_{1y}, \kappa_{1\theta y}$ and $\kappa_{2\theta}, \kappa_{2y}, \kappa_{2\theta y}$ are the bending strains for the top and bottom shells, respectively and they can be expressed as follows:

$$\kappa_{1\theta} = \frac{-w_{\theta\theta}}{r_1^2} \qquad \kappa_{2\theta} = \frac{-w_{\theta\theta}}{r_2^2}$$

$$\kappa_{1y} = -w_{yy} \qquad \kappa_{2y} = -w_{yy}$$

$$\kappa_{1\theta y} = \frac{-2}{r_1} w_{\theta y} \qquad \kappa_{2\theta y} = \frac{-2}{r_2} w_{\theta y}$$

The membrane strain energy functions can be expressed in terms of strains and they are given as follows:

$$U_m^1 = \frac{Eh_1 r_1}{2(1-\nu^2)} \int_{-\theta_1}^{\theta_1} \int_{-a}^{a} (\varepsilon_{1\theta})^2 + (\varepsilon_{1y})^2 + 2\nu(\varepsilon_{1\theta})(\varepsilon_{1y}) + (\frac{1-\nu}{2})(\varepsilon_{1\theta y})^2) d\theta dy \tag{3.4}$$

$$U_m^2 = \frac{Eh_2 r_2}{2(1-\nu^2)} \int_{-\theta_1}^{\theta_1} \int_{-a}^{a} (\varepsilon_{2\theta})^2 + (\varepsilon_{2y})^2 + 2\nu(\varepsilon_{2\theta})(\varepsilon_{2y}) + (\frac{1-\nu}{2})(\varepsilon_{2\theta y})^2) d\theta dy \tag{3.5}$$

where,

$\varepsilon_{1\theta}$, ε_{1y} , $\varepsilon_{1\theta y}$ and $\varepsilon_{2\theta}$, ε_{2y} , $\varepsilon_{2\theta y}$ are the nonlinear membrane strains and for the top and bottom shell units, respectively.They can be expressed in terms of the displacement as follows:

$$\varepsilon_{1\theta} = \frac{u1_\theta + w}{r_1} + \frac{1}{2}\left(\frac{w_\theta}{r_1}\right)^2 \qquad \varepsilon_{2\theta} = \frac{u2_\theta + w}{r_2} + \frac{1}{2}\left(\frac{w_\theta}{r_2}\right)^2$$

$$\varepsilon_{1y} = v1_y + \frac{1}{2}\left(w_y\right)^2 \qquad \varepsilon_{2y} = v2_y + \frac{1}{2}\left(w_y\right)^2$$

$$\varepsilon_{1\theta y} = u1_y + \frac{v1_\theta}{r_1} + \left(\frac{w_\theta w_y}{r_1}\right) \qquad \varepsilon_{2\theta y} = u2_y + \frac{v2_\theta}{r_2} + \left(\frac{w_\theta w_y}{r_2}\right)$$

The average shear strains $\gamma_{\theta r}$ and γ_{yr} are obtained from Figure 2.2 which is plotted to show deformed and undeformed sections of the shell unit

$$\gamma_{\theta r} = \phi_{\theta} + \theta_{\theta}$$

$$\gamma_{\theta r} = \frac{-\partial w}{\partial \theta} + \frac{\partial u}{\partial r}$$

$$\gamma_{\theta r} = (\frac{1}{r_1})\frac{-\partial w}{\partial \theta} + [u1 - u2 - \frac{\partial w}{\partial \theta}(\frac{1}{r_1}\frac{h_1}{2} + \frac{1}{r_2}\frac{h_2}{2}]/t$$

$$\gamma_{\theta r} = \frac{(u1 - u2 - (\frac{1}{r_1}\frac{h_1}{2} + \frac{1}{r_2}\frac{h_2}{2} + \frac{t}{r_1})\frac{\partial w}{\partial \theta})}{t}$$

$$\gamma_{yr} = \phi_{y} + \theta_{y}$$

$$\gamma_{yr} = \frac{-\partial w}{\partial y} + \frac{\partial v}{\partial r}$$

$$\gamma_{yr} = \frac{-\partial w}{\partial y} + [v1 - v2 - \frac{\partial w}{\partial y}(\frac{h_1}{2} + \frac{h_2}{2}]/t$$

$$\gamma_{yr} = \frac{(v1 - v2 - (\frac{h_1}{2} + \frac{h_2}{2} + t)\frac{\partial w}{\partial y})}{t}$$

Making use of the shear strain equations, interlayer shear strain energy expressions are written as:

$$U^{I}_{\theta r} = \int_{0}^{t}\int_{-\theta_1}^{\theta_1}\int_{-a}^{a}\frac{1}{2}G\gamma^{2}_{\theta r}dV$$

$$U^{I}_{\theta r} = \int_{-\theta_I}^{\theta_I}\int_{-a}^{a}\frac{Gtr_I}{2}\left[\frac{(u1-u2-(\frac{1}{r_1}\frac{h_1}{2}+\frac{1}{r_2}\frac{h_2}{2}+\frac{t}{r_1})\frac{\partial w}{\partial\theta})}{t}\right]^{2}d\theta dy \tag{3.6}$$

$$U^{I}_{yr} = \int_{0}^{t}\int_{-\theta_1}^{\theta_1}\int_{-a}^{a}\frac{1}{2}G\gamma^{2}_{yr}dV$$

$$U^{I}_{yr} = \int_{-\theta_I}^{\theta_I}\int_{-a}^{a}\frac{Gtr_I}{2}\left[\frac{(v1-v2-(\frac{h_1}{2}+\frac{h_2}{2}+t)\frac{\partial w}{\partial y})}{t}\right]^{2}d\theta dy \tag{3.7}$$

This problem has a uniformly distributed load and the load potential function can be written as:

$$\Omega = -\int_{-\theta_I}^{\theta_I}\int_{-a}^{a}qwr_I d\theta dy \tag{3.8}$$

where,

i = 1, 2 denotes the top and bottom shells, respectively,

E = Young modulus of the glass shells,

G = interlayer shear modulus,

h_i = thickness of the shell,

r_i = radius of the shell,

ν = Poisson's ratio of the glass,

r_I = radius of the interlayer,

t = thickness of the interlayer,

w = radial deflection of laminated glass unit for the top and bottom shell,

$u1$, $u2$ = circumferential displacements of top and bottom glass shells, respectively.

$v1$, $v2$ = axial displacements of top and bottom glass shells, respectively

The total potential energy Π of the system is written by substituting the Equations (3.2), (3.3), (3.4), (3.5), (3.7) and (3.8) into Equation (3.1).

$$\Pi = \int_{v} (U_m^1 + U_m^2 + U_b^1 + U_b^2 + U_{yr}^I + U_{\theta r}^I + \Omega) dV$$

$$\Pi = \int_{-\theta_1}^{\theta_1} \int_{-a}^{a} F t r d\theta dy$$

Here F can be expressed as:

$$F = \frac{Gr_1}{2t}\left[(u1 - u2 - (\frac{1}{r_1}\frac{h_1}{2} + \frac{1}{r_2}\frac{h_2}{2} + \frac{t}{r_1})\frac{\partial w}{\partial \theta})^2 + (v1 - v2 - (\frac{h_1}{2} + \frac{h_2}{2} + t)\frac{\partial w}{\partial y})^2\right]$$
$$+ \frac{Eh_1^3 r_1}{24(1-\nu^2)}\left[\left(-\frac{w_{\theta\theta}^2}{r_1^2}\right)^2 + \left(-w_{yy}\right)^2 + 2\nu\left(-\frac{w_{\theta\theta}^2}{r_1^2}\right)\left(-w_{yy}\right) + \left(\frac{1-\nu}{2}\right)\left(-\frac{2}{r_1}w_{\theta y}\right)^2\right]$$
$$+ \frac{Eh_1 r_1}{2(1-\nu^2)}\left[\varepsilon_{1\theta}^2 + \varepsilon_{1y}^2 + 2\nu\varepsilon_{1\theta}\varepsilon_{1y} + \frac{(1-\nu)}{2}\varepsilon_{1\theta y}^2\right]$$
$$+ \frac{Eh_2 r_2}{2(1-\nu^2)}\left[\varepsilon_{2\theta}^2 + \varepsilon_{2y}^2 + 2\nu\varepsilon_{2\theta}\varepsilon_{2y} + \frac{(1-\nu)}{2}\varepsilon_{2\theta y}^2\right]$$
$$+ \frac{Eh_2^3 r_2}{24(1-\nu^2)}\left[\left(-\frac{w_{\theta\theta}^2}{r_2^2}\right)^2 + \left(-w_{yy}\right)^2 + 2\nu\left(-\frac{w_{\theta\theta}^2}{r_2^2}\right)\left(-w_{yy}\right) + \left(\frac{1-\nu}{2}\right)\left(-\frac{2}{r_2}w_{\theta y}\right)^2\right] - qwr_1$$

Minimum potential energy theorem, which states that corresponding to the satisfaction of stable equilibrium of all geometric possible configurations of a body is identified by minimum value for the potential energy, and variational approach are used to solve this problem. The total potential energy of the system is written respect to the radial and in plane displacements $u1$, $u2$, $v1$, $v2$ and w. Euler Equation which is given by Langhaar (1962), is applied to the total potential energy to obtain the governing differential equations of the system.

Euler Equation in its most general form is:

$$\frac{\partial F}{\partial u_i} - \frac{\partial}{\partial \theta}\left(\frac{\partial F}{\partial ui_\theta}\right) - \frac{\partial}{\partial y}\left(\frac{\partial F}{\partial ui_y}\right) + \frac{\partial^2}{\partial \theta^2}\left(\frac{\partial F}{\partial ui_{\theta\theta}}\right) + \frac{\partial^2}{\partial \theta \partial y}\left(\frac{\partial F}{\partial ui_{\theta y}}\right) + \frac{\partial^2}{\partial y^2}\left(\frac{\partial F}{\partial ui_{yy}}\right) = 0$$

where,

ui denotes $u1$, $u2$, $v1$, $v2$ and w respectively,

ui_θ is the first derivative of ui with respect to θ,

ui_y is the first derivative of ui with respect to y,

$ui_{\theta\theta}$ is the second derivative of ui with respect to θ,

ui_{yy} is the second derivative of ui with respect to y,

$ui_{\theta y}$ is the second order cross derivative of ui.

Mathematical calculations give the following five nonlinear governing equations of laminated glass shell unit, which are obtained with respect to radial and in-plane displacement:

$$\frac{\partial(N1_{y\theta})}{\partial y} + \frac{1}{r_1}\frac{\partial N1_\theta}{\partial \theta} - \frac{Gr_1}{tr_1}(u1 - u2 - \left(\frac{1}{r_1}\frac{h_1}{2} + \frac{1}{r_2}\frac{h_2}{2} + \frac{t}{r_1}\right)\frac{\partial w}{\partial \theta}) = 0 \qquad (3.9)$$

$$\frac{\partial(N2_{y\theta})}{\partial y} + \frac{1}{r_2}\frac{\partial N2_\theta}{\partial \theta} + \frac{Gr_1}{tr_2}(u1 - u2 - \left(\frac{1}{r_1}\frac{h_1}{2} + \frac{1}{r_2}\frac{h_2}{2} + \frac{t}{r_1}\right)\frac{\partial w}{\partial \theta}) = 0 \qquad (3.10)$$

$$\frac{1}{r_1}\frac{\partial(N1_{y\theta})}{\partial\theta}+\frac{\partial N1_y}{\partial y}-\frac{Gr_1}{tr_1}\left(v1-v2\left(\frac{h_1}{2}+\frac{h_2}{2}+t\right)\frac{\partial w}{\partial y}\right)=0 \tag{3.11}$$

$$\frac{1}{r_2}\frac{\partial(N2_{y\theta})}{\partial\theta}+\frac{\partial N2_y}{\partial y}+\frac{Gr_1}{tr_2}\left(v1-v2_{-}\left(\frac{h_1}{2}+\frac{h_2}{2}+t\right)\frac{\partial w}{\partial y}\right)=0 \tag{3.12}$$

$$\begin{aligned}
&-qr_1+N1_\theta+N1_\theta-\left(N1_y r_1+N2_y r_2\right)\left(\frac{\partial^2 w}{\partial y^2}\right)-\left(\frac{N1_\theta}{r_1}+\frac{N2_\theta}{r_2}\right)\left(\frac{\partial^2 w}{\partial\theta^2}\right)\\
&-\left(2N1_{\theta y}+2N2_{\theta y}\right)\left(\frac{\partial^2 w}{\partial\theta\partial y}\right)\\
&+\frac{Gr_1}{t}\left(\frac{h_1}{2}+\frac{h_2}{2}+t\right)\left(\frac{\partial v1}{\partial y}-\frac{\partial v2}{\partial y}-\left(\frac{h_1}{2}+\frac{h_2}{2}+t\right)\frac{\partial^2 w}{\partial y^2}\right)\\
&+\frac{Gr_1}{t}\left(\frac{1}{r_1}\frac{h_1}{2}+\frac{1}{r_2}\frac{h_2}{2}+\frac{t}{r_1}\right)\left(\frac{\partial u1}{\partial\theta}-\frac{\partial u2}{\partial\theta}-\left(\frac{1}{r_1}\frac{h_1}{2}+\frac{1}{r_2}\frac{h_2}{2}+\frac{t}{r_1}\right)\frac{\partial^2 w}{\partial\theta^2}\right)\\
&+\frac{Gr_1}{t}\left(\frac{1}{r_1}-\frac{1}{r_2}\right)\left[u1-u2-\left(\frac{1}{r_1}\frac{h_1}{2}+\frac{1}{r_2}\frac{h_2}{2}+\frac{t}{r_1}\right)\frac{\partial w}{\partial\theta}\right]\\
&+\frac{Eh_1^3}{12\left(1-\nu^2\right)}\left[r_1\frac{\partial^4 w}{\partial y^4}+\frac{2}{r_1}\frac{\partial^4 w}{\partial y^2\partial\theta^2}+\frac{1}{r_1^3}\frac{\partial^4 w}{\partial\theta^4}\right]\\
&+\frac{Eh_2^3}{12\left(1-\nu^2\right)}\left[r_2\frac{\partial^4 w}{\partial y^4}+\frac{2}{r_2}\frac{\partial^4 w}{\partial y^2\partial\theta^2}+\frac{1}{r_2^3}\frac{\partial^4 w}{\partial\theta^4}\right]=0
\end{aligned} \tag{3.13}$$

where,

$$N1_\theta=\frac{Eh_1}{(1-\nu^2)}(\varepsilon_{1\theta}+\nu\varepsilon_{1y}) \qquad N2_\theta=\frac{Eh_2}{(1-\nu^2)}(\varepsilon_{2\theta}+\nu\varepsilon_{2y})$$

$$N1_y=\frac{Eh_1}{(1-\nu^2)}(\varepsilon_{1y}+\nu\varepsilon_{1\theta}) \qquad N2_y=\frac{Eh_2}{(1-\nu^2)}(\varepsilon_{2y}+\nu\varepsilon_{2\theta})$$

$$N1_{\theta y}=\frac{Eh_1}{2(1+\nu)}(\varepsilon_{1\theta y}) \qquad N2_{\theta y}=\frac{Eh_2}{2(1+\nu)}(\varepsilon_{2\theta y})$$

The governing equations in extended form are as follows.

$$\left(\frac{1}{r_1^2}\frac{\partial^2}{\partial\theta^2}+\frac{1-\nu}{2}\frac{\partial^2}{\partial y^2}-\frac{Gr_1(1-\nu^2)}{Eh_1r_1t}\right)u1=\frac{\partial w}{\partial\theta}\left(\frac{1}{r_1^2}+\frac{1}{r_1^3}\frac{\partial^2 w}{\partial\theta^2}+\frac{(1-\nu)}{2r_1}\frac{\partial^2 w}{\partial y^2}\right)+$$
$$\frac{Gr_1(1-\nu^2)}{Eh_1r_1t}\left(-u2-\left(\frac{1}{r_1}\frac{h_1}{2}+\frac{1}{r_2}\frac{h_2}{2}+\frac{t}{r_1}\right)\frac{\partial w}{\partial\theta}\right)-\frac{\partial w}{\partial y}\frac{\partial^2 w}{\partial\theta\partial y}\left(\frac{1+\nu}{2r_1}\right)-\frac{\partial^2 v1}{\partial\theta\partial y}\left(\frac{1+\nu}{2r_1}\right)$$

$$\left(\frac{1}{r_2^2}\frac{\partial^2}{\partial\theta^2}+\frac{1-\nu}{2}\frac{\partial^2}{\partial y^2}-\frac{Gr_1(1-\nu^2)}{Eh_2r_2t}\right)u2=\frac{Gr_1(1-\nu^2)}{Eh_2r_2t}\left(u1-\left(\frac{1}{r_1}\frac{h_1}{2}+\frac{1}{r_2}\frac{h_2}{2}+\frac{t}{r_1}\right)\frac{\partial w}{\partial\theta}\right)$$
$$-\frac{\partial w}{\partial\theta}\left(\frac{1}{r_2^2}+\frac{1}{r_2^3}\frac{\partial^2 w}{\partial\theta^2}+\frac{(1-\nu)}{2r_2}\frac{\partial^2 w}{\partial y^2}\right)-\frac{\partial w}{\partial y}\frac{\partial^2 w}{\partial\theta\partial y}\left(\frac{1+\nu}{2r_2}\right)-\frac{\partial^2 v2}{\partial\theta\partial y}\left(\frac{1+\nu}{2r_2}\right)$$

$$\left(\frac{\partial^2}{\partial y^2}+\frac{1-\nu}{2r_1^2}\frac{\partial^2}{\partial\theta^2}-\frac{Gr_1(1-\nu^2)}{Eh_1r_1t}\right)v1=\frac{Gr_1(1-\nu^2)}{Eh_1r_1t}\left(-v2-\left(\frac{h_1}{2}+\frac{h_2}{2}+t\right)\frac{\partial w}{\partial y}\right)$$
$$-\frac{\partial w}{\partial y}\left(\frac{\nu}{r_1}+\frac{\partial^2 w}{\partial y^2}+\frac{(1-\nu)}{2r_1^2}\frac{\partial^2 w}{\partial\theta^2}\right)-\frac{\partial w}{\partial\theta}\frac{\partial^2 w}{\partial\theta\partial y}\left(\frac{1+\nu}{2r_1^2}\right)-\frac{\partial^2 u1}{\partial\theta\partial y}\left(\frac{1+\nu}{2r_1}\right)$$

$$\left(\frac{\partial^2}{\partial y^2}+\frac{1-\nu}{2r_2^2}\frac{\partial^2}{\partial\theta^2}-\frac{Gr_1(1-\nu^2)}{Eh_2r_2t}\right)v2=\frac{Gr_1(1-\nu^2)}{Eh_1r_1t}\left(v1-\left(\frac{h_1}{2}+\frac{h_2}{2}+t\right)\frac{\partial w}{\partial y}\right)$$
$$-\frac{\partial w}{\partial y}\left(\frac{\nu}{r_2}+\frac{\partial^2 w}{\partial y^2}+\frac{(1-\nu)}{2r_2^2}\frac{\partial^2 w}{\partial\theta^2}\right)-\frac{\partial w}{\partial\theta}\frac{\partial^2 w}{\partial\theta\partial y}\left(\frac{1+\nu}{2r_2^2}\right)-\frac{\partial^2 u2}{\partial\theta\partial y}\left(\frac{1+\nu}{2r_2}\right)$$

$$\frac{E}{12(1-\nu^2)}\left[\left(\frac{h_1^3}{r_1^3}+\frac{h_2^3}{r_2^3}\right)\frac{\partial^4}{\partial\theta^4}+(r_1h_1^3+r_2h_2^3)\frac{\partial^4}{\partial y^4}+\left(\frac{2h_1^3}{r_1}+\frac{2h_2^3}{r_2}\right)\frac{\partial^4}{\partial y^2\partial\theta^2}\right]w$$

$$+\frac{E}{(1-\nu^2)}\left(\frac{h_1}{r_1}+\frac{h_2}{r_2}\right)w-\frac{Gr_1}{t}\left[\left(\frac{1}{r_1}\frac{h_1}{2}+\frac{1}{r_2}\frac{h_2}{2}+\frac{t}{r_1}\right)^2\frac{\partial^2}{\partial\theta^2}+\left(\frac{h_1}{2}+\frac{h_2}{2}+t\right)^2\frac{\partial^2}{\partial y^2}\right.$$

$$\left.-\left(\frac{1}{r_1}\frac{h_1}{2}+\frac{1}{r_2}\frac{h_2}{2}+\frac{t}{r_1}\right)\left(\frac{1}{r_1}-\frac{1}{r_2}\right)\frac{\partial}{\partial\theta}\right]w=qr_1+\frac{Eh_1}{(1+\nu)}\left[\left(\frac{\partial u1}{\partial y}+\frac{1}{r_1}\frac{\partial v1}{\partial\theta}+\frac{1}{r_1}\frac{\partial w}{\partial\theta}\frac{\partial w}{\partial y}\right)\right]\frac{\partial^2 w}{\partial y\partial\theta}$$

$$+\frac{Eh_2}{(1+\nu)}\left[\left(\frac{\partial u2}{\partial y}+\frac{1}{r_2}\frac{\partial v2}{\partial\theta}+\frac{1}{r_2}\frac{\partial w}{\partial\theta}\frac{\partial w}{\partial y}\right)\right]\frac{\partial^2 w}{\partial y\partial\theta}$$

$$-\frac{Eh_1}{(1-\nu^2)}\left[\left(\frac{1}{r_1}\frac{\partial u1}{\partial\theta}+\frac{1}{2r_1^2}\frac{\partial^2 w}{\partial\theta^2}\right)+\nu\left(\frac{\partial v1}{\partial y}+\frac{1}{2}\frac{\partial^2 w}{\partial y^2}\right)\right]$$

$$-\frac{Eh_2}{(1-\nu^2)}\left[\left(\frac{1}{r_2}\frac{\partial u2}{\partial\theta}+\frac{1}{2r_2^2}\frac{\partial^2 w}{\partial\theta^2}\right)+\nu\left(\frac{\partial v2}{\partial y}+\frac{1}{2}\frac{\partial^2 w}{\partial y^2}\right)\right]$$

$$+\frac{Eh_1}{(1-\nu^2)r_1}\left[\left(\frac{1}{r_1}\frac{\partial u1}{\partial\theta}+\frac{w}{r_1}+\frac{1}{2r_1^2}\frac{\partial^2 w}{\partial\theta^2}\right)+\nu\left(\frac{\partial v1}{\partial y}+\frac{1}{2}\frac{\partial^2 w}{\partial y^2}\right)\right]\frac{\partial^2 w}{\partial\theta^2}$$

$$+\frac{Eh_2}{(1-\nu^2)r_2}\left[\left(\frac{1}{r_2}\frac{\partial u2}{\partial\theta}+\frac{w}{r_2}+\frac{1}{2r_2^2}\frac{\partial^2 w}{\partial\theta^2}\right)+\nu\left(\frac{\partial v2}{\partial y}+\frac{1}{2}\frac{\partial^2 w}{\partial y^2}\right)\right]\frac{\partial^2 w}{\partial\theta^2}$$

$$+\frac{Eh_1}{(1-\nu^2)}\left[\left(\frac{\partial v1}{\partial y}+\frac{1}{2}\frac{\partial^2 w}{\partial y^2}\right)+\nu\left(\frac{1}{r_1}\frac{\partial u1}{\partial\theta}+\frac{w}{r_1}+\frac{1}{2r_1^2}\frac{\partial^2 w}{\partial\theta^2}\right)\right]\frac{\partial^2 w}{\partial y^2}$$

$$+\frac{Eh_2}{(1-\nu^2)}\left[\left(\frac{\partial v2}{\partial y}+\frac{1}{2}\frac{\partial^2 w}{\partial y^2}\right)+\nu\left(\frac{1}{r_2}\frac{\partial u2}{\partial\theta}+\frac{w}{r_2}+\frac{1}{2r_2^2}\frac{\partial^2 w}{\partial\theta^2}\right)\right]\frac{\partial^2 w}{\partial y^2}$$

$$-\frac{Gr_1}{t}\left(\frac{h_1}{2}+\frac{h_2}{2}+t\right)\left(\frac{\partial v1}{\partial y}-\frac{\partial v2}{\partial y}\right)-\frac{Gr_1}{t}\left(\frac{1}{r_1}\frac{h_1}{2}+\frac{1}{r_2}\frac{h_2}{2}+\frac{t}{r_1}\right)\left(\frac{\partial u1}{\partial\theta}-\frac{\partial u2}{\partial\theta}\right)$$

$$+\frac{Gr_1}{t}\left(\frac{1}{r_1}-\frac{1}{r_2}\right)(u1-u2)$$

In the above equations, the left hand side contains only the linear terms. All the nonlinear terms are collected on the right hand side of the equation to be able to employ the iterative finite difference method which will be presented in the next chapter.

Because of symmetry, only a quarter of the shell is considered. For the case of fixed supported shell subjected to uniform pressure, the obtained boundary conditions are as follows. And the pictorial presentation of boundary conditions of fixed supported cylindrical shell is given Figure 3.2.

Boundary Condition along the centerline θ=0

$u1 = 0 \quad u2 = 0 \quad \frac{\partial v1}{\partial \theta} = 0 \quad \frac{\partial v2}{\partial \theta} = 0 \quad \frac{\partial \mathrm{w}}{\partial \theta} = 0$ Symmetry

Boundary Condition along the edge θ=θ_1

$u1 = 0 \quad u2 = 0 \quad v1 = 0 \quad v2 = 0 \quad \mathrm{w} = 0 \quad \frac{\partial \mathrm{w}}{\partial \theta} = 0$

Boundary Condition along the centerline y=0

$\frac{\partial u1}{\partial y} = 0 \quad \frac{\partial u2}{\partial y} = 0 \quad v1 = 0 \quad v2 = 0 \quad \frac{\partial \mathrm{w}}{\partial \mathrm{y}} = 0$ Symmetry

Boundary Condition along the edge y=y_1

$u1 = 0 \quad u2 = 0 \quad v1 = 0 \quad v2 = 0 \quad \mathrm{w} = 0 \quad \frac{\partial \mathrm{w}}{\partial \mathrm{y}} = 0$

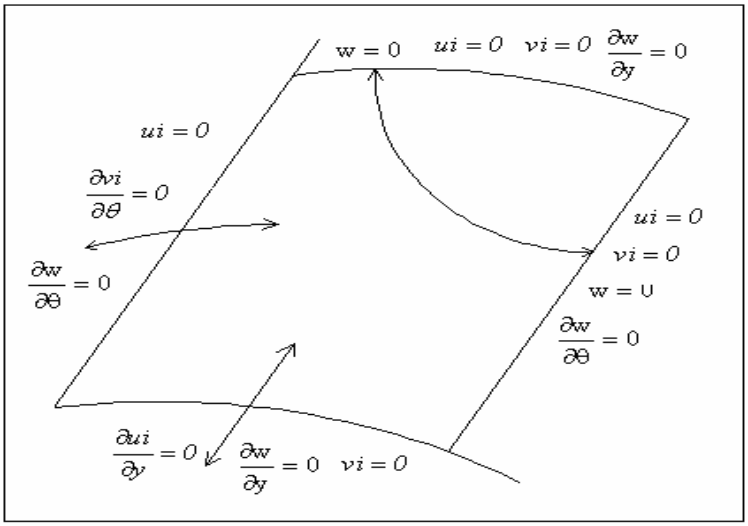

Figure 3.2 Pictorial presentation of boundary conditions for the fixed supported laminated cylindrical glass shell

3.4 Finite Difference Expressions for Field and Boundary Equations and The Iterative Solution Technique

3.4.1 Application of Finite Difference Method (FDM)

Due to symmetry of geometry only one quarter of the shell is considered in the analysis. The governing differential equations of laminated glass shell unit are given in Equations 3.7 through 3.11. It is found that the differential equations of *u1, u2, v1 and v2* are linear while the field equation for radial displacement , w, is nonlinear. Close form solution of these nonlinear governing differential equations is not known. Therefore, to solve the equations an iterative technique has to be adopted.

Finite difference method is used to convert the governing differential equations into discrete values of *u1, u2, v1, v2* and *w* at every point of the finite difference mesh. Nonlinear partial differential equations are arranged in such a way that the left-hand side of the governing equations becomes linear; all the nonlinear terms are collected on the right hand side of the equality. The equations in the matrix form are obtained for radial and in-plane displacements. While full coefficient matrices are obtained for in-plane displacements, symmetric banded coefficient matrix is obtained for radial displacement. Because of the large memory necessity, the modified strongly implicit procedure, which was proposed by Schneider and Zedan (1981) is employed for the in plane displacements.

The algebraic equations for the radial displacement are stored in matrix A. Therefore, the system of equation can be written as:

$$[A]\{w\} = \{q + f_1(w,u1,u2,v1,v2)\}$$

where,

$\{w\}$ = the radial displacement vector,

q= applied pressure magnitude,

[A] = coefficient matrix for radial displacement.

[A] is symmetric and banded coefficient matrix, and the elements are stored in banded forms. The right-hand side vector includes applied load and the other terms calculated at every point inside the domain.

In this chapter, the coefficient matrices, and the corresponding right-hand side vectors inside the domain as well as those at the boundaries are presented. For the radial deflection, the finite difference mesh size is chosen to be n_θ x n_y, where n_θ and n_y being the number of subdivisions in the θ and y directions, respectively. The size of coefficient matrix A is ($n_\theta n_y$, $2n_\theta+1$). In order to reduce the total number of equations the radial deflection value at the fixed supported edges which is zero, is not incorporated. Finite difference expression for radial deflection field equation inside the domain is:

For i=3,4,...n_θ-2, j=3,4,...n_y-2

$$Cw_{i,j} + Bw_{i+1,j} + Bw_{i-1,j} + Hw_{i+2,j} + Hw_{i-2,j} + Jw_{i,j+1} + Jw_{i,j-1} + Gw_{i,j+2} + Gw_{i,j-2} + Fw_{i+1,j+1} + Fw_{i+1,j-1} + Fw_{i-1,j+1} + Fw_{i-1,j-1} = RHS_{i,j} \tag{3.14}$$

where,

$$C = \frac{E\left(h_1^3 r_1 + h_2^3 r_2\right)}{2\left(1-\nu^2\right)h_y^4} + \frac{E}{2\left(1-\nu^2\right)h_\theta^4}\left(\frac{h_1^3}{r_1^3} + \frac{h_2^3}{r_2^3}\right) + \frac{4E}{6\left(1-\nu^2\right)h_\theta^2 h_y^2}\left(\frac{h_1^3}{r_1} + \frac{h_2^3}{r_2}\right)$$
$$+ \frac{E}{\left(1-\nu^2\right)}\left[\frac{h_1}{r_1} + \frac{h_2}{r_2}\right] + \frac{2Gr_1}{th_y^2}\left(\frac{h_1}{2} + \frac{h_2}{2} + t\right)^2 + \frac{2Gr_1}{th_\theta^2}\left(\frac{1}{r_1}\frac{h_1}{2} + \frac{1}{r_2}\frac{h_2}{2} + \frac{t}{r_1}\right)^2$$

$$J = \frac{-4E\left(h_1^3 r_1 + h_2^3 r_2\right)}{12\left(1-\nu^2\right)h_y^4} - \frac{4E}{12\left(1-\nu^2\right)h_\theta^2 h_y^2}\left(\frac{h_1^3}{r_1} + \frac{h_2^3}{r_2}\right) - \frac{Gr_1}{th_y^2}\left(\frac{h_1}{2} + \frac{h_2}{2} + t\right)^2$$

$$G = \frac{E\left(h_1^3 r_1 + h_2^3 r_2\right)}{12\left(1-\nu^2\right)h_y^4}$$

$$H = \frac{E}{12\left(1-\nu^2\right)h_\theta^4}\left(\frac{h_1^3}{r_1^3} + \frac{h_2^3}{r_2^3}\right)$$

$$B = \frac{-4E}{12(1-\nu^2)h_\theta^4}\left(\frac{h_1^3}{r_1^3}+\frac{h_2^3}{r_2^3}\right)-\frac{4E}{12(1-\nu^2)h_\theta^2 h_y^2}\left(\frac{h_1^3}{r_1}+\frac{h_2^3}{r_2}\right)$$
$$-\frac{Gr_1}{th_\theta^2}\left(\frac{1}{r_1}\frac{h_1}{2}+\frac{1}{r_2}\frac{h_2}{2}+\frac{t}{r_1}\right)^2-\frac{Gr_1}{2th_\theta}\left(\frac{1}{r_1}-\frac{1}{r_2}\right)\left(\frac{1}{r_1}\frac{h_1}{2}+\frac{1}{r_2}\frac{h_2}{2}+\frac{t}{r_1}\right)$$

$$F = \frac{E}{6(1-\nu^2)h_\theta^2 h_y^2}\left(\frac{h_1^3}{r_1}+\frac{h_2^3}{r_2}\right)$$

$$RHS_{i,j} = \frac{Eh_1}{(1-\nu^2)}\left[\frac{1}{r_1}(\varepsilon_{1\theta}+\nu\varepsilon_{1y})\frac{\partial^2 w}{\partial\theta^2}+r_1(\varepsilon_{1y}+\nu\varepsilon_{1\theta})\frac{\partial^2 w}{\partial y^2}+(1-\nu)\varepsilon_{1\theta y}\frac{\partial^2 w}{\partial\theta\partial y}\right]$$
$$+\frac{Eh_2}{(1-\nu^2)}\left[\frac{1}{r_2}(\varepsilon_{2\theta}+\nu\varepsilon_{2y})\frac{\partial^2 w}{\partial\theta^2}+r_2(\varepsilon_{2y}+\nu\varepsilon_{2\theta})\frac{\partial^2 w}{\partial y^2}+(1-\nu)\varepsilon_{2\theta y}\frac{\partial^2 w}{\partial\theta\partial y}\right]$$
$$-\frac{Eh_1}{(1-\nu^2)}\left[\left(\frac{1}{r_1}\frac{\partial u1}{\partial\theta}+\frac{1}{2r_1^2}\frac{\partial^2 w}{\partial\theta^2}\right)+\nu\left(\frac{\partial v1}{\partial y}+\frac{1}{2}\frac{\partial^2 w}{\partial y^2}\right)\right]$$
$$-\frac{Eh_2}{(1-\nu^2)}\left[\left(\frac{1}{r_2}\frac{\partial u2}{\partial\theta}+\frac{1}{2r_2^2}\frac{\partial^2 w}{\partial\theta^2}\right)+\nu\left(\frac{\partial v2}{\partial y}+\frac{1}{2}\frac{\partial^2 w}{\partial y^2}\right)\right]$$
$$-\frac{Gr_1}{t}\left(\frac{1}{r_1}\frac{h_1}{2}+\frac{1}{r_2}\frac{h_2}{2}+\frac{t}{r_1}\right)\left(\frac{\partial u1}{\partial\theta}-\frac{\partial u2}{\partial\theta}\right)-\frac{Gr_1}{t}\left(\frac{h_1}{2}+\frac{h_2}{2}+t\right)\left(\frac{\partial v1}{\partial y}-\frac{\partial v2}{\partial y}\right)$$
$$-\frac{Gr_1}{t}\left(\frac{1}{r_1}-\frac{1}{r_2}\right)(u1-u2)+qr_1$$

The general equation is modified at the shell boundaries and the following equations are obtained for fixed supported shell:

<u>For i=1, j=1</u>

$$\frac{C}{4}w_{i,j}+\frac{B}{2}w_{i+1,j}+\frac{H}{2}w_{i+2,j}+\frac{J}{2}w_{i,j+1}+\frac{G}{2}w_{i,j+2}+Fw_{i+1,j+1}=\frac{RHS_{i,j}}{4}$$

For i=1, j=2

$$\frac{C+G}{2}w_{i,j} + Bw_{i+1,j} + Hw_{i+2,j} + \frac{J}{2}w_{i,j-1} + \frac{J}{2}w_{i,j+1} + \frac{G}{2}w_{i,j+2} + Fw_{i+1,j+1} + Fw_{i+1,j-1} = \frac{RHS_{i,j}}{2}$$

For i=1, j=3,4,...n_y-1

$$\frac{C}{2}w_{i,j} + Bw_{i+1,j} + Hw_{i+2,j} + \frac{J}{2}w_{i,j-1} + \frac{J}{2}w_{i,j+1} + \frac{G}{2}w_{i,j+2} + \frac{G}{2}w_{i,j-2} + Fw_{i+1,j+1} + Fw_{i+1,j-1} = \frac{RHS_{i,j}}{2}$$

For i=1, j=n_y

$$\frac{C+G}{2}w_{i,j} + Bw_{i+1,j} + Hw_{i+2,j} + \frac{J}{2}w_{i,j-1} + \frac{G}{2}w_{i,j-2} + Fw_{i+1,j-1} = \frac{RHS_{i,j}}{2}$$

For i=2, j=1

$$\frac{C+H}{2}w_{i,j} + \frac{B}{2}w_{i+1,j} + \frac{H}{2}w_{i+2,j} + \frac{B}{2}w_{i-1,j} + Gw_{i,j+2} + Jw_{i,j+1} + Fw_{i+1,j+1} + Fw_{i-1,j+1} = \frac{RHS_{i,j}}{2}$$

For i=2, j=2

$$(C+G+H)w_{i,j} + Bw_{i+1,j} + Bw_{i-1,j} + Hw_{i+2,j} + Jw_{i,j+1} + Jw_{i,j-1} + Gw_{i,j-2} + Fw_{i+1,j+1} + Fw_{i+1,j-1} + Fw_{i-1,j+1} + Fw_{i-1,j-1} = RHS_{i,j}$$

For i=2, j=3,4,....n_y-2

$$(C+H)w_{i,j} + Bw_{i+1,j} + Bw_{i-1,j} + Hw_{i+2,j} + Jw_{i,j+1} + Jw_{i,j-1} + Gw_{i,j-2} + Gw_{i,j+2} + Fw_{i+1,j+1} + Fw_{i+1,j-1} + Fw_{i-1,j+1} + Fw_{i-1,j-1} = RHS_{i,j}$$

For i=2, j=n_y-1

$$(C+H)w_{i,j} + Bw_{i+1,j} + Bw_{i-1,j} + Hw_{i+2,j} + Jw_{i,j+1} + Jw_{i,j-1} + Gw_{i,j-2} + Fw_{i+1,j+1} + Fw_{i+1,j-1} + Fw_{i-1,j+1} + Fw_{i-1,j-1} = RHS_{i,j}$$

For i=2, j=n_y

$$(C+G+H)w_{i,j} + Bw_{i+1,j} + Bw_{i-1,j} + Hw_{i+2,j} + Jw_{i,j-1} + Gw_{i,j-2} + Fw_{i+1,j-1} + Fw_{i-1,j-1} = RHS_{i,j}$$

For i=3,4…. .n_θ-2, j=1

$$\frac{C}{2}w_{i,j} + \frac{B}{2}w_{i+1,j} + \frac{B}{2}w_{i-1,j} + \frac{H}{2}w_{i+2,j} + \frac{H}{2}w_{i-2,j} + Jw_{i,j+1} + Gw_{i,j+2} + Fw_{i+1,j+1} + Fw_{i-1,j+1} = \frac{RHS_{i,j}}{2}$$

For i=n_θ-1, j=1

$$\frac{C}{2}w_{i,j} + \frac{B}{2}w_{i-1,j} + \frac{B}{2}w_{i+1,j} + \frac{H}{2}w_{i-2,j} + Jw_{i,j+1} + Gw_{i,j+2} + Fw_{i-1,j+1} + Fw_{i+1,j+1} = \frac{RHS_{i,j}}{2}$$

For i=n_θ-1, j=3,4...n_y-2

$$Cw_{i,j} + Bw_{i+1,j} + Bw_{i-1,j} + Hw_{i-2,j} + Jw_{i,j+1} + Jw_{i,j-1} + Gw_{i,j-2} + Gw_{i,j+2} + Fw_{i+1,j+1} + Fw_{i+1,j-1} + Fw_{i-1,j+1} + Fw_{i-1,j-1} = RHS_{i,j}$$

For i=n_θ, j=3,4,...n_y-2

$$(C+H)w_{i,j} + Bw_{i-1,j} + Hw_{i-2,j} + Jw_{i,j+1} + Jw_{i,j-1} + Gw_{i,j-2} + Gw_{i,j+2} + Fw_{i-1,j+1} + Fw_{i-1,j-1} = RHS_{i,j}$$

For i=n_θ, j=n_y-1

$$(C+H)w_{i,j} + Bw_{i-1,j} + Hw_{i-2,j} + Jw_{i,j+1} + Jw_{i,j-1} + Gw_{i,j-2} + Fw_{i-1,j+1} + Fw_{i-1,j-1} = RHS_{i,j}$$

For i=n_θ, j=1

$$(\frac{C+H}{2})w_{i,j} + \frac{B}{2}w_{i-1,j} + \frac{H}{2}w_{i-2,j} + Jw_{i,j+1} + Gw_{i,j+2} + Fw_{i-1,j+1} = \frac{RHS_{i,j}}{2}$$

For i=n_θ-1, j=2

$$(C+G)w_{i,j} + Bw_{i-1,j} + Bw_{i-1,j} + Hw_{i-2,j} + Jw_{i,j+1} + Jw_{i,j-1} + Gw_{i,j+2} + Fw_{i-1,j+1}$$
$$+ Fw_{i-1,j-1} + Fw_{i+1,j+!} + Fw_{i+1,j-1} = RHS_{i,j}$$

For i=n_θ, j=2

$$(C+G+H)w_{i,j} + Bw_{i-1,j} + Hw_{i-2,j} + Jw_{i,j+1} + Jw_{i,j-1} + Gw_{i,j+2} + Fw_{i-1,j+1} +$$
$$Fw_{i-1,j-1} = RHS_{i,j}$$

For i=n_θ, j=n_y

$$(C+G+H)w_{i,j} + Bw_{i-1,j} + Hw_{i-2,j} + Jw_{i,j-1} + Gw_{i,j-2} + Fw_{i-1,j-1} = RHS_{i,j}$$

For i=n_θ-1, j=n_y-1

$$Cw_{i,j} + Bw_{i+1,j} + Bw_{i-1,j} + Hw_{i-2,j} + Jw_{i,j+1} + Jw_{i,j-1} + Gw_{i,j-2} + Fw_{i+1,j+1} + Fw_{i+1,j-1}$$
$$+ Fw_{i-1,j+1} + Fw_{i-1,j-1} = RHS_{i,j}$$

For i=3,4,...n_θ-2, j=2

$$(C+G)w_{i,j} + Bw_{i+1,j} + Bw_{i-1,j} + Hw_{i-2,j} + Hw_{i+2,j} + Jw_{i,j+1} + Jw_{i,j-1} + Gw_{i,j+2}$$
$$+ Fw_{i+1,j+1} + Fw_{i+1,j-1} + Fw_{i-1,j+1} + Fw_{i-1,j-1} = RHS_{i,j}$$

For i=3,4,...n_θ-2, j=n_y-1

$$Cw_{i,j} + Bw_{i+1,j} + Bw_{i-1,j} + Hw_{i-2,j} + Hw_{i+2,j} + Jw_{i,j+1} + Jw_{i,j-1} + Gw_{i,j-2} + Fw_{i+1,j+1} + Fw_{i+1,j-1} + Fw_{i-1,j+1} + Fw_{i-1,j-1} = RHS_{i,j}$$

For i=3,4,...n_θ-2, j=n_y

$$(C+G)w_{i,j} + Bw_{i+1,j} + Bw_{i-1,j} + Hw_{i-2,j} + Hw_{i+2,j} + Jw_{i,j-1} + Gw_{i,j+-2} + Fw_{i+1,j-1} + Fw_{i-1,j-1} = RHS_{i,j}$$

For i=n_θ-1, j=n_y

$$(C+G)w_{i,j} + Bw_{i+1,j} + Bw_{i-1,j} + Hw_{i-2,j} + Jw_{i,j-1} + Gw_{i,j-2} + Fw_{i+1,j-1} + Fw_{i-1,j-1} = RHS_{i,j}$$

Equations (3.13)-(3.16) given below are modified at the boundaries of the laminated unit with respect to boundary conditions. Because of the nature of the problem, full coefficient matrices are obtained for circumferential and axial displacements. To provide decrease in computation time and storage Asik (2003) stored the coefficients of circumferential and axial displacement as column vectors. To obtain the circumferential and axial displacement Modified Strongly Implicit Method (MSI), which is proposed by Schinder and Zedan (1981), is employed.

Finite difference mesh size for the in-plane displacement is $n_\theta \times n_y$. If full coefficient matrix is used to obtain the axial and circumferential displacement total number of elements of coefficient matrix will be $2\times(n_\theta+1)^2\times(n_y+1)^2$. But if the coefficients are stored in vectors and MSI method is employed to obtain the circumferential and axial displacements, total number of elements in coefficient vectors will be $2\times5\times(n_\theta+1)\times(n_y+1)$.

$$APU1_{(i,j)}\,u1_{(i,j)} = ASU1_{(i,j)}\,u1_{(i,j-1)} + ANU1_{(i,j)}\,u1_{(i,j+1)} + AWU1_{(i,j)}\,u1_{(i-1,j)} + AEU1_{(i,j)}\,u1_{(i+1,j)} - FU1(i,j) \tag{3.15}$$

$$APU2_{(i,j)}\,u2_{(i,j)} = ANU2_{(i,j)}\,u2_{(i,j+1)} + ASU2_{(i,j)}\,u2_{(i,j-1)} + AWU2_{(i,j)}\,u2_{(i-1,j)} + AEU2_{(i,j)}\,u2_{(i+1,j)} - FU2(i,j) \tag{3.16}$$

$$APV1_{(i,j)}\,v1_{(i,j)} = ASV1_{(i,j)}\,v1_{(i,j-1)} + ANV1_{(i,j)}\,v1_{(i,j+1)} + AWV1_{(i,j)}\,v1_{(i-1,j)} + AEV1_{(i,j)}\,v1_{(i+1,j)} - FV1(i,j) \tag{3.17}$$

$$APV2_{(i,j)}\,v2_{(i,j)} = ASV2_{(i,j)}\,v2_{(i,j-1)} + ANV2_{(i,j)}\,v2_{(i,j+1)} + AWV2_{(i,j)}\,v2_{(i-1,j)} + AEV2_{(i,j)}\,v2_{(i+1,j)} - FV2(i,j) \tag{3.18}$$

where

$$APU1_{(i,j)} = \frac{(1-\nu)}{h_y^2} + \frac{2}{r_1^2 h_\theta^2} + \frac{G(1-\nu^2)r_1}{Eh_1\,tr_1}$$

$$AWU1_{(i,j)} = AEU1_{(i,j)} = \frac{1}{r_1^2 h_\theta^2}$$

$$ANU1_{(i,j)} = ASU1_{(i,j)} = \frac{(1-\nu)}{2h_y^2}$$

$$APV1_{(i,j)} = +\frac{(1-\nu)}{h_\theta^2 r_1^2} + \frac{2}{h_y^2} + \frac{G(1-\nu^2)r_1}{Eh_1 tr_1}$$

$$AWV1_{(i,j)} = AEV1_{(i,j)} = \frac{(1-\nu)}{2r_1^2 h_\theta^2}$$

$$ASV1_{(i,j)} = ANV1_{(i,j)} = \frac{1}{h_y^2}$$

$$APU2_{(i,j)} = +\frac{(1-\nu)}{h_y^2} + \frac{2}{r_2^2 h_\theta^2} + \frac{G(1-\nu^2)r_1}{Eh_2\,tr_2}$$

$$AWU2_{(i,j)} = AEU2_{(i,j)} = \frac{1}{r_2^2 h_\theta^2}$$

$$ANU2_{(i,j)} = ASU2_{(i,j)} = \frac{(1-\nu)}{2h_y^2}$$

$$APV2_{(i,j)} = +\frac{(1-\nu)}{h_\theta^2 r_2^2} + \frac{2}{h_y^2} + \frac{G(1-\nu^2)r_1}{Eh_2 t r_2}$$

$$AWV2_{(i,j)} = AEV2_{(i,j)} = \frac{(1-\nu)}{2r_2^2 h_\theta^2}$$

$$ASV2_{(i,j)} = ANV2_{(i,j)} = \frac{1}{h_y^2}$$

$$FU1(i,j) = \frac{G(1-\nu^2)r_1}{Eh_2 t r_2}[-u2 - (\frac{1}{r_1}\frac{h_1}{2} + \frac{1}{r_2}\frac{h_2}{2} + \frac{t}{r_1})\frac{\partial w}{\partial \theta}] - w_y w_{\theta y}\left(\frac{1+\nu}{2r_2^2}\right)$$
$$- w_\theta\left(w_{\theta\theta} + \frac{\nu}{r_1} + \frac{(1-\nu)w_{yy}}{2r_1^2}\right) - v2_{\theta y}\left(\frac{1+\nu}{2r_1}\right)$$

$$FU2(i,j) = \frac{G(1-\nu^2)r_1}{Eh_2 t r_2}[u1 - (\frac{1}{r_1}\frac{h_1}{2} + \frac{1}{r_2}\frac{h_2}{2} + \frac{t}{r_1})\frac{\partial w}{\partial \theta}] - w_y w_{\theta y}\left(\frac{1+\nu}{2r_1^2}\right)$$
$$- w_\theta\left(w_{\theta\theta} + \frac{\nu}{r_2} + \frac{(1-\nu)w_{yy}}{2r_2^2}\right) - v2_{\theta y}\left(\frac{1+\nu}{2r_2}\right)$$

$$FV1(i,j) = \frac{G(1-\nu^2)r_1}{Eh_1 t r_1}[-v2 - (\frac{h_1}{2} + \frac{h_2}{2} + t)\frac{\partial w}{\partial y}] - w_\theta w_{\theta y}\left(\frac{1+\nu}{2r_1^2}\right)$$
$$- w_y\left(w_{yy} + \frac{\nu}{r_1} + \frac{(1-\nu)w_{\theta\theta}}{r_1^2}\right) - u1_{\theta y}\left(\frac{1+\nu}{2r_1}\right)$$

$$FV2(i,j) = \frac{G(1-\nu^2)r_1}{Eh_2 t r_2}[v1 - (\frac{h_1}{2} + \frac{h_2}{2} + t)\frac{\partial w}{\partial y}] - w_\theta w_{\theta y}\left(\frac{1+\nu}{2r_2^2}\right)$$
$$- w_y\left(w_{yy} + \frac{\nu}{r_2} + \frac{(1-\nu)w_{\theta\theta}}{r_2^2}\right) - u2_{\theta y}\left(\frac{1+\nu}{2r_2}\right)$$

In the above equations h_θ is the increment in θ direction and h_y is the increment in y direction. $FU1(i,j), FU2(i,j), FV1(i,j)$ and $FV2(i,j)$ are the right hand sides of

governing equations of $u1$, $u2$, $v1$ and $v2$, respectively at each discrete point. These are the governing equations and boundary conditions for the cylindrical shell. The general equations for circumferential displacement (u1) are modified at the shell boundaries and the following equations are obtained for fixed supported shell:

For i=2, j=1

$$APU1_{(i,j)}u1_{(i,j)} + \left(ANU1_{(i,j)} + ASU1_{(i,j)}\right)u1_{(i,j+1)} + AEU1_{(i,j)}u1_{(i+1,j)} = FU1_{(i,j)}$$

For i=3,4,….n_θ-1, j=1

$$APU1_{(i,j)}u1_{(i,j)} + \left(ANU1_{(i,j)} + ASU1_{(i,j)}\right)u1_{(i,j+1)} + AEU1_{(i,j)}u1_{(i+1,j)} + AWU1_{(i,j)}u1_{(i+1,j)} = FU1_{(i,j)}$$

For i=n_θ, j=1

$$APU1_{(i,j)}u1_{(i,j)} + \left(ANU1_{(i,j)} + ASU1_{(i,j)}\right)u1_{(i,j+1)} + AWU1_{(i,j)}u1_{(i+1,j)} = FU1_{(i,j)}$$

For i=2, j=2,3,…..n_y-1

$$APU1_{(i,j)}u1_{(i,j)} + ANU1_{(i,j)}u1_{(i,j+1)} + ASU1_{(i,j)}u1_{(i,j-1)} + AEU1_{(i,j)}u1_{(i+1,j)} = FU1_{(i,j)}$$

For i=2, j=n_y

$$APU1_{(i,j)}u1_{(i,j)} + ASU1_{(i,j)}u1_{(i,j-1)} + AEU1_{(i,j)}u1_{(i+1,j)} = FU1_{(i,j)}$$

For i=3,4,….n_θ-1 . j=2,3,…..n_y-1

$$APU1_{(i,j)}u1_{(i,j)} + ANU1_{(i,j)}u1_{(i,j+1)} + ASU1_{(i,j)}u1_{(i,j-1)} + AWU1_{(i,j)}u1_{(i-1,j)} + AEU1_{(i,j)}u1_{(i+1,j)} = FU1_{(i,j)}$$

For i=3,4,….n_θ-1, j= n_y

$$APU1_{(i,j)}u1_{(i,j)} + ASU1_{(i,j)}u1_{(i,j-1)} + AWU1_{(i,j)}u1_{(i-1,j)} + AEU1_{(i,j)}u1_{(i+1,j)} = FU1_{(i,j)}$$

For i=n_θ, j=2,3,…..n_y-1

$$APU1_{(i,j)}u1_{(i,j)} + ANU1_{(i,j)}u1_{(i,j+1)} + ASU1_{(i,j)}u1_{(i,j-1)} + AWU1_{(i,j)}u1_{(i-1,j)} = FU1_{(i,j)}$$

For i=n_θ, j=n_y

$$APU1_{(i,j)}u1_{(i,j)} + ASU1_{(i,j)}u1_{(i,j-1)} + AWU1_{(i,j)}u1_{(i-1,j)} = FU1_{(i,j)}$$

The general equations for circumferential displacement (u2) are obtained for fixed supported shell as follows:

For i=2, j=1

$$APU2_{(i,j)}u2_{(i,j)} + \left(ANU2_{(i,j)} + ASU2_{(i,j)}\right)u2_{(i,j+1)} + AEU2_{(i,j)}u2_{(i+1,j)} = FU2_{(i,j)}$$

For i=3,4,….n_θ-1, j=1

$$APU2_{(i,j)}u2_{(i,j)} + \left(ANU2_{(i,j)} + ASU2_{(i,j)}\right)u2_{(i,j+1)} + AEU2_{(i,j)}u2_{(i+1,j)} + AWU2_{(i,j)}u2_{(i+1,j)} = FU2_{(i,j)}$$

For i=n_θ, j=1

$$APU2_{(i,j)}u2_{(i,j)} + \left(ANU2_{(i,j)} + ASU2_{(i,j)}\right)u2_{(i,j+1)} + AWU2_{(i,j)}u2_{(i+1,j)} = FU2_{(i,j)}$$

For i=2, j=2,3,…..n_y-1

$$APU2_{(i,j)}u2_{(i,j)} + ANU2_{(i,j)}u2_{(i,j+1)} + ASU2_{(i,j)}u2_{(i,j-1)} + AEU2_{(i,j)}u2_{(i+1,j)} = FU2_{(i,j)}$$

For i=2, j=n_y

$$APU2_{(i,j)}u2_{(i,j)} + ASU2_{(i,j)}u2_{(i,j-1)} + AEU2_{(i,j)}u2_{(i+1,j)} = FU2_{(i,j)}$$

For i=3,4,….n_θ-1 . j=2,3,…..n_y-1

$$APU2_{(i,j)}u2_{(i,j)} + ANU2_{(i,j)}u2_{(i,j+1)} + ASU2_{(i,j)}u2_{(i,j-1)} + AWU2_{(i,j)}u2_{(i-1,j)} + AEU2_{(i,j)}u2_{(i+1,j)} = FU2_{(i,j)}$$

For i=3,4,….n_θ-1, j= n_y

$$APU2_{(i,j)}u2_{(i,j)} + ASU2_{(i,j)}u2_{(i,j-1)} + AWU2_{(i,j)}u2_{(i-1,j)} + AEU2_{(i,j)}u2_{(i+1,j)} = FU2_{(i,j)}$$

For i=n_θ, j=2,3,…..n_y-1

$$APU2_{(i,j)}u2_{(i,j)} + ANU2_{(i,j)}u2_{(i,j+1)} + ASU2_{(i,j)}u2_{(i,j-1)} + AWU2_{(i,j)}u2_{(i-1,j)} = FU2_{(i,j)}$$

For i=n_θ, j=n_y

$$APU\ 2_{(i,j)}u2_{(i,j)} + ASU\ 2_{(i,j)}u2_{(i,j-1)} + AWU\ 2_{(i,j)}u2_{(i-1,j)} = FU\ 2_{(i,j)}$$

Modified axial displacement (v1) at the shell boundaries are obtained for fixed supported shell as follows:

For i=1, j=2

$$APV1_{(i,j)}v1_{(i,j)} + ANV1_{(i,j)}v1_{(i,j+1)} + \left(AEV1_{(i,j)} + AWV1_{(i,j)}\right)v1_{(i+1,j)} = FV1_{(i,j)}$$

For i=2,3,….n_θ-1, j=2

$$APV1_{(i,j)}v1_{(i,j)} + ANV1_{(i,j)}v1_{(i,j+1)} + AWV1_{(i,j)}v1_{(i-1,j)} + AEV1_{(i,j)}v1_{(i+1,j)} = FV1_{(i,j)}$$

For i=n_θ, j=2

$$APV1_{(i,j)}v1_{(i,j)} + ANV1_{(i,j)}v1_{(i,j+1)} + AWV1_{(i,j)}v1_{(i-1,j)} = FV1_{(i,j)}$$

For i=1, j=3,4,…..n_y-1

$$APV1_{(i,j)}v1_{(i,j)} + ASV1_{(i,j)}v1_{(i,j-1)} + ANV1_{(i,j)}v1_{(i,j+1)} + \left(AEV1_{(i,j)} + AWV1_{(i,j)}\right)v1_{(i+1,j)} = FV1_{(i,j)}$$

For i=1, j=n_y

$$APV1_{(i,j)}v1_{(i,j)} + ASV1_{(i,j)}v1_{(i,j-1)} + \left(AEV1_{(i,j)} + AWV1_{(i,j)}\right)v1_{(i+1,j)} = FV1_{(i,j)}$$

For i=2,3,….n_θ-1, j=3,4,…..n_y-1

$$APV1_{(i,j)}v1_{(i,j)} + ASV1_{(i,j)}v1_{(i,j-1)} + ANV1_{(i,j)}v1_{(i,j+1)} + AWV1_{(i,j)}v1_{(i-1,j)} + AEV1_{(i,j)}v1_{(i+1,j)} = FV1_{(i,j)}$$

For i=2,3,….n_θ-1, j=n_y

$$APV1_{(i,j)}v1_{(i,j)} + ASV1_{(i,j)}v1_{(i,j-1)} + AWV1_{(i,j)}v1_{(i-1,j)} + AEV1_{(i,j)}v1_{(i+1,j)} = FV1_{(i,j)}$$

For i=n_θ, j=3,4,…..n_y-1

$$APV1_{(i,j)}v1_{(i,j)} + ASV1_{(i,j)}v1_{(i,j-1)} + ANV2_{(i,j)}v1_{(i,j+1)} + AWV2_{(i,j)}v1_{(i-1,j)} = FV1_{(i,j)}$$

For i=n_θ, j=n_y

$$APV1_{(i,j)}v1_{(i,j)} + ASV1_{(i,j)}v1_{(i,j-1)} + AWV1_{(i,j)}v1_{(i-1,j)} = FV1_{(i,j)}$$

Modified axial displacement (v2) at the shell boundaries are obtained for fixed supported shell as follows:

For i=1, j=2

$$APV2_{(i,j)}v2_{(i,j)} + ANV2_{(i,j)}v2_{(i,j+1)} + \left(AEV2_{(i,j)} + AWV2_{(i,j)}\right)v2_{(i+1,j)} = FV2_{(i,j)}$$

For i=2,3,….n_θ-1, j=2

$$APV2_{(i,j)}v2_{(i,j)} + ANV2_{(i,j)}v2_{(i,j+1)} + AWV2_{(i,j)}v2_{(i-1,j)} + AEV2_{(i,j)}v2_{(i+1,j)} = FV2_{(i,j)}$$

For i=n_θ, j=2

$$APV2_{(i,j)}v2_{(i,j)} + ANV2_{(i,j)}v2_{(i,j+1)} + AWV2_{(i,j)}v2_{(i-1,j)} = FV2_{(i,j)}$$

For i=1, j=3.4…..n_y-1

$$APV2_{(i,j)}v2_{(i,j)} + ASV2_{(i,j)}v2_{(i,j-1)} + ANV2_{(i,j)}v2_{(i,j+1)} + \left(AEV2_{(i,j)} + AWV2_{(i,j)}\right)v2_{(i+1,j)} = FV2_{(i,j)}$$

For i=1, j=n_y

$$APV2_{(i,j)}v2_{(i,j)} + ASV2_{(i,j)}v2_{(i,j-1)} + \left(AEV2_{(i,j)} + AWV2_{(i,j)}\right)v2_{(i+1,j)} = FV2_{(i,j)}$$

For i=2,3,….n_θ-1, j=3,4,…..n_y-1

$$APV2_{(i,j)}v2_{(i,j)} + ASV2_{(i,j)}v2_{(i,j-1)} + ANV2_{(i,j)}v2_{(i,j+1)} + AWV2_{(i,j)}v2_{(i-1,j)} + AEV2_{(i,j)}v2_{(i+1,j)} = FV2_{(i,j)}$$

For i=2,3,….n_θ-1, j=n_y

$$APV2_{(i,j)}v2_{(i,j)} + ASV2_{(i,j)}v2_{(i,j-1)} + AWV2_{(i,j)}v2_{(i-1,j)} + AEV2_{(i,j)}v2_{(i+1,j)} = FV2_{(i,j)}$$

For i=n_θ, j=3,4,…..n_y-1

$$APV2_{(i,j)}v2_{(i,j)} + ASV2_{(i,j)}v2_{(i,j-1)} + ANV2_{(i,j)}v2_{(i,j+1)} + AWV2_{(i,j)}v2_{(i-1,j)} = FV2_{(i,j)}$$

For i=n_θ, j=n_y

$$APV2_{(i,j)}v2_{(i,j)} + ASV2_{(i,j)}v2_{(i,j-1)} + AWV2_{(i,j)}v2_{(i-1,j)} = FV2_{(i,j)}$$

3.4.2 Solution Algorithm

Using finite difference method, governing differential equations 3.7 through 3.11 are converted into algebraic equations at every point of the domain. The equations are obtained in matrix form as:

$$[A]\{w\}_{(i)}^{(k)} = \{q + f_1(w,u1,u2,v1,v2)\}_{(i)}^{(k)} \tag{3.19}$$

In above equations {w} denotes the radial displacement vector while {U} denotes the in-plane displacement vector for *u1, u2*, *v1, v2*and q designates the applied pressure. Subscripts (i) denote the iteration number while superscripts (k) designate the increment number.

Coefficient matrice [A] is linear while the right hand side vectors f_1 is nonlinear. To transform nonlinear algebraic equations into the set of quasi linear equations the values of *w, u1, u2, v1* and *v2* from the (i-1)*th* iteration are put into right hand side of equation 3.17 of the i*th* iteration. Value of radial displacement w for i *th* iteration is

obtained from equation 3.17. The new value of radial displacement is used to calculate the right hand side of equation of equation of *u1, u2, v1* and *v2*. Then equations are solved to obtain *u1, v1,* and *v2*. The solution procedure is repeated until convergence is achieved.

The steps of an iterative procedure are listed below:

1. assume *w*, *u1, u2, v1, v2,*
2. calculate RHS of governing equation for the radial displacement,
3. obtain w(i.j) from $\underline{A}\,\underline{w} = \underline{R}$
4. recalculate $w(i,j) = \alpha w(i,j) + (1-\alpha) w_0(i,j),$

where α is under relaxation parameter. This parameter is used in order to overcome convergence difficulties. α is calculated by interpolation regarding the non-dimensional maximum displacement $2 * w_{(1,1)} / (h_1 + h_2)$ as a result of numerical experiment and $w_{0(i,j)}$ is the radial displacement that is calculated in the previous step. Radial displacement w is interpolated by using $\alpha\left(\frac{w_{\max}}{h}\right)$ and in-plane displacement is extrapolated by using $\beta = 1.4$

5. if $\frac{\sum_{i,j} \left| w_{(i,j)} - w_{o(i,j)} \right|}{(num * w_{\max})} \le tol$ then stop the iteration,
6. calculate $FU1_{(i,j)}$ and $u1$ from governing equation of $u1$,
7. calculate $FU2_{(i,j)}$ and $u2$ from governing equation of $u2$,
8. calculate $FV1_{(i,j)}$ and $v1$ from governing equation of $v1$,
9. calculate $FV2_{(i,j)}$ and $v2$ from governing equation of $v2$,
10. back to step 2.

The described iterative procedure is implemented by developing a computer code, which is written in FORTRAN.

3.5 Verification of Model

To verify the present model first monolithic glass is considered. Results obtained from the analysis for clamped cylindrical shell under lateral pressure are compared with the results, which are obtained using finite element package program (ABAQUS version 6.7.1) and with the published results in literature for monolithic case. The length and radius of the model considered are 0.508 m and 2.54 m, respectively. The thickness of the monolithic unit is 3.175 mm. The values of Young's modulus of elasticity and Poisson's ratio of glass are assumed as $E = 31.03 * 10^4$ kPa and $\nu = 0.30$, respectively. The same model was solved by Plazotto [37] for several mesh arrangement by using finite element method. Plazotto's results for different mesh values, Abaqus results and current model's result are presented in Table 3.1. It is observed that when the load is increased center displacement begins to increase. Comparison of the results obtained by using the present model, Plazotto's model and ABAQUS is taking place in Figure 3.3. Results match quite well for monolithic case.

Table 3.1 Comparison of the deflections for the monolithic cylindrical shell

Load	Plazotto's Solution (mm)					Abaqus	Model
(kN/m^2)	4*4L	8*8L	4*4Q	4*6Q	8*8Q	(mm)	(mm)
0.276	0.303	0.305	0.311	0.308	0.308	0.306	0.301
0.552	0.639	0.652	0.659	0.653	0.659	0.656	0.646
0.827	1.018	1.063	1.054	1.052	1.078	1.076	1.058
1.103	1.454	1.589	1.516	1.533	1.622	1.632	1.608
1.379	1.971	2.391	2.077	2.162	2.505	2.624	2.645
1.655	2.606	4.317	2.802	3.132	5.048	5.601	5.997
1.931	3.417	6.455	3.818	4.912	7.047	7.345	7.740
2.206	4.448	7.719	5.245	6.603	8.206	8.430	8.796
2.482	5.591	8.641	6.691	7.735	9.065	9.257	9.607
2.758	6.634	9.383	7.804	8.585	9.762	9.937	10.279

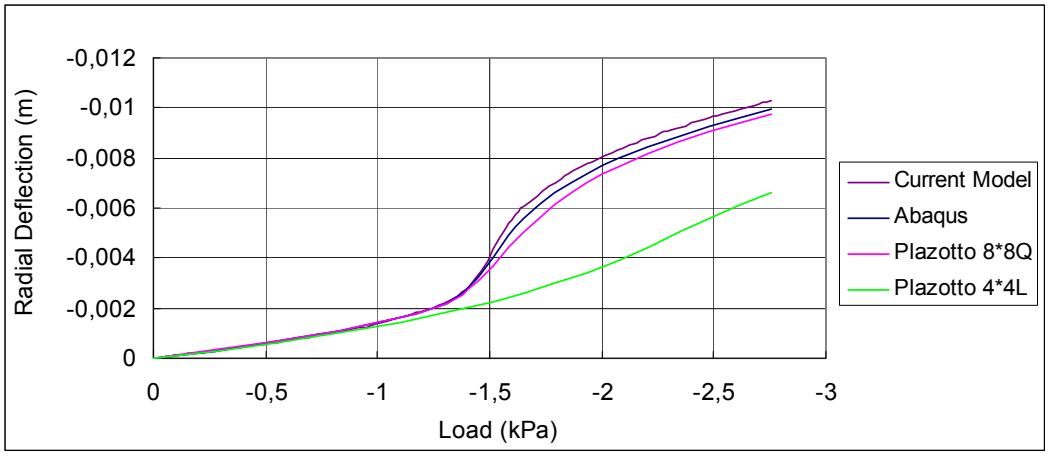

Figure 3.3 Comparison of central deflection values for monolithic case

Present model is developed to analyze the laminated glass shell, which consists of two glass shells and an interlayer. To verify the developed for the laminated glass shell, finite element method is used. The laminated glass shell unit considered has a length of 0.508 m and a radius of 2.54 m. Each glass shell has a thickness of 2.5 mm. The thickness of the inner core is 0.76 mm. The total thickness of the unit is 5.76 mm. The Young's modulus and Poisson's ratio of glass are taken to be 72 GPa and 0.25, respectively; but the shear modulus and Poisson's ratio of the interlayer are taken as 1000 kPa and 0.29, respectively. The physical properties of laminated glass shell unit are given in Table 3.2. The three dimensional finite element model is generated and solved with ABAQUS version 6.7. Load is uniformly distributed. To perform large deformation analysis ''geometric nonlinearity'' option is used. Twenty node quadratic brick elements (C3D20R) are used in meshing because the program gives more accurate results where large deformations are involved and leads to faster convergence. Because of the symmetry only a quarter of the shell unit is solved. The boundaries are modeled as clamped edge. At the fixed ends of the unit, vertical and horizontal degrees of freedom of all the nodes of the unit are set to be zero. The unit is divided into nearly 2000 elements to obtain convergence. Comparison of the results of finite element model and current model is taking place in Table 3.3, Figures 3.4 and 3.5. The difference between the stress and displacement results is 11% at most. A view of contours of radial deflection obtained from ABAQ

US is seen in Figures 3.6. From Figure 3.6 it can be seen that radial deflection takes its maximum value at the center of unit.

Table 3.2 Physical properties of laminated glass shell unit

	Dimensions (mm)				Modulus	
	Thickness	Length	Radius	θ	E	G
Glass 1	2,5	508	2540	0,2	72 GPa	28.8 GPa
PVB	0.76	508	2538,37	0,2	2900 kPa	1000 kPa
Glass 2	2,5	508	2537,74	0,2	72 GPa	28.8 GPa

Table 3.3 Comparison of the results for the fixed supported laminated cylindrical shell

	Displacement (mm)			Maximum Stress (MPa)		
Load (kPa)	FEM	Model	% Error	FEM	Model	% Error
0	0.000	0.000	0	0.000	0.000	0
0.1	0.003	0.003	8.8	0.120	0.112	6.5
0.2	0.005	0.006	8.8	0.240	0.225	6.5
0.3	0.008	0.009	8.9	0.361	0.337	6.5
0.4	0.010	0.012	8.9	0.481	0.449	6.5
0.5	0.013	0.015	8.9	0.607	0.562	7.4
0.6	0.016	0.017	8.9	0.721	0.674	6.5
0.7	0.019	0.020	9	0.841	0.786	6.5
0.8	0.021	0.023	9	0.961	0.898	6.5
0.9	0.024	0.026	8.9	1.081	1.011	6.5
1	0.026	0.029	9	1.216	1.123	7.7
2	0.053	0.058	9.1	2.430	2.242	7.7
3	0.078	0.086	9.3	3.640	3.358	7.7
4	0.104	0.115	9.4	4.846	4.472	7.7
5	0.129	0.142	9.5	6.050	5.582	7.7
6	0.154	0.170	9.6	7.251	6.689	7.7
7	0.178	0.198	9.7	8.449	7.794	7.8
8	0.203	0.225	9.8	9.644	8.896	7.8
9	0.227	0.252	9.9	10.840	9.995	7.8
10	0.250	0.278	10	12.030	11.091	7.8
20	0.476	0.533	10.7	23.880	21.871	8.4
30	0.685	0.771	11.1	36.010	32.549	9.6
40	0.881	0.994	11.4	48.170	42.995	10.7
50	1.067	1.202	11.3	60.330	53.286	11.7

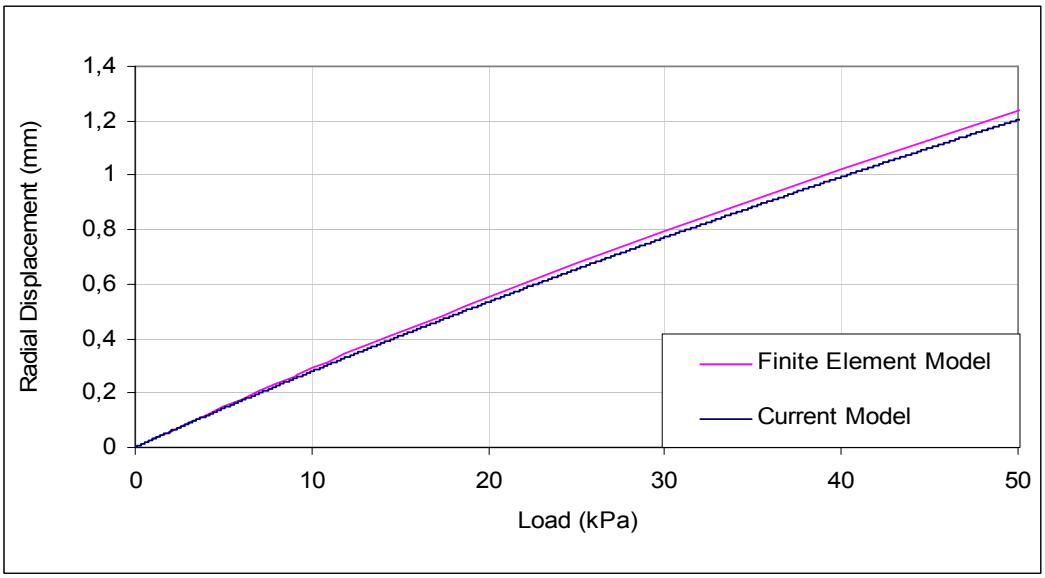

Figure 3.4 Comparison of the central deflection values for laminated cylindirical glass shell

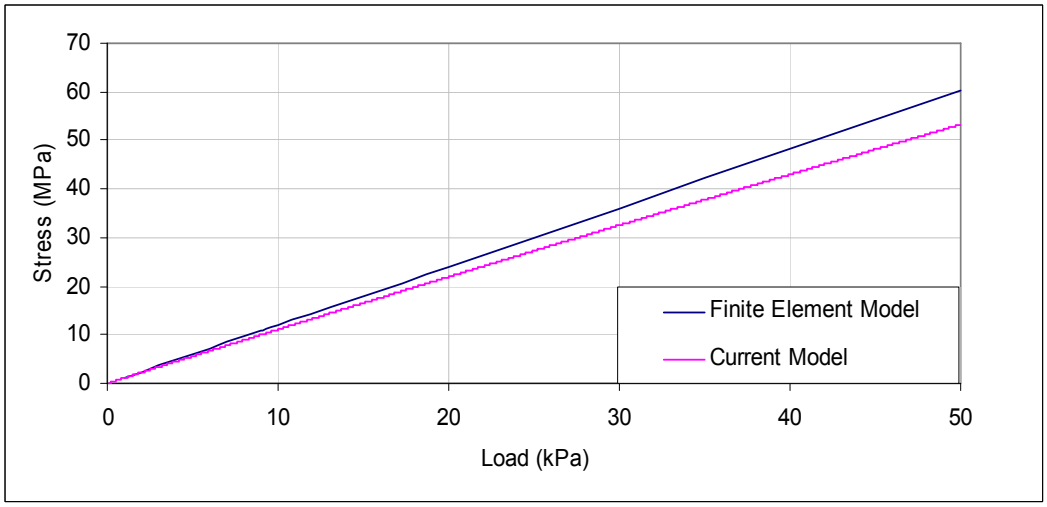

Figure 3.5 Comparison of the stress values for the laminated cylindrical glass shell

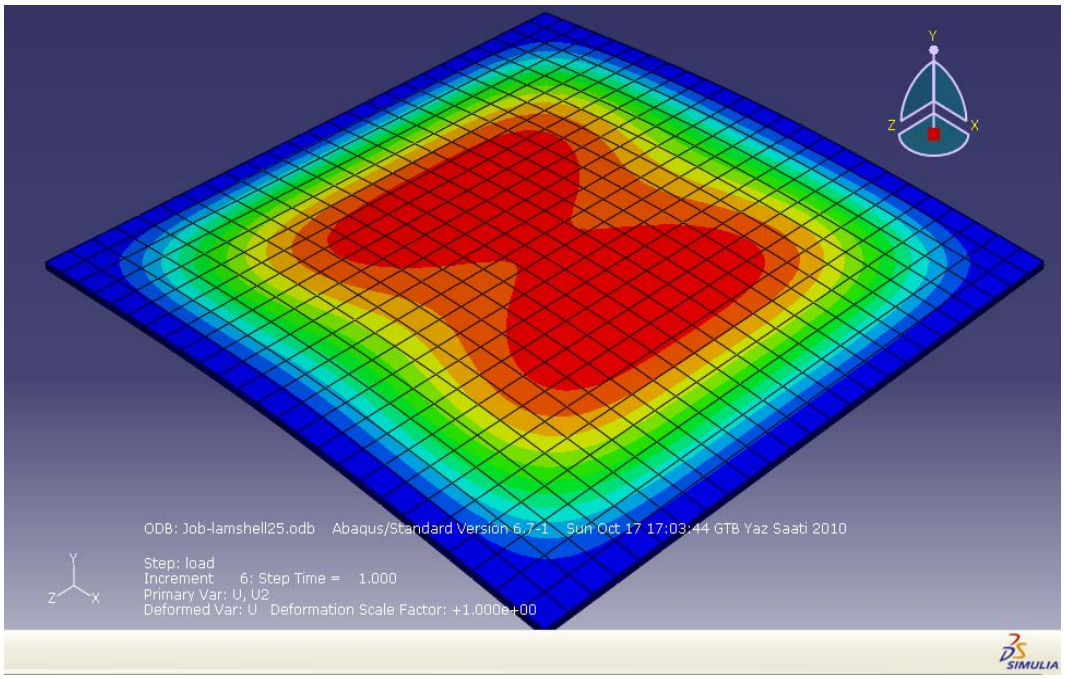

Figure 3.6 A view of contours of radial deflection obtained from ABAQUS

3.6 Numerical Solution and Results

3.6.1 Numerical Results for Fixed Supported Cylindrical Shell Subjected to Uniform Distributed Load Towards Out of the Top Shell Surface

Fixed laminated glass shell tested has 0.508 m in length and 2.54 m radius. It is consisting of two glass shells and each of them has a thickness of 2.5 mm. The thickness of the inner core is 0.76 mm. The total thickness of the unit is 5.76 mm. The Young's modulus and Poisson's ratio of glass are taken to be 72 GPa and 0.25, respectively. Shear modulus and Poisson's ratio of the interlayer are taken as 1000 kPa and 0.29, respectively. Physical properties of laminated unit are given in Table 3.2. Figures 3.7 and 3.8 show the comparison of linear and nonlinear approach to predict the behavior of the clamped cylindrical shell. Linear and nonlinear solution

results are plotted as normalized deflection versus load in Figure 3.7. The level of nonlinearity may be defined as $\frac{w_{max}}{h}$ ratio, where w_{max} is the deflection at the center of the shell, and h is the thickness of the single glass sheets. Separation between linear and nonlinear solutions starts when $\frac{w_{max}}{h} > 0.08$. It can be said that nonlinear solution should be considered when the ratio of maximum deflection to thickness of a single glass shell is greater than 0.08. It is observed that this ratio (the level of nonlinearity) is about 0.5 for a load P=50 kPa in Figure 3.7. The central deflection obtained from the linear approach is almost 1.2 times of the deflection obtained by nonlinear approach at load P=50 kPa. Figure 3.8 is plotted to observe stress versus load for linear and nonlinear behavior. In contrary to the deflection values, stress values of nonlinear behavior are higher than stress values, which are obtained for linear behavior. Because there are ignored nonlinear terms in stress formulation of linear approach.

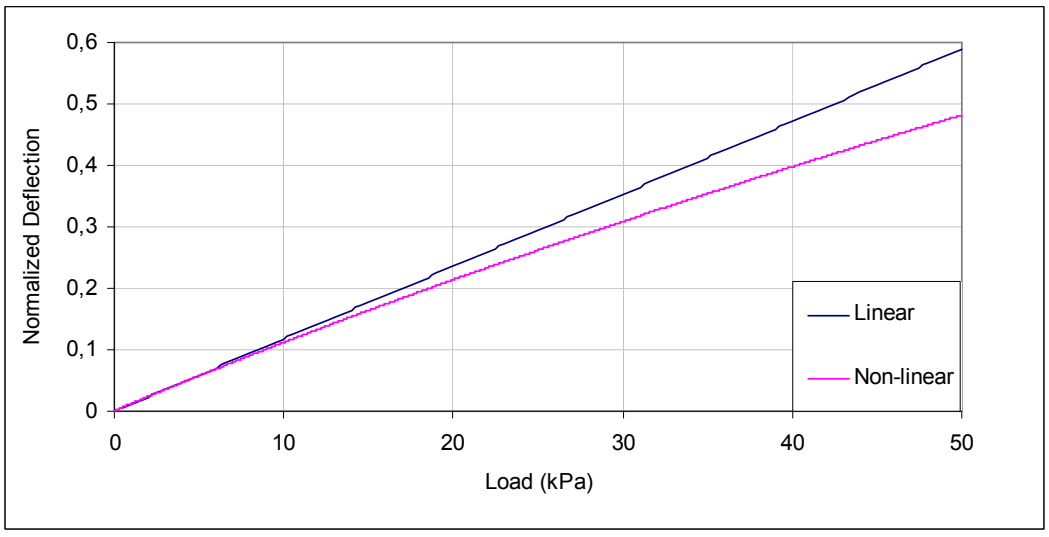

Figure 3.7 Normalized maximum deflection ($\frac{w_{max}}{h}$) versus load for clamped cylindrical shell

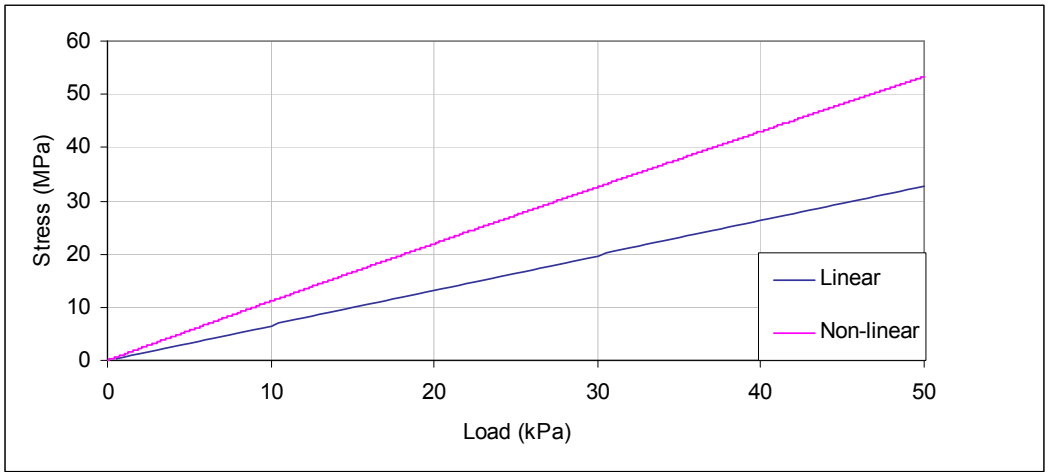

Figure 3.8 Stress versus load for clamped cylindrical shell.

The developed model is able to predict the behavior of monolithic, layered and laminated glass shells.

Figures 3.9 and 3.10 are plotted to compare the behavior of true monolithic, equivalent monolithic, laminated and layered glass shells. In the figures below, the origin of coordinate system is considered at the center of the laminated glass shell. Figures 3.9 and 3.10 are the deflection and maximum stress versus load graphs, respectively. The behavior of laminated glass shell is close to the behavior of layered glass shell as seen in Figures 3.9 and 3.10. Their behavior is bounded by two limiting cases which are monolithic and layered behavior. While layered glass, which has two glass sheets with no connection between them, is found to be the upper bound of laminated glass behavior; true monolithic glass, which has only one glass sheet with thickness equal to the total thickness of glass sheets plus the interlayer thickness in laminated shell unit, is found to be the lower bound, rather than that of an equivalent monolithic glass which has a glass sheet having the thickness equal to the total glass thickness of laminated glass unit.

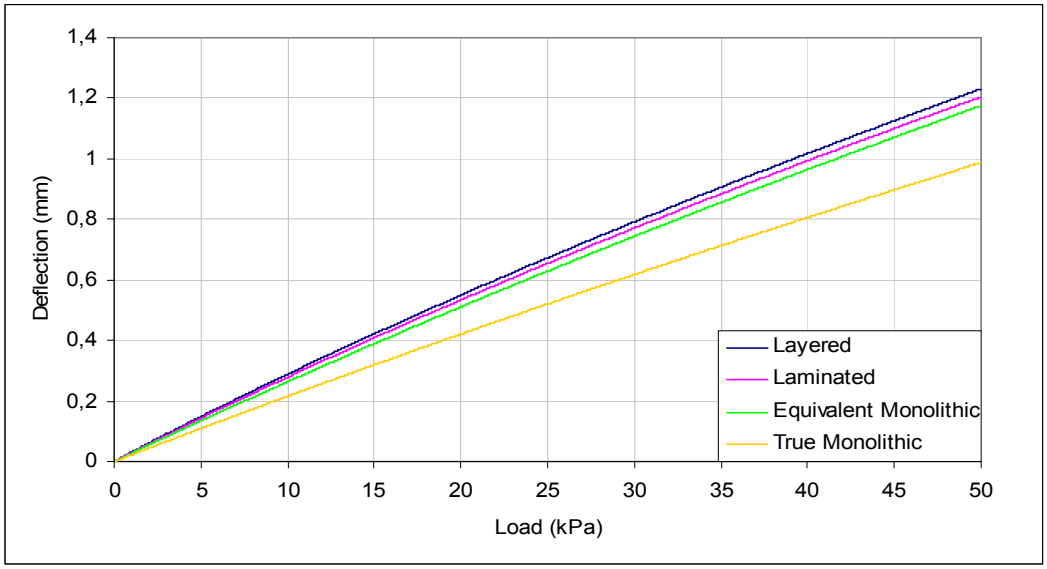

Figure 3.9 Maximum deflection versus load

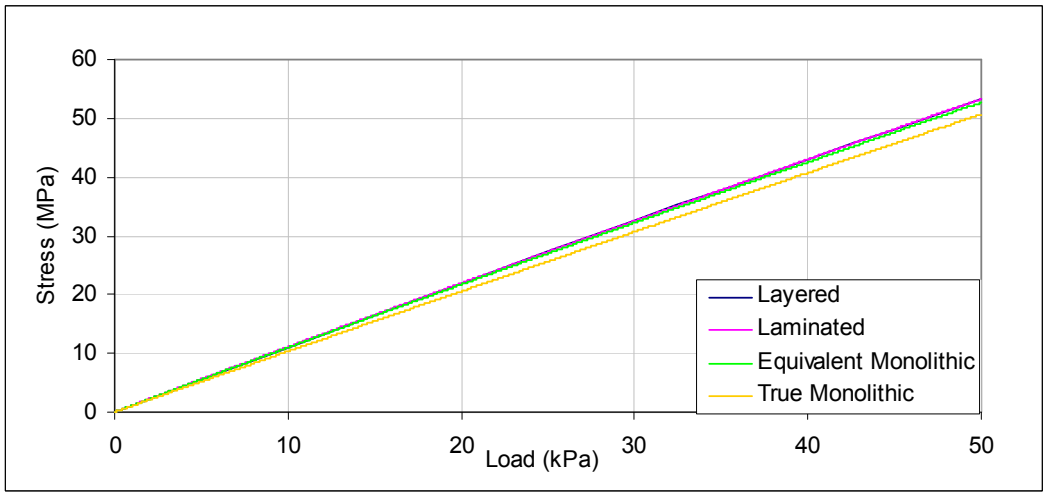

Figure 3.10 Maximum stress versus load

Figures 3.11 and 3.12 represent the circumferential deflection in θ direction (u1 and u2) along the centerline at y=0 for top and bottom glass units, respectively. Circumferential deflections are zero at θ=0 and θ=θ_1. Circumferential deflections in θ direction take their maximum values close to the midpoint of the quarter shell. There is a slight difference between the circumferential deflections of top and bottom glass sheets. Circumferential deflection of the top glass is larger than the bottom glass. Both of them are negative. When the load is increased the deflection curves are

getting closer to each other and the curvature of deflection lines increases. The ratio of maximum deflection value at 10 kPa to that at 5 kPa is nearly 2, while it is nearly 1 for those at 50 kPa and at 45 kPa. The reason of this behavior is the nonlinearity of the shell unit.

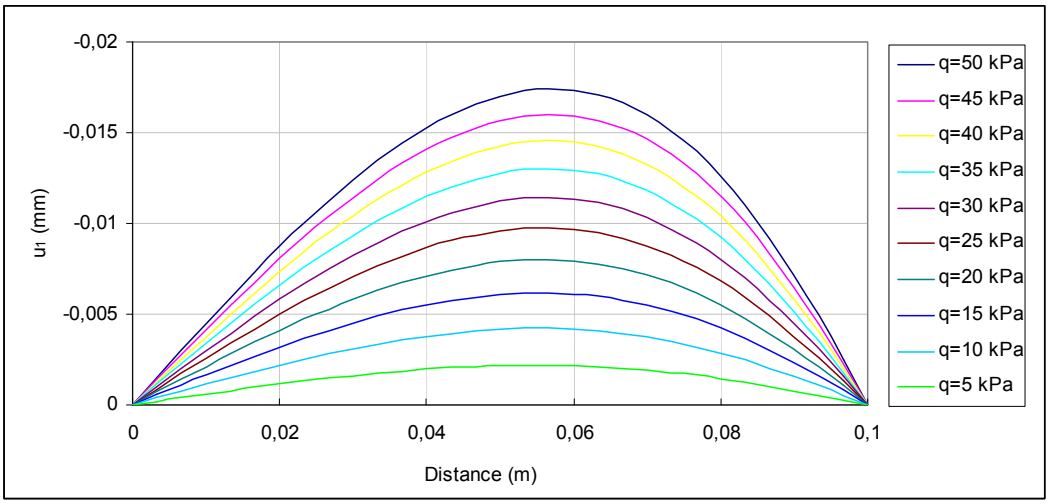

Figure 3.11 Circumferential displacement of the top glass unit along the center line at y=0

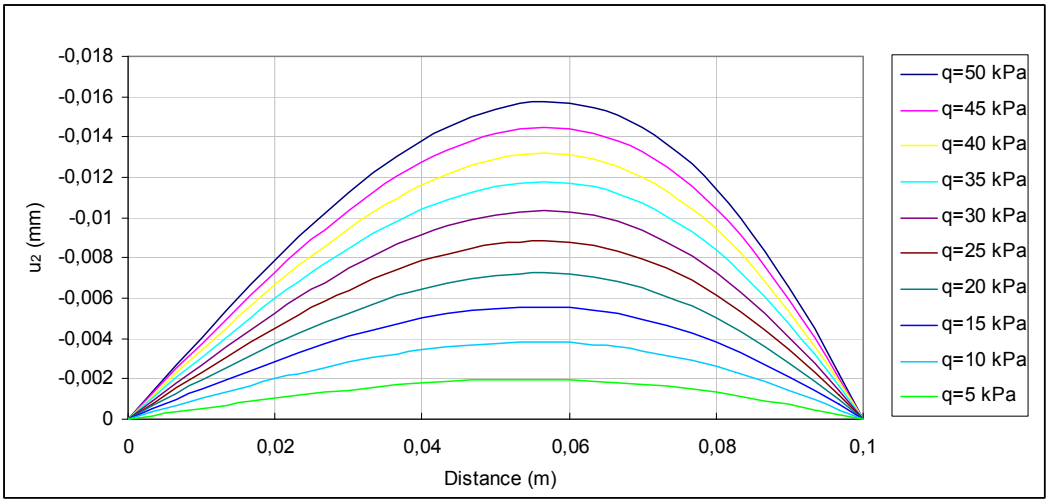

Figure 3.12 Circumferential displacement of the bottom glass unit along the centerline at y=0

Figures 3.13 and 3.14 are plotted to represent the axial deflections (v1 and v2) along the center line at θ=0 for top and bottom glass units, respectively. Axial deflections v_1 and v_2 are zero at along the center line at y=0 and at the edge $y=y_1$ in accordance with the geometry of shell unit. Axial deflections take the value of zero also at a node inside the domain. The location of zero point is found to shift toward the edge for high values of applied pressure on top surface. From Figure 3.14 it is observed that zero point of bottom glass sheet inside the domain is the same for all load values. They take their maximum values at the midpoint of the quarter laminated glass unit. Axial deflections v_1 and v_2 along the center line at θ=0 take both positive and negative values. Axial deflection at the top shell is nearly half of that of the bottom shell. Radial deflections along the center line at y=0 are illustrated in Figure 3.15 for different load levels. Radial displacements take their maximum value at the center of the unit while they are zero at the shell boundaries. Because of the nonlinearity, radial deflections are getting closer to each other when the load is increased.

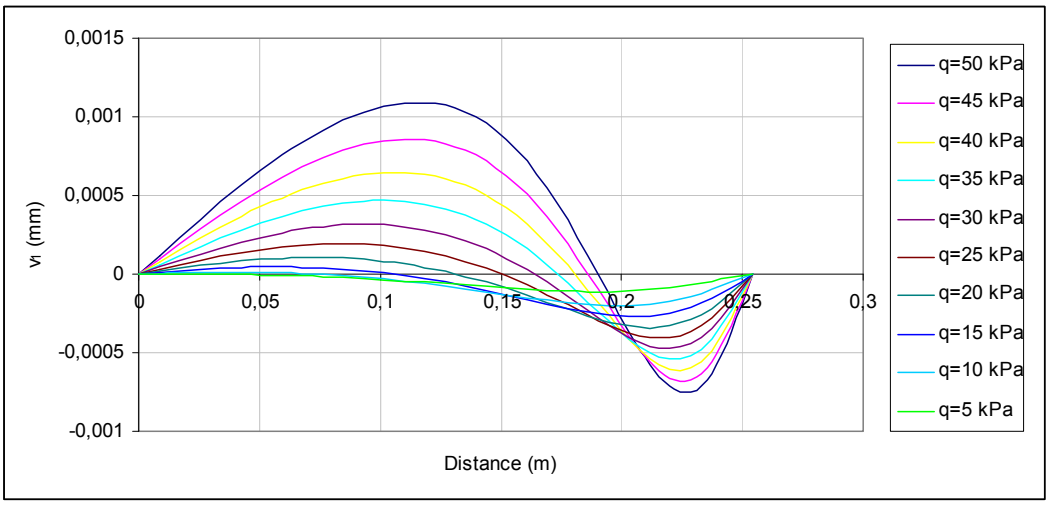

Figure 3.13 Axial displacement of the top glass unit along the center line at θ=0

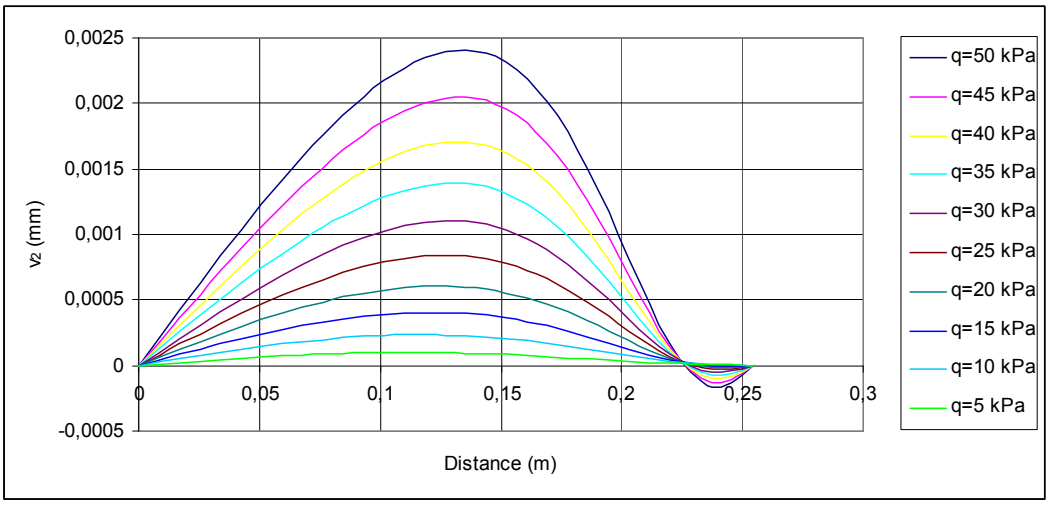

Figure 3.14 Axial displacement of the bottom glass unit along the center line at θ=0

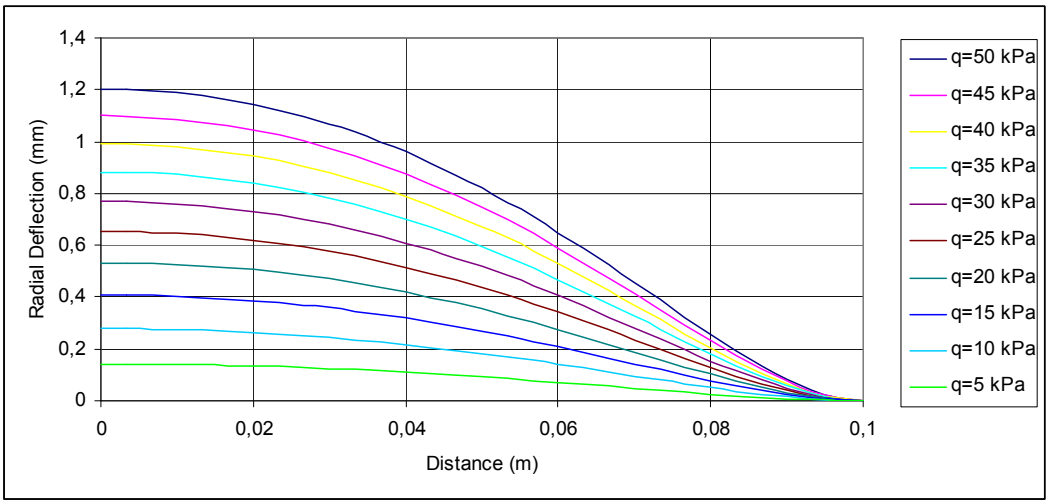

Figure 3.15 Radial displacement of the unit along the centerline at y=0

Figures 3.16-3.20 illustrate the radial, circumferential and axial displacements along the diagonal of the laminated glass shell unit. Radial displacements take their maximum value at the center of the unit. The circumferential displacement of the top glass ply in θ direction is larger than the axial displacement of the bottom glass ply as seen in Figures 3.17 and 3.18. Axial displacements are zero at the center and at the corner of the shell. In addition to the center and corner of the unit, axial deflections along the diagonal are zero at a point inside the domain as it is observed from

Figures 3.19 and 3.20. The point shifts toward the center while the load is decreasing. They take positive values near the center while they are negative near the corner of the unit. The negative values are absolutely greater than the positive values. The circumferential displacement (u1) of the top glass ply is larger than the circumferential displacement of the bottom glass ply. The effect of geometric nonlinearity is observed since displacement curves for increasing load values are getting closer to each other.

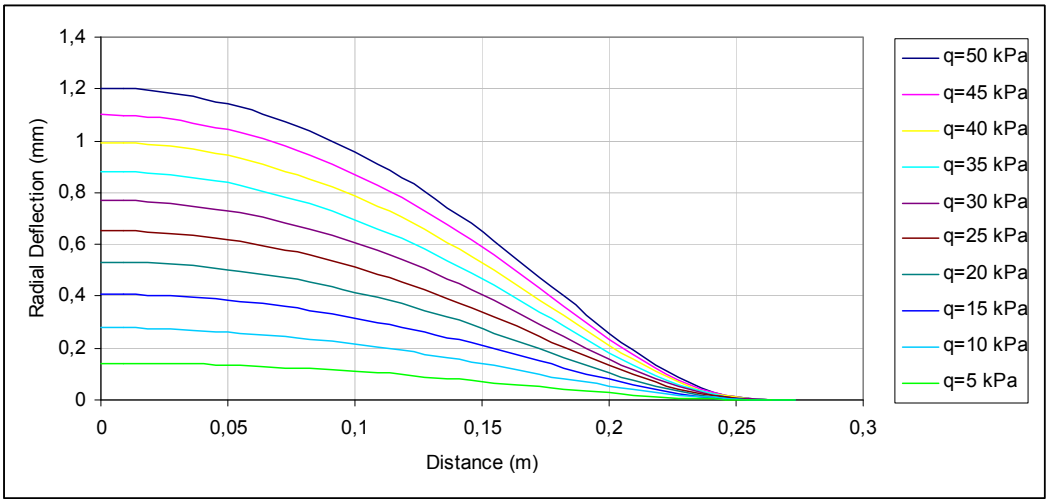

Figure 3.16 Radial displacement of the shell along the diagonal

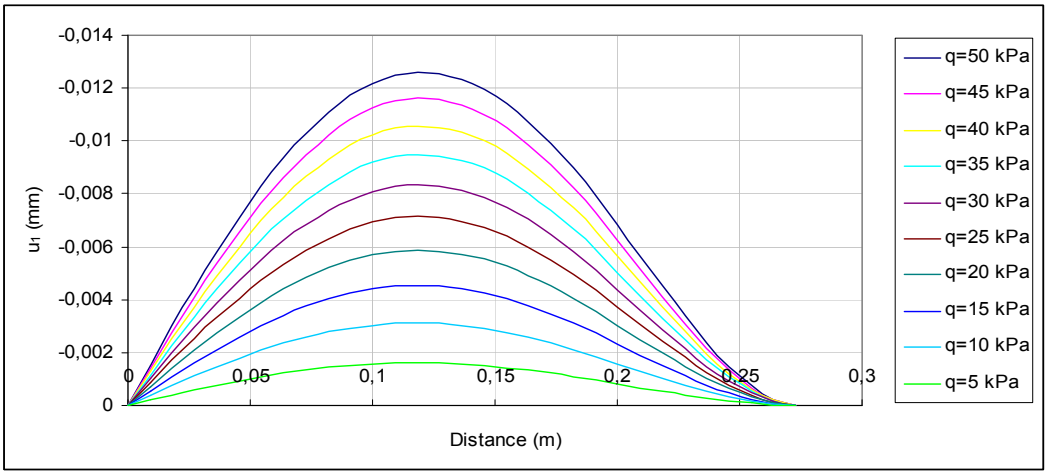

Figure 3.17 Circumferential displacement of the top glass shell along the diagonal

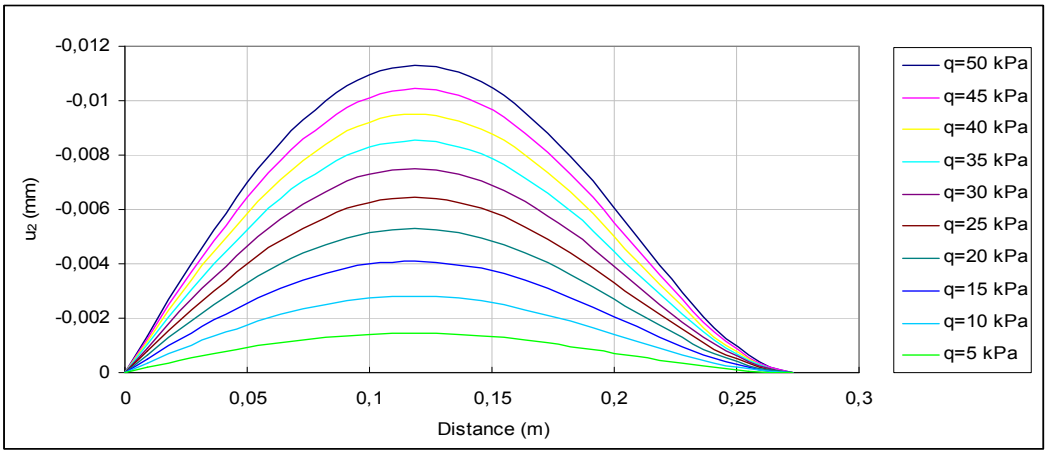

Figure 3.18 Circumferential displacement of the bottom glass shell along the diagonal

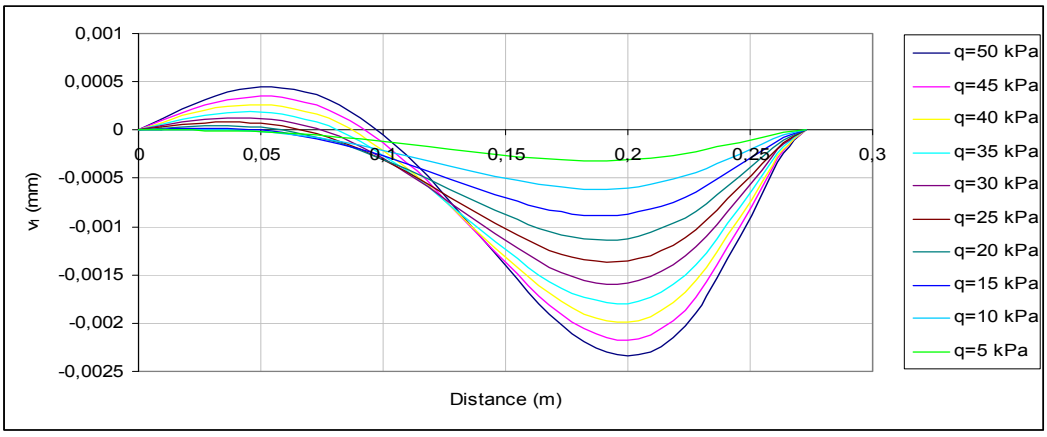

Figure 3.19 Axial displacement of the top glass shell along the diagonal

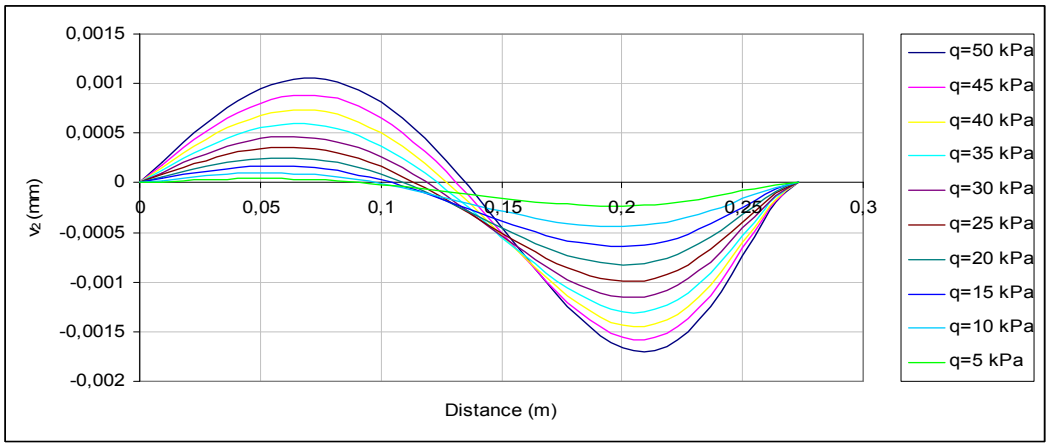

Figure 3.20 Axial displacement of the bottom glass shell along the diagonal

Figures 3.21-3.24 are plotted to consider the maximum and minimum principal stresses for the top surface of the top shell and for the bottom surface of the bottom shell of laminated glass unit. Figures 3.21 and 3.22 represent maximum and minimum principal stresses at top surface of the top glass unit along the center line at y=0 for different load values, respectively. Maximum and minimum principal stresses from Figures 3.21 and 3.22 are observed as tension at the top surface of the top glass. They take their maximum values at the support of the unit at $\theta=\theta_1$. The value of maximum principal stress at top surface is 50 MPa for the applied 50 kPa load while it is 28 MPa for bottom surface.

Maximum and minimum principal stresses of the bottom surface of the bottom glass along the centerline at y =0 are presented in Figures 3.23 and 3.24, respectively. While principal stresses of the bottom surface of the bottom glass are tension at the center, they are compression at the boundary of the unit. Unlike maximum stresses on the top surface, maximum stresses on the bottom surface take their maximum value at the center of the shell.

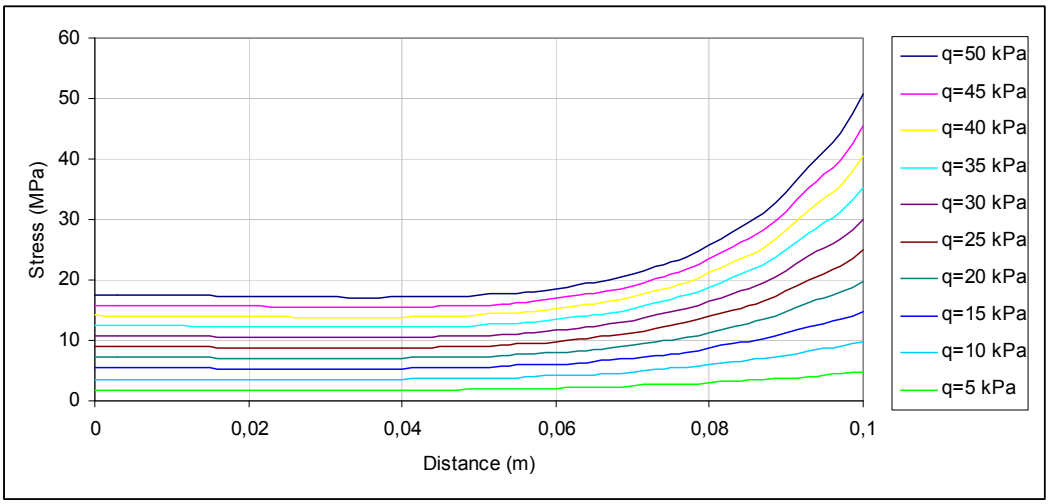

Figure 3.21 Maximum stresses on the top surface of the top glass along the center line at y=0

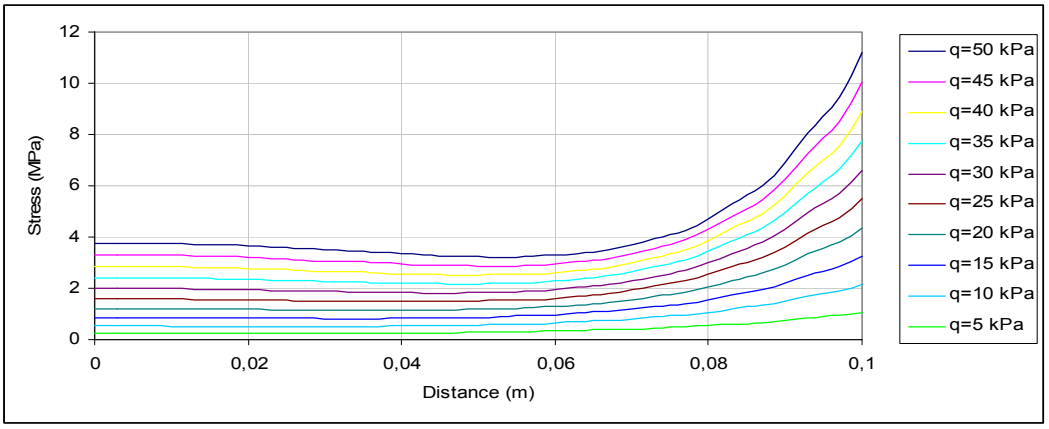

Figure 3.22 Minimum stresses on the top surface of the top glass along the center line at y=0

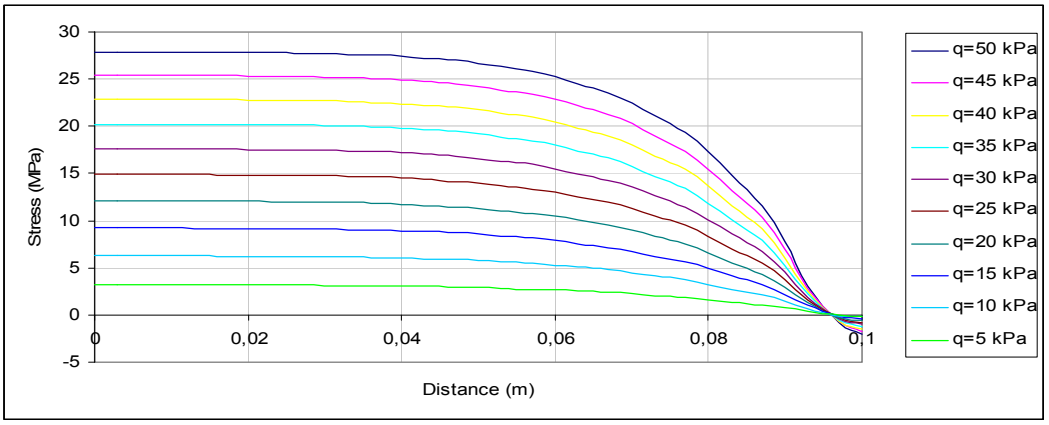

Figure 3.23 Maximum stresses on the bottom surface of the bottom glass along the center line at y=0

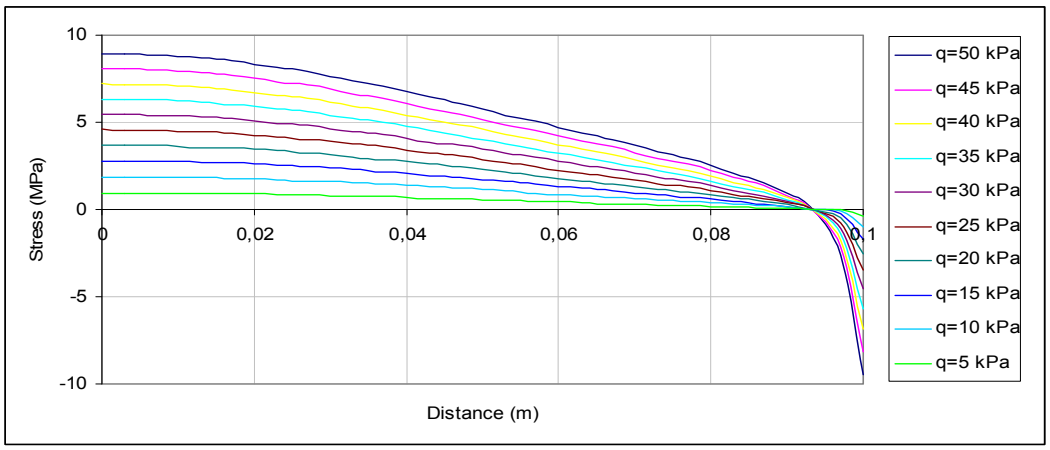

Figure 3.24 Minimum stresses on the bottom surface of the bottom glass along the center line at y=0

Figures 3.25 and 3.28 are plotted to illustrate the maximum and minimum principal stresses at the bottom surface of the top shell and on the top surface of the bottom shell along θ direction of the laminated shell unit. Because of the perfect bound between the glass sheets and PVB film, stress at top surface of PVB interlayer is equal to the stress at the bottom surface of the top glass sheets and stress at the bottom surface of PVB interlayer is equal to the stress at the top surface of the bottom glass sheet. Figures 3.25 and 3.26 present the maximum principal stress on the top and bottom surface of PVB interlayer, respectively. While maximum principal stresses on the bottom surface of interlayer are tension along the center line at y=0, they are both tension and compression at the bottom surface of top shell. Maximum principal stress at the bottom surface of interlayer is nearly twice of maximum principal stress on top surface of interlayer PVB. Figures 3.27 and 3.28 show minimum principal stress on the bottom surface of the top shell and on the top surface of the bottom shell along the center line at y=0, respectively. Minimum principal stresses on the bottom surface of the top shell are tension till a point which is 0.003 m away from the edge of the unit. They take their maximum value as tension at the center of unit. Minimum principal stresses on the top surface of the bottom shell are tension along θ direction. They take their maximum value at the edge of the unit. Minimum principal stresses on the top surface of the bottom shell are slightly higher than that of the bottom surface of the top shell.

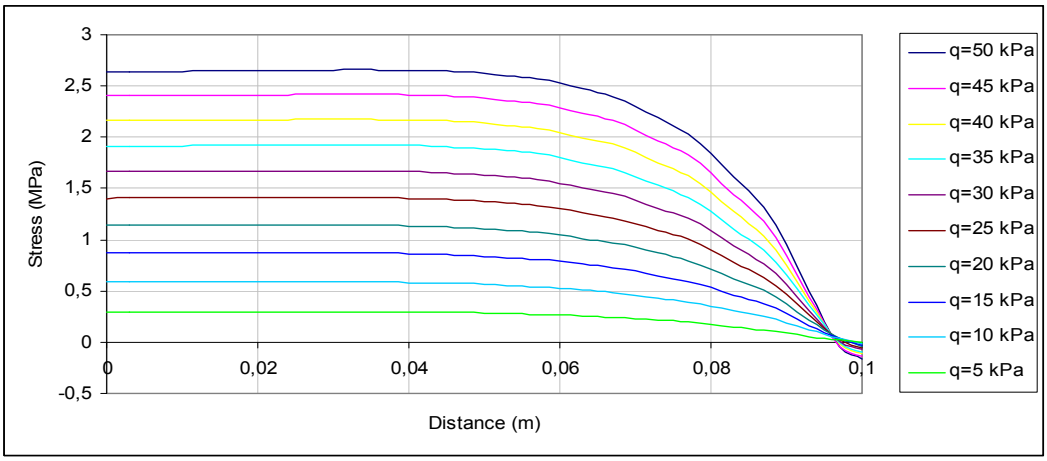

Figure 3.25 Maximum stresses on the bottom surface of the top shell along the center line at y=0

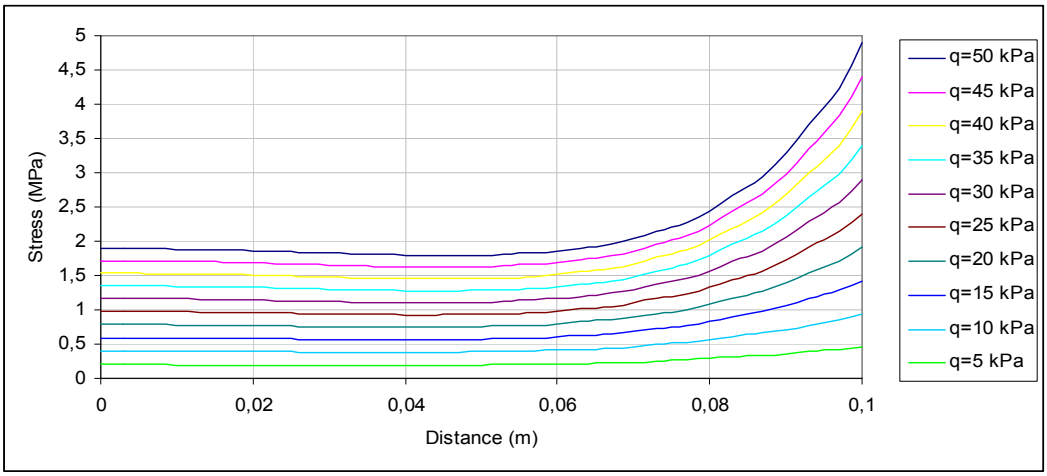

Figure 3.26 Maximum stresses on the top surface of the bottom shell along center line at y=0

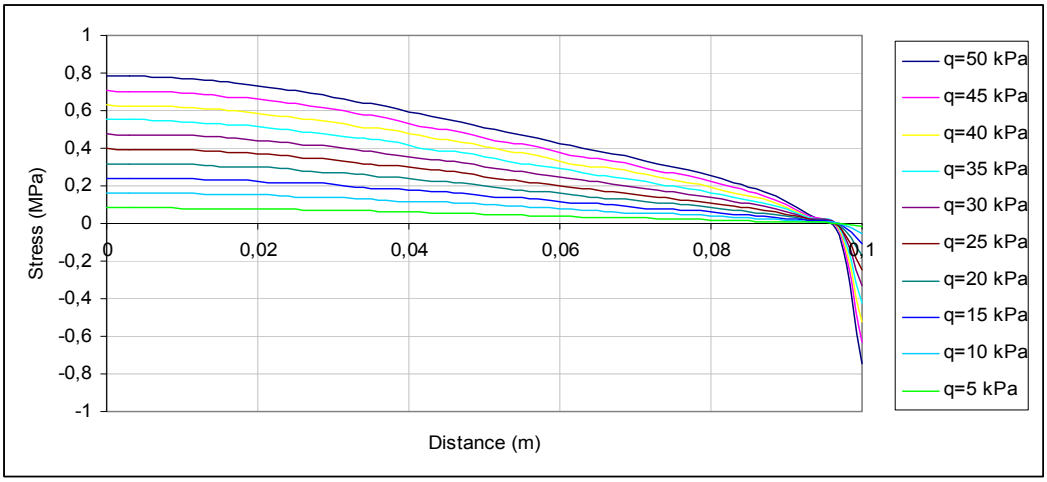

Figure 3.27 Minimum stresses on the bottom surface of the top shell along center line at y=0

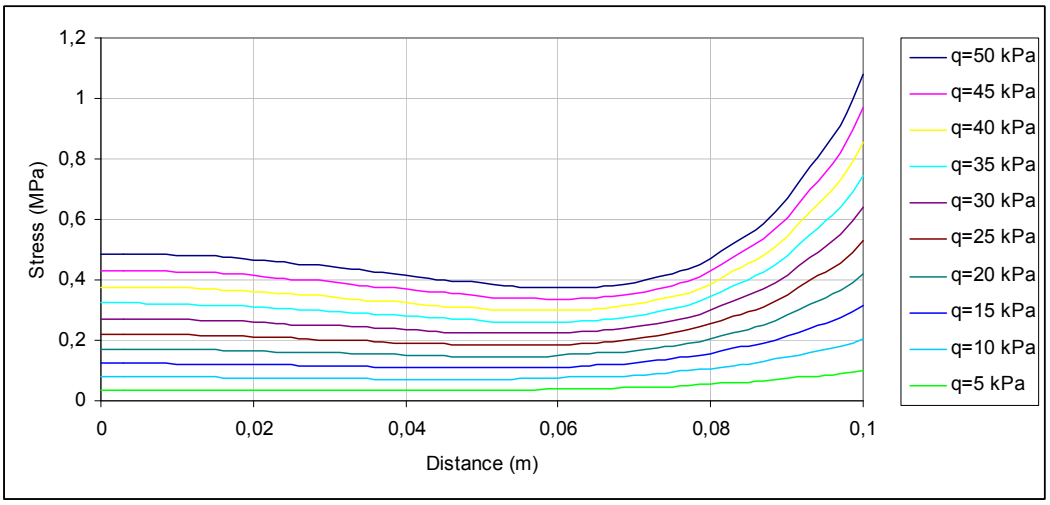

Figure 3.28 Minimum stresses on the top surface of the bottom shell along center line at y=0

Figure 3.29-3.32 are plotted to represent the maximum and minimum principal stresses on the top surface of the top glass unit and on the bottom surface of the bottom glass unit, respectively along the center line at θ=0 of the shell unit. Maximum stress on the top surface of the shell is tension; it takes its maximum value at the boundary of the unit. As it is seen from Figure 3.29 maximum stresses on the top surface of the top glass is tension along the center line at θ=0 . They take their maximum value at the boundary of unit. Figure 3.30 illustrates how minimum principal stress changes on top surface along the y-axis. At the origin, they are tension and they change their sign at a point close to 0.1 while the load is increasing. Close to boundary of unit, they change their sign again and they become tension. At the point where maximum principal stress is minimum, minimum principal stress makes a peak. They take their maximum value at the boundary. As it is seen from Figure 3.31 maximum stress of bottom surface is tension near the center while it is compression near the edge. Maximum stress lines on top face of top ply are nearly straight because they get smaller very slowly till a point which is 0.042 away from the boundary. At that point, they take their minimum value. After that point they start to increase and at the boundary they take their maximum value. Minimum stress lines at the bottom surface of the unit along the center line at θ=0 are illustrated in

Figure 3.32. It is observed that minimum stresses on bottom surface of the unit take their maximum value at the center of the shell as compression.

Figures 3.33-3.36 show how maximum and minimum principal stresses change along the diagonal of the shell unit on the top and bottom surfaces, respectively. While minimum principal stresses on the bottom surface are tension near the center, they are compression near the edges. Figures 3.33 and 3.35 illustrate maximum principal stresses as tension on the top and bottom surfaces. It should be underlined that, in Figures 3.34 and 3.36, absolute minimum stresses on the top surface occur as compression, while it is tension at the bottom surface.

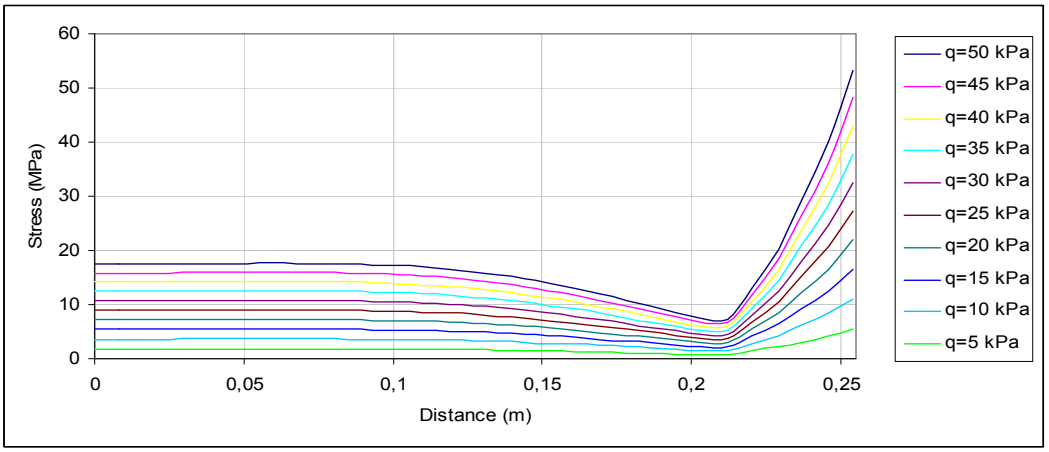

Figure 3.29 Maximum stresses on the top surface of the top glass along the center line at θ=0

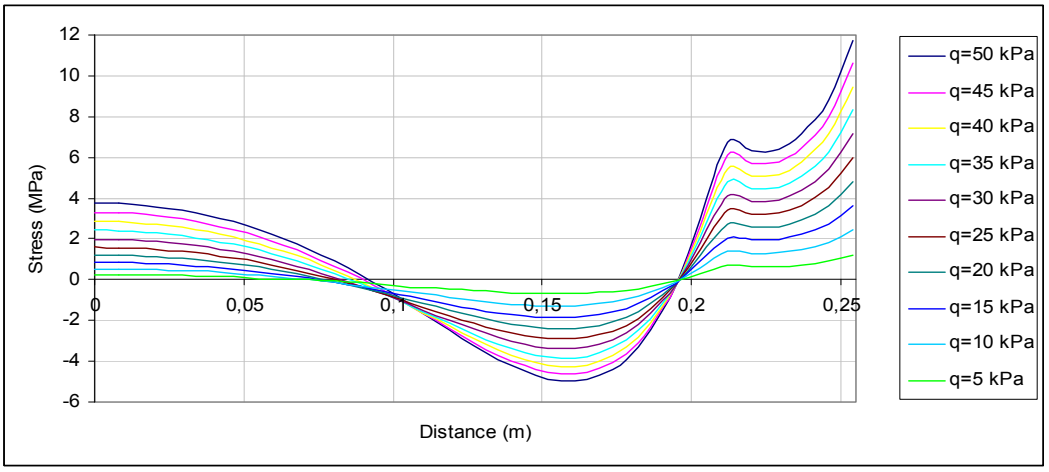

Figure 3.30 Minimum stresses on the top surface of the top glass along the center line at θ=0

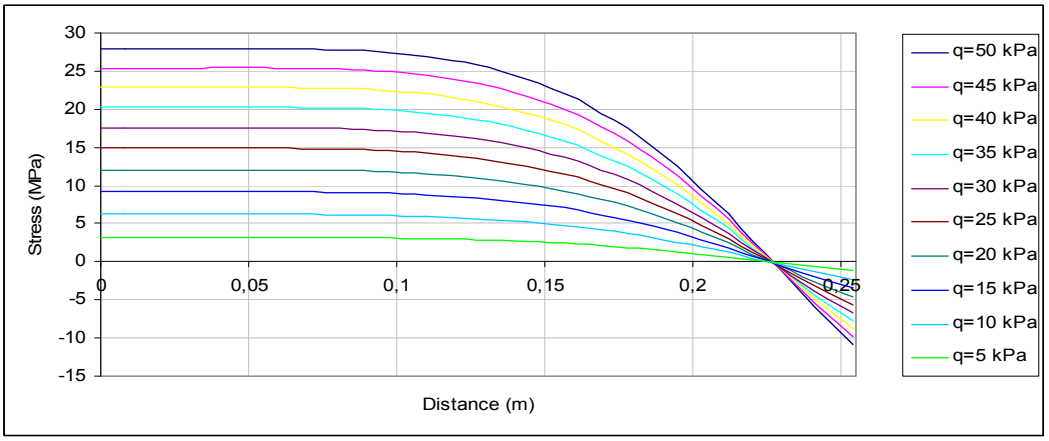

Figure 3.31 Maximum stresses on the bottom surface of the bottom shell along the center line at θ=0

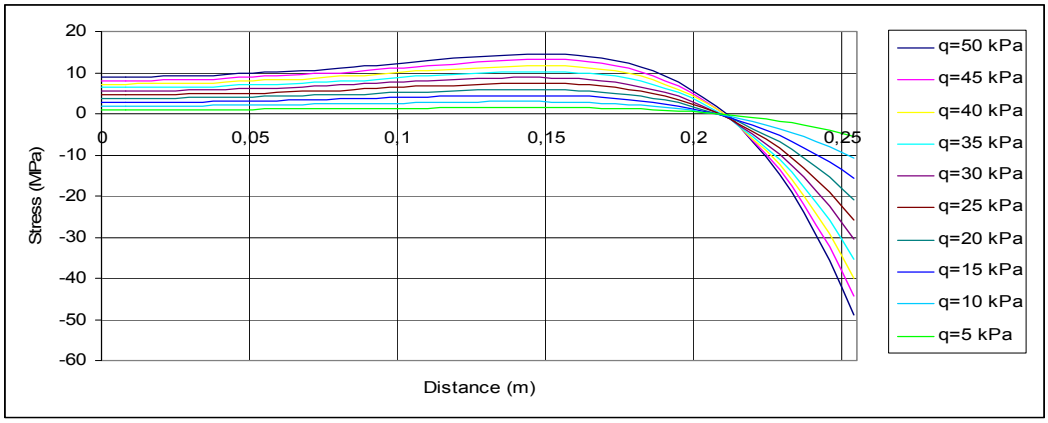

Fi

Figure 3.32 Minimum stresses on the bottom surface of the bottom shell along the center line at θ=0

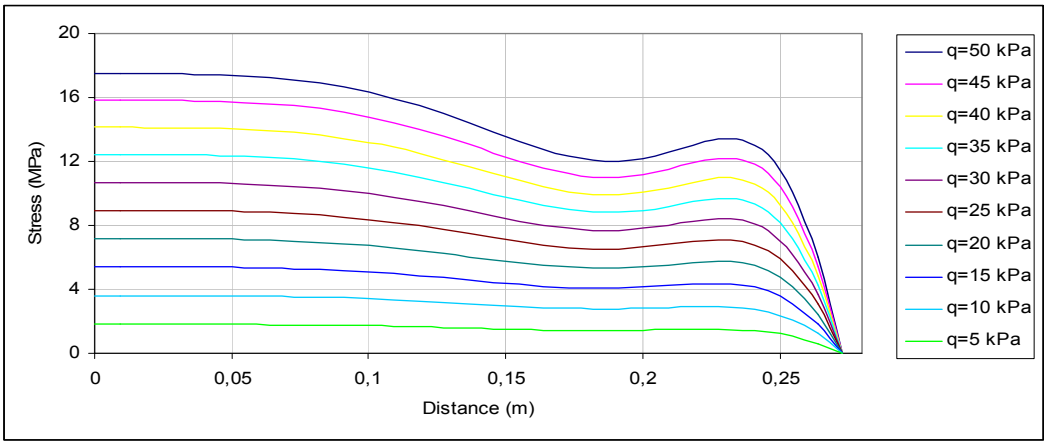

Figure 3.33 Maximum stresses on the top surface of the top shell along the diagonal

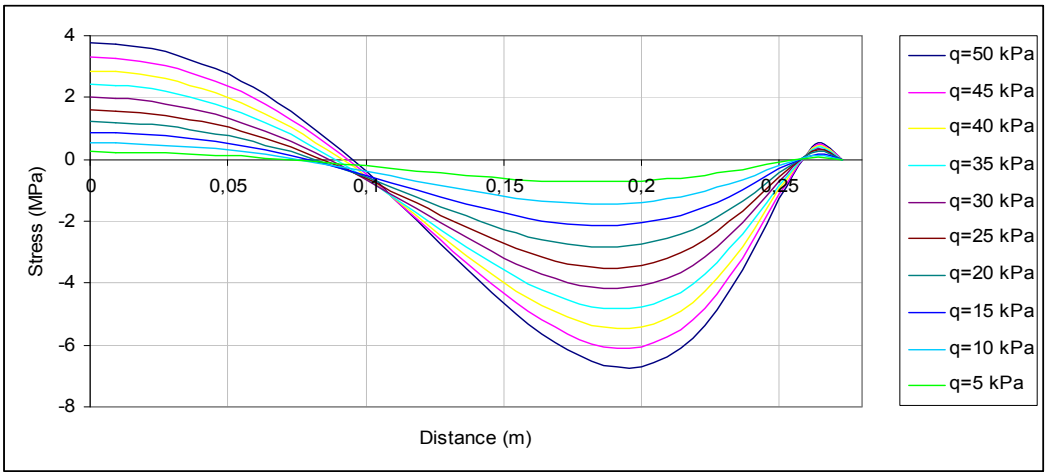

Figure 3.34 Minimum stresses on the top surface of the top shell along the diagonal

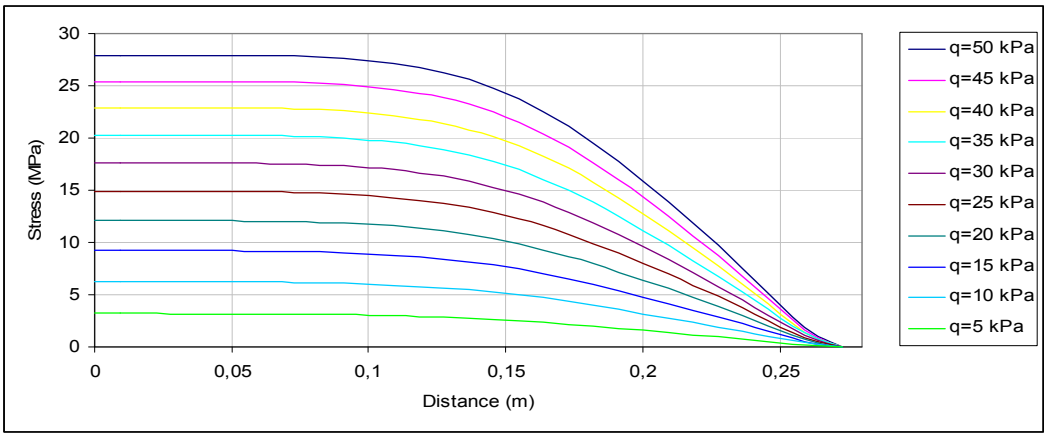

Figure 3.35 Maximum stresses on the bottom surface of the bottom shell along the diagonal

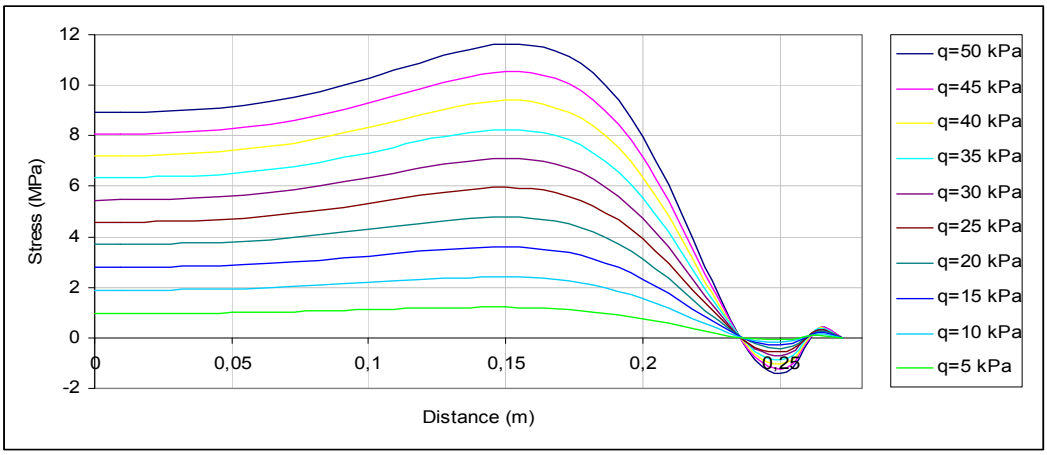

Figure 3.36 Minimum stresses on the bottom surface of the bottom shell along the diagonal

Function of shear stress of interlayer along the center line at y=0 and along the centerline at θ=0 is plotted in Figures 3.37 and 3.38. For fixed supported shell, it is observed that shear stress is maximum close to the supports and zero at the center and boundaries. Shear stress at the center and at the boundaries of unit is zero because of the geometry of unit as we expected.

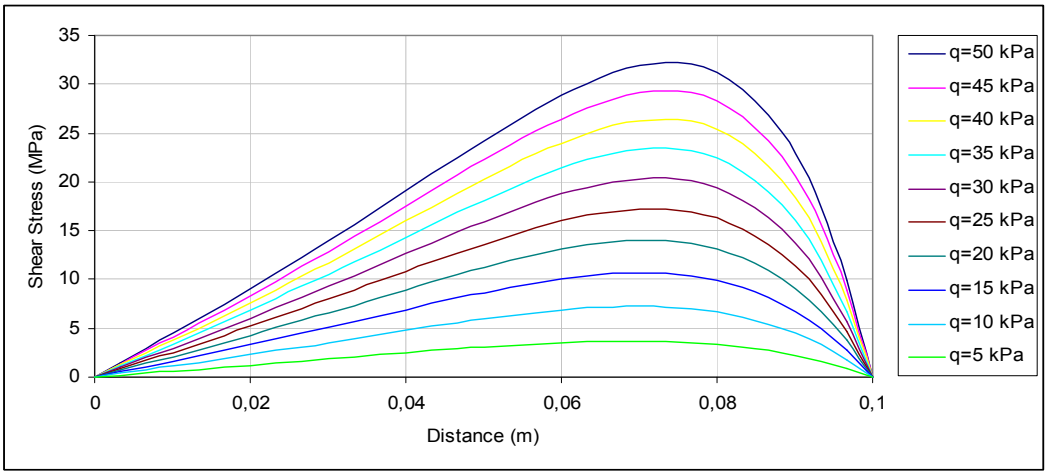

Figure 3.37 Shear stresses along θ direction

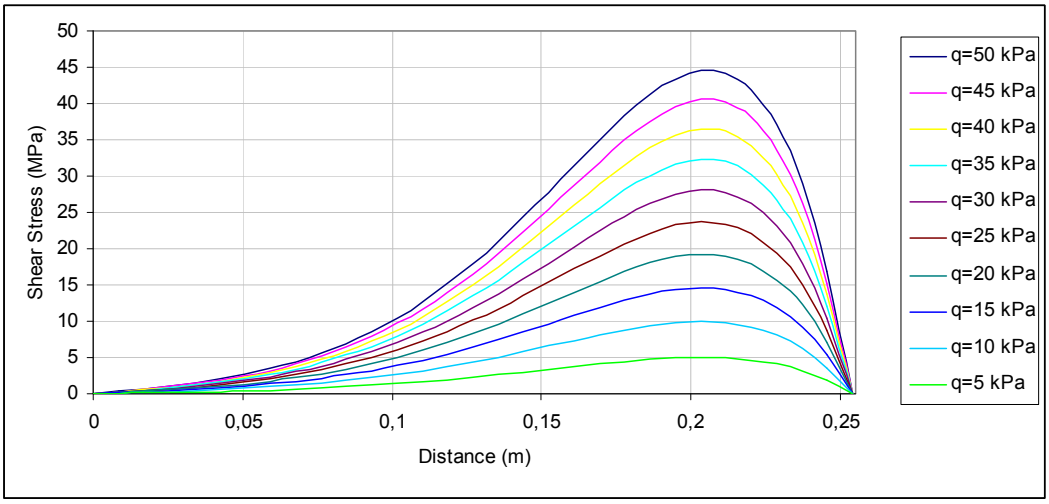

Figure 3.38 Shear stresses along y direction

In order to have detailed information, the contour of the radial deflection is given for the quarter of the shell unit. Radial deflection contours are plotted for applied pressure q=10, 20, 30, 40 and 50 kPa in Figures 3.39-3.43. Maximum radial deflection is at the center of the unit. They are getting smaller towards the corner of

the unit. The numbers, which are seen on horizontal and vertical axes, are the distances from the center.

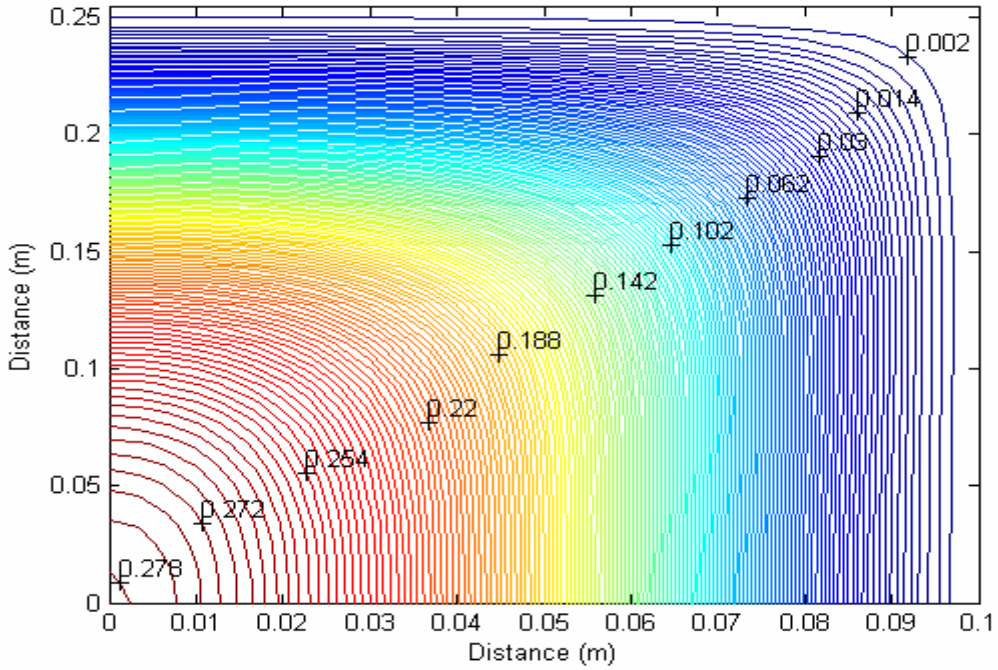

Figure 3.39 Contours of radial displacement (mm) for q=10 kPa

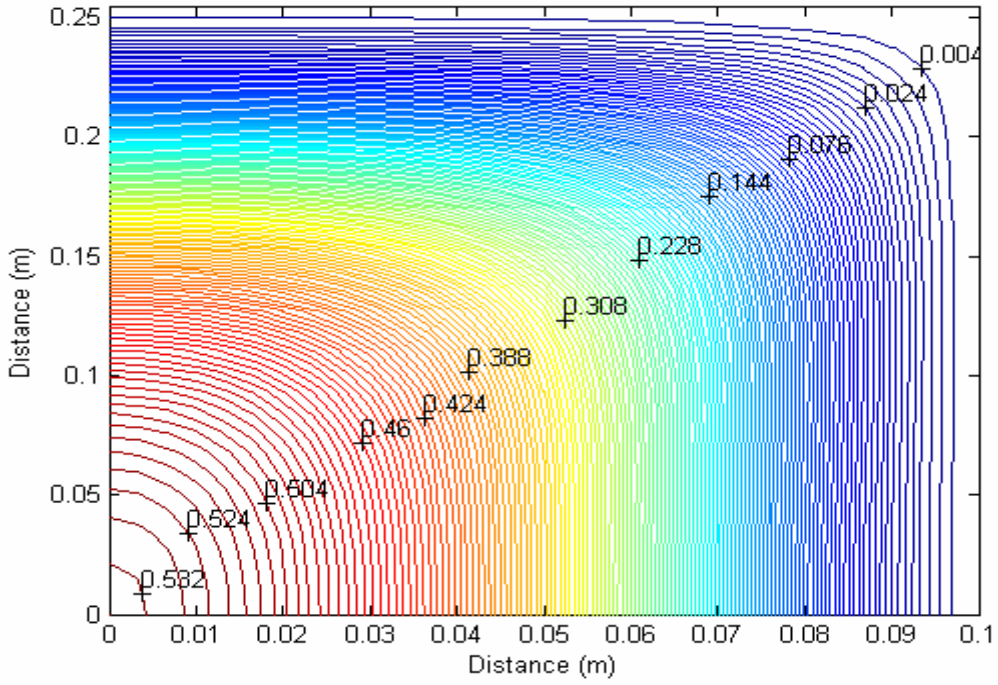

Figure 3.40 Contours of radial displacement (mm) for q=20 kPa

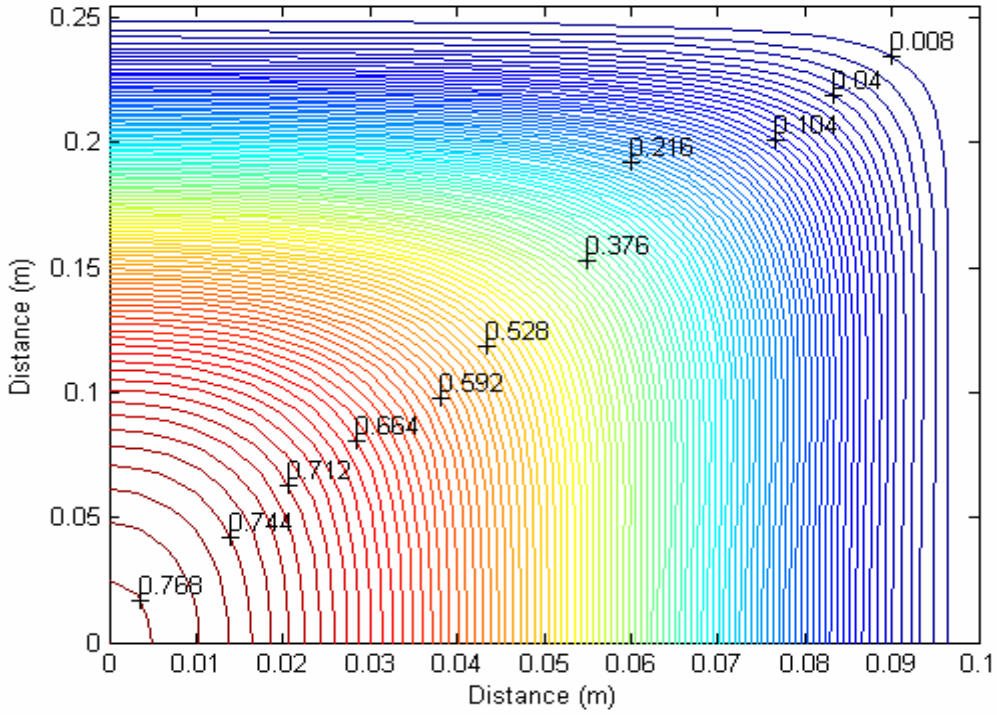

Figure 3.41 Contours of radial displacement (mm) for q=30 kPa

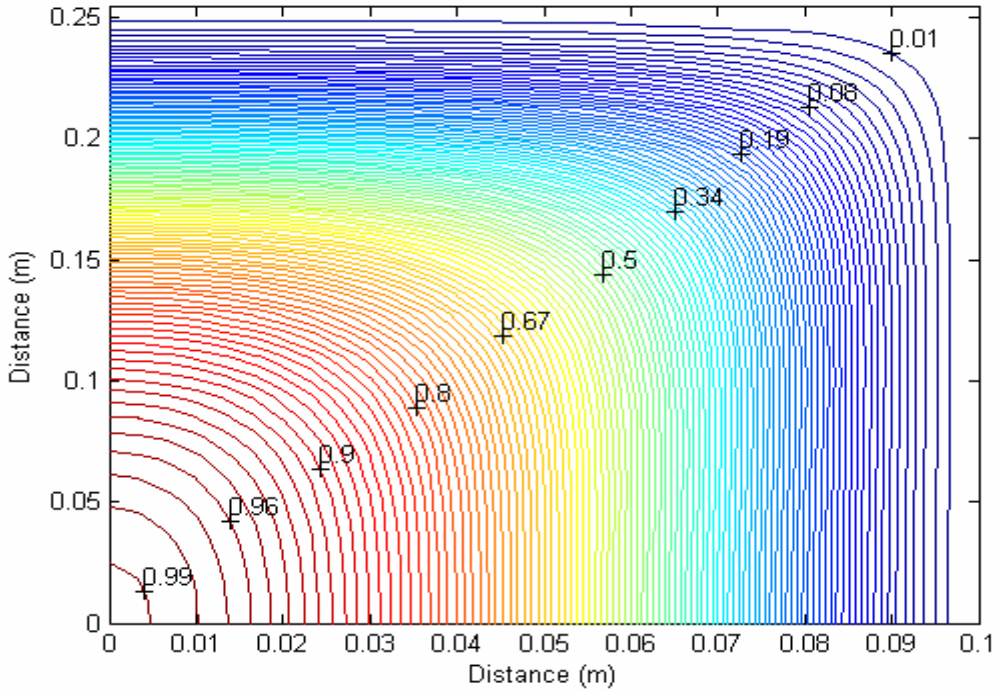

Figure 3.42 Contours of radial displacement (mm) for q=40 kPa

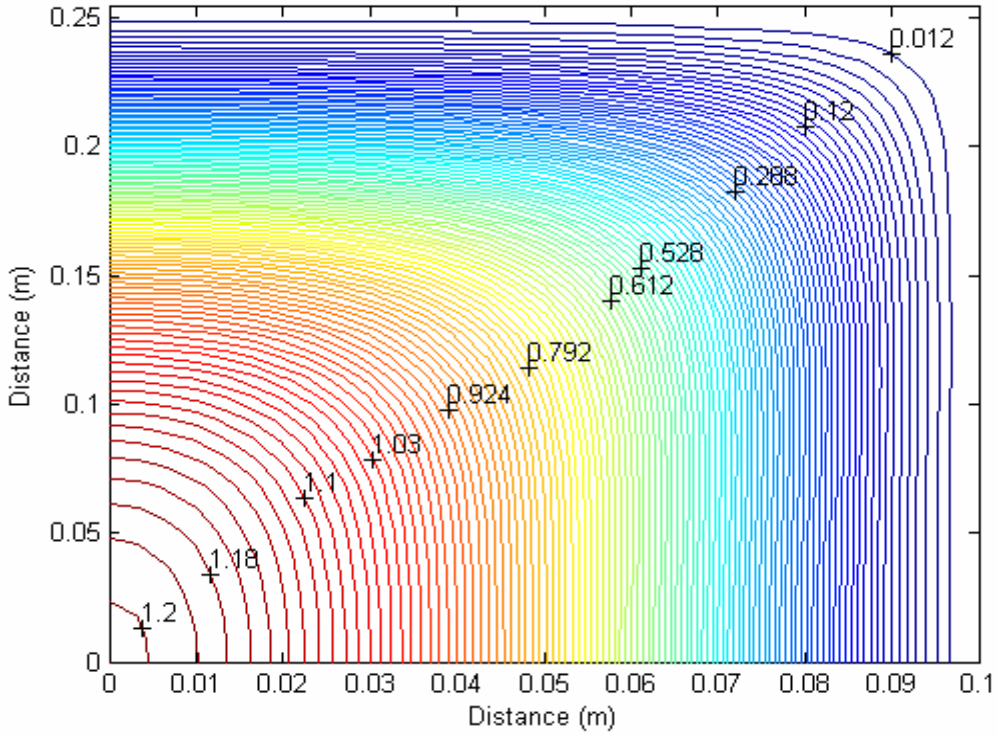

Figure 3.43 Contours of radial displacement (mm) for q=50 kPa

Figures 3.44-3.55 illustrate principal stress contours for the first quarter of laminated glass shell unit. Principal stress contours are plotted for applied pressure q= 10, 30, 50, 70, 90, 100 kPa. Contours of maximum principal stress on the top face of top glass unit are given in Figures 3.44-3.49 and minimum principal stress on the top surface of the top glass are given in Figures 3.50-3.55. Maximum principal stresses on the top surface take their maximum value at the intersection of upper boundary and symmetry axes of the unit. Maximum principal stresses on the top surface are in tension at every point of the shell unit. They are zero at the corner of the unit. Minimum principal stresses on the top surface of the top glass take their maximum value at the intersection of upper boundary and center line of the unit. The place of minimum value of minimum principal stress move horizontally towards the corner of the unit for increasing load levels. Minimum principal stress at the top surface of the top glass could be tension or compression as observed in Figures 3.50-3.55. They take zero values at the corner of unit.

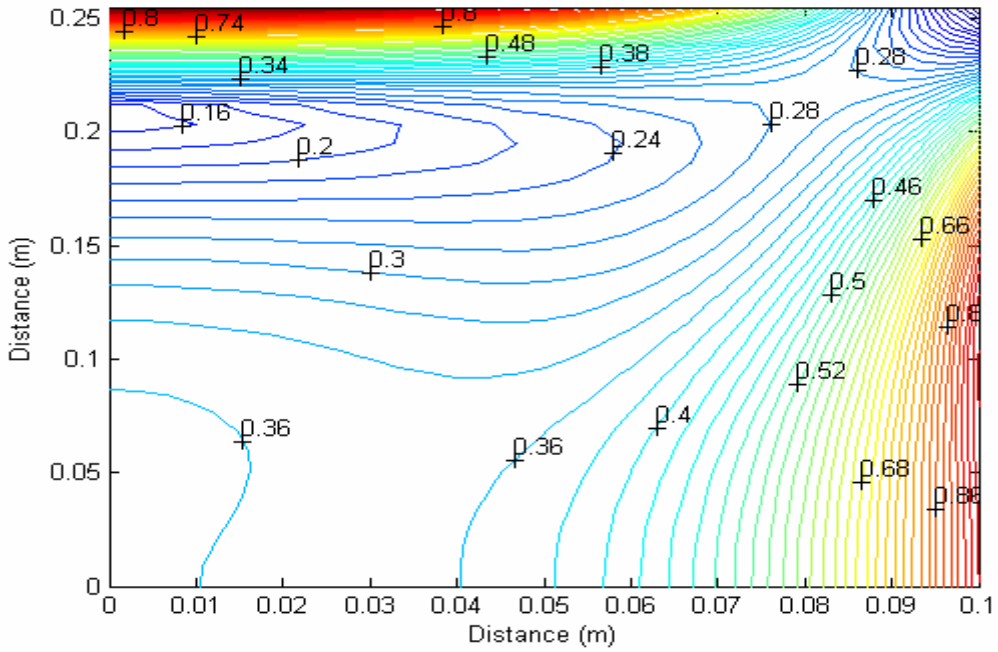

Figure 3.44 Contours of maximum principal stresses (*10^4 kPa) on the top surface of the top shell for q= 10 kPa.

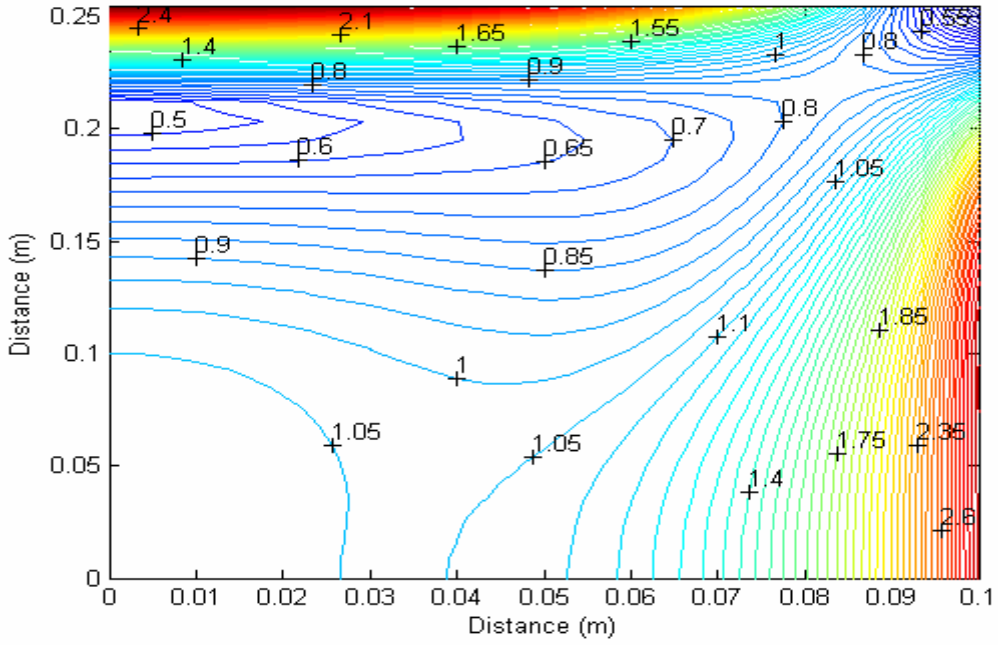

Figure 3.45 Contours of maximum principal stresses (*10^4 kPa) on the top surface of the top shell for q= 30 kPa.

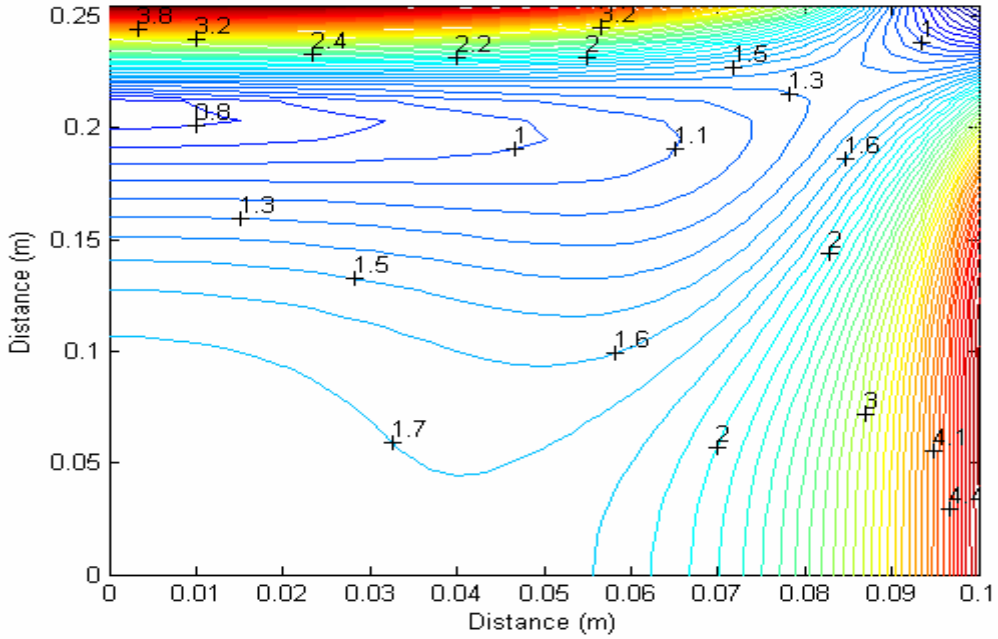

Figure 3.46 Contours of maximum principal stresses (*10^4 kPa) on the top surface of the top shell for q= 50 kPa.

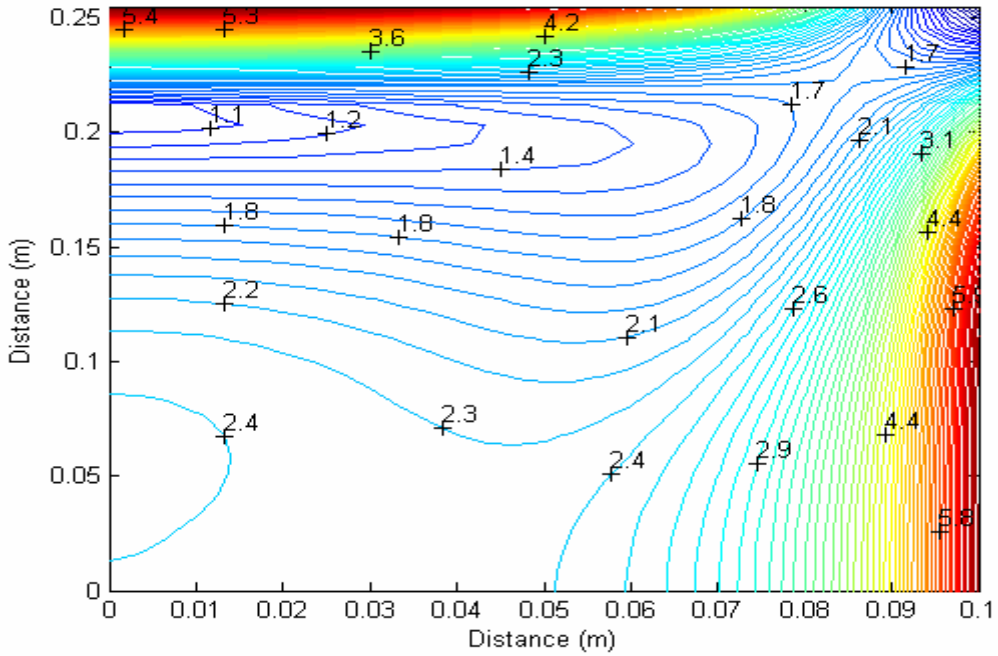

Figure 3.47 Contours of maximum principal stresses (*10^4 kPa) on the top surface of the top shell for q= 70 kPa.

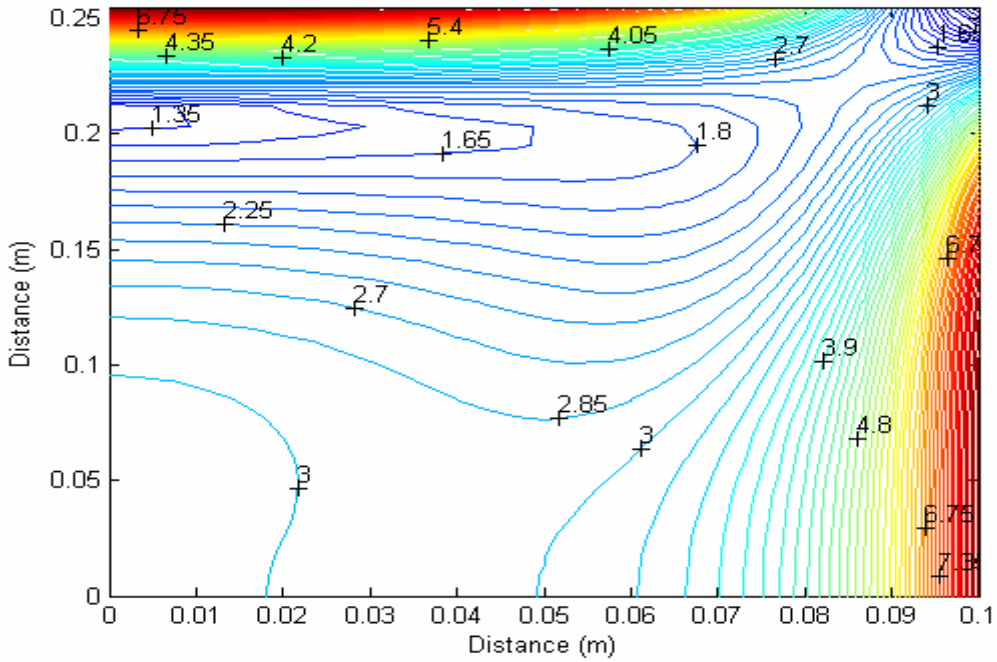

Figure 3.48 Contours of maximum principal stresses (*10^4 kPa) on the top surface of the top shell for q= 90 kPa

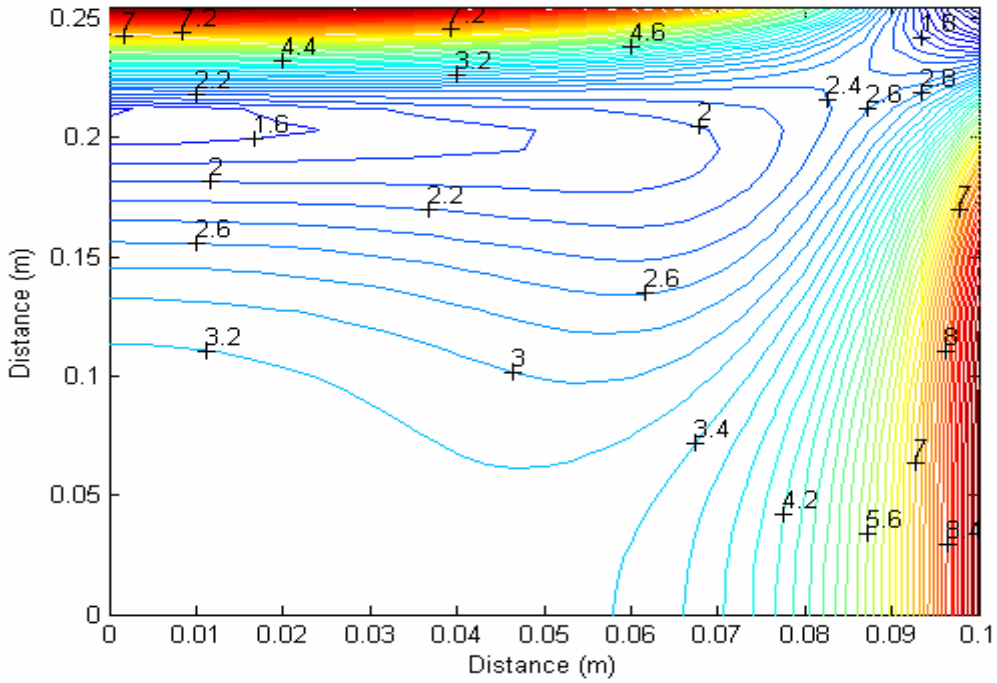

Figure 3.49 Contours of maximum principal stresses (*10^4 kPa) on the top surface of the top shell for q= 100 kPa

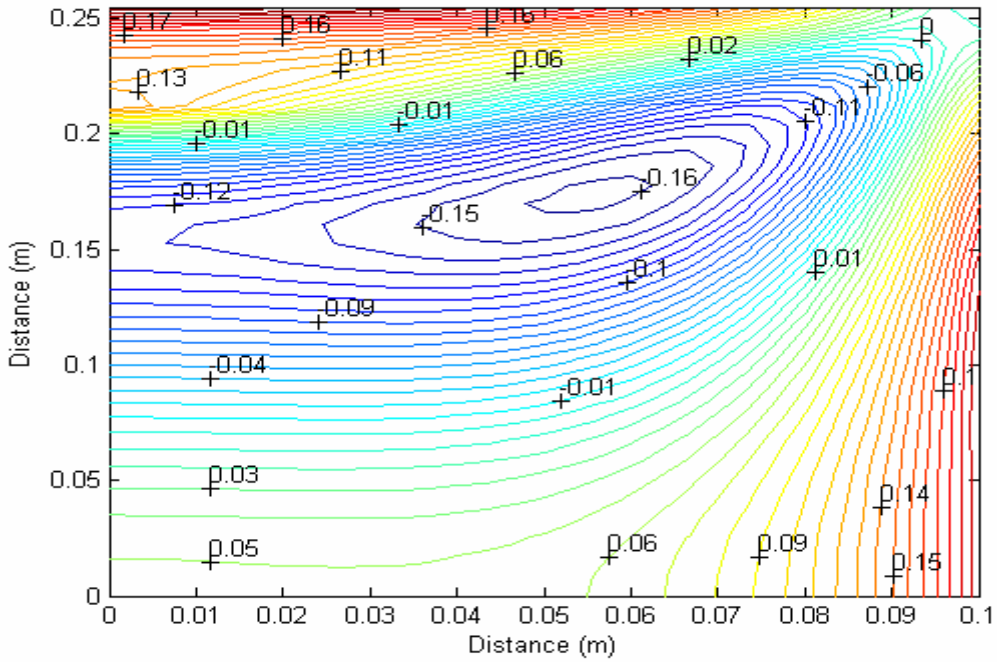

Figure 3.50 Contours of minimum principal stresses (*10^4 kPa) on the top surface of the top shell for q= 10 kPa

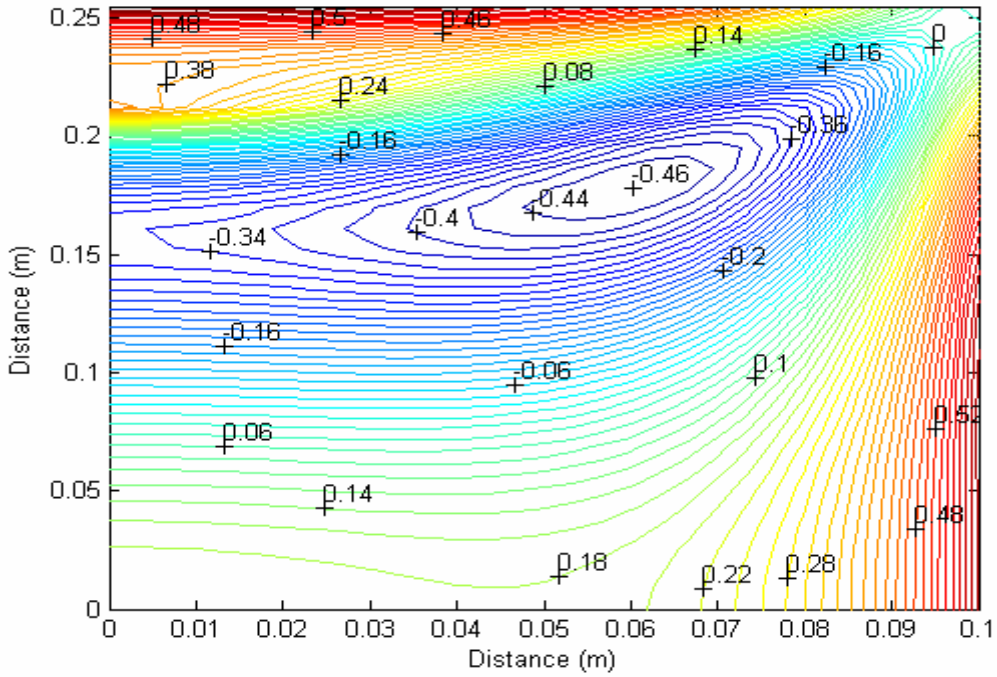

Figure 3.51 Contours of minimum principal stresses (*10^4 kPa) on the top surface of the top shell for q= 30 kPa

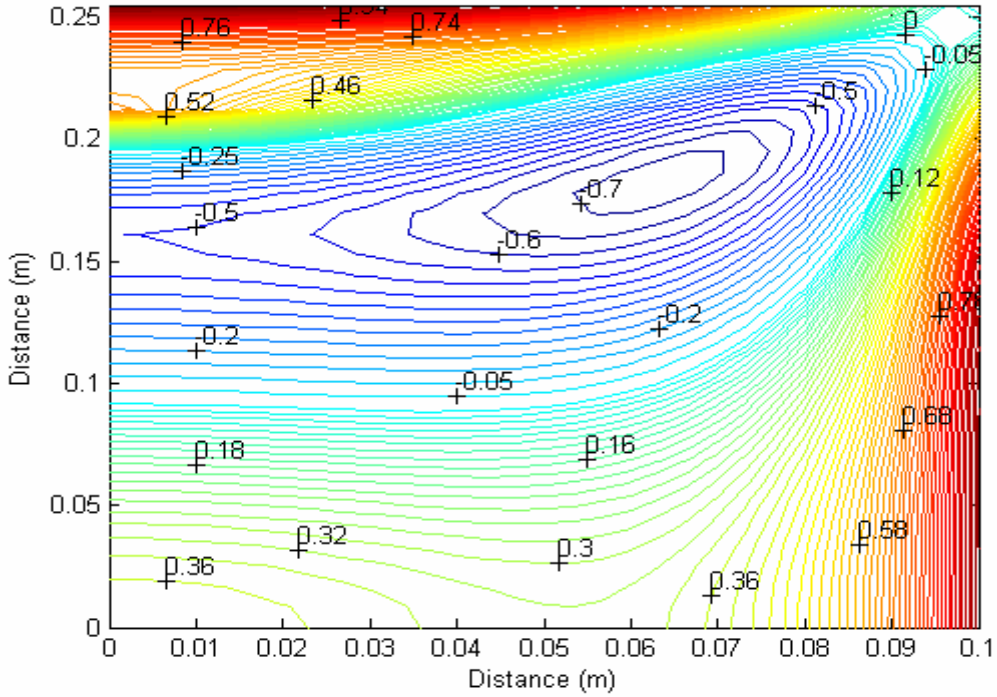

Figure 3.52 Contours of minimum principal stresses (*10^4 kPa) on the top surface of the top shell for q= 50 kPa

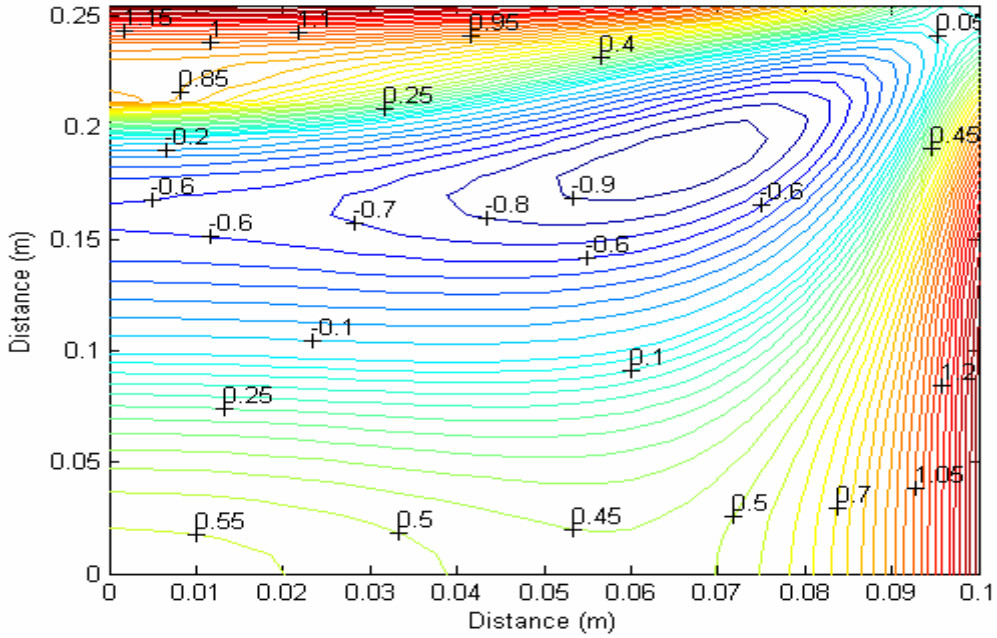

Figure 3.53 Contours of minimum principal stresses (*10^4 kPa) on the top surface of the top shell for q= 70 kPa

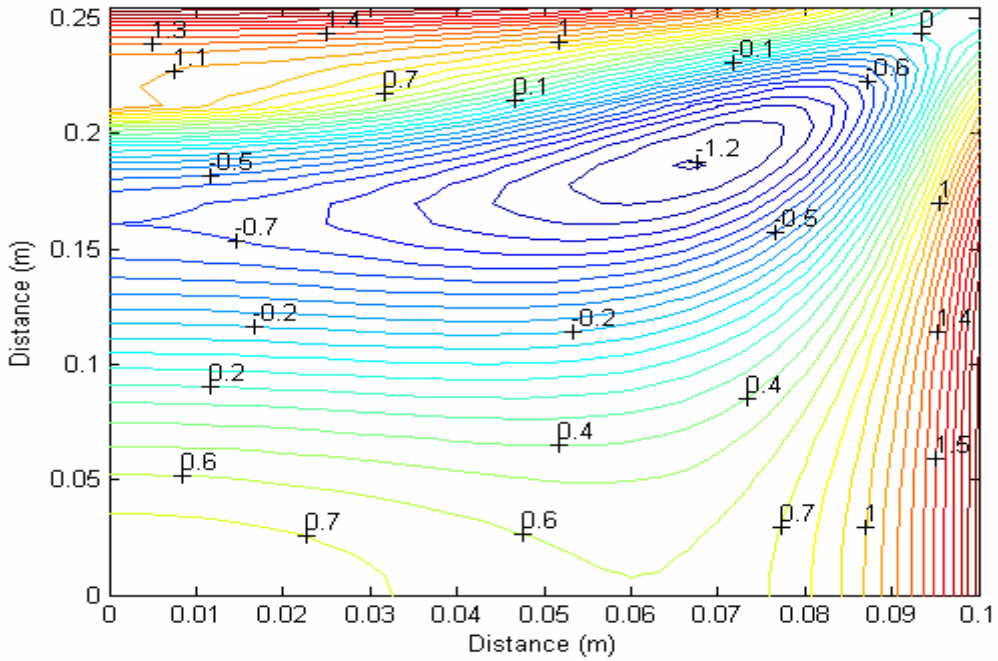

Figure 3.54 Contours of minimum principal stresses (*10^4 kPa) on the top surface of the top shell for q= 90 kPa

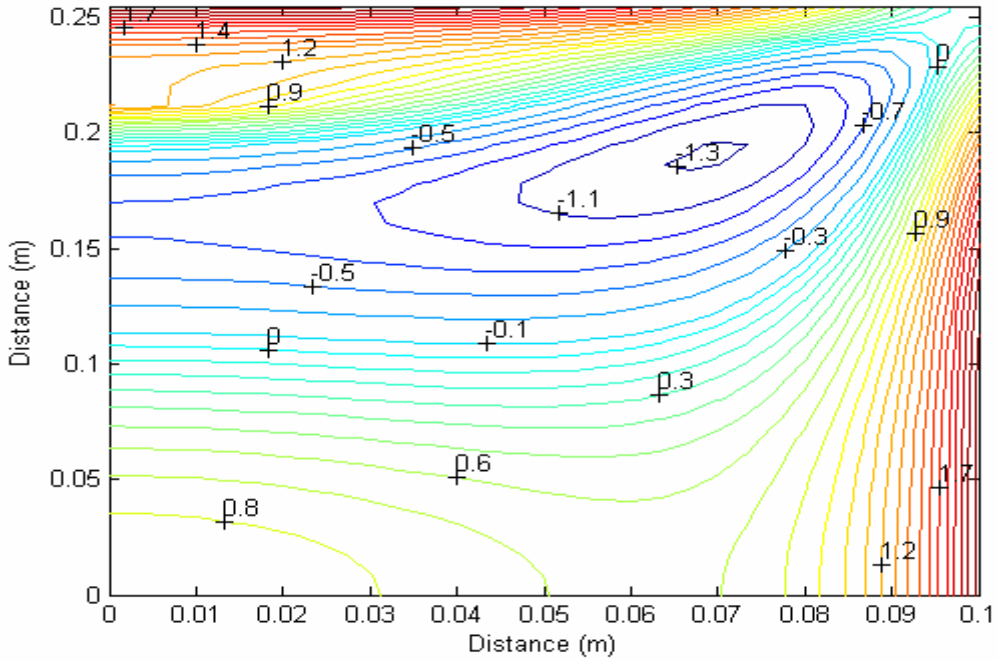

Figure 3.55 Contours of minimum principal stresses (*10^4 kPa) on the top surface of the top shell for q= 100 kPa

Maximum principal stresses at bottom surface of bottom glass are illustrated in Figures 3.56-3.62 for q=5, 20, 30, 50, 70, 90, 100 kPa. Maximum principal stresses on the bottom surface of the bottom glass surface take their maximum value close to the center of the unit as shown in Figure 3.56 for q=5 kPa which can be accepted as linear behavior. It moves on the y-axis while load is increasing. Figures 3.56-3.62 illustrate that maximum principal stress could be tension or compression on the bottom surface of the bottom glass sheet. While they are compression near the boundaries, they are tension around the center. Maximum stresses at the bottom surface of the bottom glass take their minimum value at the left hand side of the upper bound.

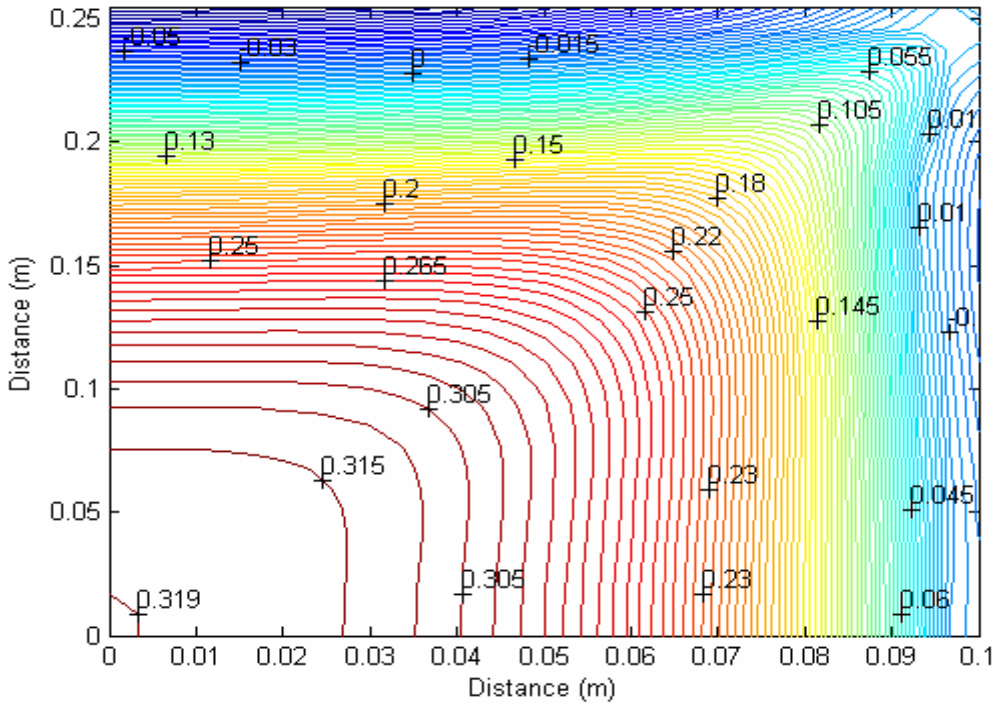

Figure 3.56 Contours of maximum principal stresses (*10^4 kPa) on the bottom surface of the bottom shell for q= 5 kPa

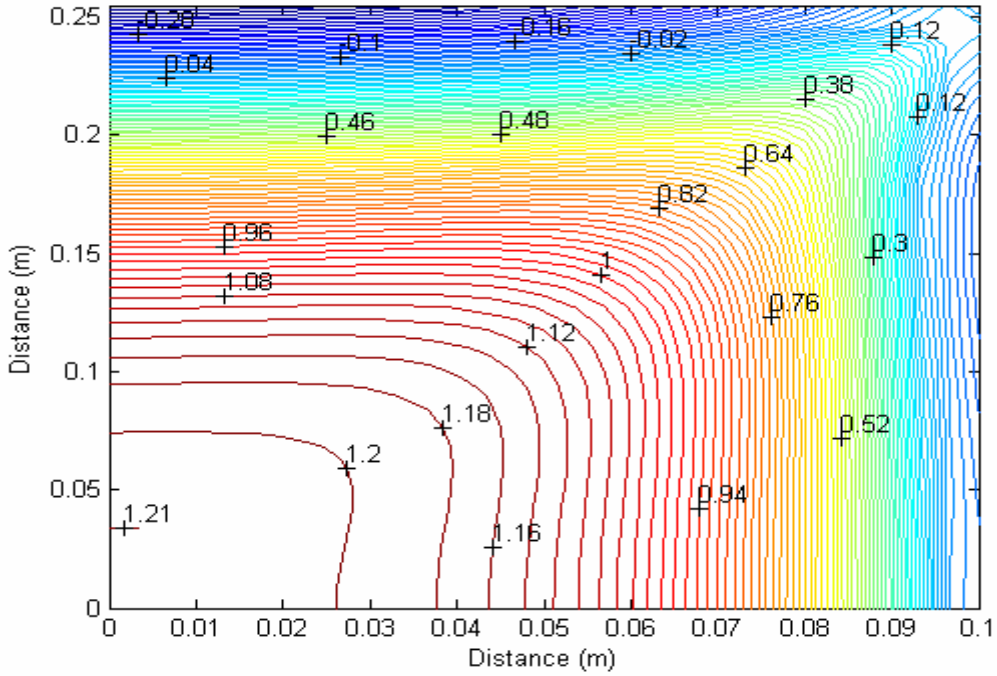

Figure 3.57 Contours of maximum principal stresses (*10^4 kPa) on the bottom surface of the bottom shell for q= 20 kPa

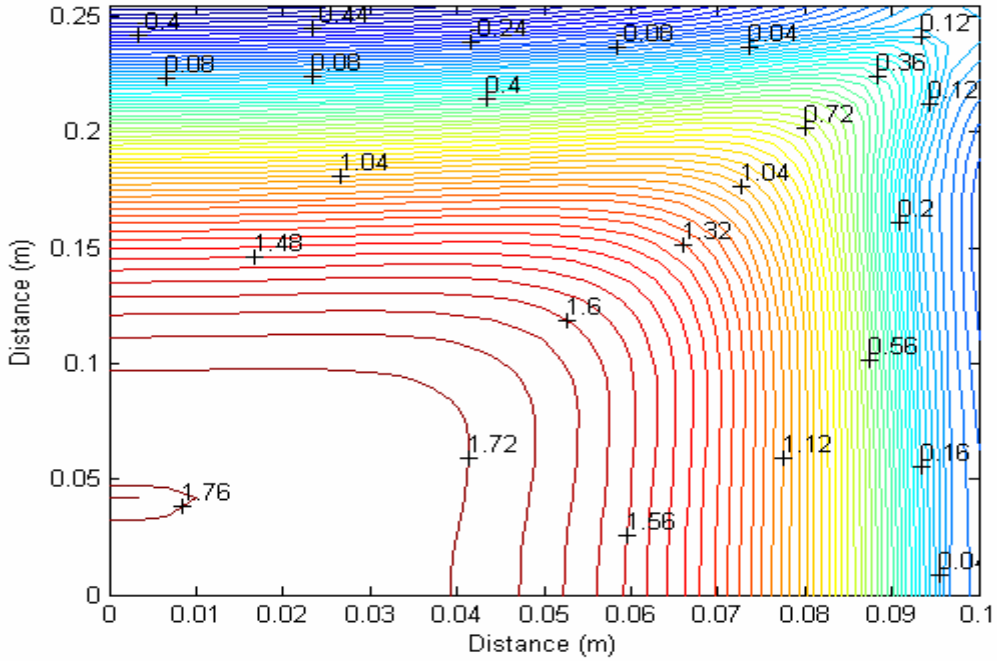

Figure 3.58 Contours of maximum principal stresses (*10^4 kPa) on the bottom surface of the bottom shell for q= 30 kPa

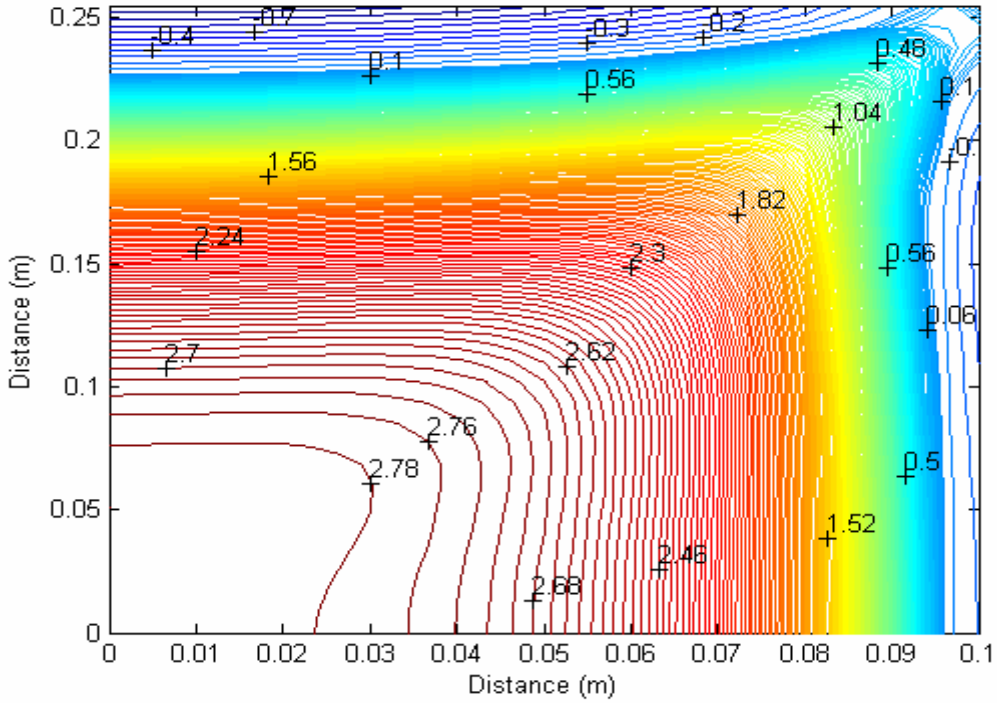

Figure 3.59 Contours of maximum principal stresses (*10^4 kPa) on the bottom surface of the bottom shell for q= 50 kPa

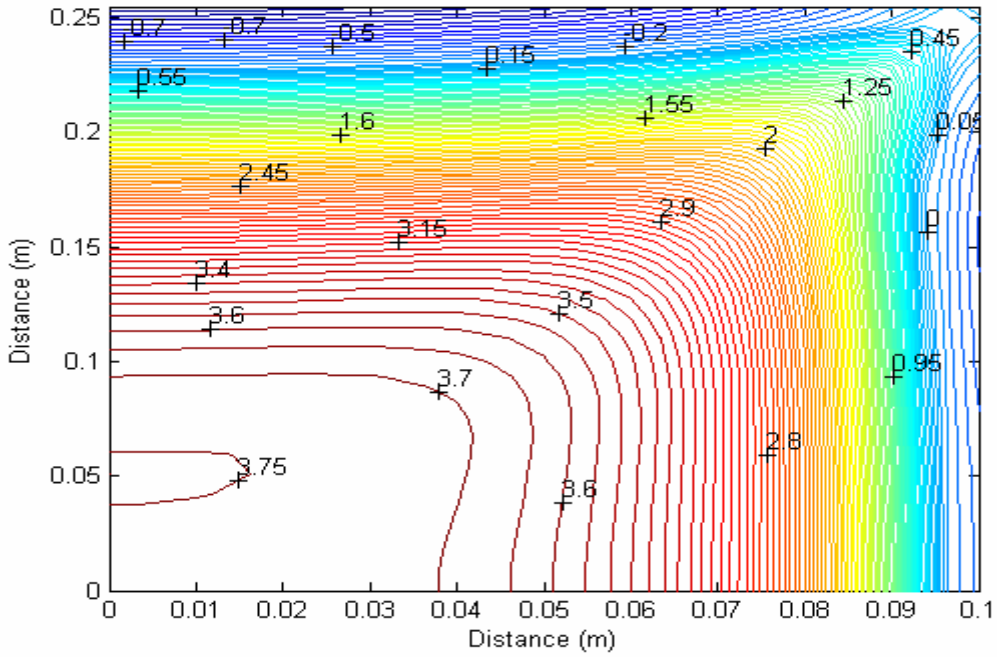

Figure 3.60 Contours of maximum principal stresses (*10^4 kPa) on the bottom surface of the bottom shell for q= 70 kPa

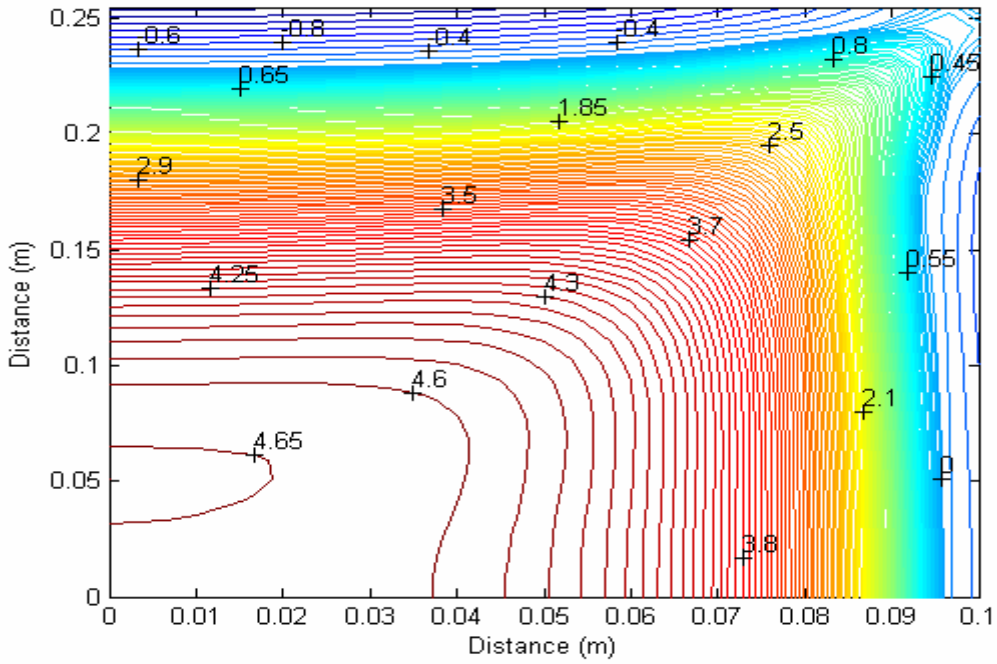

Figure 3.61 Contours of maximum principal stresses (*10^4 kPa) on the bottom surface of the bottom shell for q= 90 kPa

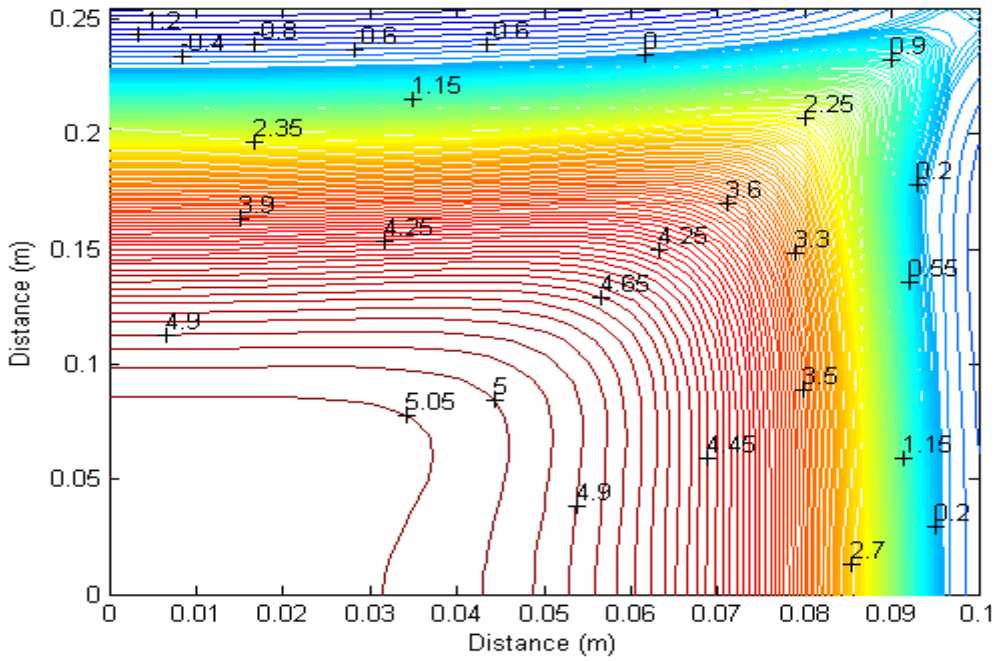

Figure 3.62 Contours of maximum principal stresses (*10^4 kPa) on the bottom surface of the bottom shell for q= 100 kPa

Contours of minimum principal stress on the bottom face of the bottom glass are illustrated in Figures 3.63- 3.68. Minimum principal stresses take both positive and negative values. They are compression close to boundaries of the shell unit. The maximum negative value of minimum principal stress is at the intersection of center and top boundary of the unit. The maximum positive value of minimum principal stress moves toward the top boundary for higher pressure values.

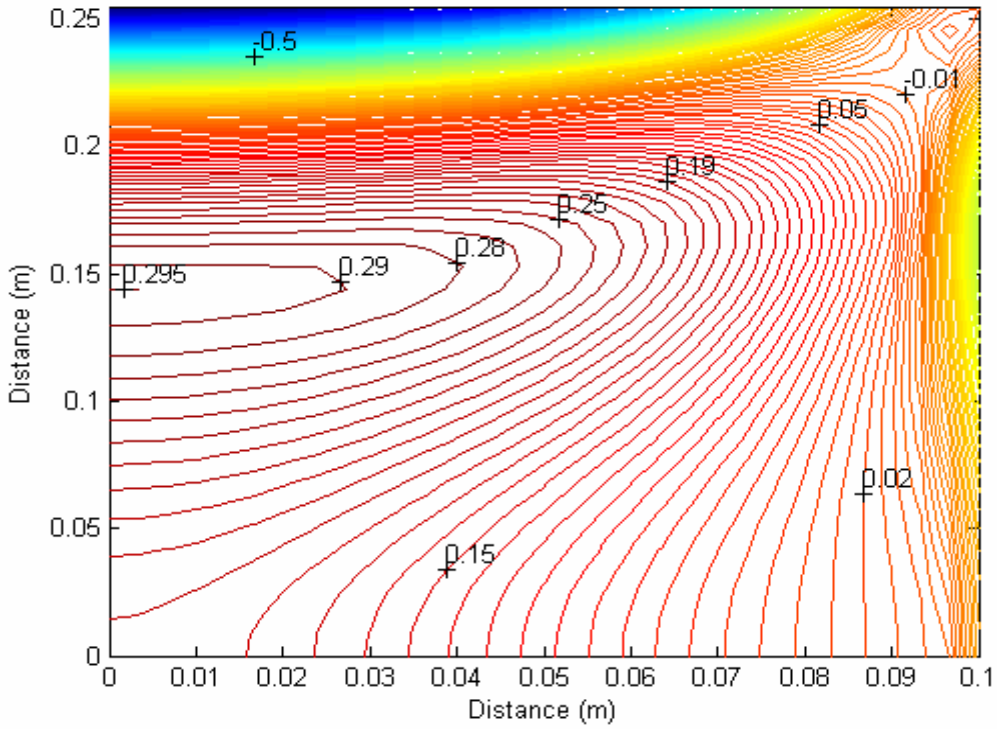

Figure 3.63 Contours of minimum principal stresses (*10^4 kPa) on the bottom surface of the bottom shell for q= 10 kPa

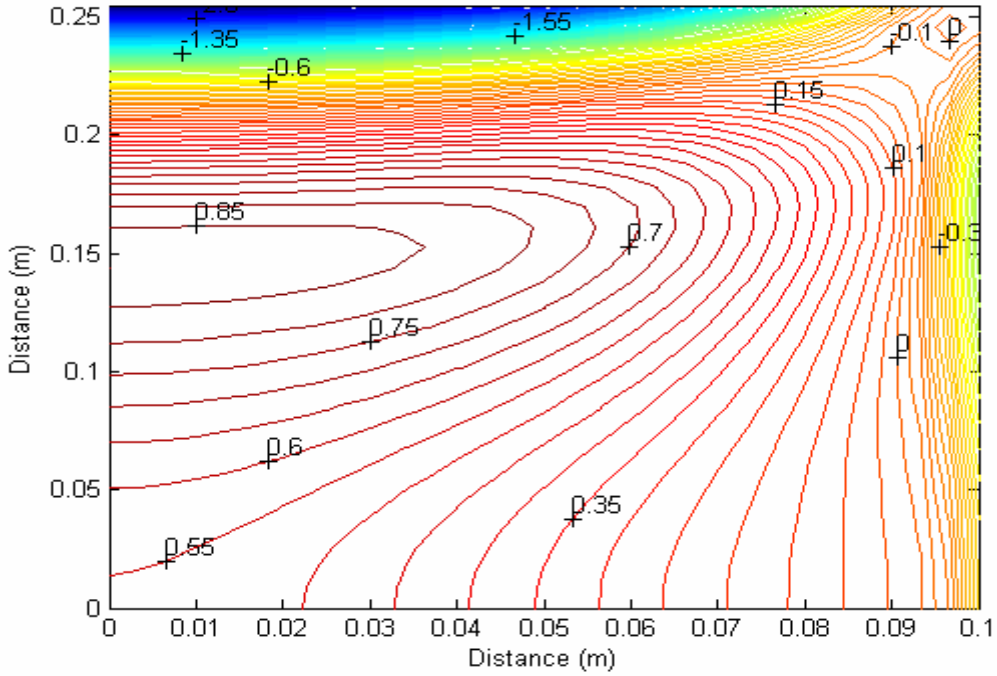

Figure 3.64 Contours of minimum principal stresses (*10^4 kPa) on the bottom surface of the bottom shell for q= 30 kPa

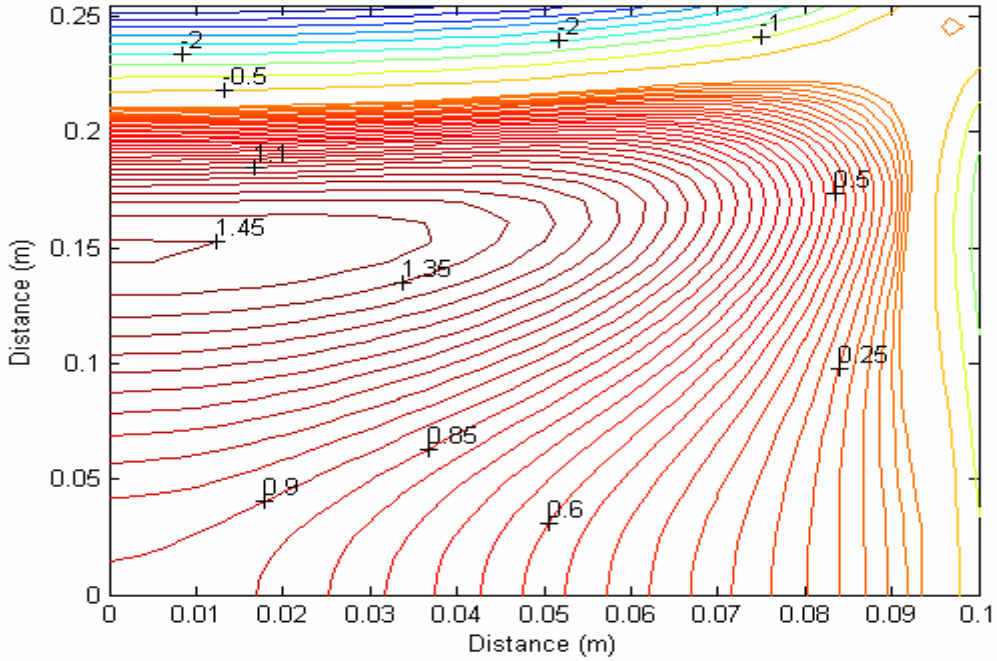

Figure 3.65 Contours of minimum principal stresses (*10^4 kPa) on the bottom surface of the bottom shell for q= 50 kPa

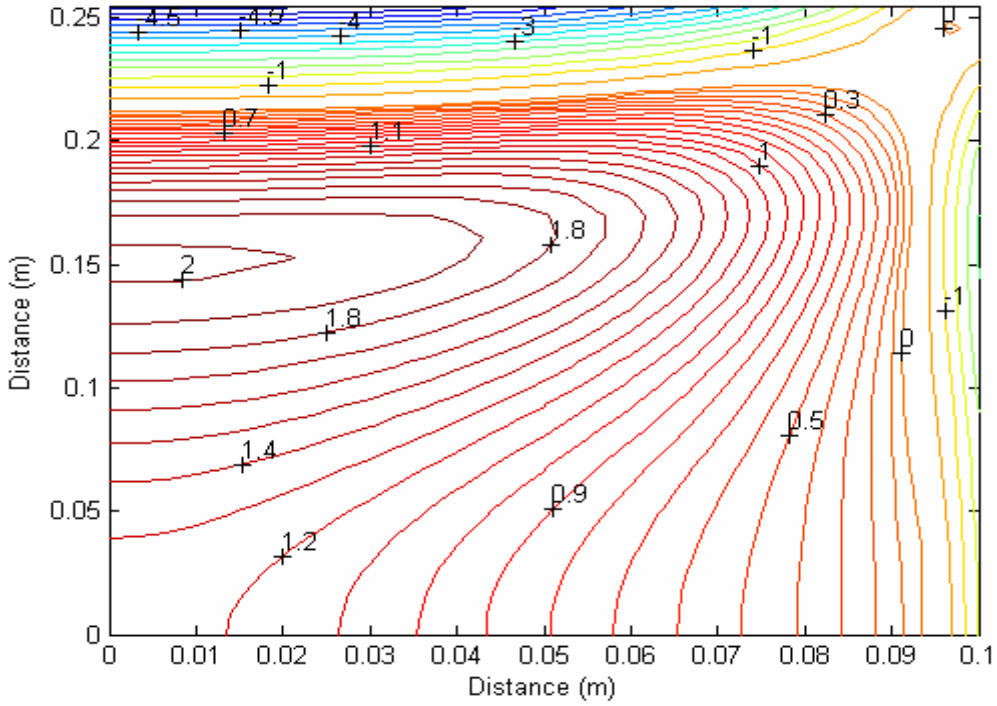

Figure 3.66 Contours of minimum principal stresses (*10^4 kPa) on the bottom surface of the bottom shell for q= 70 kPa

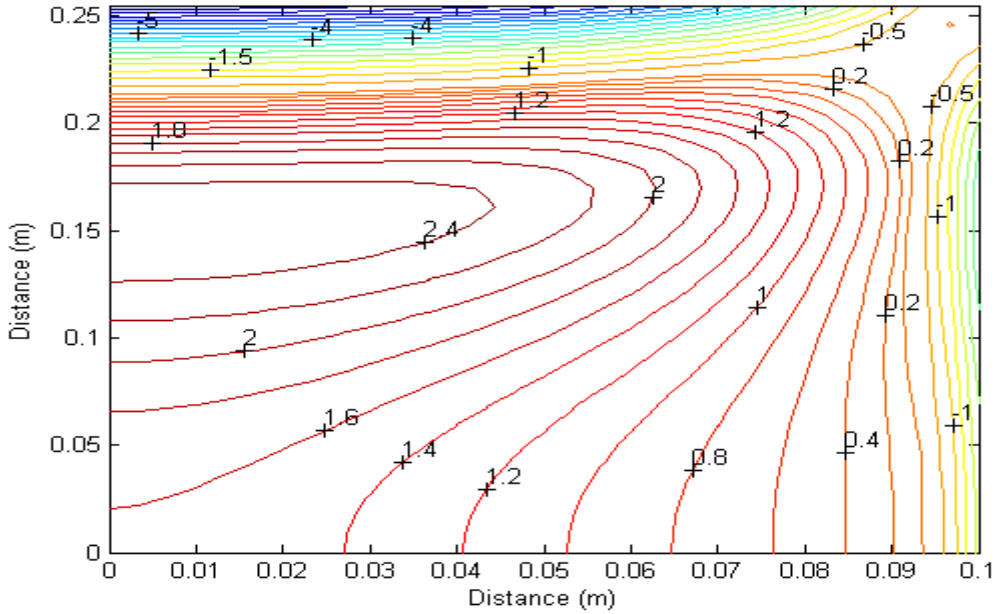

Figure 3.67 Contours of minimum principal stresses (*10^4 kPa) on the bottom surface of the bottom shell for q= 90 kPa

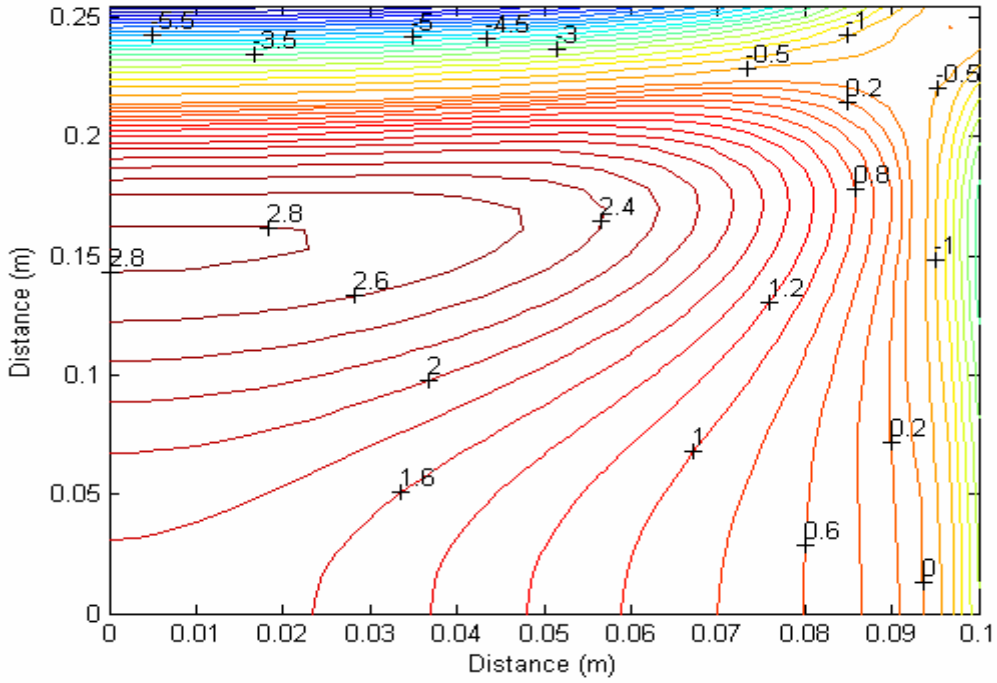

Figure 3.68 Contours of minimum principal stresses (*10^4 kPa) on the bottom surface of the bottom shell for q= 100 kPa

Because of the perfect bound between the polyvinyl butyral interlayer and glass sheets, stress on bottom surface of top glass is equal to the stress on the top surface of interlayer and stress on the bottom surface of PVB interlayer. Maximum principal stress contours for applied pressure q= 10, 30, 50, 70, 90, 100 kPa are illustrated in Figures3.69-3.74 on the bottom surface of the top shell and in Figures 3.75-3.81 on the top surface of the bottom shell. Maximum principal stress on the bottom surface of the top shell is at the center in Figure 3.69 for q= 10 kPa which can be accepted as linear behavior. It moves away from x and y-axis towards the corner of quarter shell for higher load values. Maximum principal stress on the bottom surface of the top shell could be tension or compression. They are in compression along the boundaries of the unit. Maximum principal stresses on the top surface of the bottom shell take their maximum value at upper left corner of the unit for applied load till 100 kPa. For 100 kPa load they take their maximum value at the right boundary. Maximum

principal stresses are on tension for every load value and at everywhere of the shell unit. They take their minimum value at the upper right corner of the unit.

Minimum principal stress contours for applied pressure q= 10, 30, 50, 70, 90, 100 kPa are illustrated in Figures3.82-3.87 on the bottom surface of the top shell and in Figures 3.88-3.93 on the top surface of the bottom shell. Minimum principal stresses on the bottom surface of the top shell take their maximum value at the middle of the left center line while they take their minimum value at the upper left corner. They could be both tension and compression. They are on tension near the boundaries of quarter shell. Minimum principal stresses on the top surface of the bottom shell take their maximum value at the upper left corner. They take their minimum value close to the center of quarter shell for q=10 kPa, it moves towards the corner for higher load values. Minimum principal stress on the top surface of the bottom shell could be tension or compression. They take zero value inside the domain.

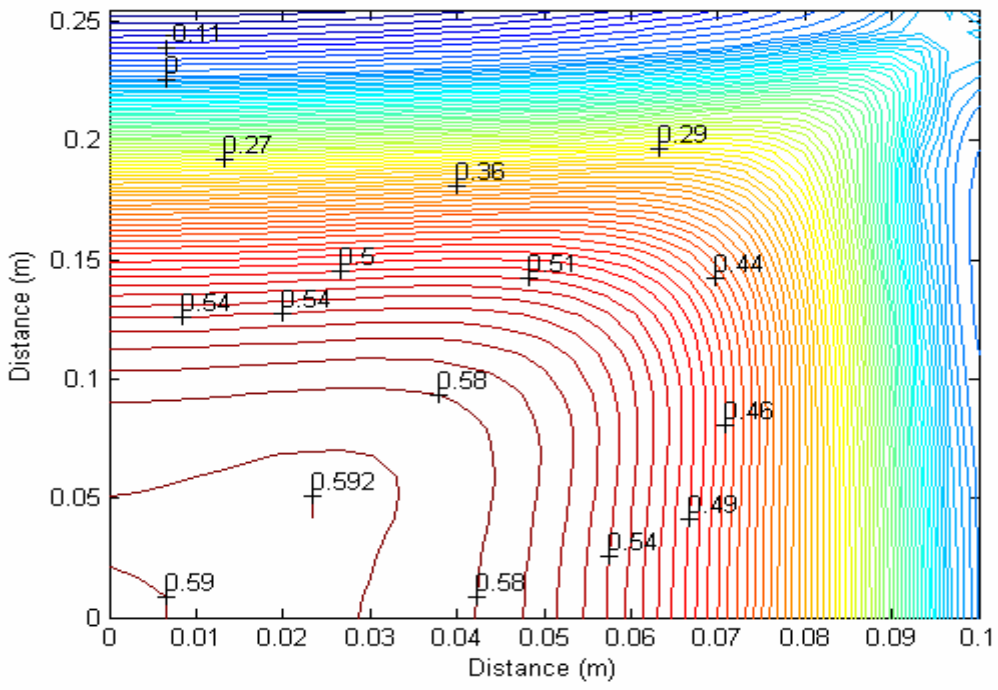

Figure 3.69 Contours of maximum principal stresses (*10^4 kPa) on the bottom surface of the top shell for q= 10 kPa

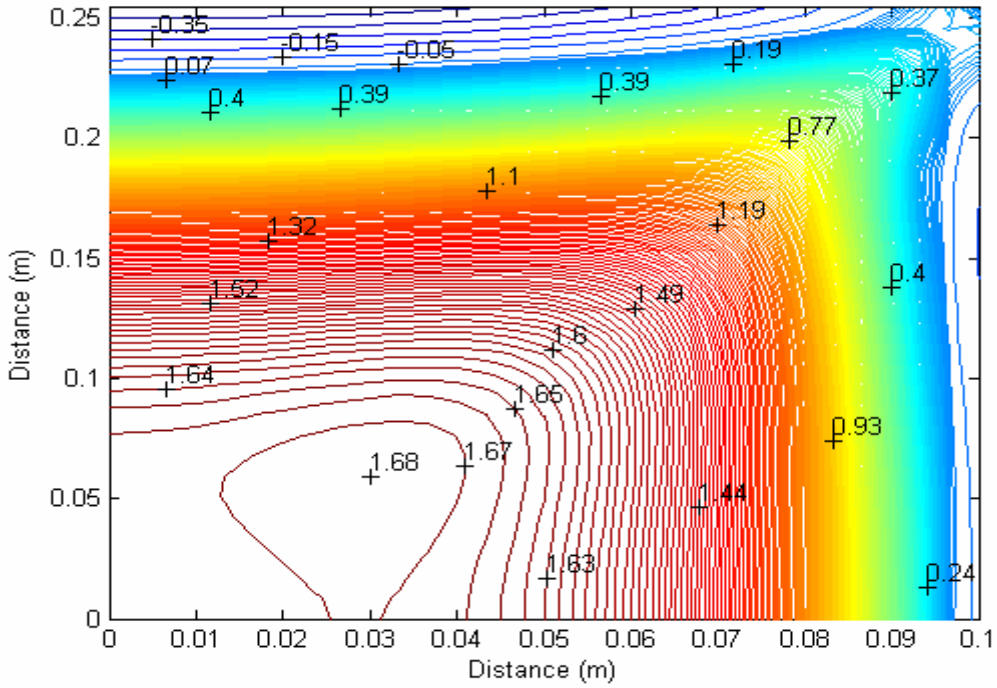

Figure 3.70 Contours of maximum principal stresses (*10^4 kPa) on the bottom surface of the top shell for q= 30 kPa

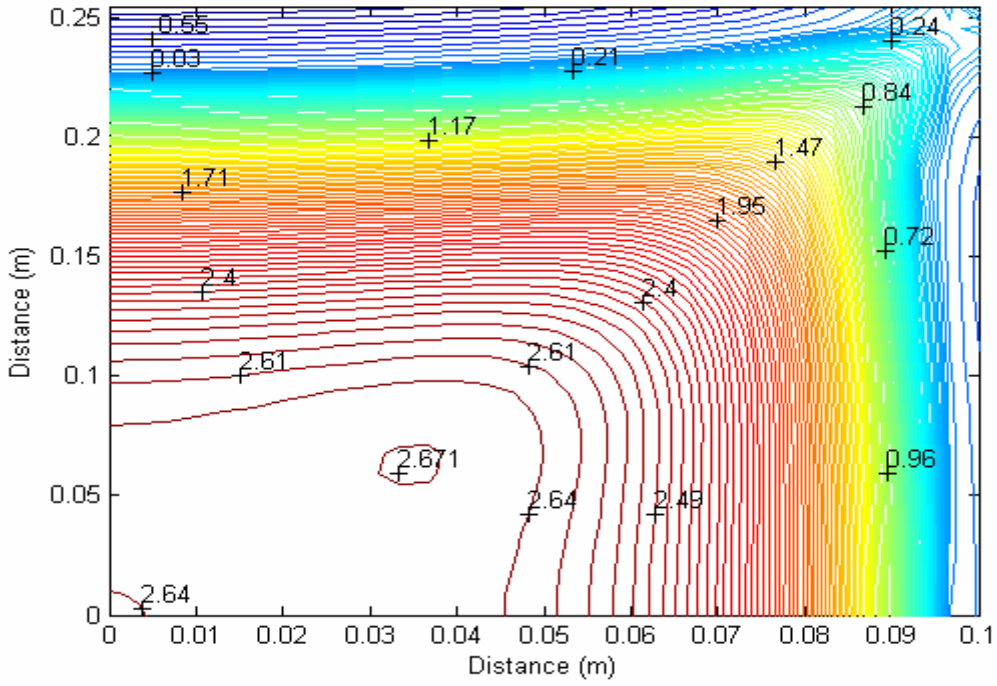

Figure 3.71 Contours of maximum principal stresses (*10^4 kPa) on the bottom surface of the top shell for q= 50 kPa

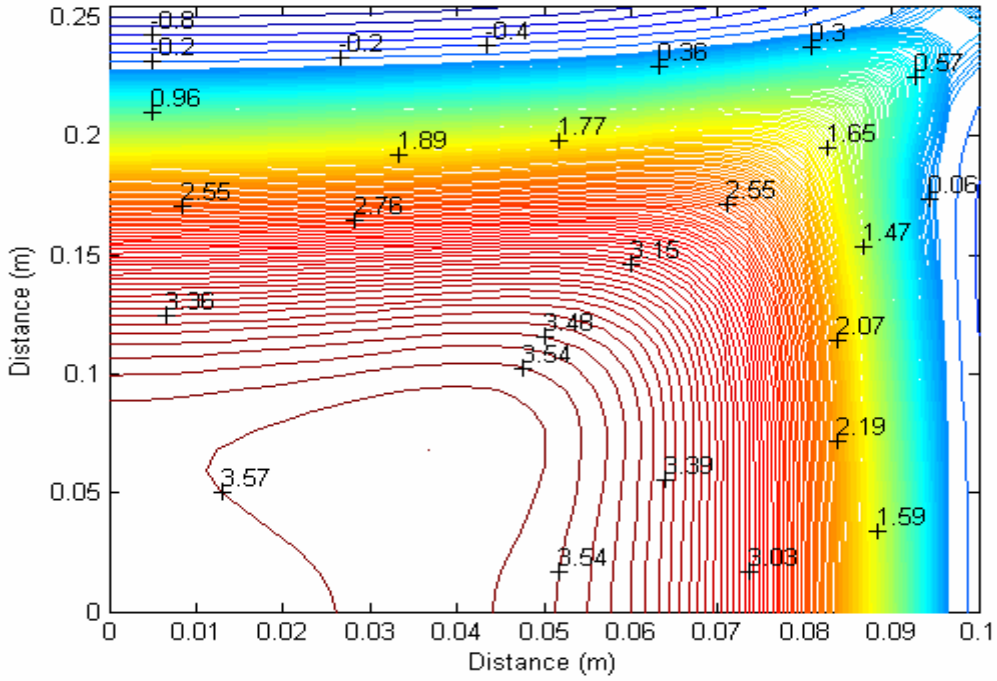

Figure 3.72 Contours of maximum principal stresses (*10^4 kPa) on the bottom surface of the top shell for q= 70 kPa

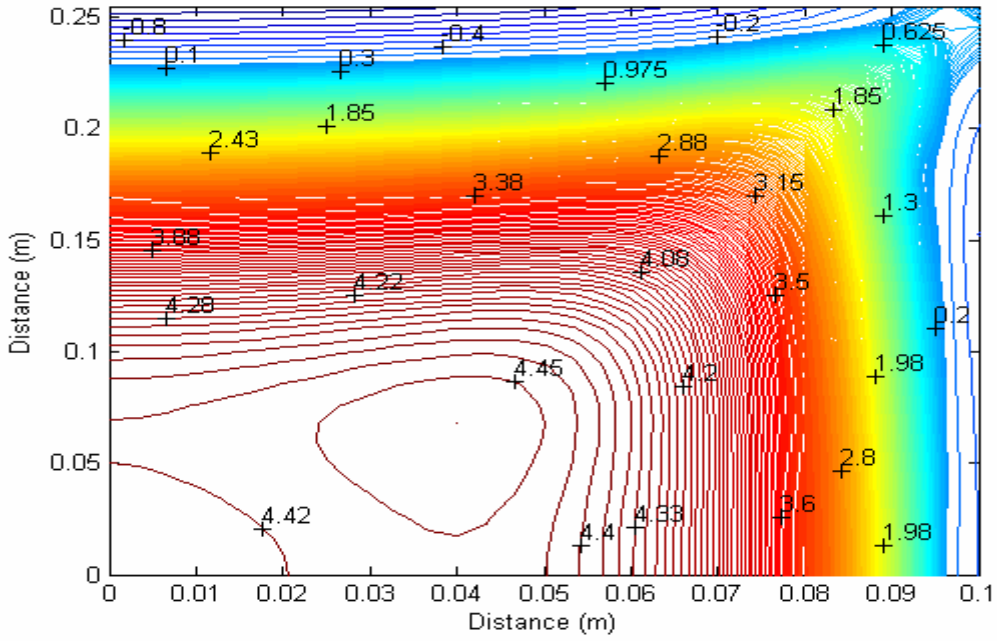

Figure 3.73 Contours of maximum principal stresses (*10^4 kPa) on the bottom surface of the top shell for q= 90 kPa

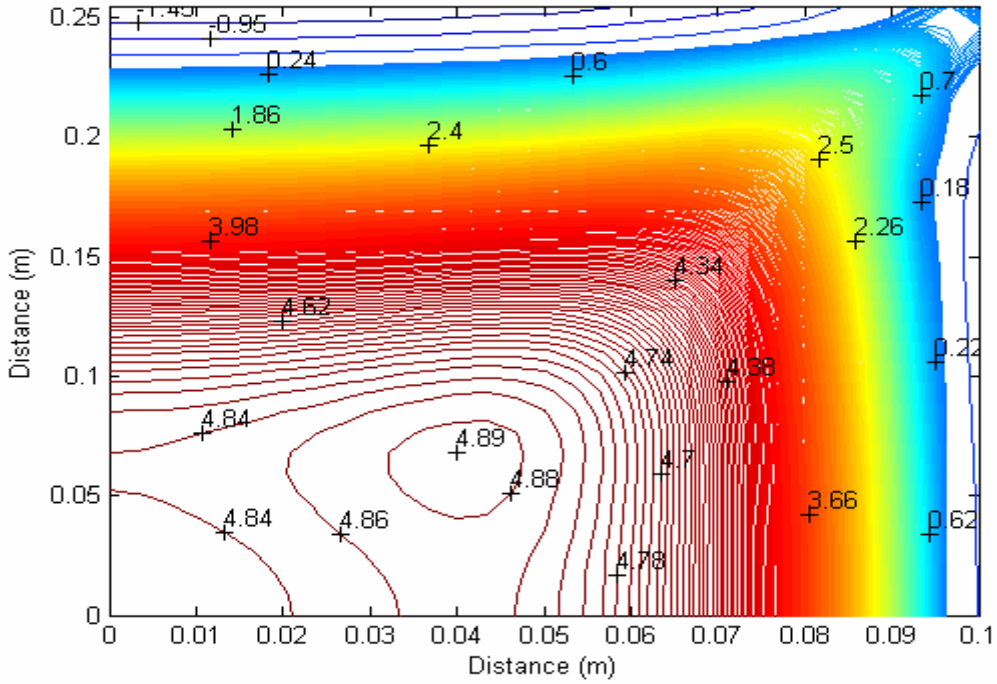

Figure 3.74 Contours of maximum principal stresses (*10^4 kPa) on the bottom surface of the top shell for q= 100 kPa

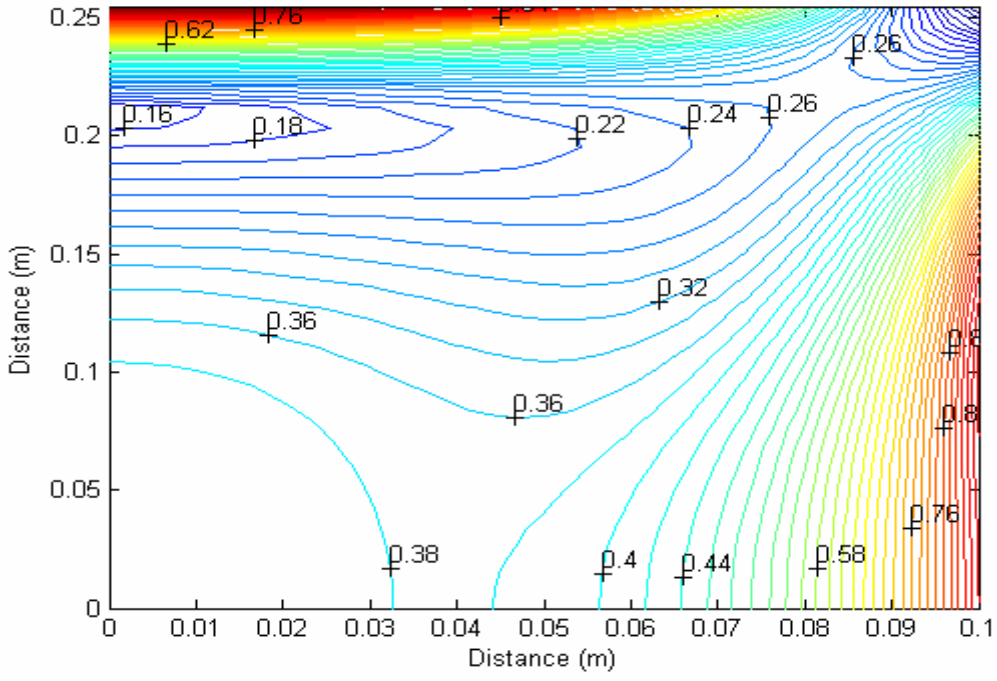

Figure 3.75 Contours of maximum principal stresses (*10^4 kPa) on the top surface of the bottom shell for q= 10 kPa

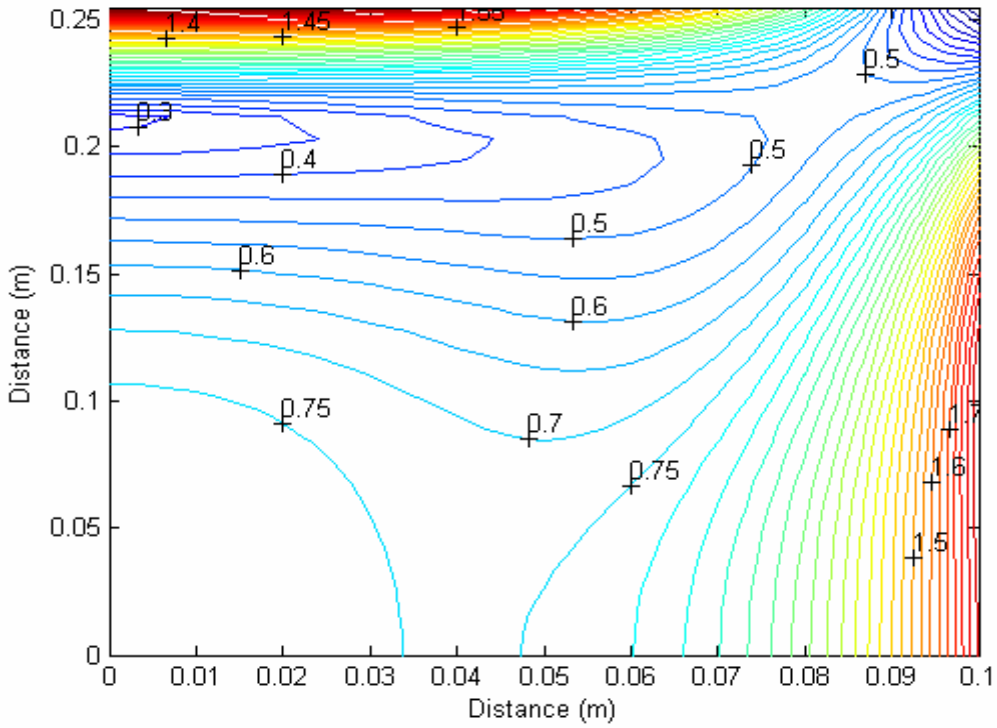

Figure 3.76 Contours of maximum principal stresses (*10^4 kPa) on the top surface of the bottom shell for q= 20 kPa

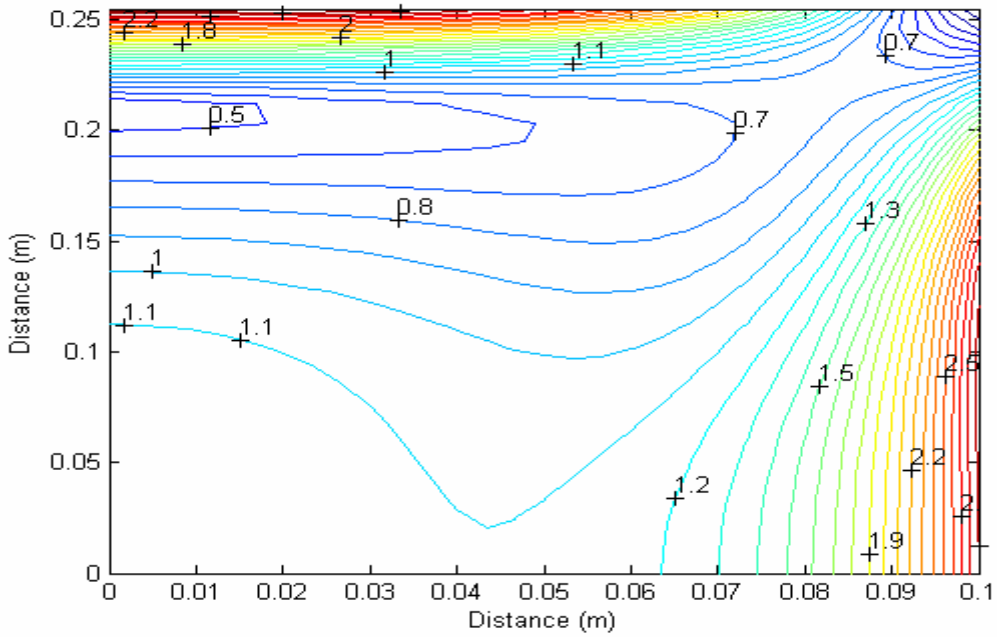

Figure 3.77 Contours of maximum principal stresses (*10^4 kPa) on the top surface of the bottom shell for q= 30 kPa

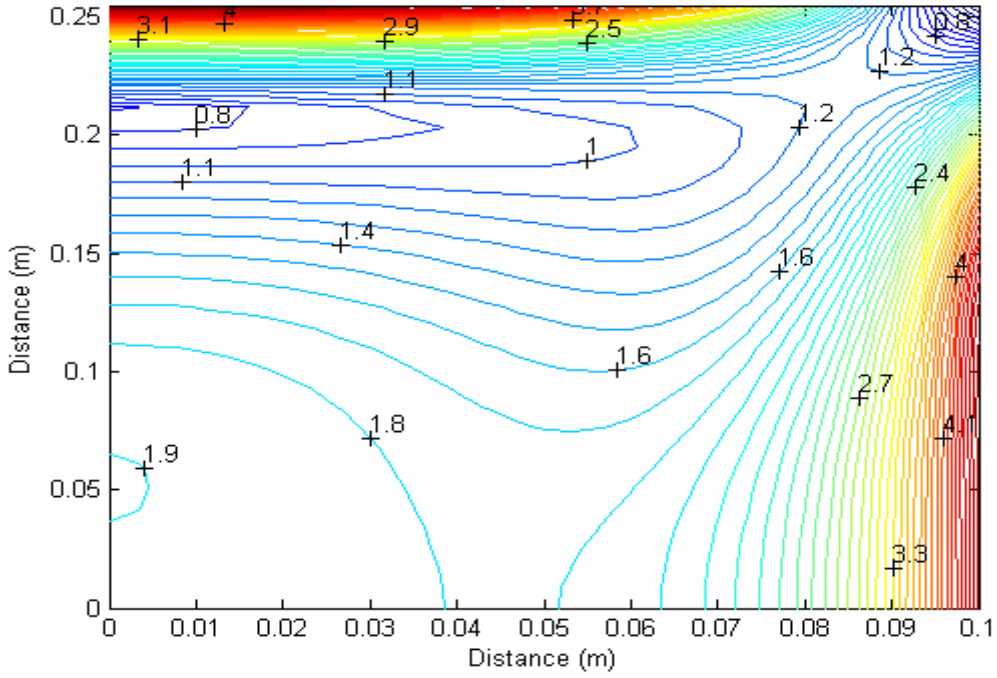

Figure 3.78 Contours of maximum principal stresses (*10^4 kPa) on the top surface of the bottom shell for q= 50 kPa

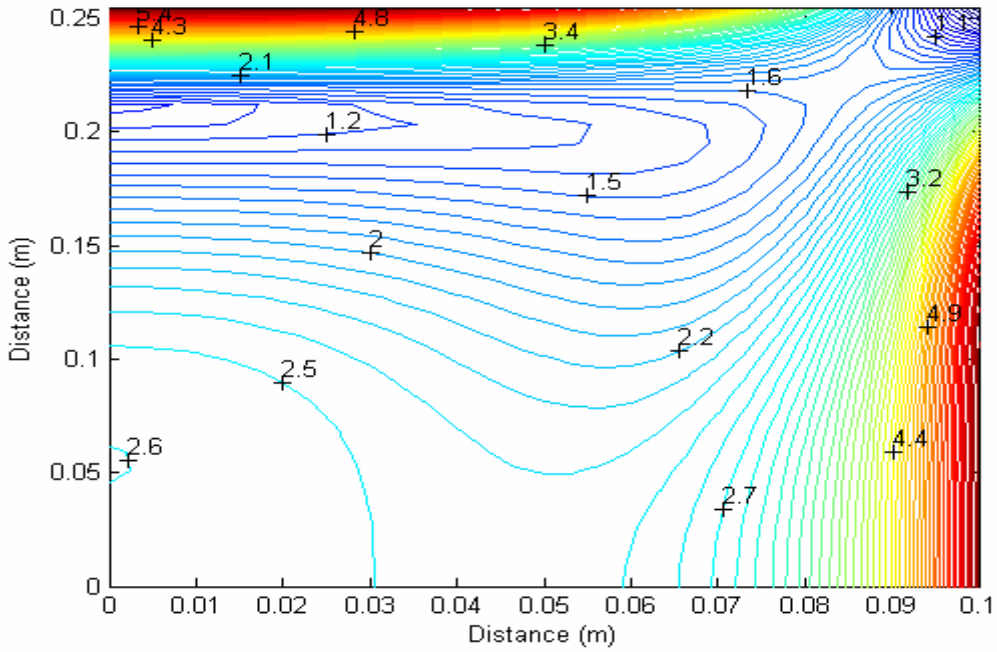

Figure 3.79 Contours of maximum principal stresses (*10^4 kPa) on the top surface of the bottom shell for q= 70 kPa

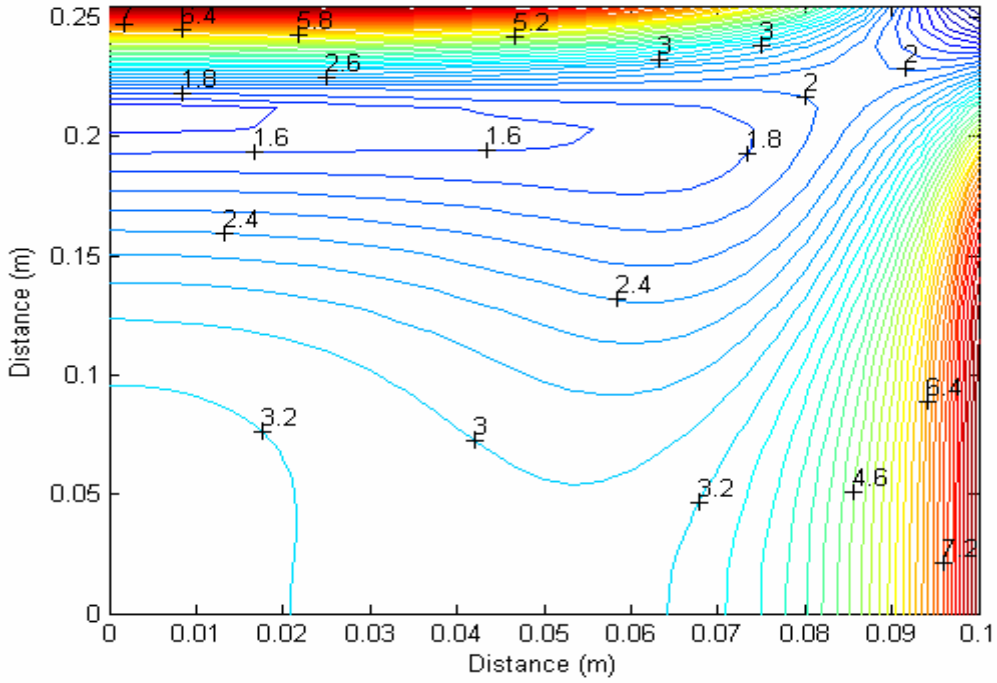

Figure 3.80 Contours of maximum principal stresses (*10^4 kPa) on the top surface of the bottom shell for q= 90 kPa

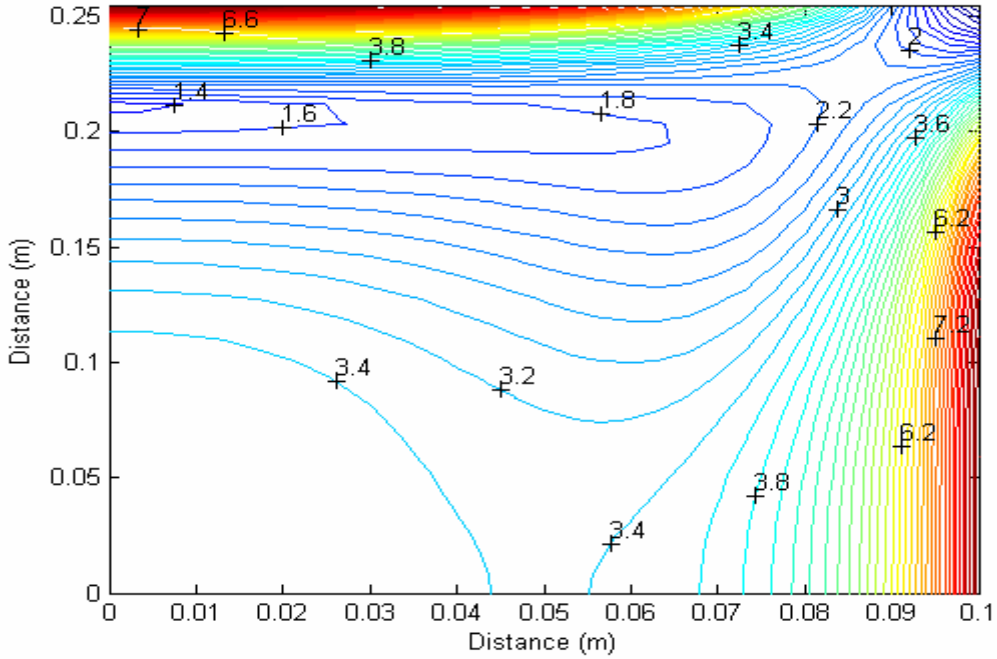

Figure 3.81 Contours of maximum principal stresses (*10^4 kPa) on the top surface of the bottom shell for q= 100 kPa

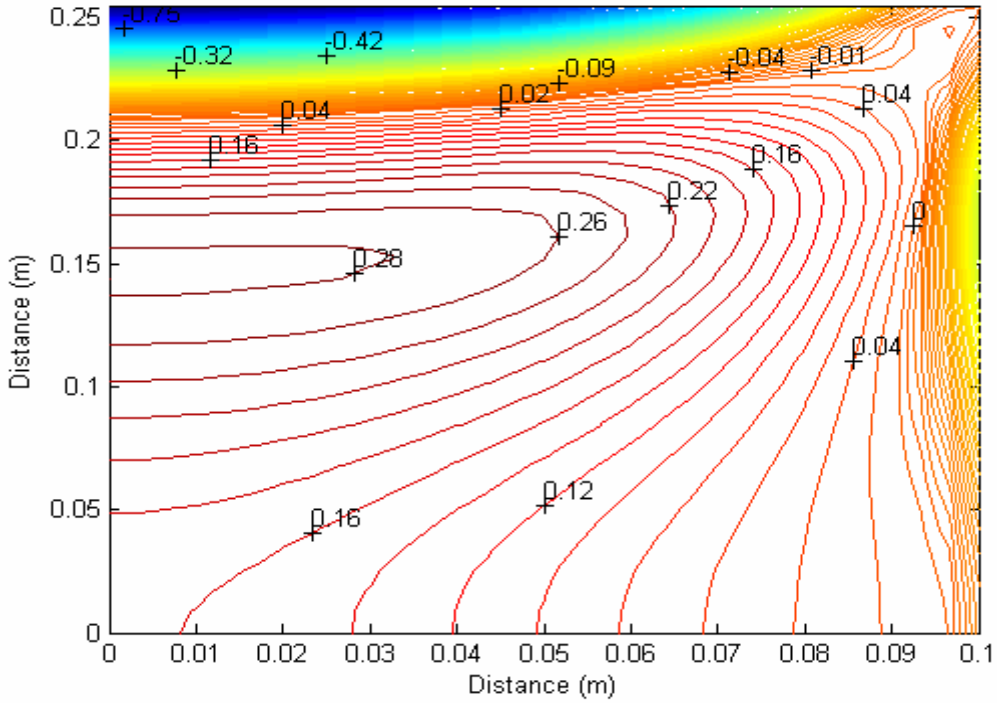

Figure 3.82 Contours of minimum principal stresses (*10^4 kPa) on the bottom surface of the top shell for q= 10 kPa

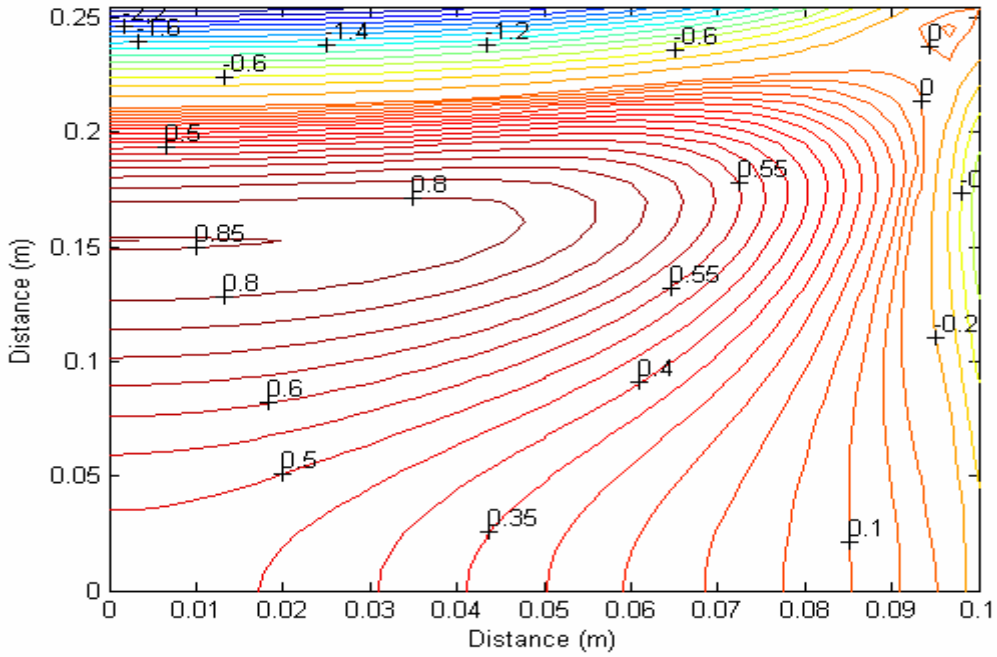

Figure 3.83 Contours of minimum principal stresses (*10^4 kPa) on the bottom surface of the top shell for q= 30 kPa

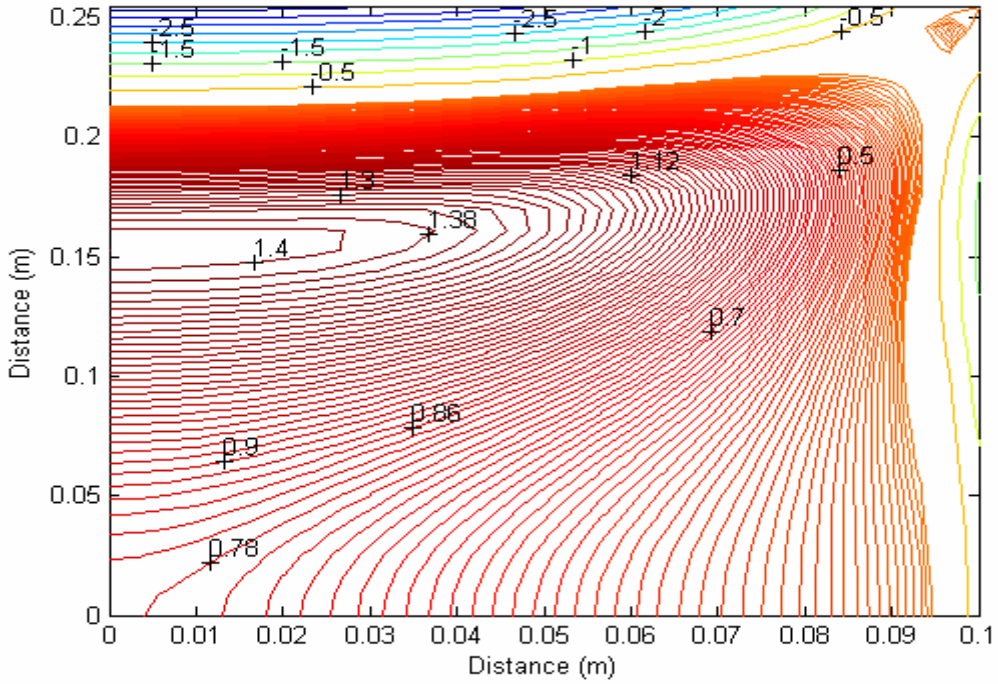

Figure 3.84 Contours of minimum principal stresses (*10^4 kPa) on the bottom surface of the top shell for q= 50 kPa

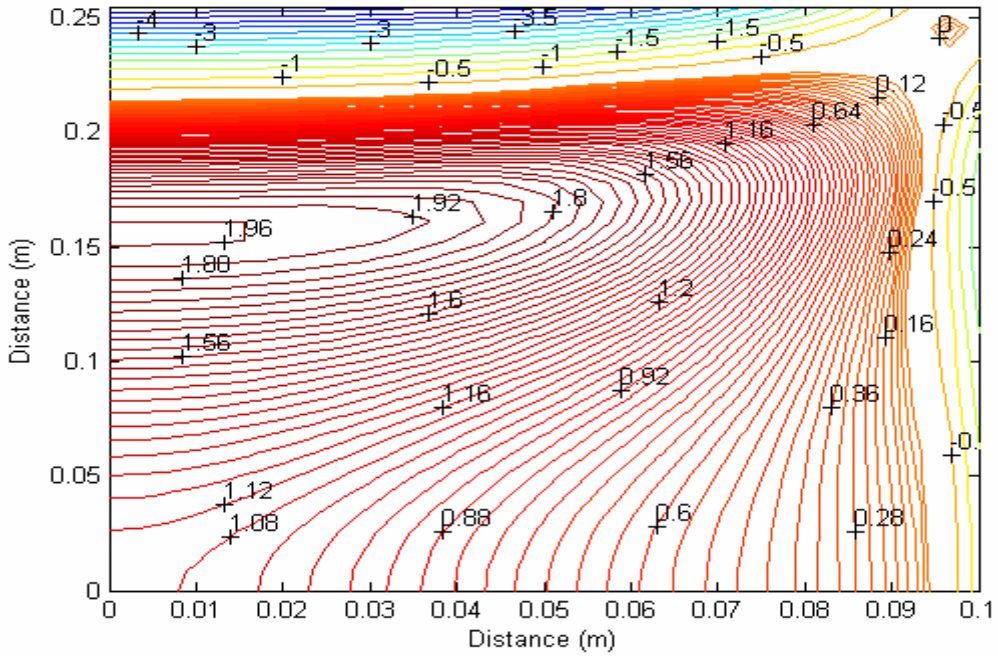

Figure 3.85 Contours of minimum principal stresses (*10^4 kPa) on the bottom surface of the top shell for q= 70 kPa

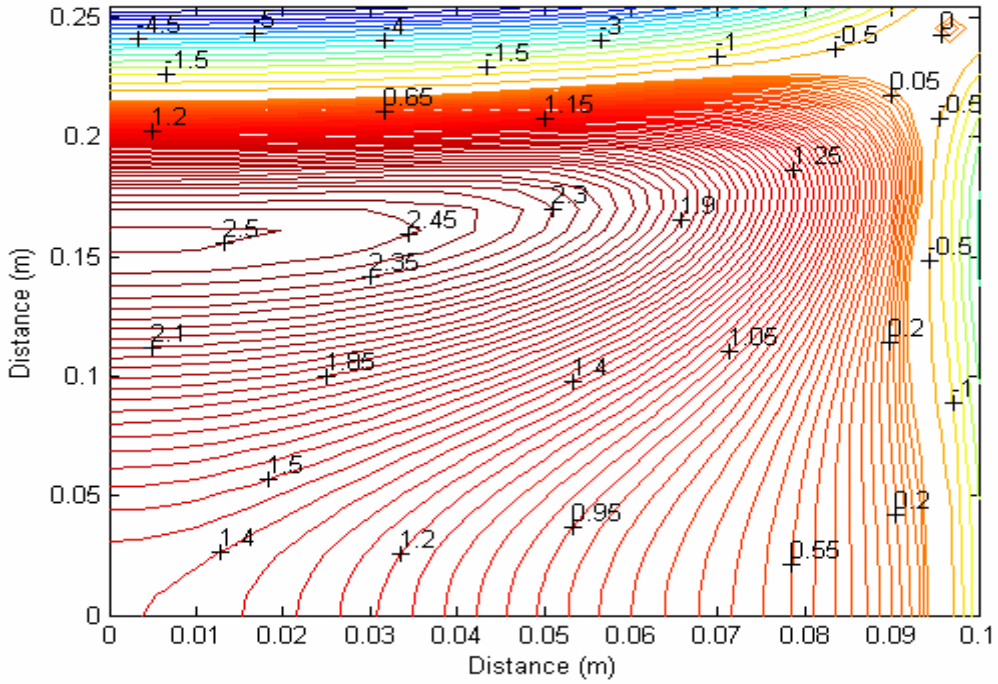

Figure 3.86 Contours of minimum principal stresses (*10^4 kPa) on the bottom surface of the top shell for q= 90 kPa

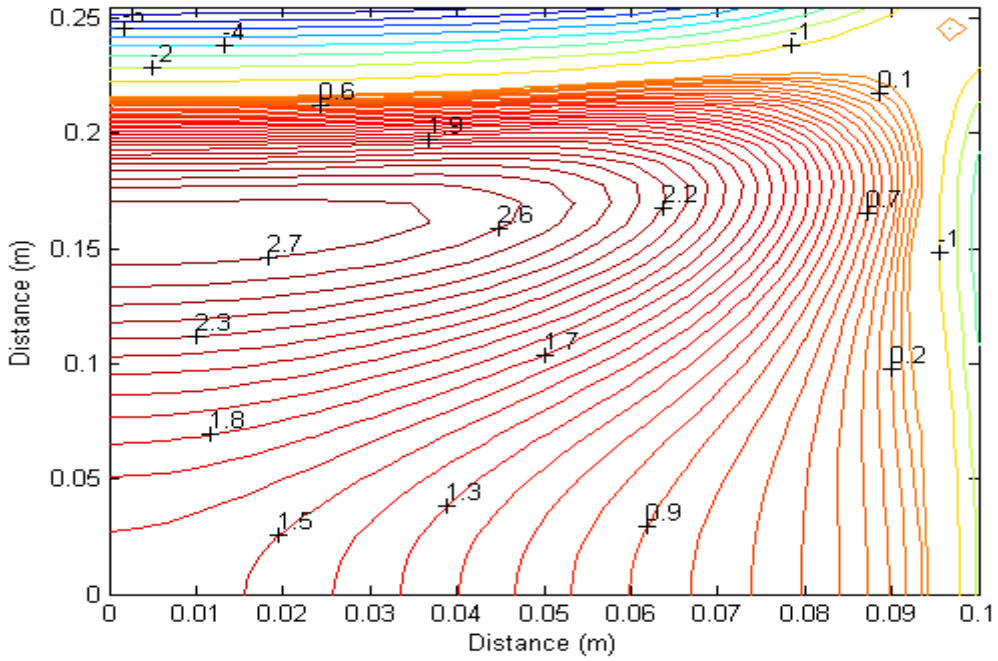

Figure 3.87 Contours of minimum principal stresses (*10^4 kPa) on the bottom surface of the top shell for q= 100 kPa

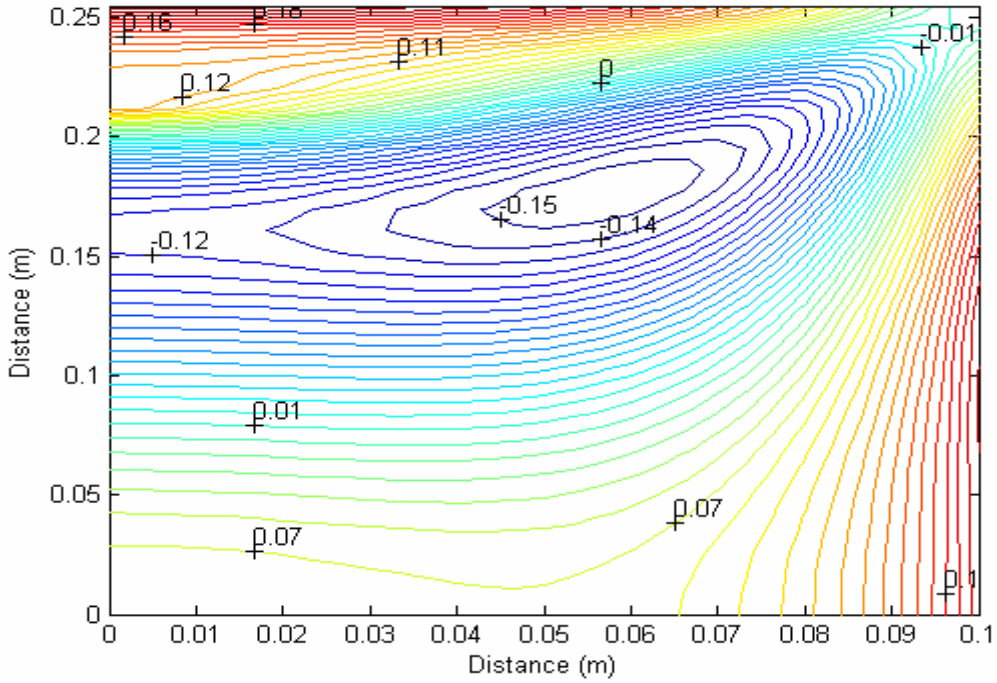

Figure 3.88 Contours of minimum principal stresses (*10^4 kPa) on the top surface of the bottom shell for q= 10 kPa

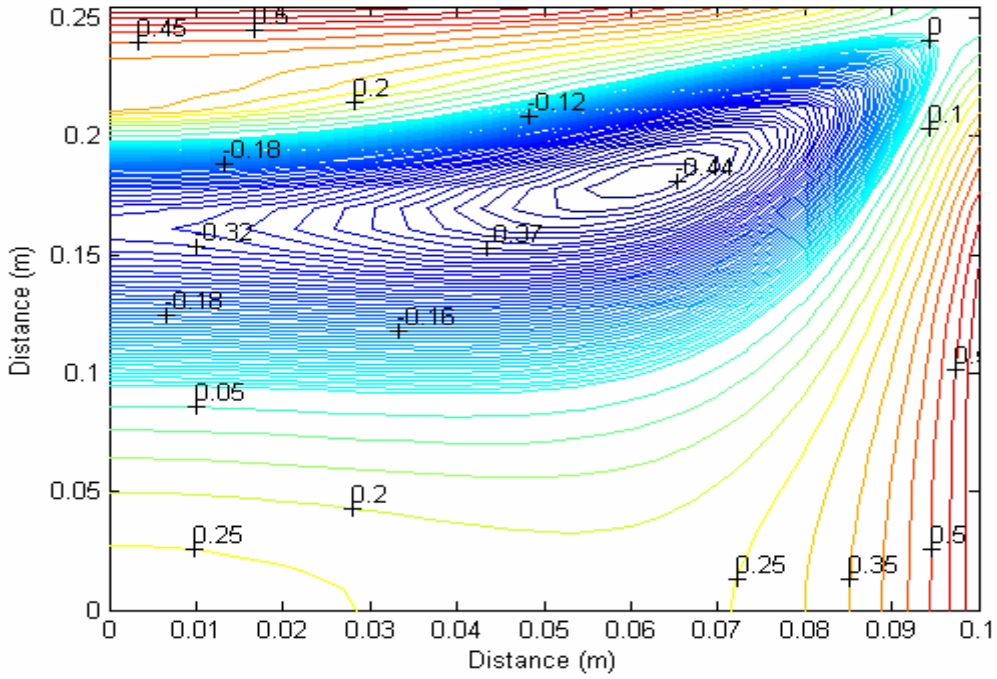

Figure 3.89 Contours of minimum principal stresses (*10^4 kPa) on the top surface of the bottom shell for q= 30 kPa

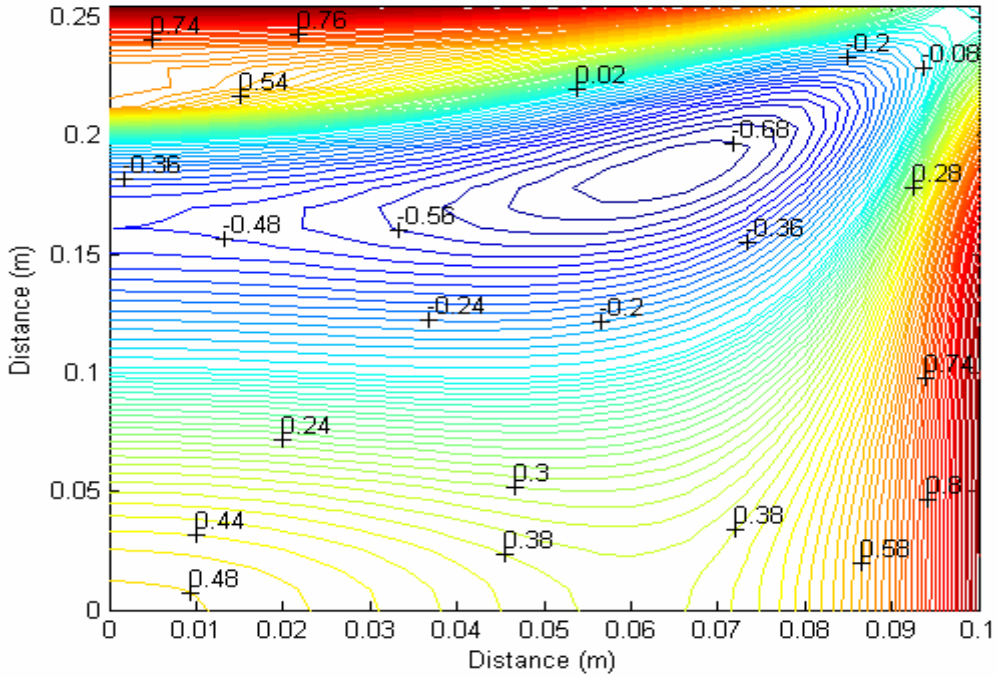

Figure 3.90 Contours of minimum principal stresses (*10^4 kPa) on the top surface of the bottom shell for q= 50 kPa

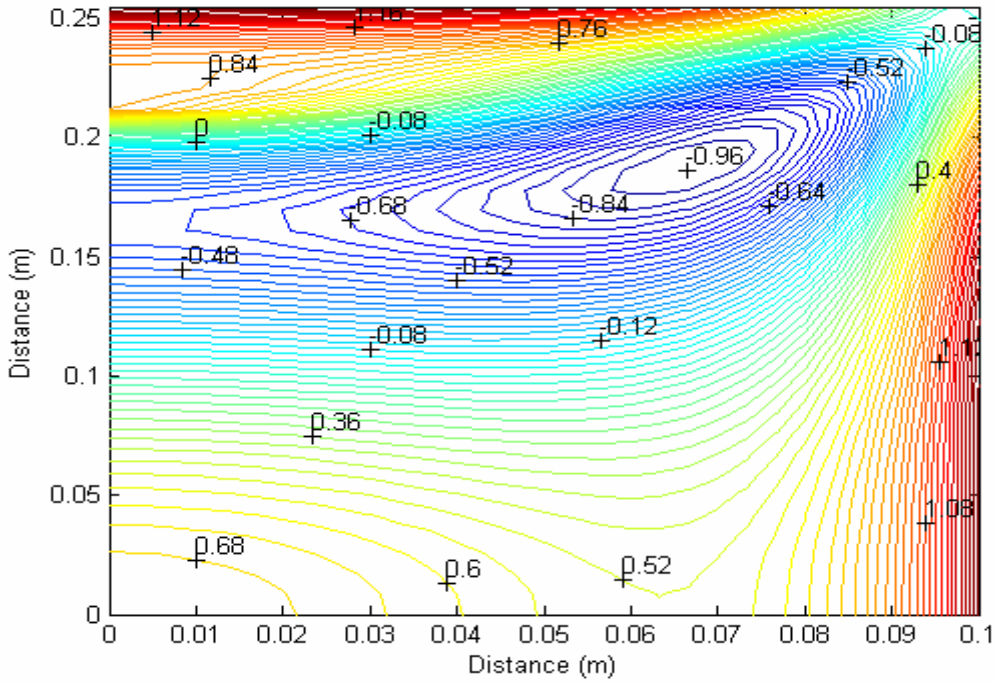

Figure 3.91 Contours of minimum principal stresses (*10^4 kPa) on the top surface of the bottom shell for q= 70 kPa

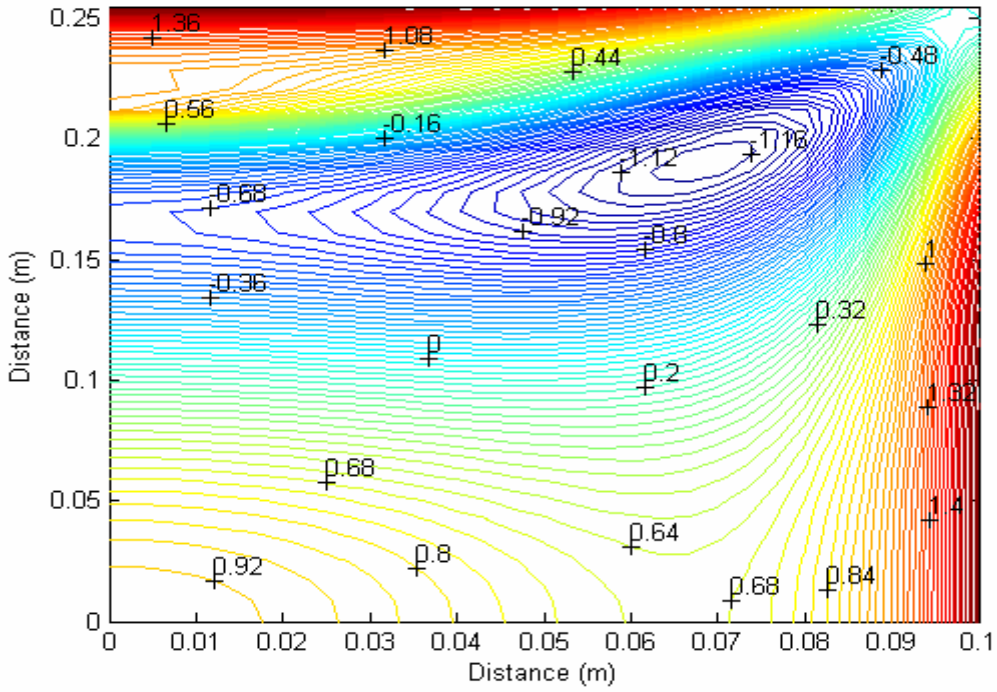

Figure 3.92 Contours of minimum principal stresses (*10^4 kPa) on the top surface of the bottom shell for q= 90 kPa

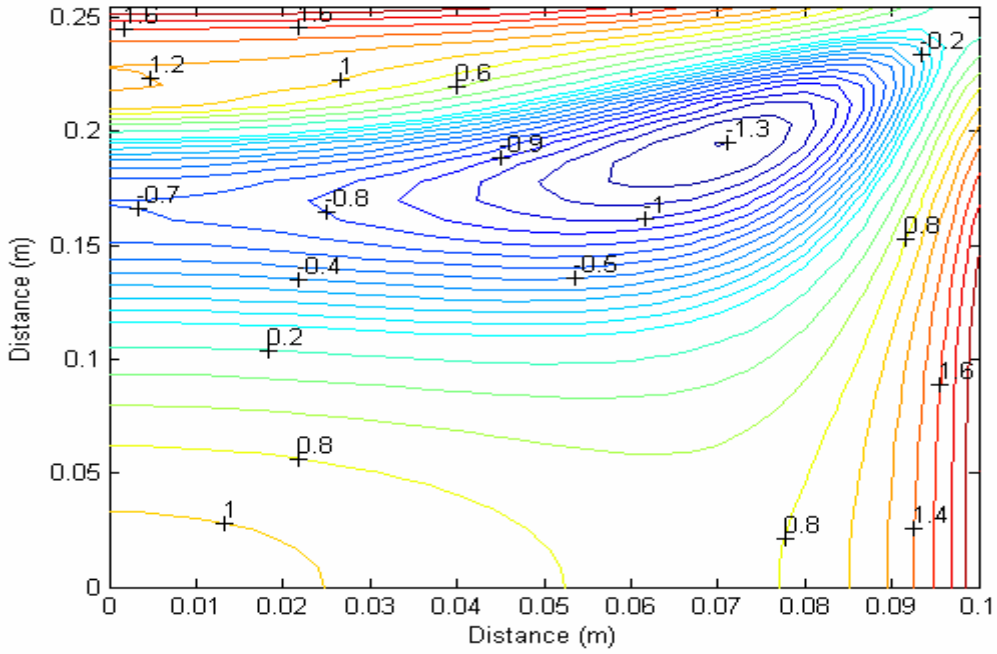

Figure 3.93 Contours of minimum principal stresses (*10^4 kPa) on the top surface of the bottom shell for q= 100 kPa

3.6.2 Strength Factor Analysis of Laminated Glass Unit

Theoretical stress analyses of monolithic and laminated glass units are conducted in order to establish the limits of behavior of laminated glass units. The strength factor (type factor) is defined as the ratio of maximum principal stress in monolithic glass unit to the maximum principal stress in laminated glass unit. If the PVB interlayer is strong enough to transfer 100 percent of shear between the glass sheets, then strength factor 1.0 will mean that radial pressure resistance of monolithic and laminated glass units are similar. Displacements and stress of laminated and monolithic glass units are compared as in order to access the strength factor value of laminated glass unit. The strength factor value for laminated unit is computed by using the formula below.

$$Strength\ Factor = \frac{Maximum\ Principal\ Stress\ in\ Monolithic\ Glass\ Unit}{Maximum\ Principal\ Stress\ in\ Laminated\ Glass\ Unit}$$

Because of large deformations in addition to the bending stresses, membrane stresses occur while the radial pressures are increasing and this causes variation to the strength factor.

For monolithic and laminated glass units, which have the same nominal glass thickness, strength factor values are assigned in Table 3.4 below:

Table 3.4 Strength Factor values in building codes

Code	Strength Factor
Uniform Building Code 1985	0.6
Basic/National Building Code 1984	
Standart Building Code 1986	0.75
Uniform Building Code 1988	
Basic/National Building Code 1987	
Standart Building Code 1988	

Strength factor value for fixed shell unit varies between 1.03-1.07 as shown in Figure 3.94. Strength factor value gets smaller while the load is increasing.

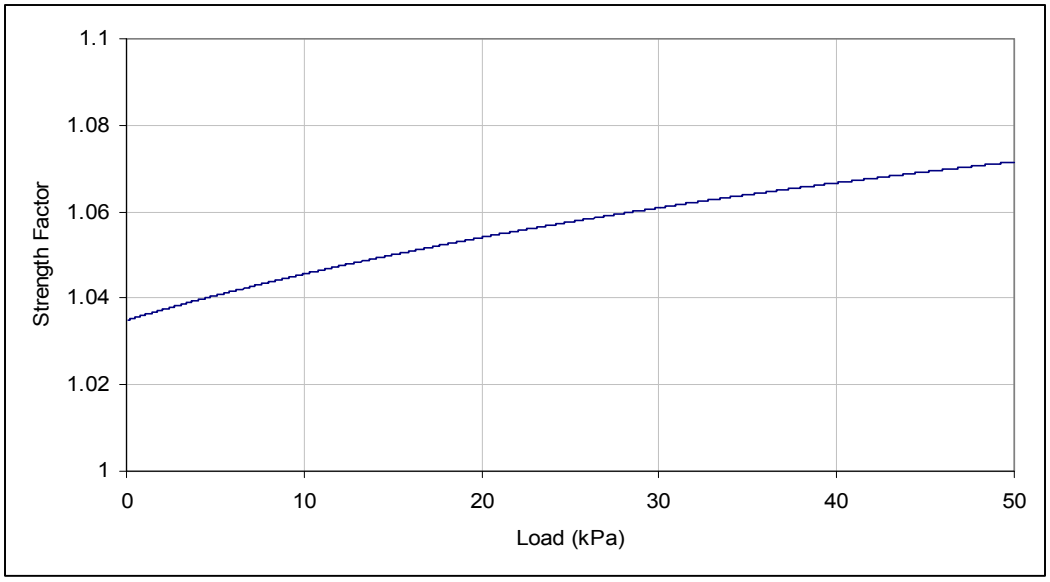

Figure 3.94 Strength factor for the fixed supported laminated cylindrical shell

3.6.3 Numerical Results for Fixed Supported Cylindrical Shell Subjected to Uniformly Distributed Load Towards the Top Shell Surface

To consider the effect of load on the behavior of laminated glass shell, the same unit is solved for the same geometry by applying the load as pressure. Fixed laminated glass shell tested has 0.508 m in length and 2.54 m radius. It is consisting of two glass shells and each of them has a thickness of 2.5 mm. The thickness of the inner core is 0.76 mm. The total thickness of the unit is 5.76 mm. The Young's modulus and Poisson's ratio of glass are taken to be 72 GPa and 0.25, respectively. Shear modulus and Poisson's ratio of the interlayer are taken as 1000 kPa and 0.29, respectively. Physical properties of laminated unit are given in Table 3.2. The results are verified by using the results of finite element package program ABAQUS. As seen in Table 3.5, Figures 3.95 and 3.96 the results are seen in good agreement till 35 kPa. Between 35 kPa and 40 kPa load, the difference between the current model and

the finite element model is between 20% and 37%. Except 35-40 kPa the results are very close to each other. The difference is less than 10%. View of radial deflection contours is given in Figure 3.97. From Figure 3.97 it can be seen that they take their maximum value at the boundaries of the unit.

Table 3.5 Comparison of the results for the fixed supported laminated cylindrical shell

	Displacement (mm)			Maximum Stress (MPa)		
Load (kN/m^2)	FEM	Model	% Error	FEM	Model	% Error
0	0.000	0.000	0.000	0.000	0.000	0.000
1	-0.031	-0.029	5.202	1.304	1.095	16.036
2	-0.062	-0.059	5.289	2.619	2.198	16.076
3	-0.094	-0.089	5.413	3.945	3.310	16.108
4	-0.127	-0.120	5.496	5.282	4.430	16.130
5	-0.159	-0.150	5.643	6.631	5.560	16.154
6	-0.192	-0.181	5.493	7.887	6.699	15.058
7	-0.226	-0.213	5.880	9.244	7.849	15.089
8	-0.261	-0.245	6.078	10.610	9.010	15.083
9	-0.296	-0.277	6.242	12.000	10.182	15.153
10	-0.331	-0.310	6.402	13.850	11.366	17.938
20	-0.734	-0.670	8.722	28.860	24.084	16.549
30	-1.314	-1.131	13.907	47.950	40.309	15.936
35	-1.830	-1.458	20.310	61.940	55.934	9.696
40	-3.284	-2.046	37.707	94.440	127.219	-34.709
45	-5.138	-4.669	9.128	146.000	165.810	-13.568
50	-6.162	-6.026	2.199	185.800	197.769	-6.442
60	-7.506	-7.511	-0.061	248.700	252.222	-1.416
70	-8.470	-8.512	-0.495	304.800	299.167	1.848
80	-9.241	-9.298	-0.619	355.000	341.159	3.899
90	-9.894	-9.955	-0.614	401.100	379.423	5.404
100	-10.460	-10.520	-0.577	443.700	414.642	6.549

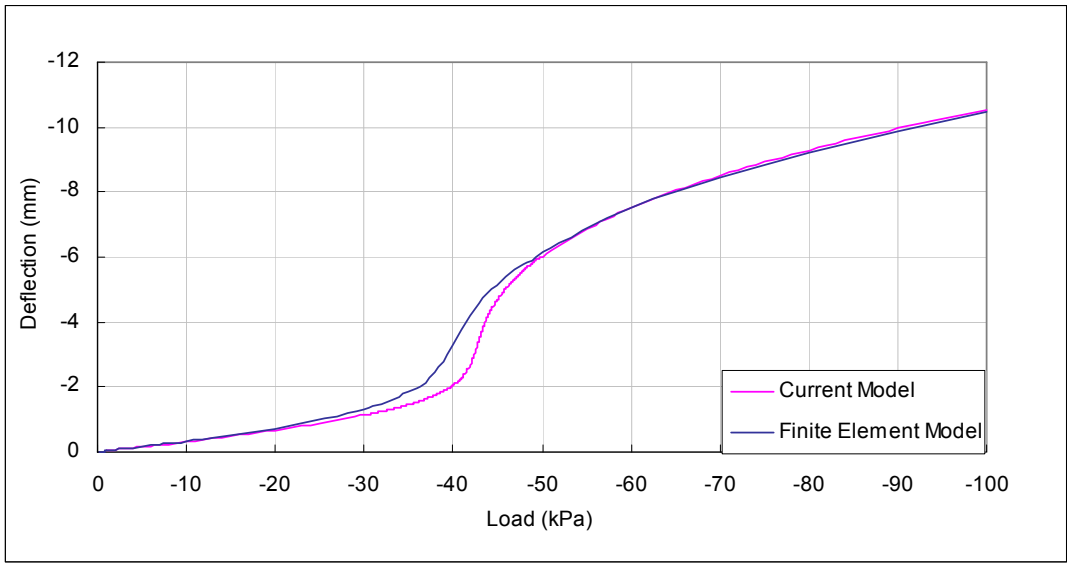

Figure 3.95 Comparison of the central deflection values for laminated glass shell

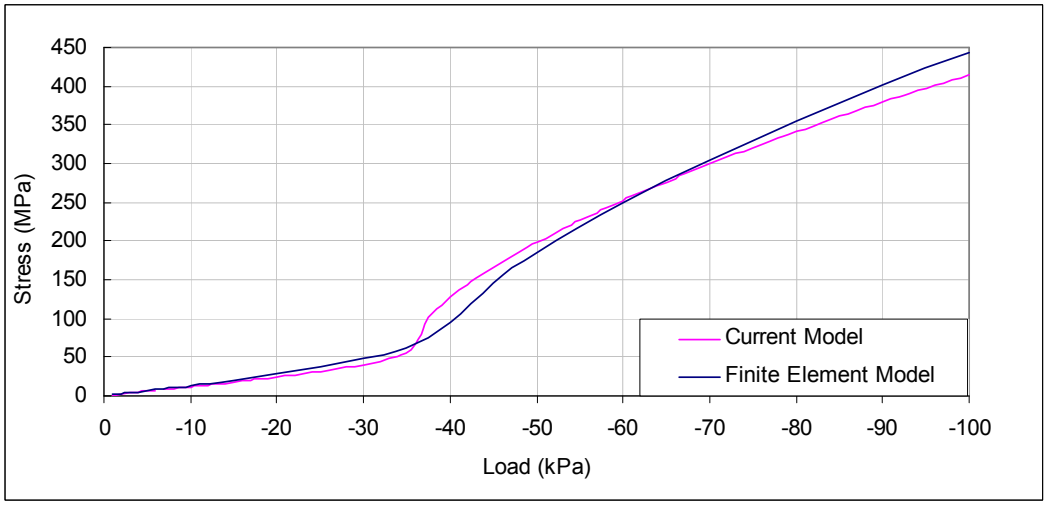

Figure 3.96 Comparison of the stress values for laminated glass shell

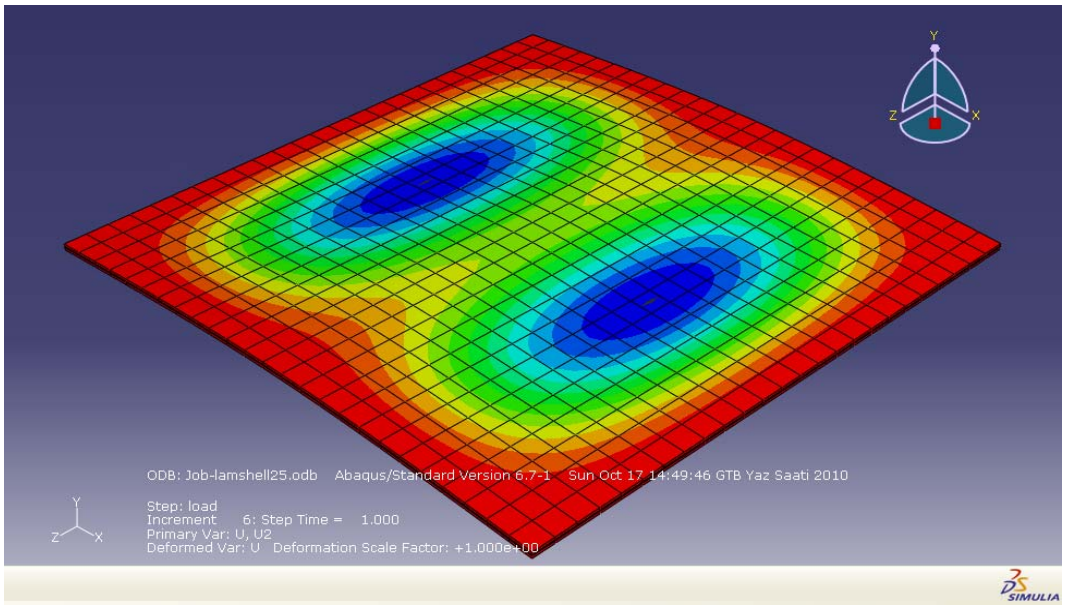

Figure 3.97 A view of radial deflection contours obtained from ABAQUS

The behavior of laminated shell unit changes according to dimension of load. If the load is applied as pressure double curvature can be seen in Figure 3.98. The behavior of monolithic shell is different from layered and laminated units because double curvature is not observable for monolithic shell. For the applied tensile load there is only one curvature and the behavior of laminated, layered and monolithic glass units are very close to each other.

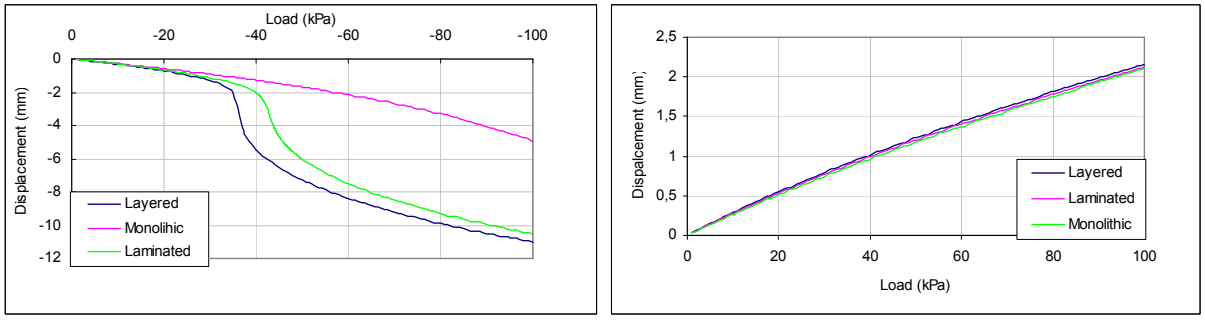

Figure 3.98 Comparison of displacement of the laminated glass subjected to uniform tension and compressive load

Figures 3.99 and 3.100 are plotted to compare the behavior of monolithic, laminated and layered glass beams. The developed model is able to predict the behavior of monolithic, layered and laminated glass shells. In Figures 3.99 and 3.100, the origin

of coordinate system is considered at the center of the laminated glass shell. The behavior of laminated glass shell is similar to the behavior of layered glass shell as seen in Figures 3.99 and 3.100. Their behavior is bounded by two limiting cases, which are monolithic and layered behavior. Behavior of monolithic glass shell is different from layered and laminated glass shell. Double curvature is not observed for monolithic case. The deflection value of laminated shell unit which is obtained for 100 kPa pressure is nearly 5 times of the same shell under 100 kPa tensile load.

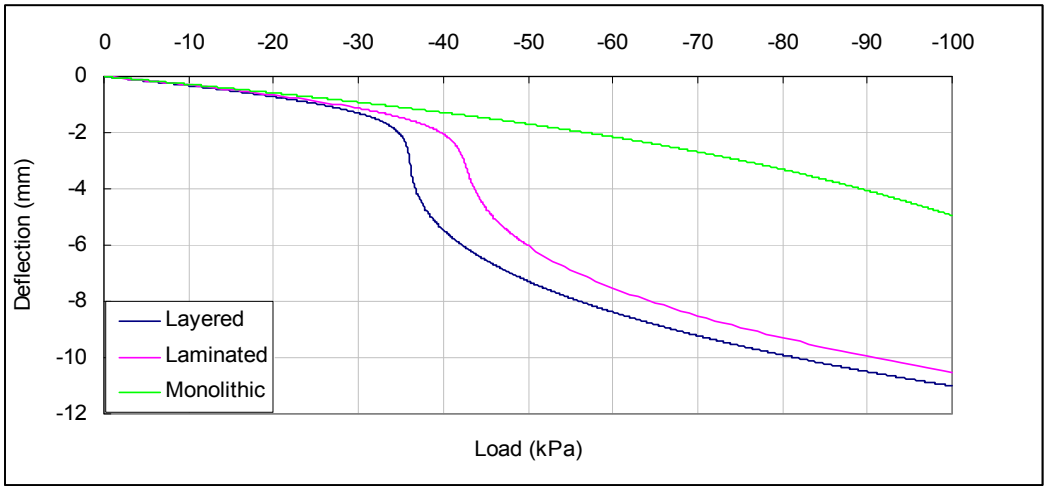

Figure 3.99 Comparison of maximum displacements of monolithic, laminated and layered glass units

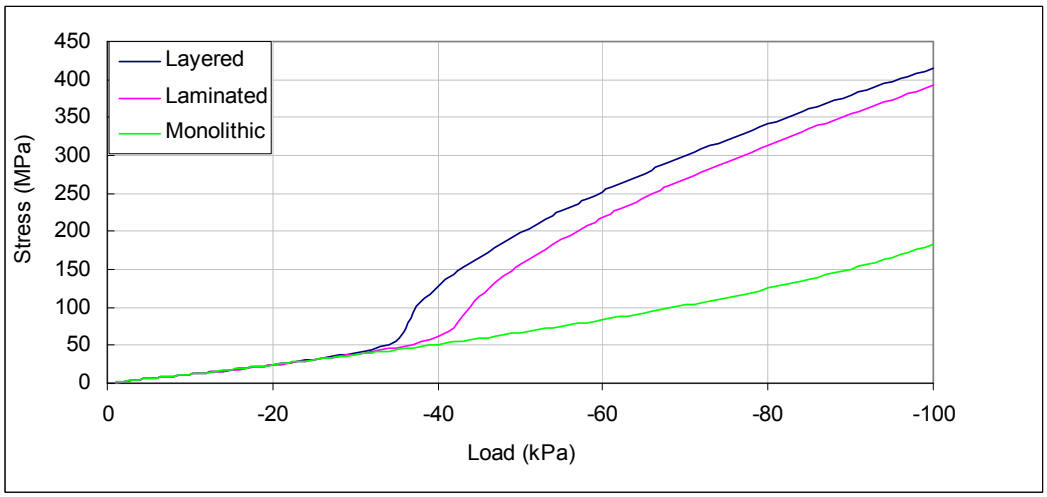

Figure 3.100 Comparison of maximum stresses of monolithic, laminated and layered glass units

Figures 3.101 and 3.102 are the circumferential displacements (u1 and u2) along the centerline at y=0 for top and and glass shells, respectively. Circumferential displacements are zero at θ=0 and θ=θ_1 as we expected. The behavior of unit changes after 40 kPa load. Circumferential displacements take their maximum values close to the midpoint of the quarter laminated glass unit for pressures under 40 kPa. The maximum deflection moves toward the center of the unit for higher pressures than 40 kPa. The deflections of the top glass ply are slightly higher than the deflections of the bottom ply. The effect of nonlinearity can be seen from the below figures clearly.

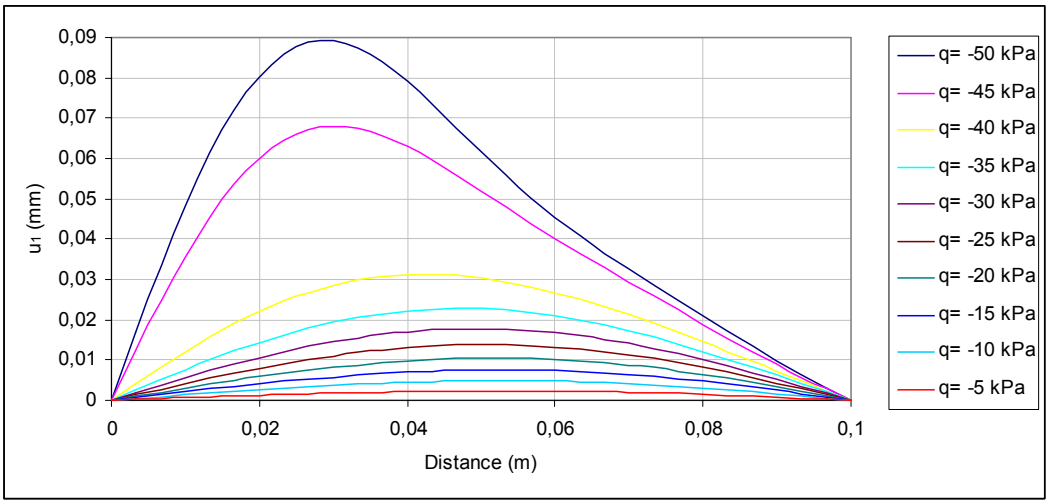

Figure 3.101 Circumferential displacement of the top glass unit along the center line at y=0

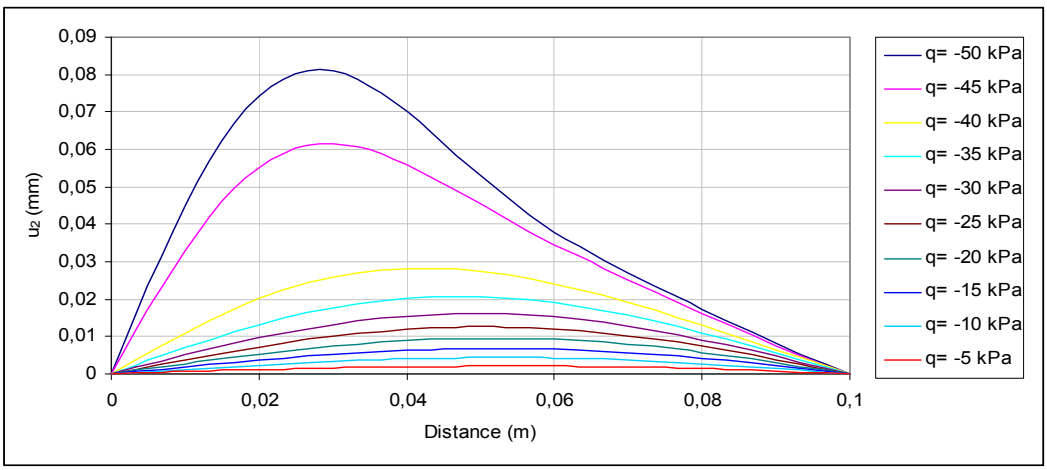

Figure 3.102 Circumferential displacement of the bottom glass unit along the center line at y=0

Figures 3.103 and 3.104 show the axial displacements (v1 and v2) along the center line at θ=0 for top and bottom glass units, respectively. Axial displacements v_1 and v_2 are zero along the center line at y=0 and $y=y_1$ as we expected. In-plane displacements of the top glass ply take positive values for pressures under 30 kPa. For pressures higher than 30 kPa they take negative values close to the boundary of the unit. The place of maximum displacement moves toward the center of the unit while the applied pressure is increasing. Axial displacements of the bottom glass ply take negative values along the length of the shell for 5 and 10 kPa loads. After 10 kPa load, they take both positive and negative values. The place of maximum displacement moves toward the center as the load is increasing. The maximum values, which are obtained for the top glass ply, are higher than that of the bottom glass ply. Figure 3.105 shows the radial displacement at the center of the shell unit along the θ direction for different load values. Radial displacements take their maximum value along the center line at θ=0 while they are zero along center line at $\theta=\theta_1$. Radial displacements are negative for applied pressure under 45 kPa; they take positive values close to boundary of the unit for pressures higher than 45 kPa.

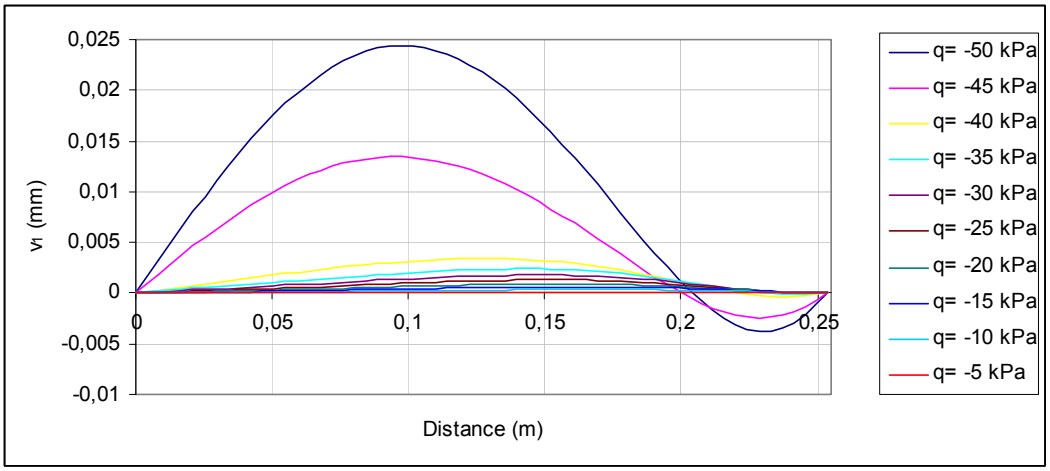

Figure 3.103 Axial displacement of the top glass unit at the center the center line at θ=0

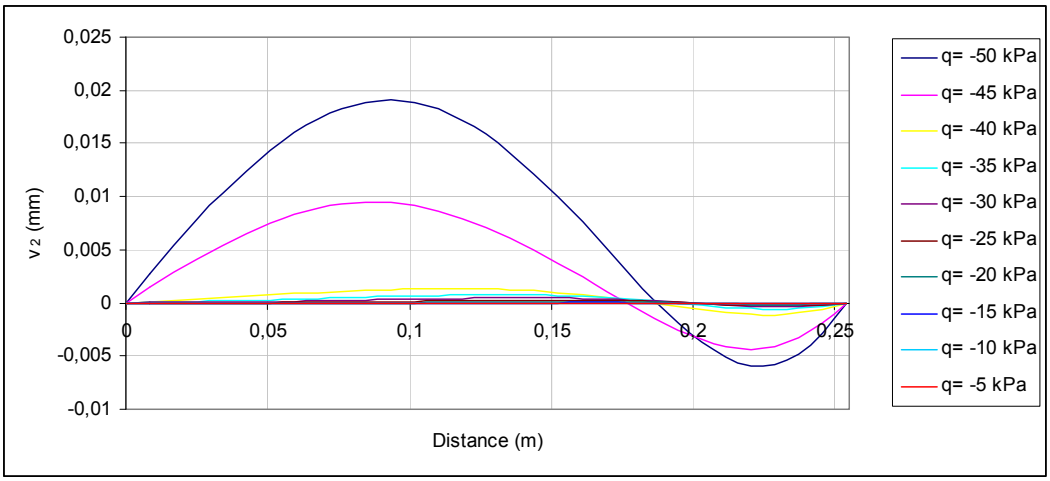

Figure 3.104 Axial displacement of the bottom glass unit along the center line at θ=0

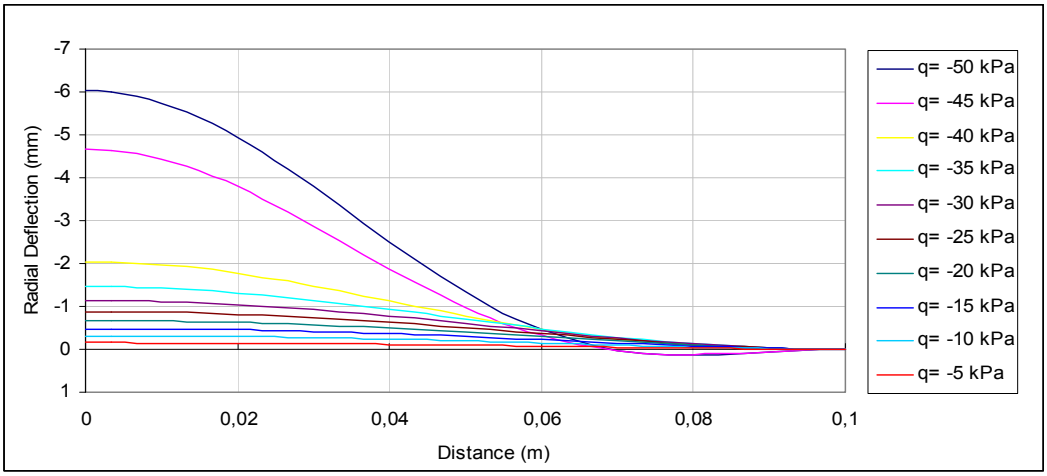

Figure 3.105 Radial displacement of the unit at the center along the center line at y=0

Figures 3.106-3.110 are the radial, circumferential and axial displacements along the diagonal of the laminated glass shell unit. While radial displacements take their maximum value along the center line at θ=0, circumferential and axial displacements are zero along the center line at θ=0. It is observed from the Figures 3.106 and 3.110 that when the curvature changes because of high nonlinearity, the behavior of displacement lines also changes.

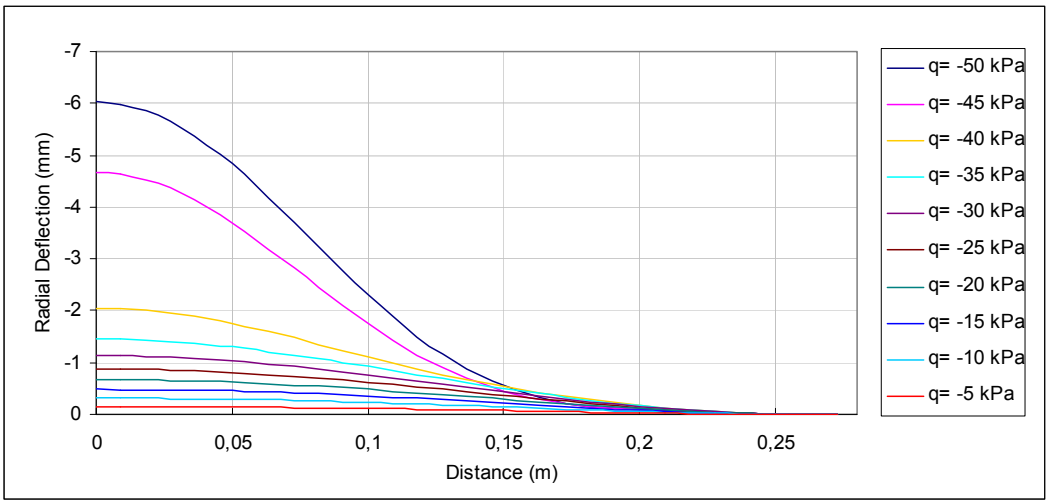

Figure 3.106 Radial displacement of the unit along the diagonal of shell

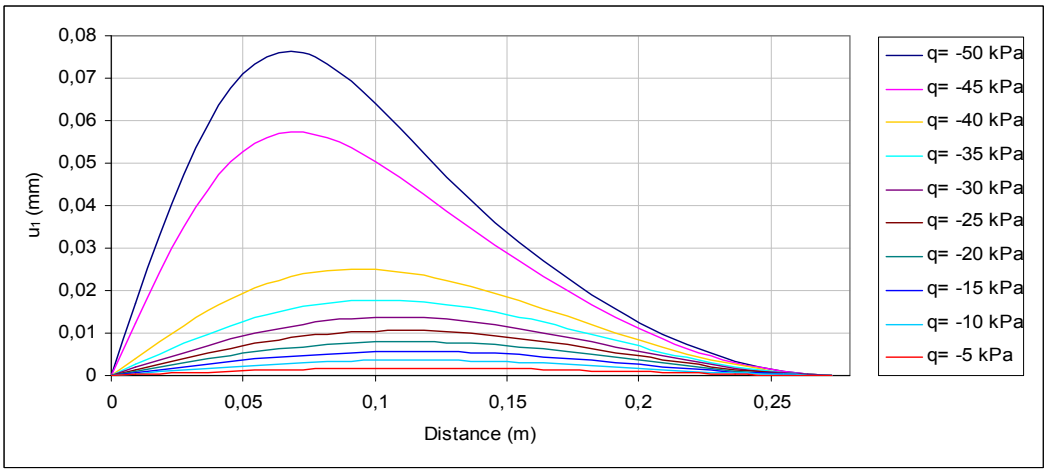

Figure 3.107 Circumferential displacement of the top glass shell along the diagonal

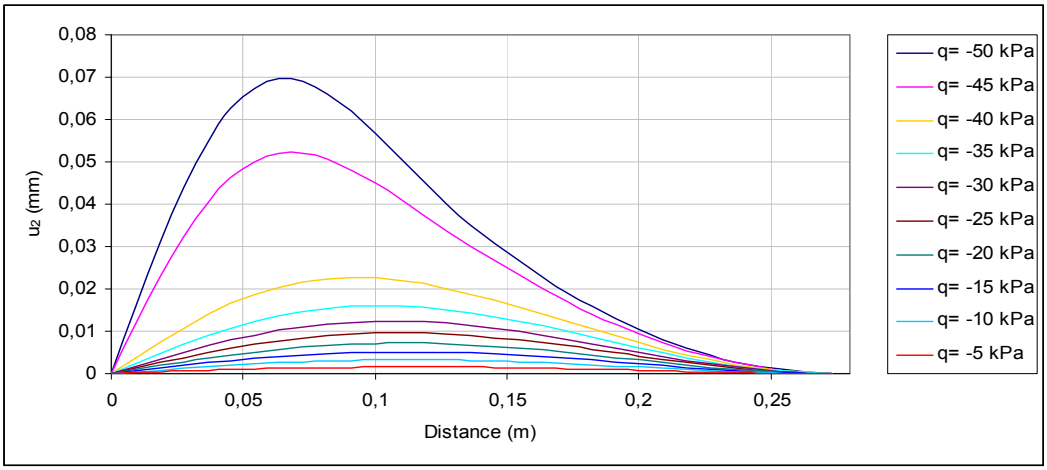

Figure 3.108 Circumferential displacement of the bottom glass shell along the diagonal

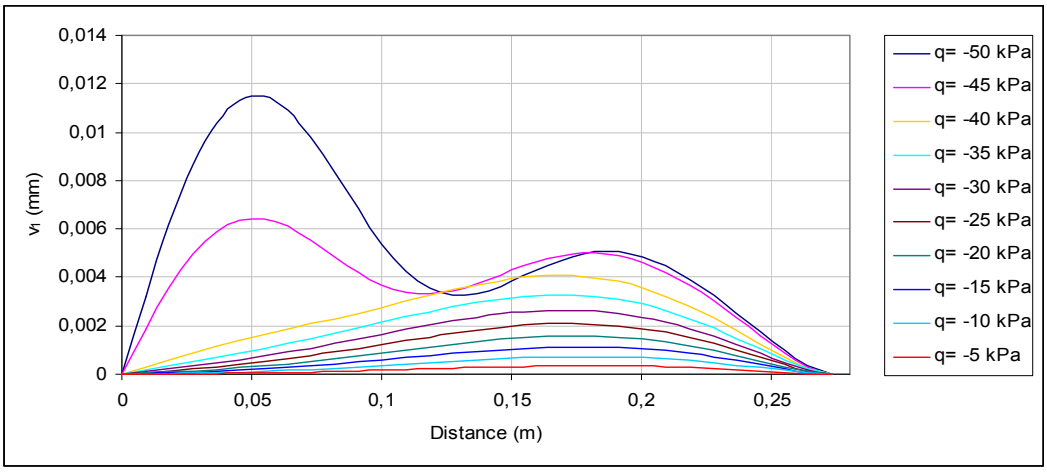

Figure 3.109 Axial displacement of the top glass shell along the diagonal

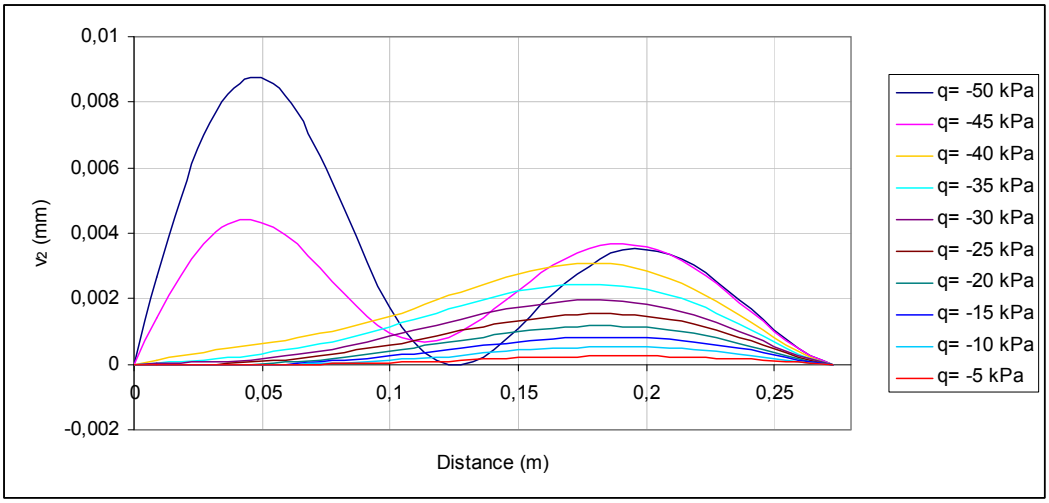

Figure 3.110 Axial displacement of the bottom glass shell along the diagonal

Figures 3.111 and 3.112 are plotted to represent the maximum principal stresses on the top and bottom surface of glass unit along the center line at y=0 for different load values. The maximum principal stresses on the top surface of the top glass are compression along the center line at y=0 till 20 kPa pressure. Between 25 and 40 kPa pressure applied they can be both tension and compression. While they are tension around the center, they take compression values at the boundary and around the boundary. Till 45 kPa, pressure they take their maximum value at the boundary of the unit as compression. For pressures higher than 45 kPa, they take their maximum value at the center as tension. On the bottom surface of the bottom glass the maximum principal stresses are compression along the center line at y=0 direction till 40 kPa pressure and they take their maximum value at the center of glass shell as

compression. For pressures higher than 40 kPa, the maximum principal stress takes both positive and negative values. They change their sign at two points along the center line at y=0 and they take their maximum value at a point close to half of the quarter unit as tension. Figures 3.113 and 3.114 represent the minimum principal stresses at the top and bottom glass unit, respectively. The minimum principal stresses on the top and bottom surface of glass unit are compression along the center line at y=0 for applied pressure till 40 kPa. For pressures higher than 40 kPa, minimum principal stresses can be both tension and compression.

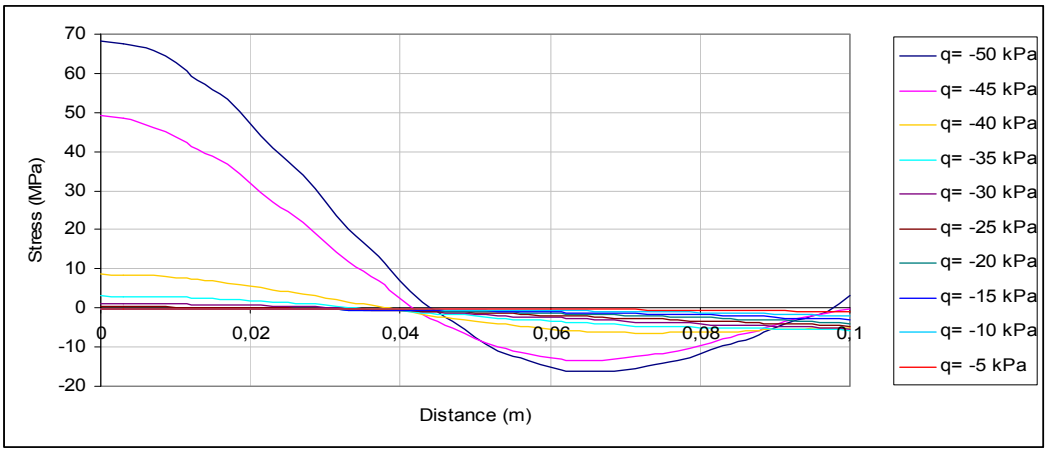

Figure 3.111 Maximum stresses on the top surface of the top glass along the center line at y=0

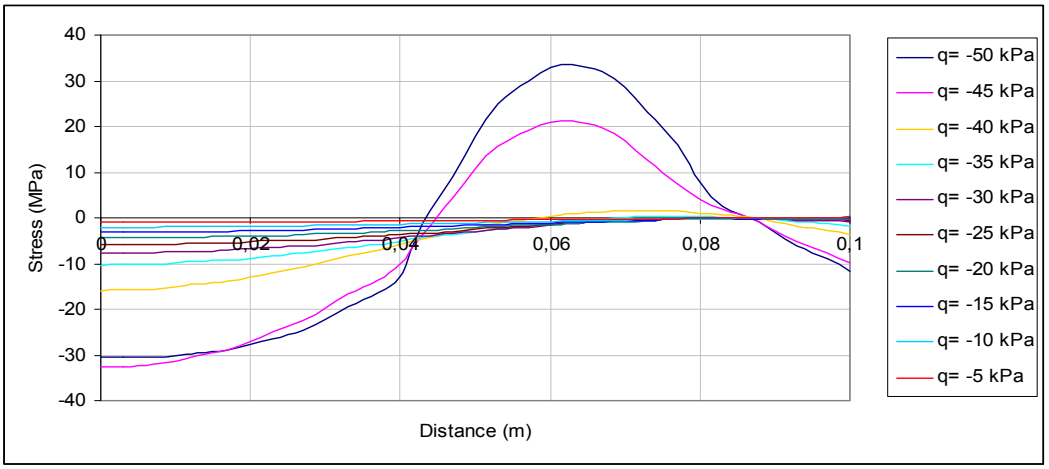

Figure 3.112 Maximum stresses on the bottom surface of the bottom glass along the center line at y=0

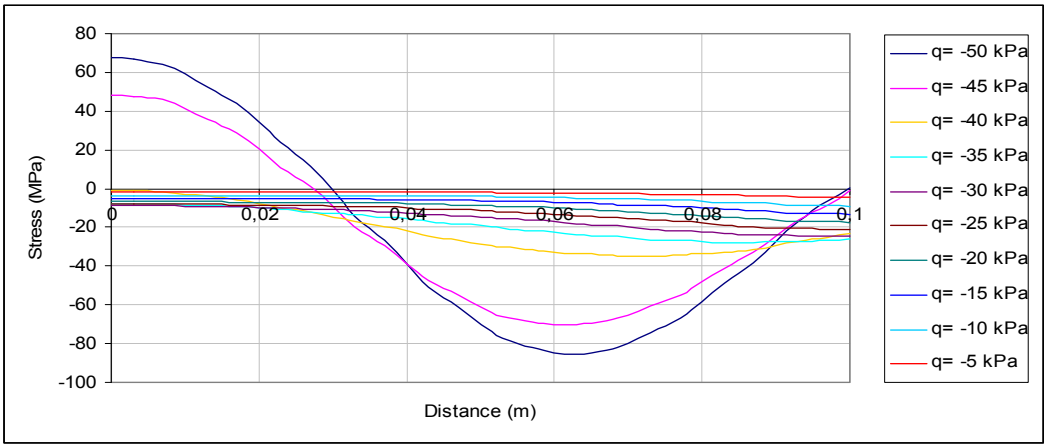

Figure 3.113 Minimum stresses on the top surface of the top glass along the center line at y=0

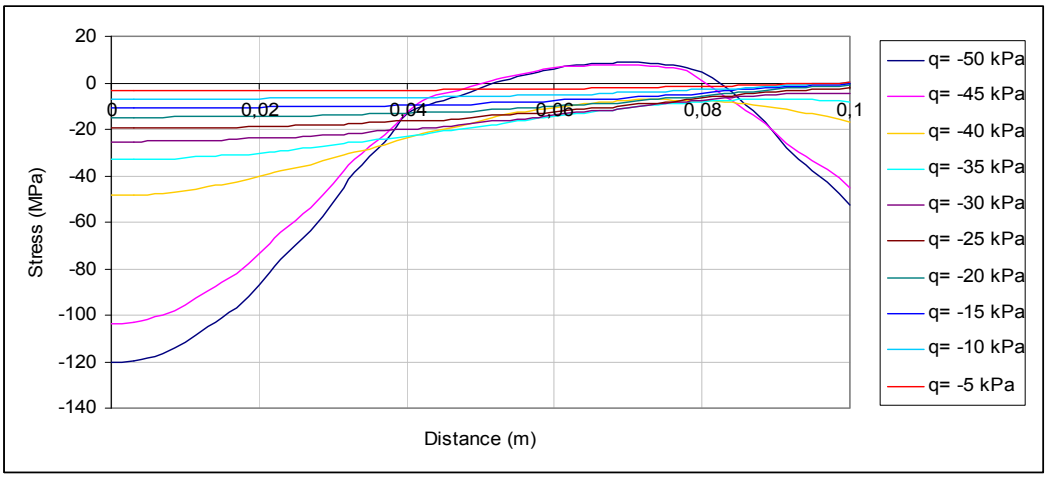

Figure 3.114 Minimum stresses on the bottom surface of the bottom glass along the center line at y=0

Figures 3.115 and 3.118 are maximum and minimum principal stresses along the center line at y=0 for clamped laminated cylindrical shell which is subjected to uniform distributed load as pressure for the bottom surface of the top shell and for the top surface of the bottom shell. Maximum principal stresses at the bottom surface of the top glass shell are compression along the center line at y=0 till 35 kPa pressure as seen in Figure 3.115. For pressures higher than 35 kPa, they could be both tension and compression. While maximum principal stresses take their maximum value at θ=0 as compression; for pressures under 45 kPa, they take their maximum value 0.06 m away from the center as tension for pressures 45 and 50 kPa. Maximum principal

stresses at the top surface of the bottom glass shell are plotted in Figure 3.116 for different load values. Maximum principal stresses at the top surface of the bottom glass shell are compression along the center line at y=0 for pressures less than 35 kPa and they take their maximum value at the edge of the unit as compression. Pressures could be both tension and compression for the values higher than 35 kPa they and they take their maximum value as tension at the center of the unit. Minimum principal stresses at the top and bottom surface of the interlayer are plotted in Figures 3.117 and 3.118, respectively. Minimum principal stresses on the bottom surface of the top glass sheel are compression along the center line at y=0. They take their maximum value at θ=0. Minimum principal stresses on the top surface of glass shell are compression for pressures less than 45 kPa and they take their maximum value at the edge of the unit for pressures higher than 45 kPa which could be both tension and compression. They take their maximum value 0.06 m away from the center as compression.

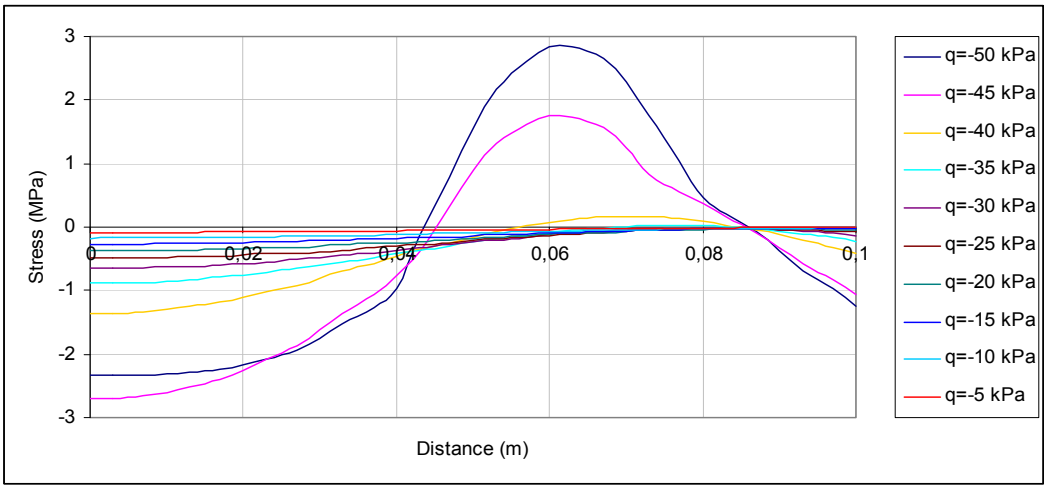

Figure 3.115 Maximum stresses at the bottom surface of the top shell along the center line at y=0

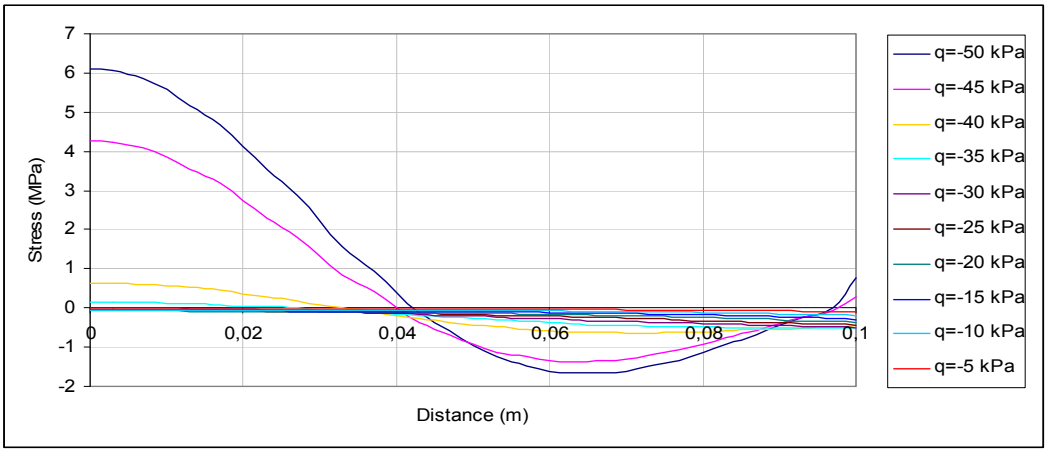

Figure 3.116 Maximum stresses at the top surface of the bottom shell along the center line at y=0

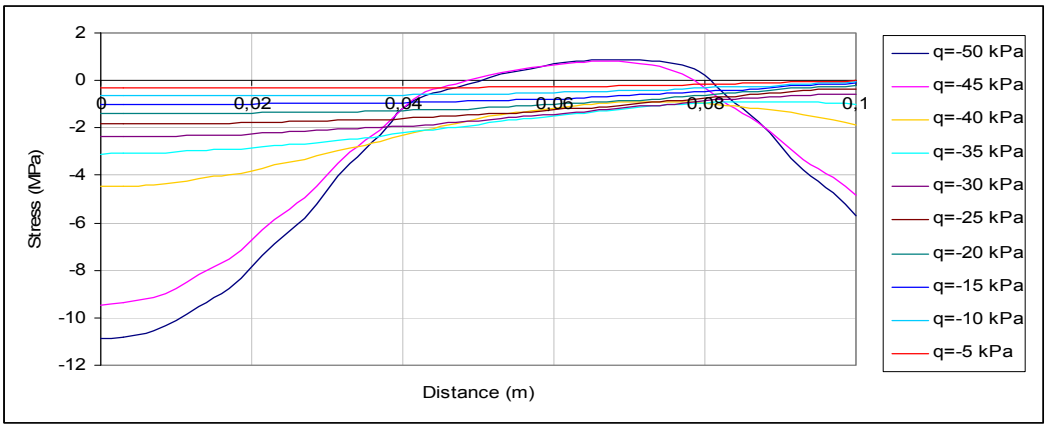

Figure 3.117 Minimum stresses at the bottom surface of the top shell along the center line at y=0

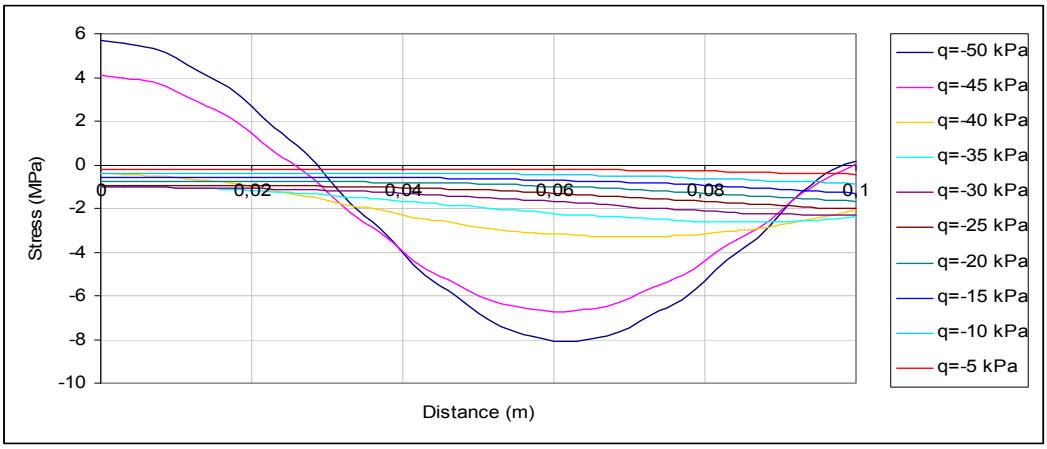

Figure 3.118 Minimum stresses at the top surface of the bottom shell along the center line at y=0

Figures 3.119 and 3.120 are plotted to represent the maximum principal stresses on the top and bottom surfaces of the glass shell unit along the center line at θ=0, respectively. The maximum stresses on the bottom surface are compression till a point close to boundary. After that point the stresses become tension. The point moves toward the center of the unit while the load is increasing. They take their maximum value at center line at y=0. The maximum stresses at the top surface are tension till a point which is 0.2 m away from the center of the unit for pressures under 45 kPa. After that point they take negative values. The maximum stress occurs at the boundary of the unit as compression. For applied pressures higher than 40 kPa the point moves toward the boundary while the load is increasing and they take their maximum value at the center of the unit. Figures 3.121 and 3.122 show the minimum principal stresses at the top and bottom surface along the y direction of glass unit, respectively. Minimum principal stresses at the top surface are compression along the center line at θ=0 till 45 kPa. 45 and 50 kPa pressures take both positive and negative values. While the minimum principal stresses take their maximum values at the boundary of the unit for top surface of the unit, they take their maximum value along the center line at y=0 for the bottom surface of unit.

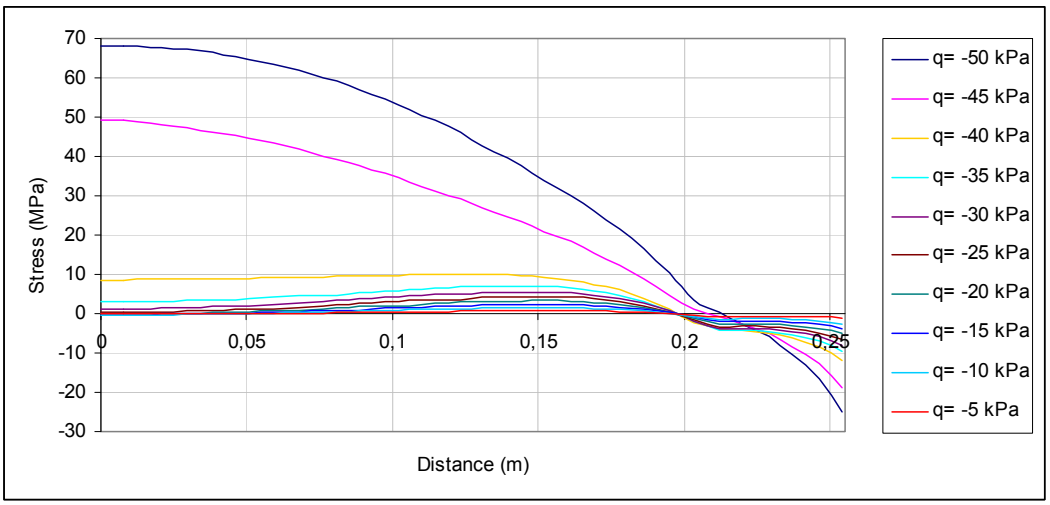

Figure 3.119 Maximum stresses on the top surface of the top glass along the center line at θ=0

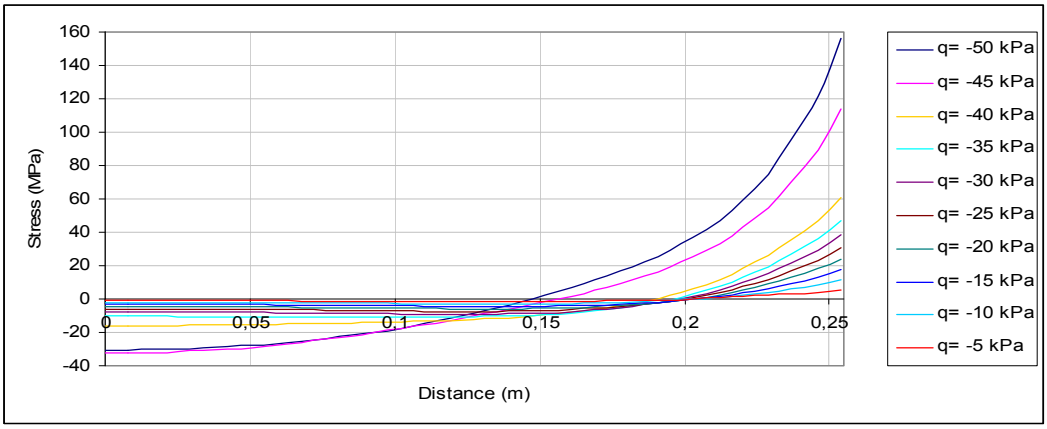

Figure 3.120 Maximum stresses on the bottom surface of the bottom glass along the center line at θ=0

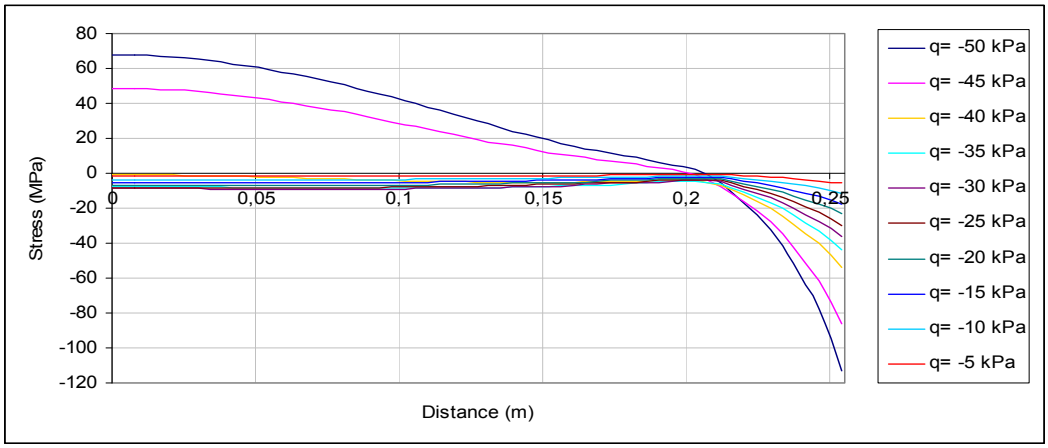

Figure 3.121 Minimum stresses on the top surface of the top glass along the center line at θ=0

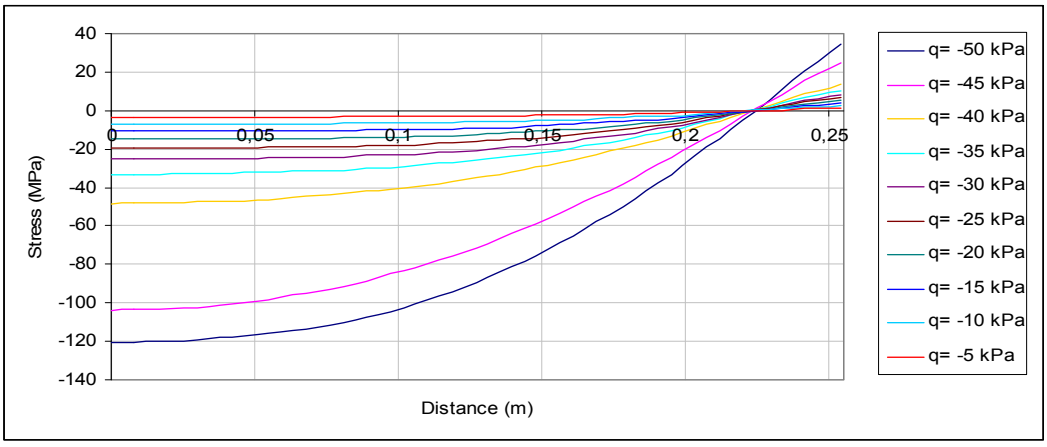

Figure 3.122 Minimum stresses on the bottom surface of the bottom glass along the center line at θ=0

Figures 3.123-3.127 are plotted in order to have detailed information about the contour of radial displacement for the quarter of the shell. Radial displacements are given for applied pressure q= 10, 20, 30, 40, 50 kPa. It is observable from the figures below that for pressures higher than 40 kPa the characteristic of contours change. It is also observed that there is a zero deflection region for pressures higher than 40 kPa. The radial deflection takes its maximum value at the center of the unit.

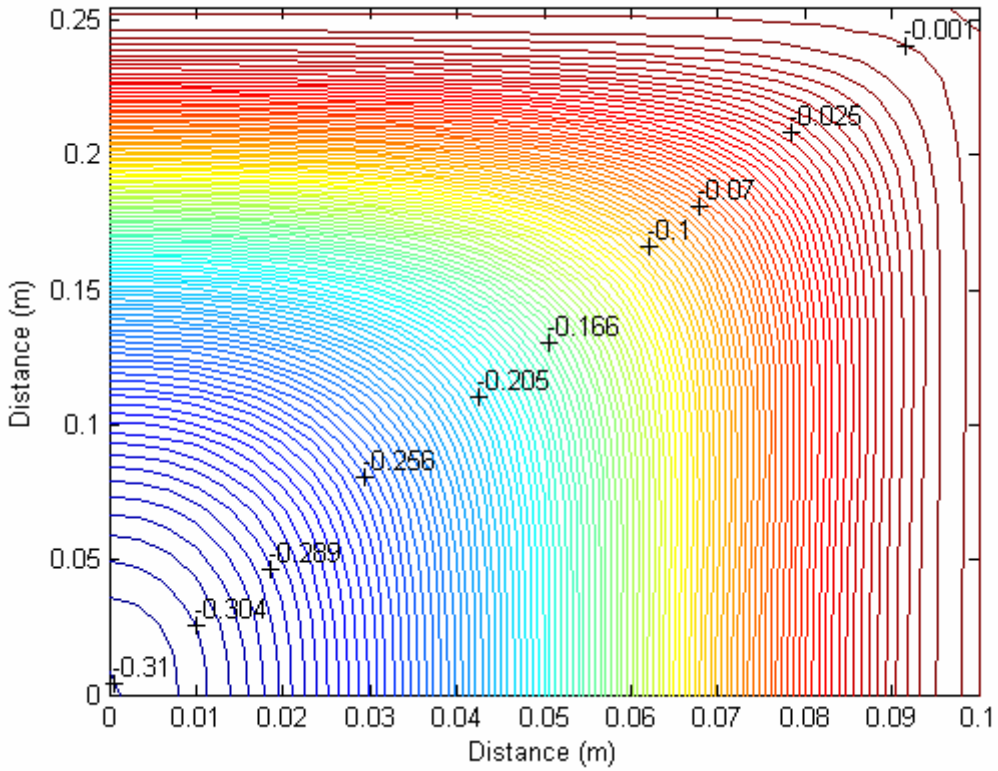

Figure 3.123 Contours of radial displacement (mm) for q=10 kPa

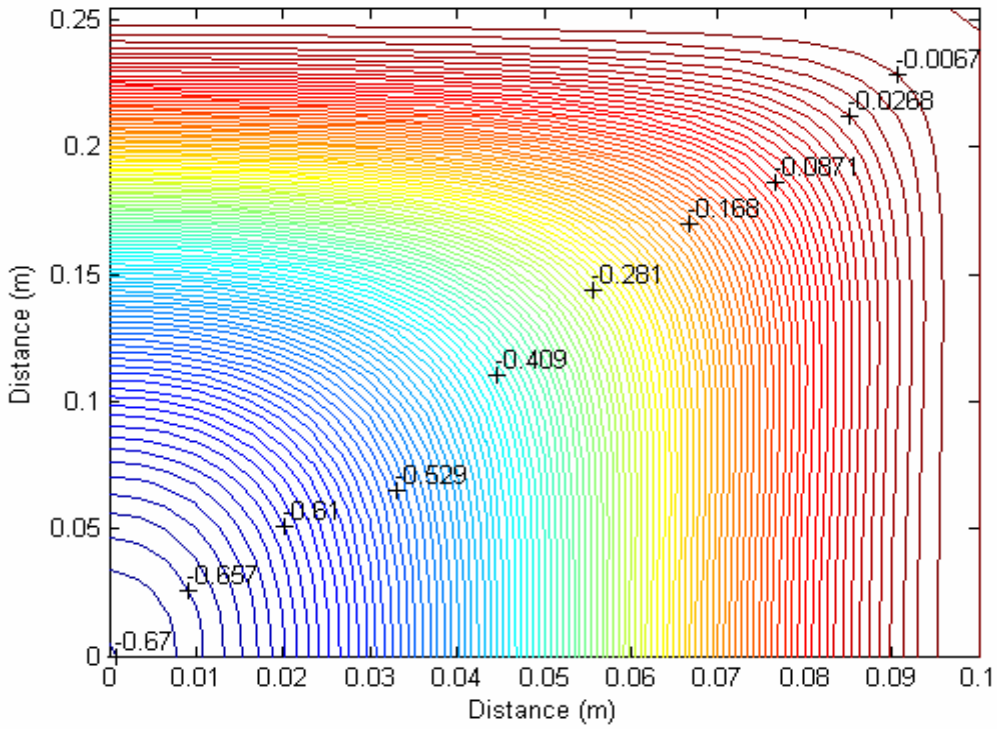

Figure 3.124 Contours of radial displacement (mm) for q=20 kPa

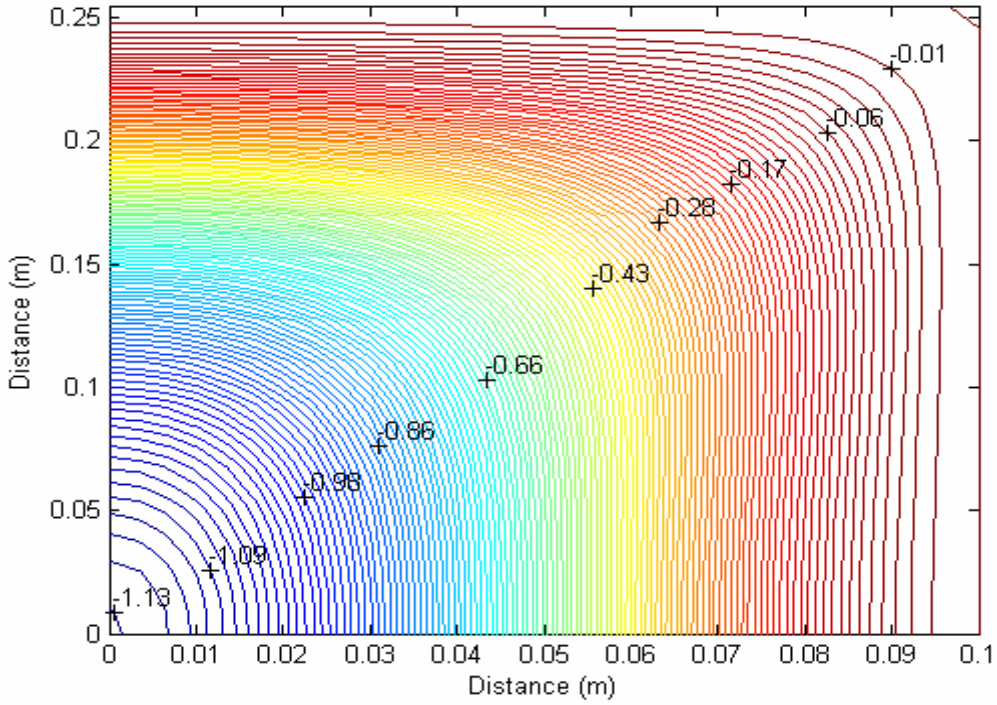

Figure 3.125 Contours of radial displacement (mm) for q=30 kPa

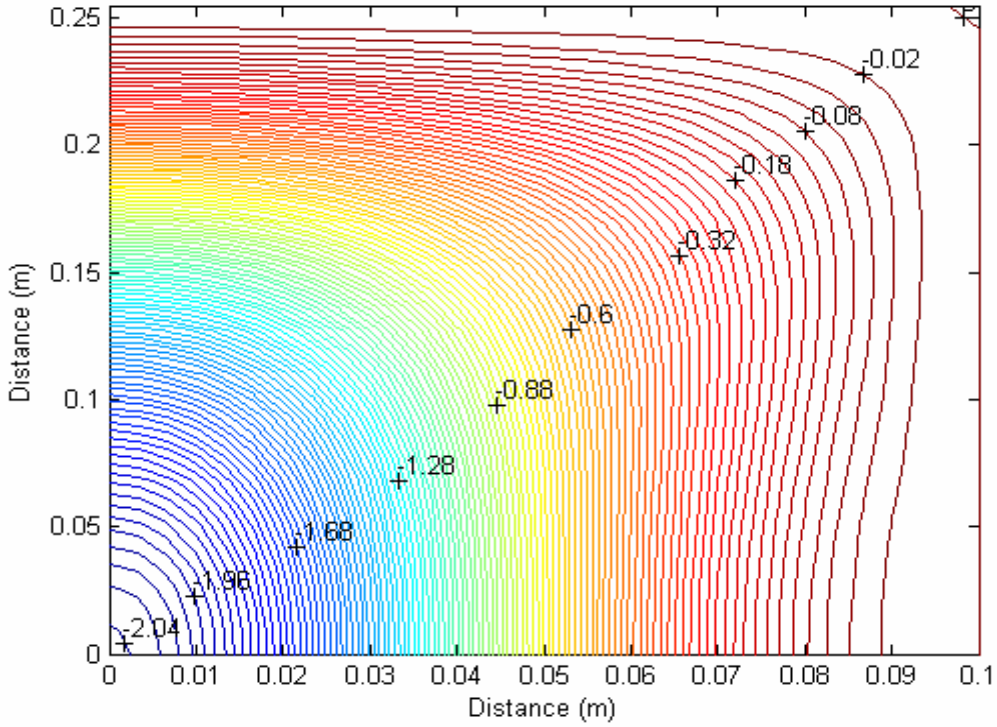

Figure 3.126 Contours of radial displacement (mm) for q=40 kPa

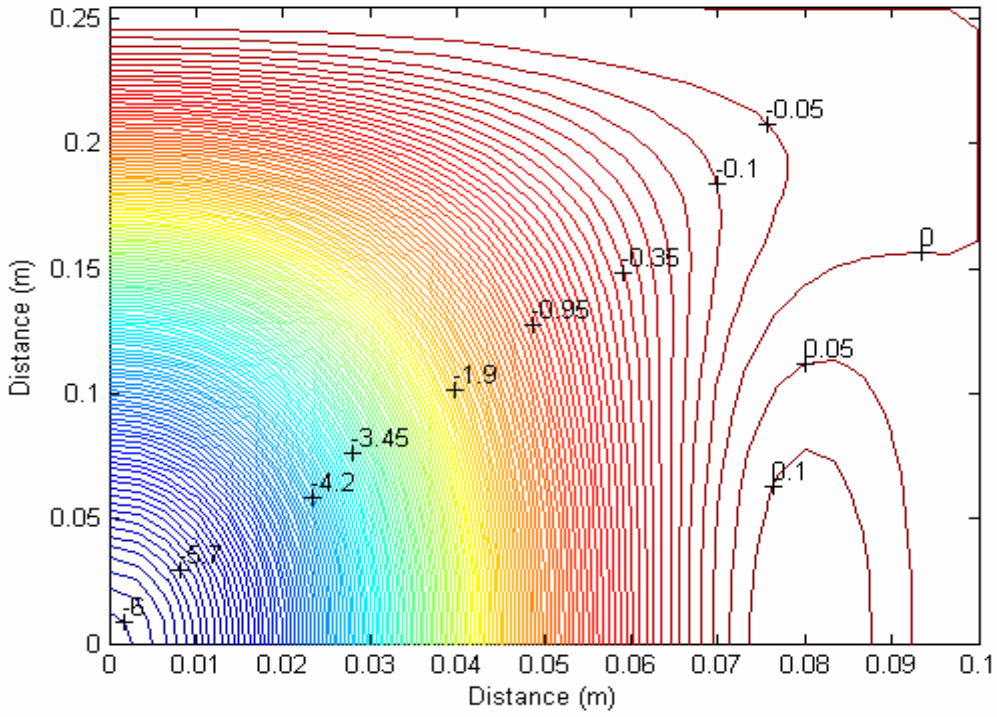

Figure 3.127 Contours of radial displacement (mm) for q=50 kPa

Figures 3.128-3.155 are plotted for the quarter of the laminated glass shell in order to have detailed information about the contour of maximum and minimum principal stress values at the top and bottom surfaces. Maximum principal stress contours are given for applied pressure q=10, 30, 40, 50, 70, 100 kPa in Figures 3.128-3.134 for the top of the unit and in Figures 3.135-3.141 for the bottom of the unit. Maximum principal stress on the top surface is close to the center of quarter shell for pressures under 50 kPa, and then it moves away from x and y-axes towards the center of the unit. For pressures higher than 50 kPa maximum principal stress on the top surface of the top glass takes place at the center of glass shell unit. Maximum principal stress on the bottom surface of the bottom glass is at the boundary of the unit. Maximum principal stress on the top and bottom surfaces of glass could be tension or compression as observed in Figures 3.128-3.141. It is observed that there is a zero stress region on the top and bottom plate. The characteristics of contours change for pressure higher than 40 kPa. Minimum principal stress contours for applied pressure are given at the top and bottom surfaces in Figures 3.142-3.148 and Figures 3.149-3.155, respectively.

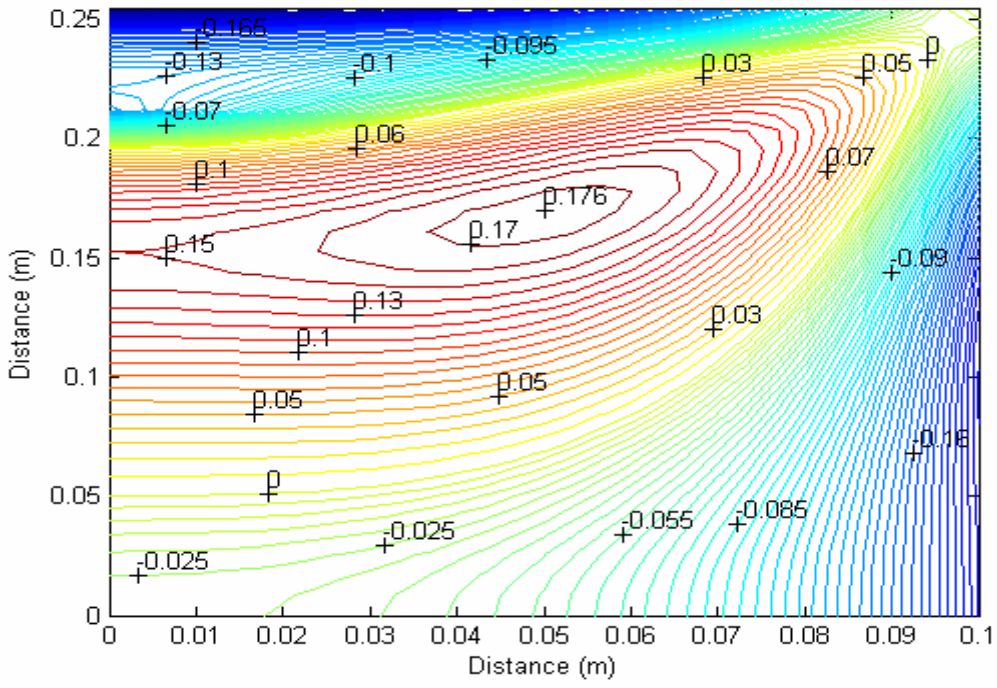

Figure 3.128 Contours of maximum principal stresses (*10^4 kPa) on the top surface of the top shell for q= 10 kPa

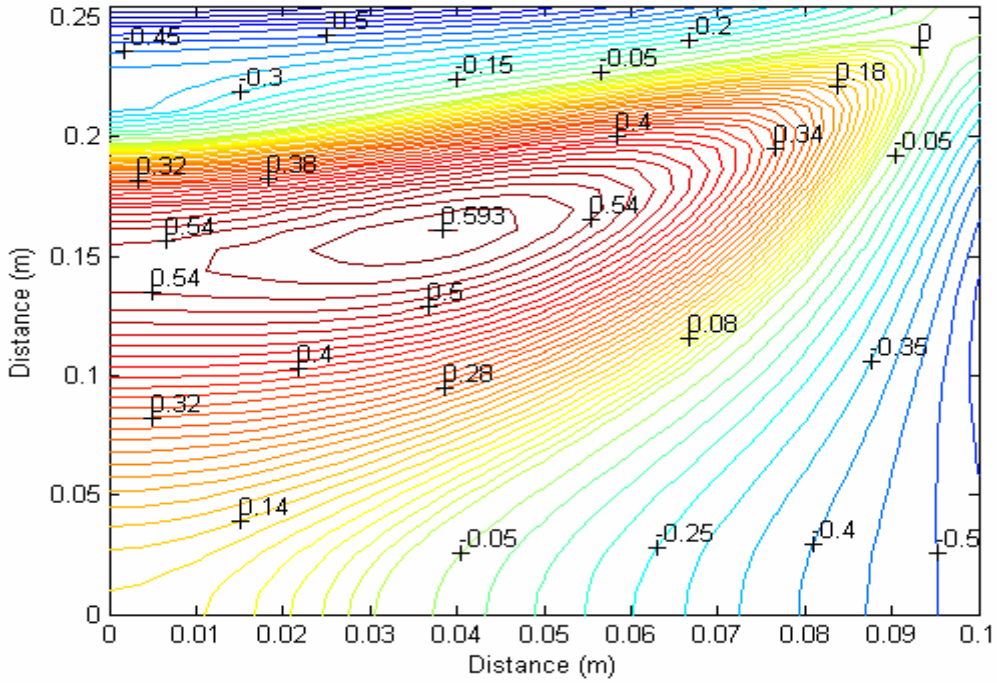

Figure 3.129 Contours of maximum principal stresses (*10^4 kPa) on the top surface of the top shell for q= 30 kPa

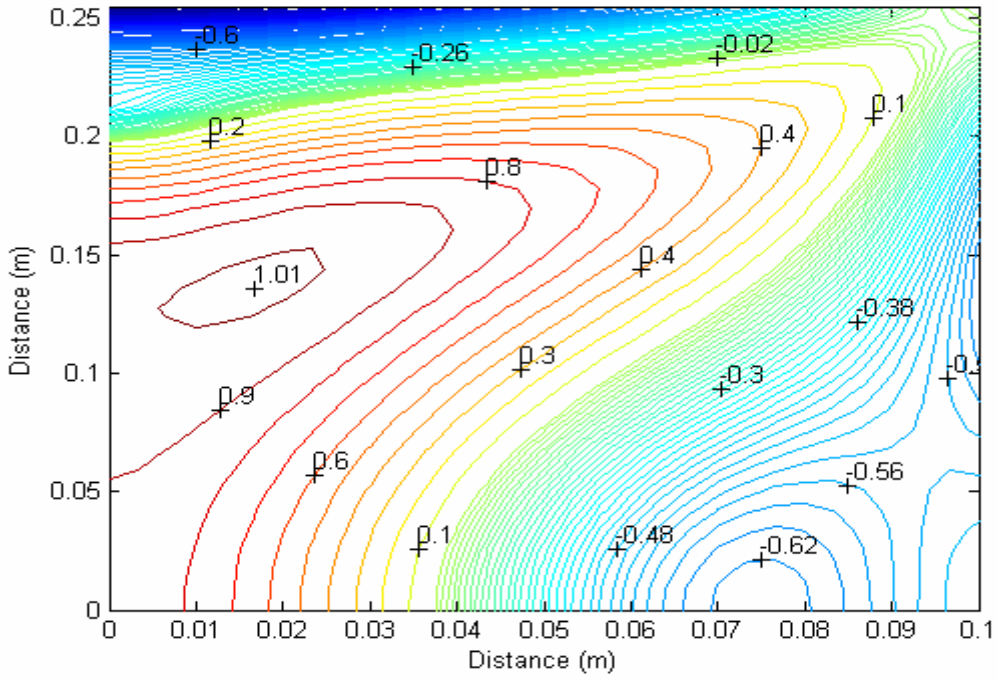

Figure 3.130 Contours of maximum principal stresses (*10^4 kPa) on the top surface of the top shell for q= 40 kPa

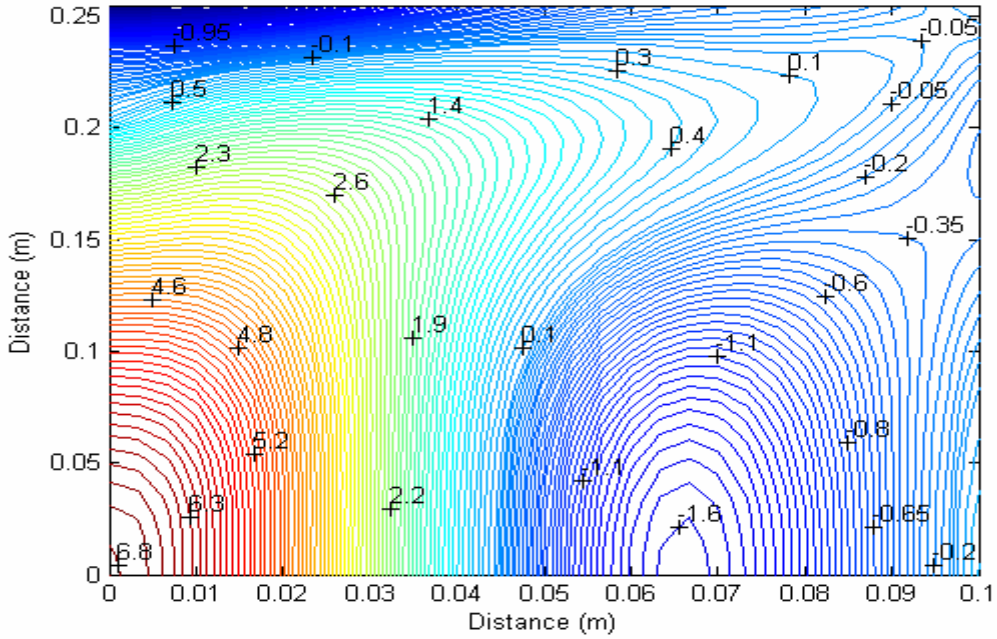

Figure 3.131 Contours of maximum principal stresses (*10^4 kPa) on the top surface of the top shell for q= 50 kPa

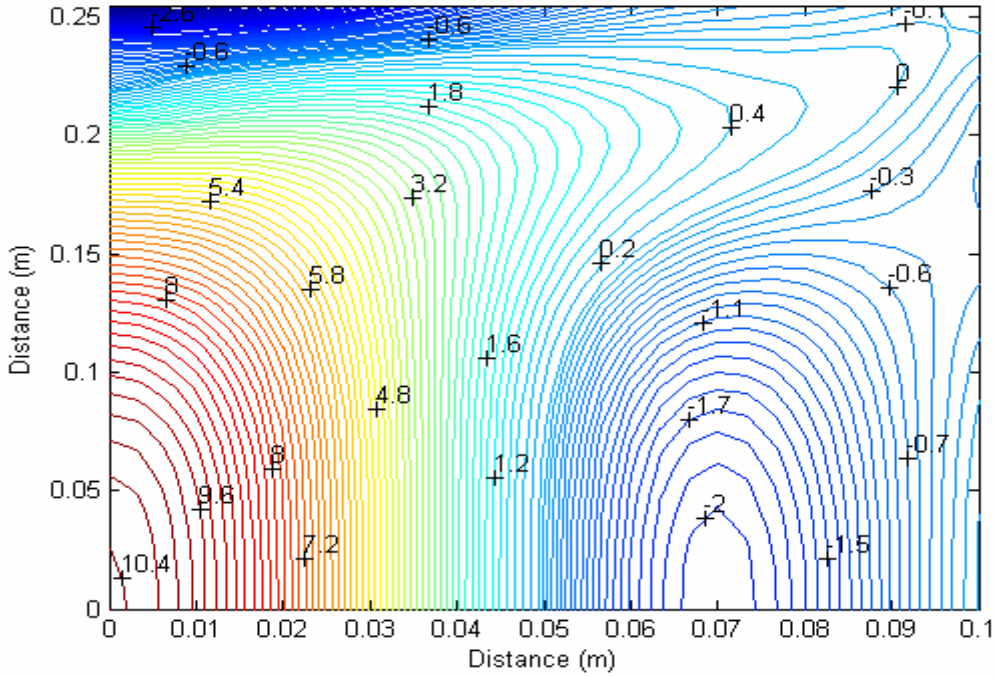

Figure 3.132 Contours of maximum principal stresses (*10^4 kPa) on the top surface of the top shell for q= 70 kPa

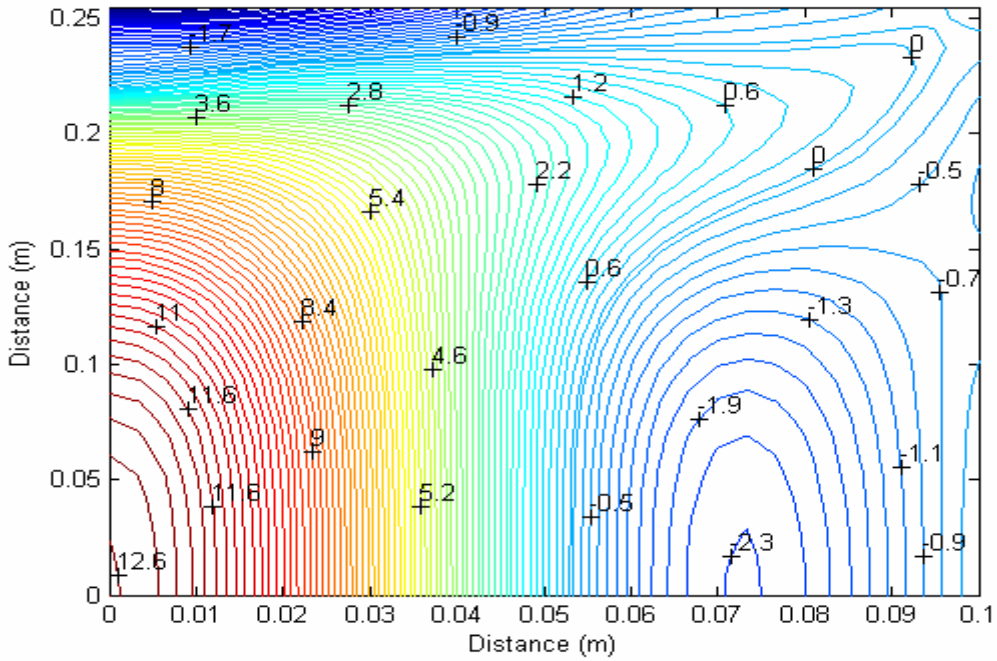

Figure 3.133 Contours of maximum principal stresses (*10^4 kPa) on the top surface of the top shell for q= 90 kPa

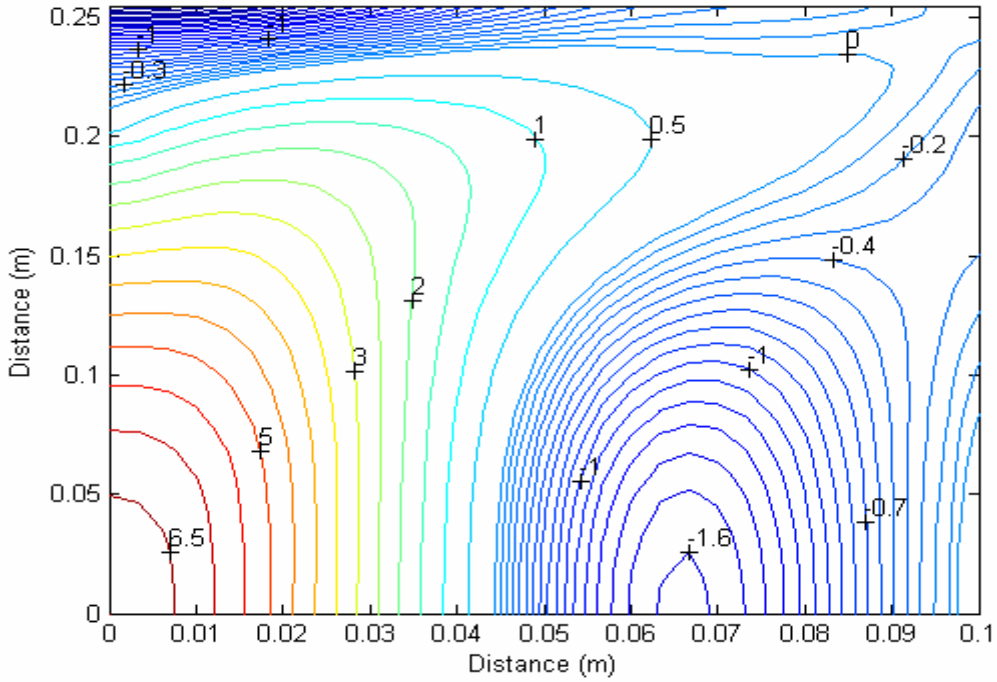

Figure 3.134 Contours of maximum principal stresses (*10^4 kPa) on the top surface of the top shell for q= 100 kPa

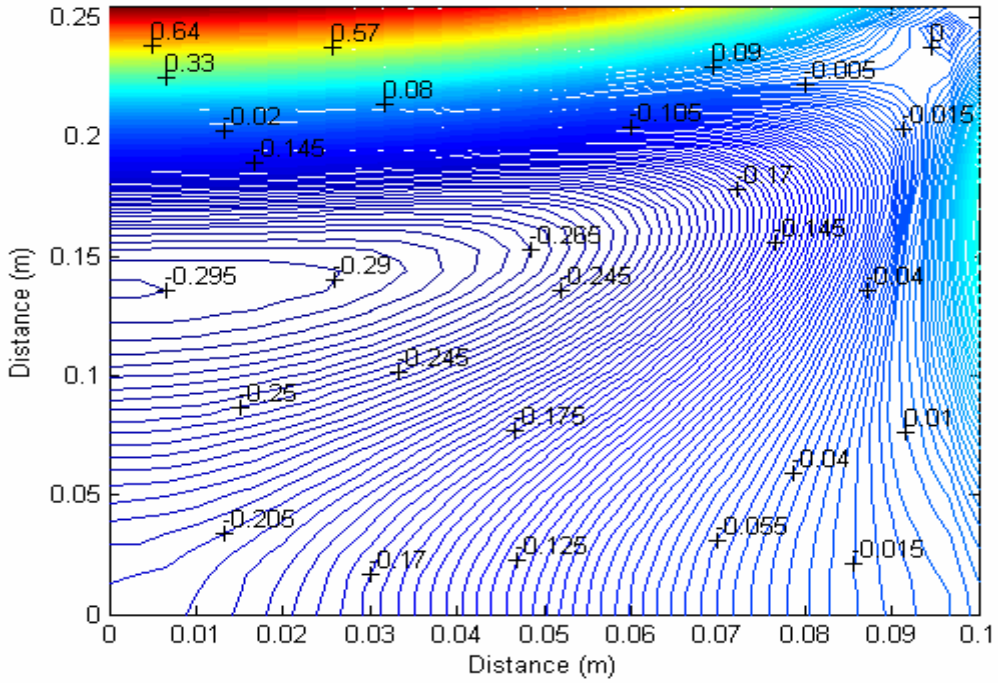

Figure 3.135 Contours of maximum principal stresses (*10^4 kPa) on the bottom surface of the bottom shell for q= 10 kPa

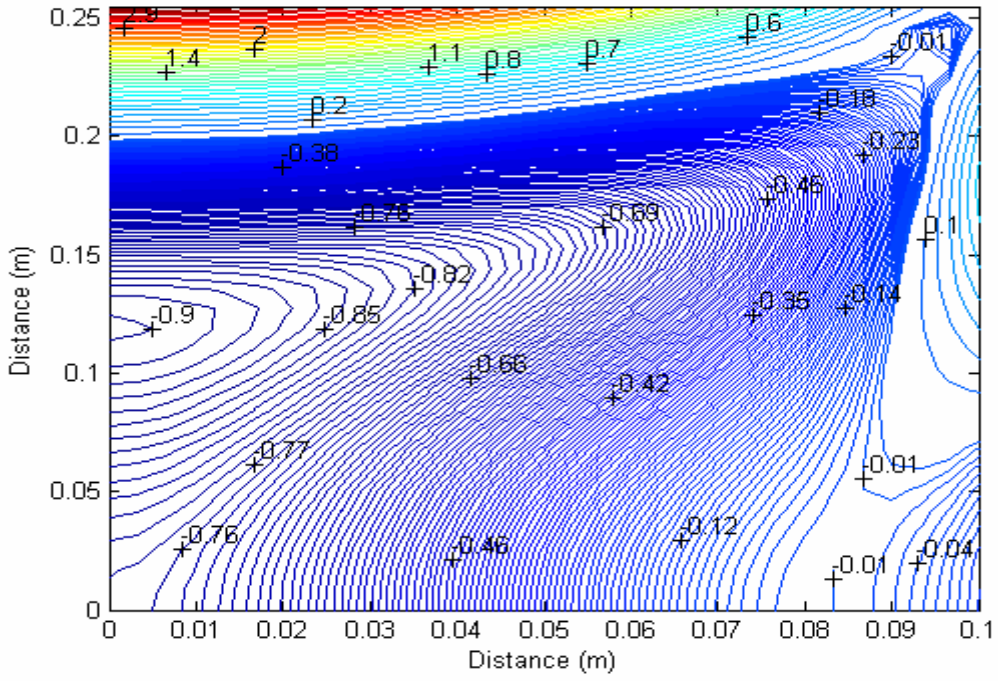

Figure 3.136 Contours of maximum principal stresses (*10^4 kPa) on the bottom surface of the bottom shell for q= 30 kPa

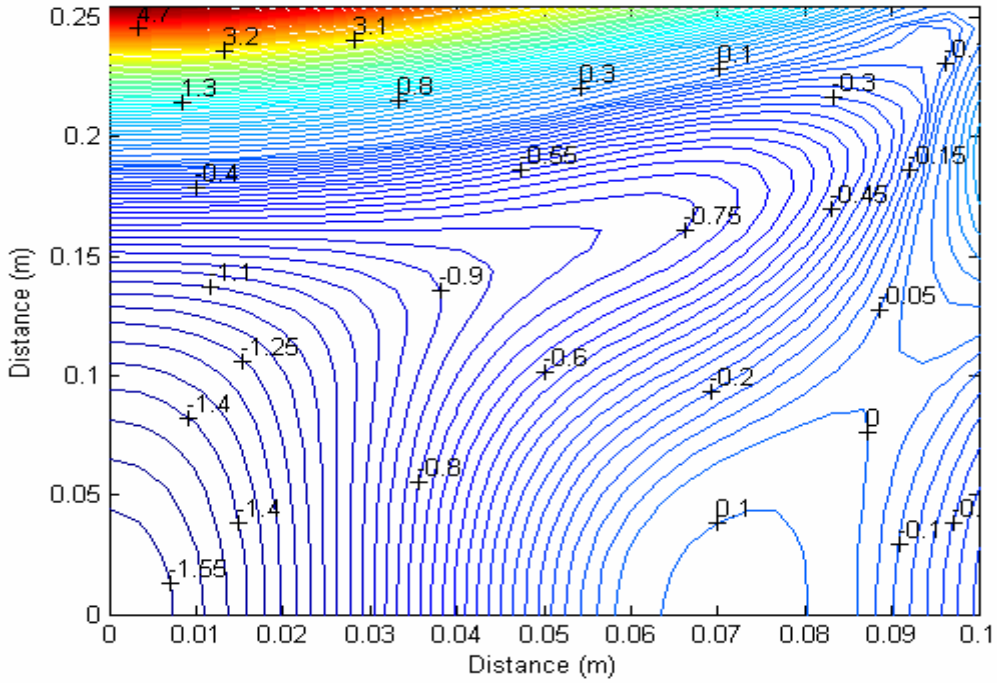

Figure 3.137 Contours of maximum principal stresses (*10^4 kPa) on the bottom surface of the bottom shell for q= 40 kPa

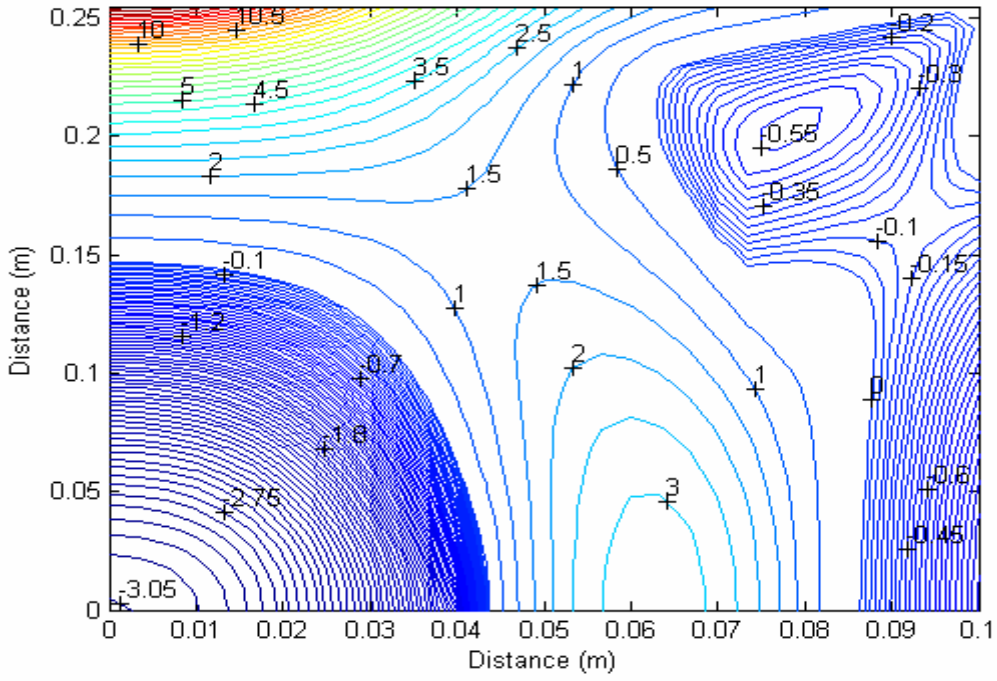

Figure 3.138 Contours of maximum principal stresses (*10^4 kPa) on the bottom surface of the bottom shell for q= 50 kPa

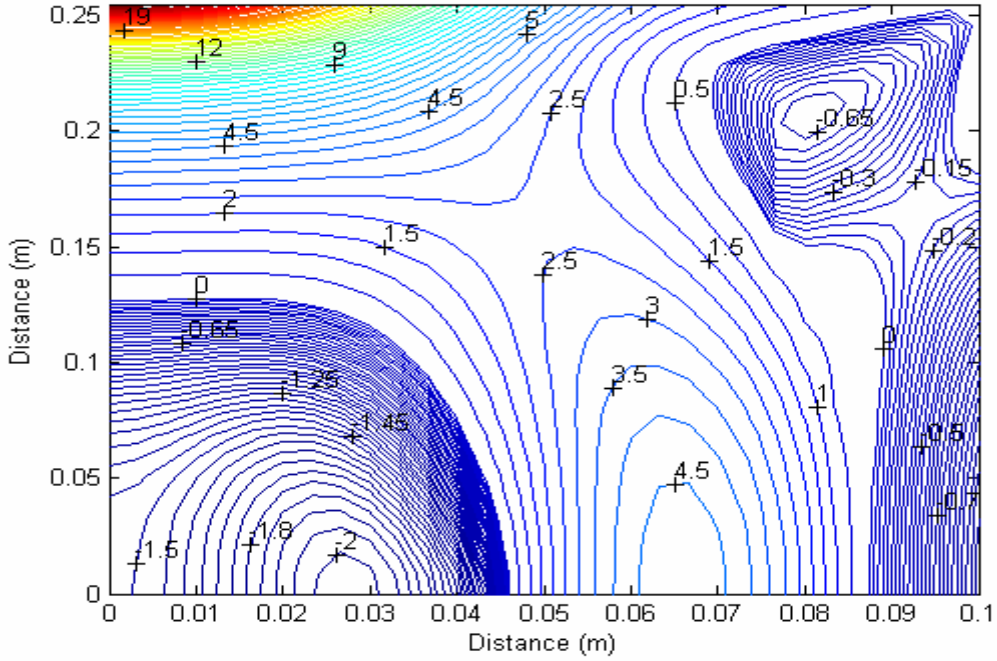

Figure 3.139 Contours of maximum principal stresses (*10^4 kPa) on the bottom surface of the bottom shell for q= 70 kPa

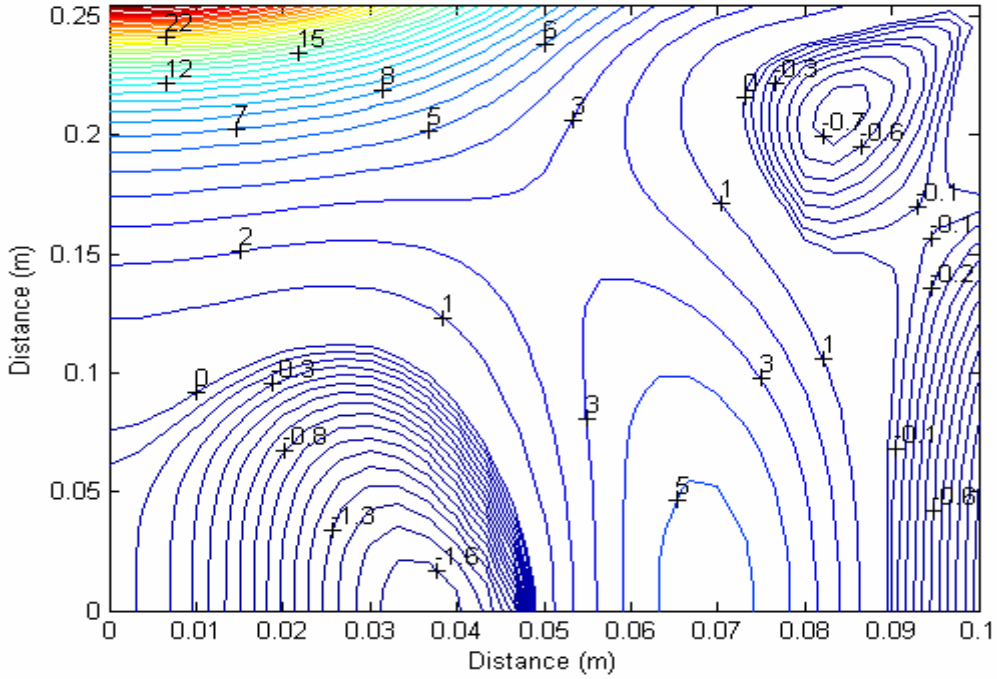

Figure 3.140 Contours of maximum principal stresses (*10^4 kPa) on the bottom surface of the bottom shell for q= 90 kPa

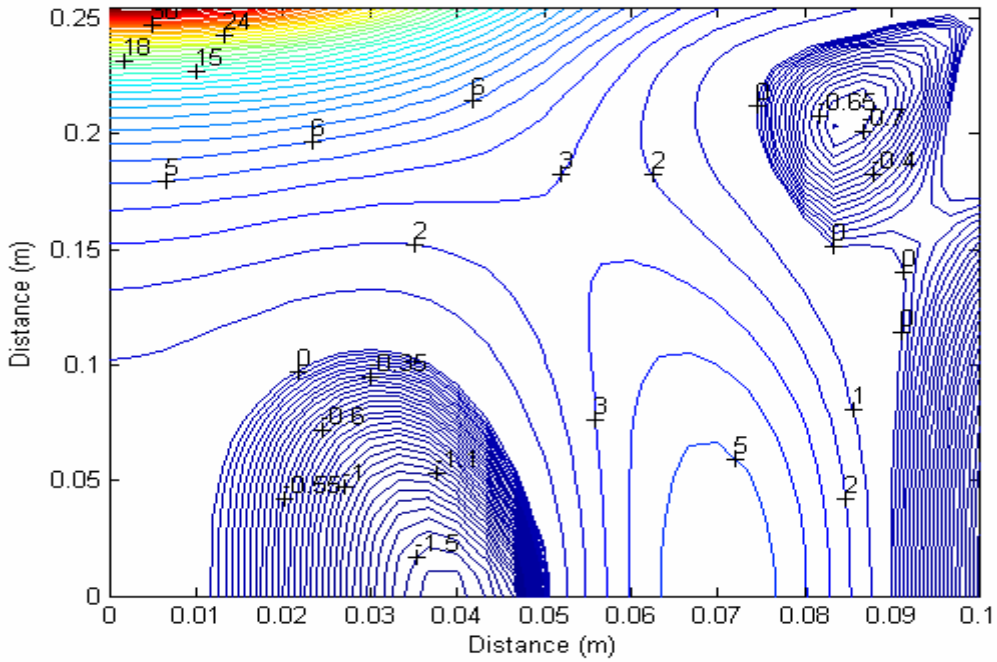

Figure 3.141 Contours of maximum principal stresses (*10^4 kPa) on the bottom surface of the bottom shell for q= 100 kPa

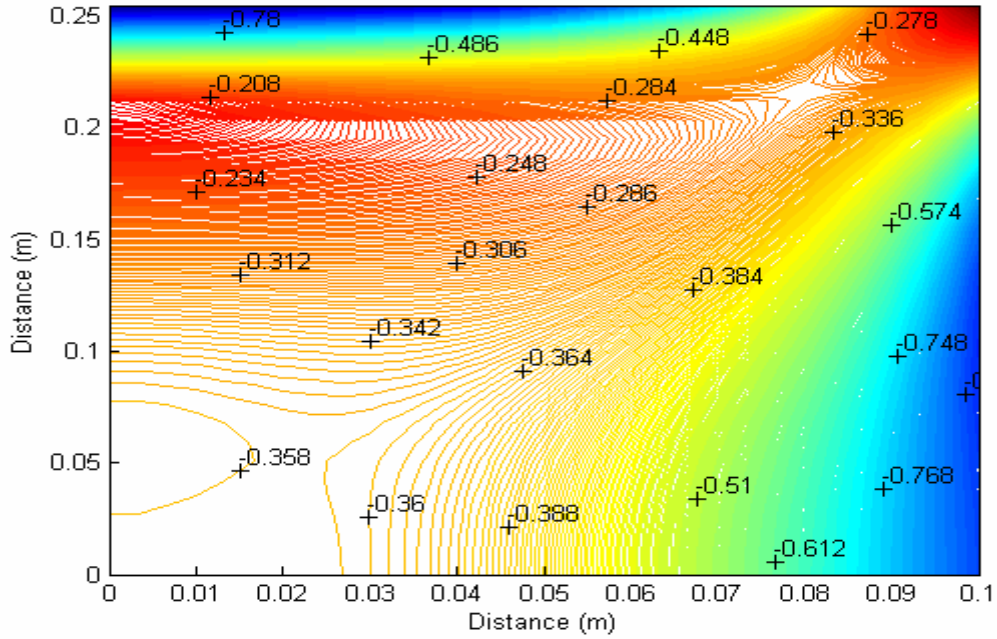

Figure 3.142 Contours of minimum principal stresses (*10^4 kPa) on the top surface of the top shell for q= 10 kPa

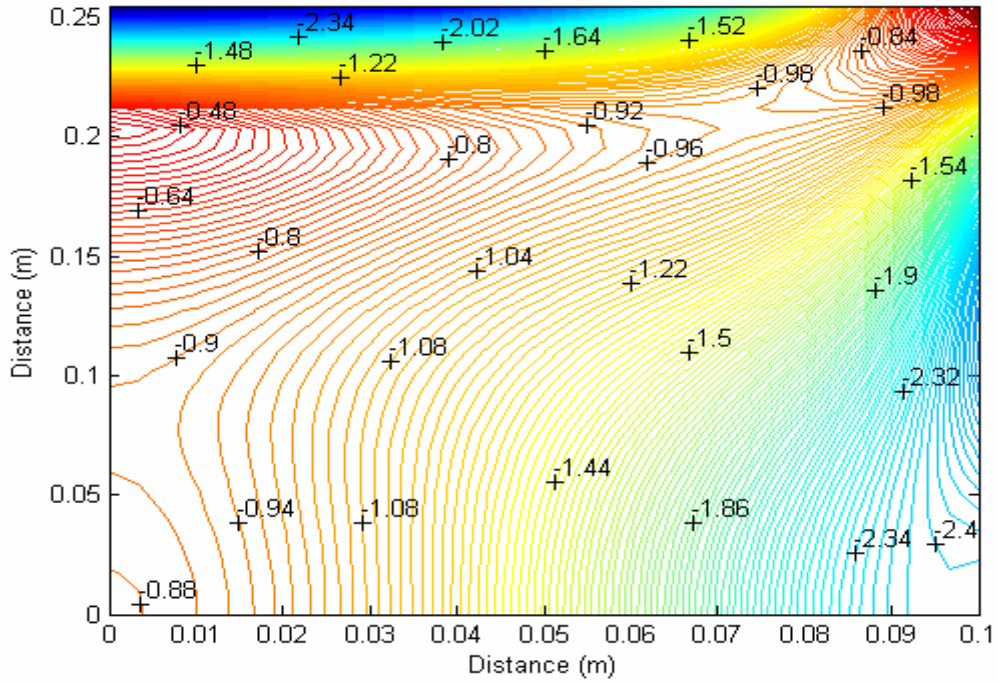

Figure 3.143 Contours of minimum principal stresses (*10^4 kPa) on the top surface of the top shell for q= 30 kPa

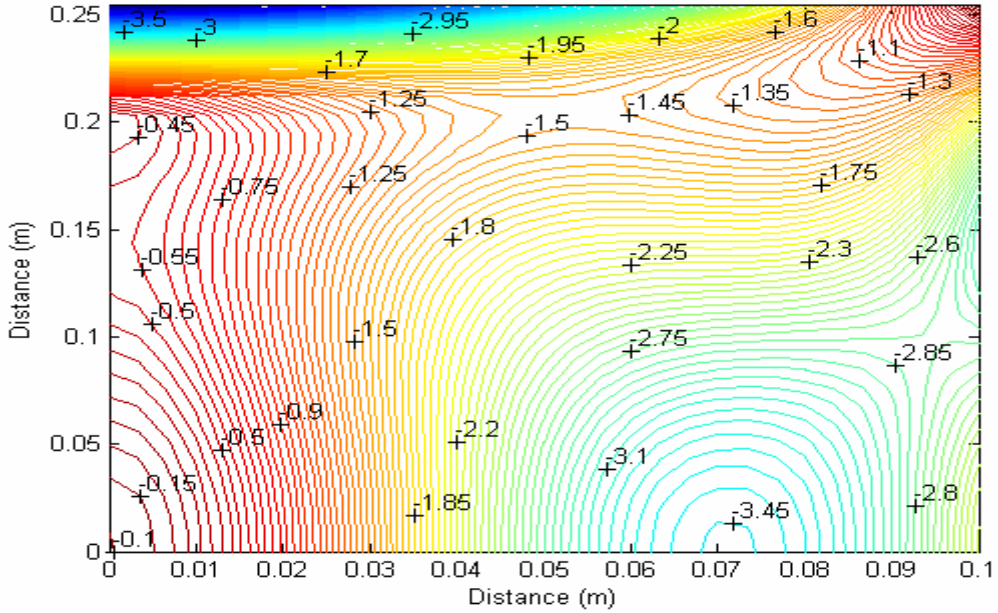

Figure 3.144 Contours of minimum principal stresses (*10^4 kPa) on the top surface of the top shell for q= 40 kPa

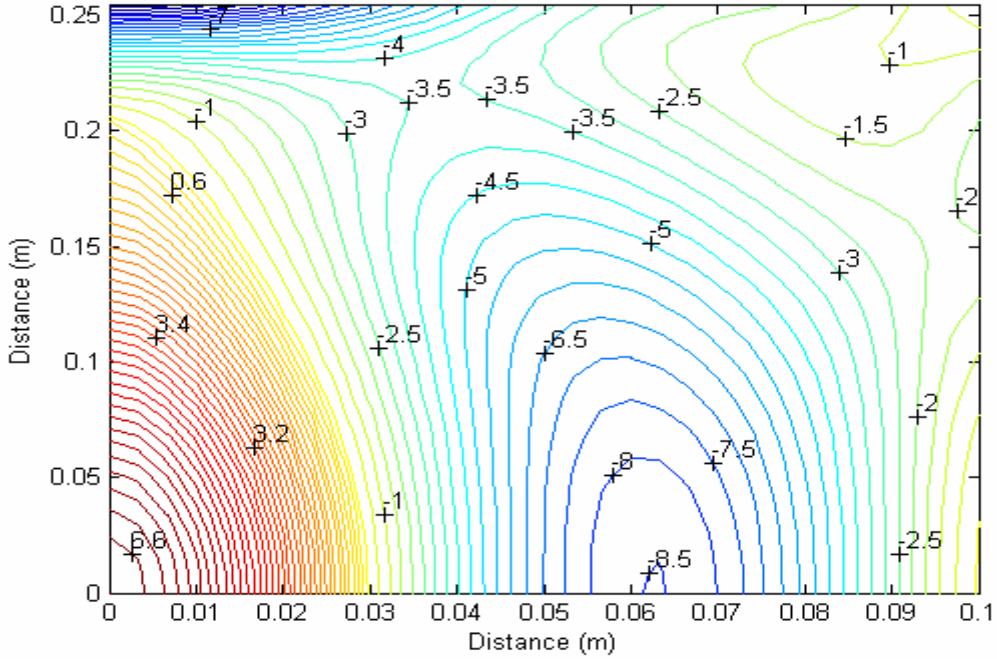

Figure 3.145 Contours of minimum principal stresses (*10^4 kPa) on the top surface of the top shell for q= 50 kPa

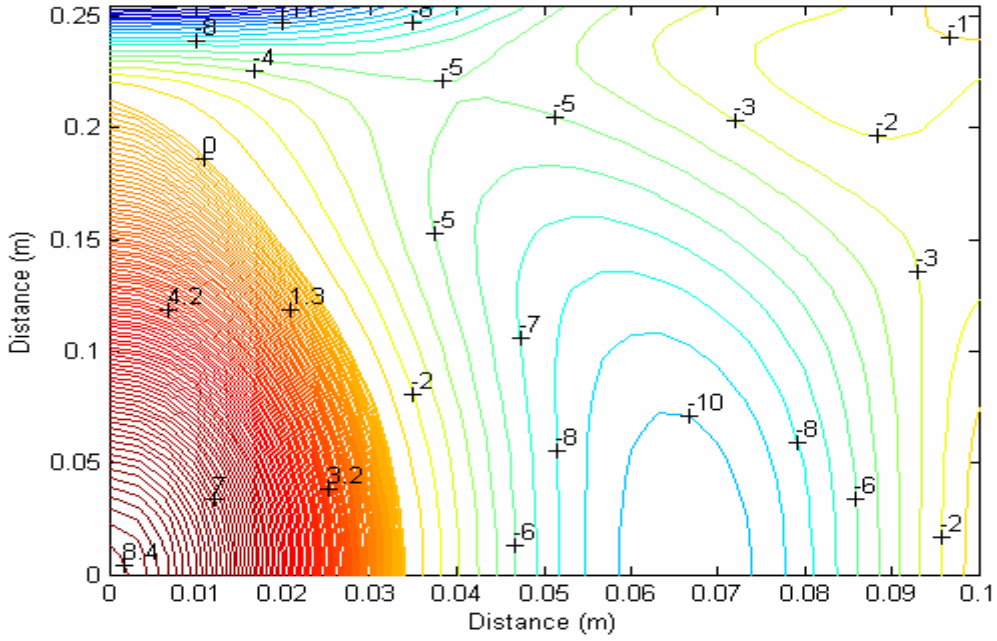

Figure 3.146 Contours of minimum principal stresses (*10^4 kPa) on the top surface of the top shell for q= 70 kPa

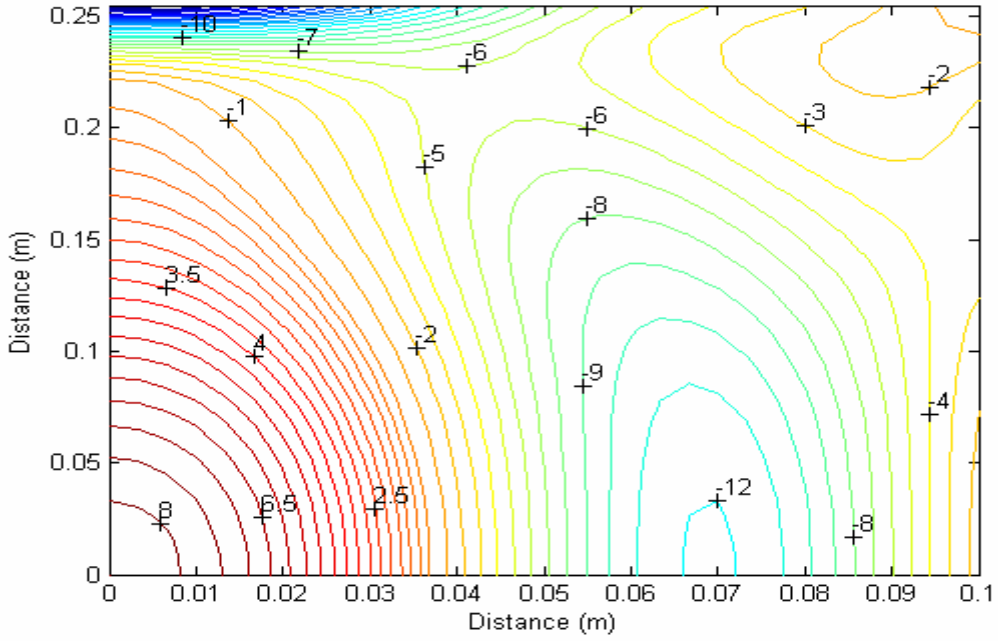

Figure 3.147 Contours of minimum principal stresses (*10^4 kPa) on the top surface of the top shell for q= 90 kPa

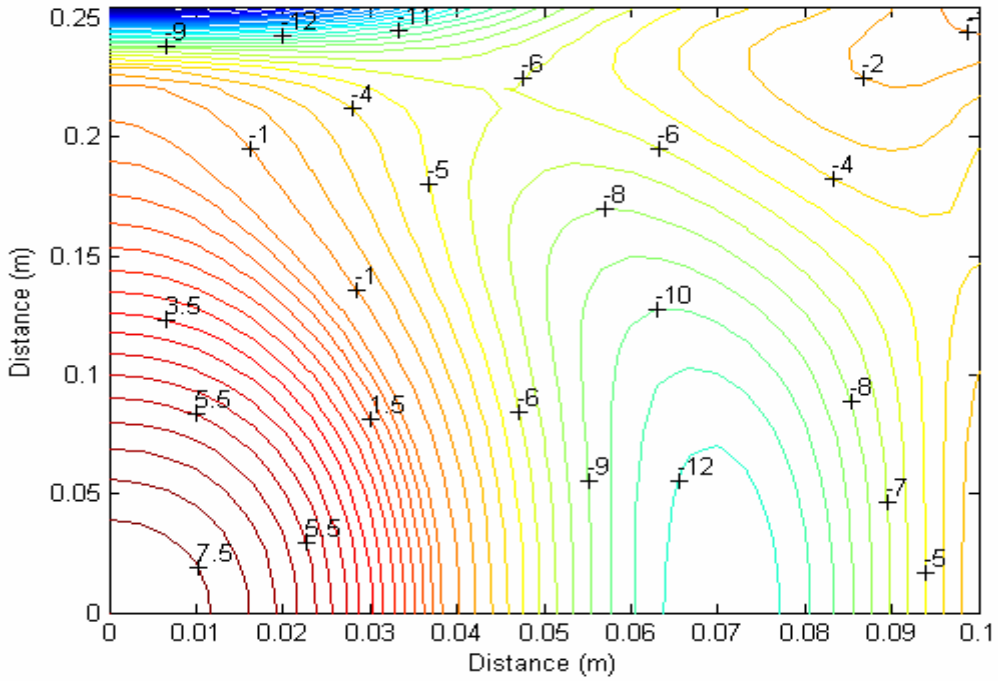

Figure 3.148 Contours of minimum principal stresses (*10^4 kPa) on the top surface of the top shell for q= 100 kPa

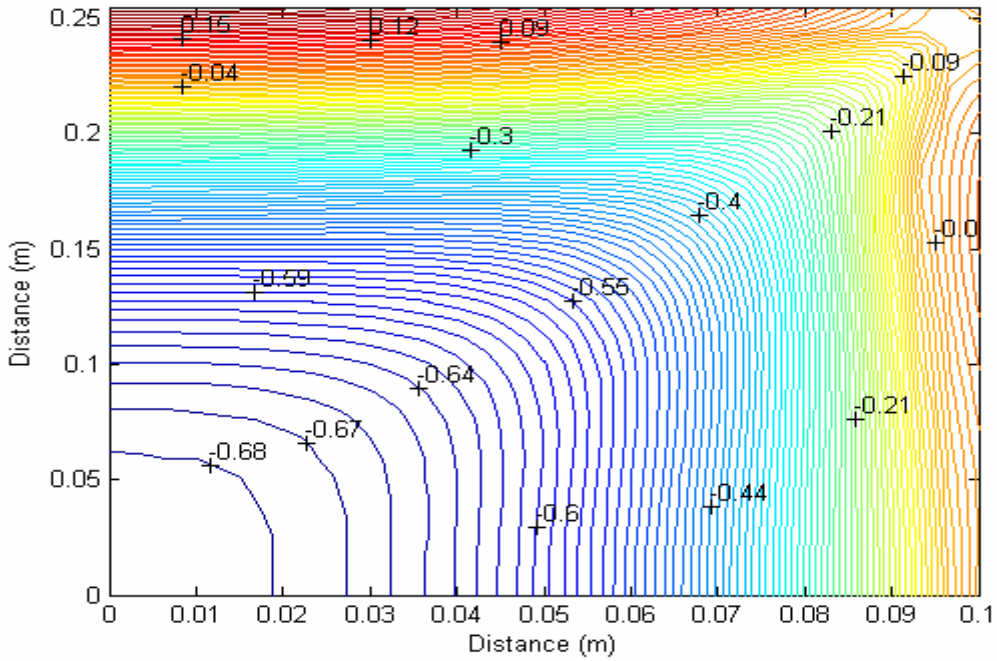

Figure 3.149 Contours of minimum principal stresses (*10^4 kPa) on the bottom surface of the bottom shell for q= 10 kPa

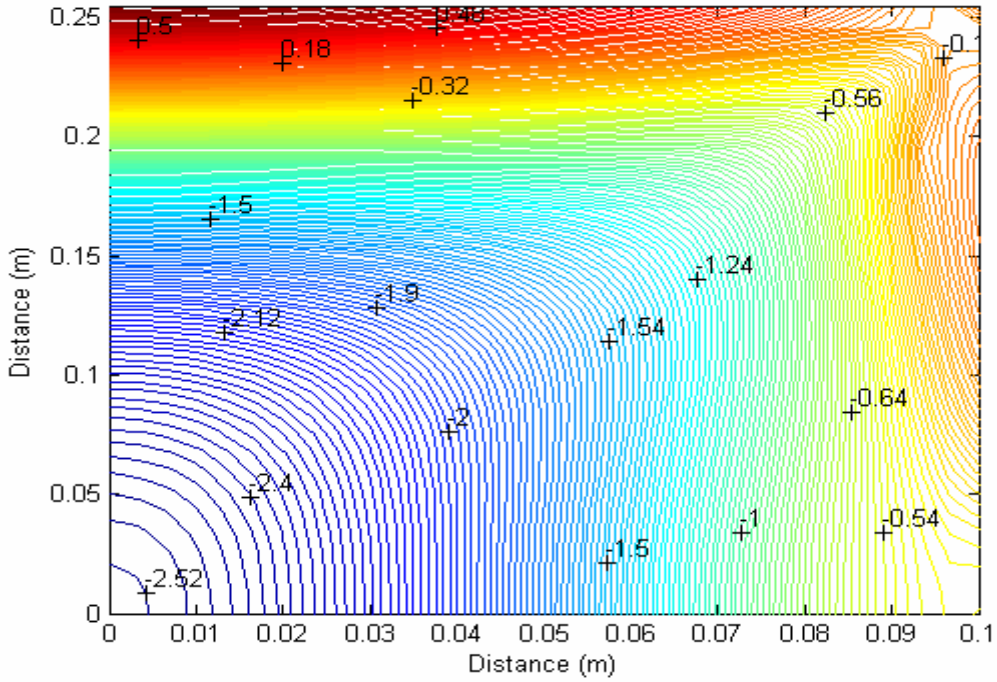

Figure 3.150 Contours of minimum principal stresses (*10^4 kPa) on the bottom surface of the bottom shell for q= 30 kPa

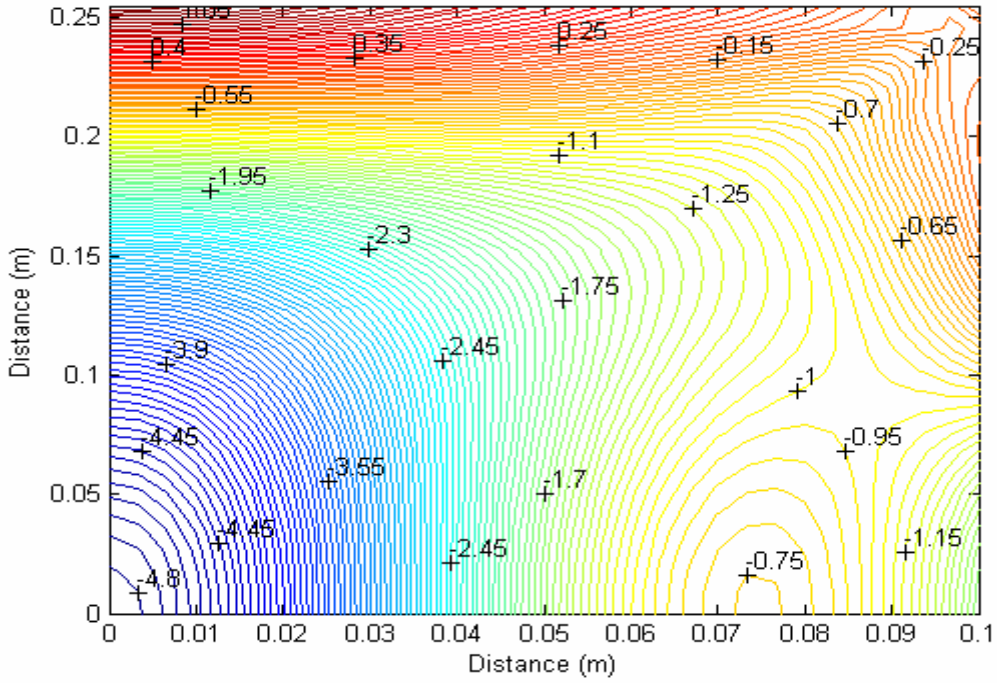

Figure 3.151 Contours of minimum principal stresses (*10^4 kPa) on the bottom surface of the bottom shell for q= 40 kPa

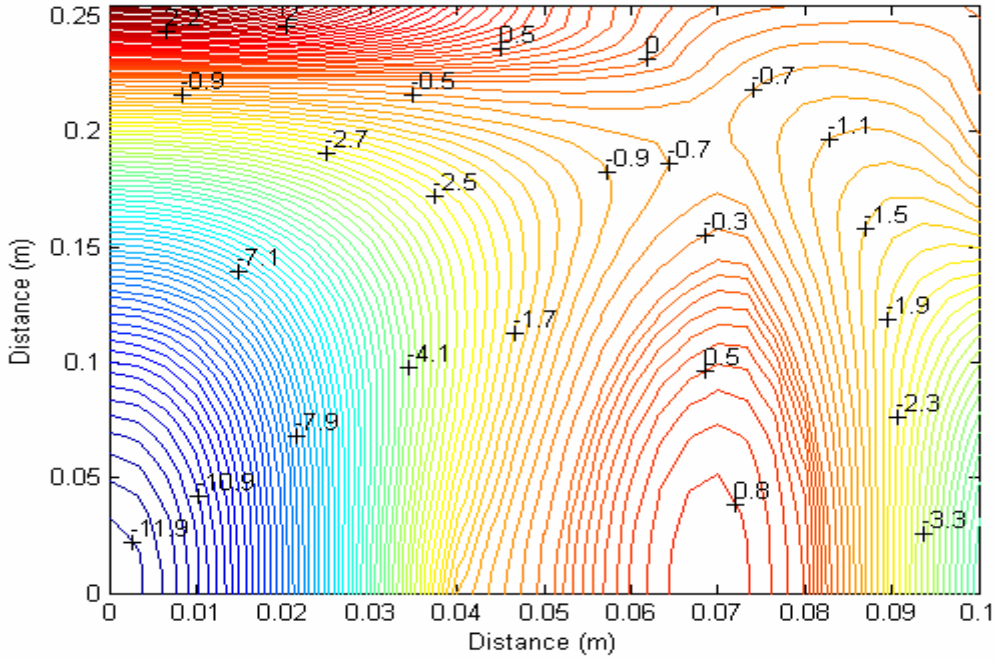

Figure 3.152 Contours of minimum principal stresses (*10^4 kPa) on the bottom surface of the bottom shell for q= 50 kPa

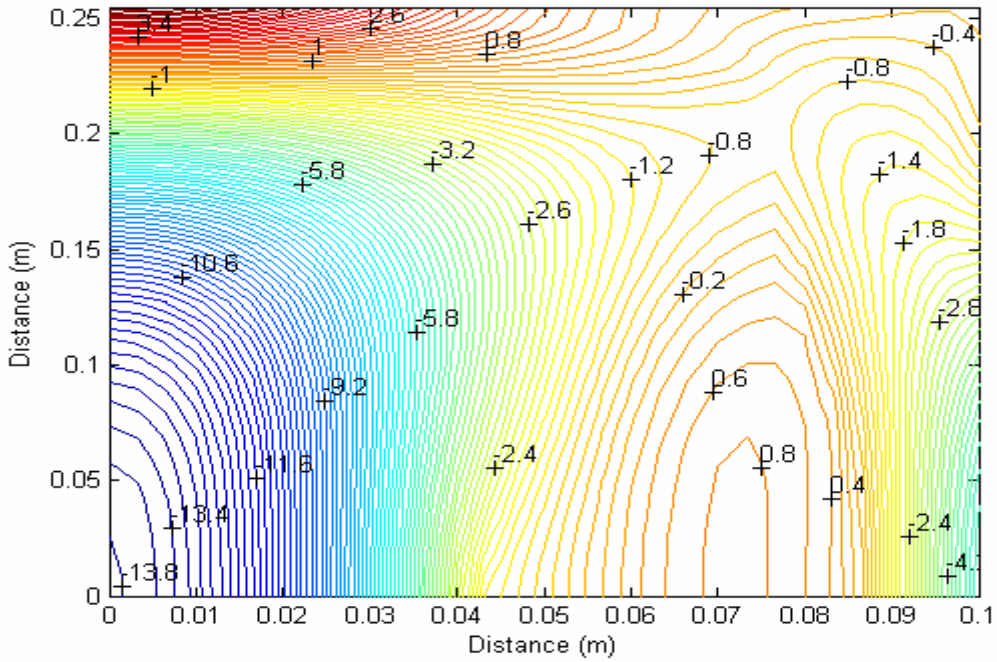

Figure 3.153 Contours of minimum principal stresses (*10^4 kPa) on the bottom surface of the bottom shell for q= 70 kPa

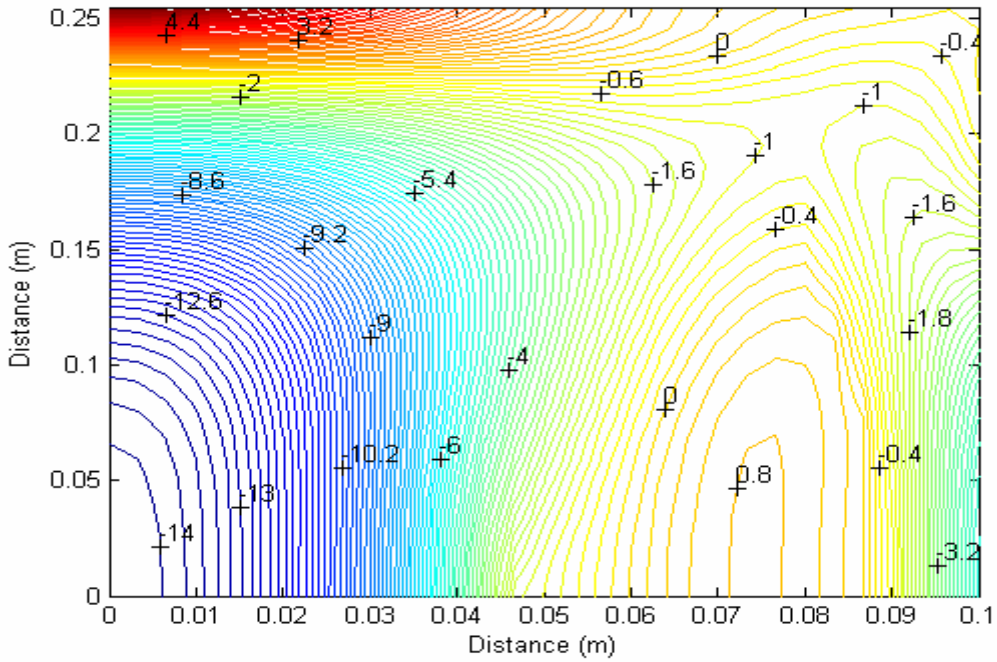

Figure 3.154 Contours of minimum principal stresses (*10^4 kPa) on the bottom surface of the bottom shell for q= 90 kPa

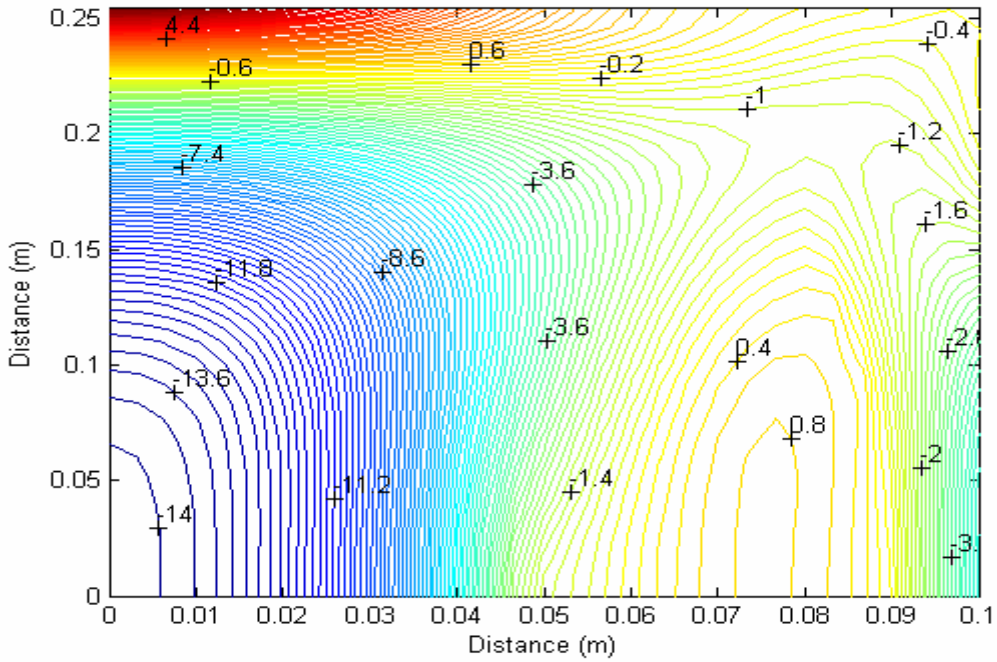

Figure 3.155 Contours of minimum principal stresses (*10^4 kPa) on the bottom surface of the bottom shell for q= 100 kPa

3.6.4 Numerical Results for Hinged Supported Cylindrical Shell Subjected to Uniform Distributed Load Towards Out of the Top Shell Surface

To consider the effect of boundary conditions on the behavior of laminated glass shell unit, the same model is verified for hinged boundary conditions. Hinged laminated glass shell tested has 0.508 m in length and 2.54 m radius. It is consisting of two glass shells and each of them has a thickness of 2.5 mm. The thickness of the inner core is 0.76 mm. The total thickness of the unit is 5.76 mm. The Young's modulus and Poisson's ratio of glass are taken to be 72 GPa and 0.25, respectively. Shear modulus and Poisson's ratio of the interlayer are taken as 1000 kPa and 0.29, respectively. Physical properties of laminated unit are given in Table 3.2.

The same governing equations (3.7)-(3.11) which are obtained for radial, circumferential and axial deflections are also valid for hinged supported shell glass. Because of symmetry, a quarter of shell is considered. For the case of hinged supported shell subjected to uniform pressure, the boundary conditions are as follows. And the pictorial presentation of boundary conditions of hinged supported cylindrical shell is given Figure 3.156.

Boundary Condition along the centerline θ=0

$$u1 = 0 \qquad u2 = 0 \qquad \frac{\partial v1}{\partial \theta} = 0 \qquad \frac{\partial v2}{\partial \theta} = 0 \qquad \frac{\partial \mathrm{w}}{\partial \theta} = 0 \qquad \text{Symmetry}$$

Boundary Condition along the edge θ=θ$_1$

$$u1 = 0 \qquad u2 = 0 \qquad v1 = 0 \qquad v2 = 0 \qquad \mathrm{w} = 0 \qquad \frac{\partial^2 \mathrm{w}}{\partial \theta^2} = 0$$

Boundary Condition along the centerline y=0

$$\frac{\partial u1}{\partial \theta} = 0 \qquad \frac{\partial u2}{\partial \theta} = 0 \qquad v1 = 0 \qquad v2 = 0 \qquad \frac{\partial \mathrm{w}}{\partial \mathrm{y}} = 0 \qquad \text{Symmetry}$$

Boundary Condition along the edge y=y$_1$

$$u1 = 0 \qquad u2 = 0 \qquad v1 = 0 \qquad v2 = 0 \qquad \mathrm{w} = 0 \qquad \frac{\partial^2 \mathrm{w}}{\partial \mathrm{y}^2} = 0$$

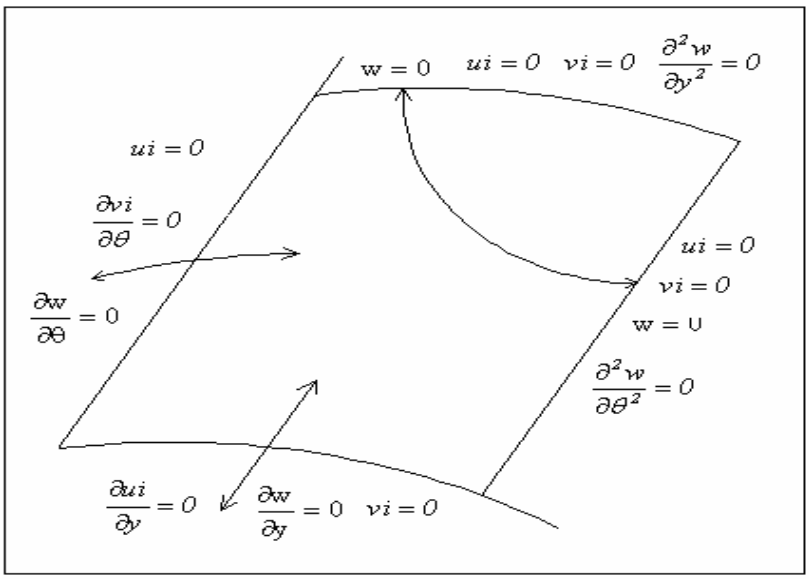

Figure 3.156 Pictorial presentation of boundary conditions for the hinged supported laminated cylindrical glass shell

The general equation is modified at the shell boundaries and the following equations are obtained for hinged supported shell:

For i=1, j=1

$$\frac{C}{4}w_{i,j}+\frac{B}{2}w_{i+1,j}+\frac{H}{2}w_{i+2,j}+\frac{J}{2}w_{i,j+1}+\frac{G}{2}w_{i,j+2}+Fw_{i+1,j+1}=\frac{RHS_{i,j}}{4}$$

For i=1, j=2

$$\frac{C+G}{2}w_{i,j}+Bw_{i+1,j}+Hw_{i+2,j}+\frac{J}{2}w_{i,j-1}+\frac{J}{2}w_{i,j+1}+\frac{G}{2}w_{i,j+2}+Fw_{i+1,j+1}$$
$$+Fw_{i+1,j-1}=\frac{RHS_{i,j}}{2}$$

For i=1, j=3...n_y-1

$$\frac{C}{2}w_{i,j}+Bw_{i+1,j}+Hw_{i+2,j}+\frac{J}{2}w_{i,j-1}+\frac{J}{2}w_{i,j+1}+\frac{G}{2}w_{i,j+2}+\frac{G}{2}w_{i,j-2}+Fw_{i+1,j+1}$$
$$+Fw_{i+1,j-1}=\frac{RHS_{i,j}}{2}$$

For i=1, j=n_y

$$\frac{C-G}{2}w_{i,j}+Bw_{i+1,j}+Hw_{i+2,j}+\frac{J}{2}w_{i,j-1}+\frac{G}{2}w_{i,j-2}+Fw_{i+1,j-1}=\frac{RHS_{i,j}}{2}$$

For i=2, j=1

$$\frac{C+H}{2}w_{i,j}+\frac{B}{2}w_{i+1,j}+\frac{H}{2}w_{i+2,j}+\frac{B}{2}w_{i-1,j}+Gw_{i,j+2}+Jw_{i,j+1}+Fw_{i+1,j+1}$$
$$+Fw_{i-1,j+1}=\frac{RHS_{i,j}}{2}$$

For i=2, j=2

$$(C+G+H)w_{i,j}+Bw_{i+1,j}+Bw_{i-1,j}+Hw_{i+2,j}+Jw_{i,j+1}+Jw_{i,j-1}+Gw_{i,j-2}$$
$$+Fw_{i+1,j+1}+Fw_{i+1,j-1}+Fw_{i-1,j+1}+Fw_{i-1,j-1}=RHS_{i,j}$$

For i=2, j=3....n_y-2

$$(C+H)w_{i,j} + Bw_{i+1,j} + Bw_{i-1,j} + Hw_{i+2,j} + Jw_{i,j+1} + Jw_{i,j-1} + Gw_{i,j-2} + Gw_{i,j+2}$$
$$+ Fw_{i+1,j+1} + Fw_{i+1,j-1} + Fw_{i-1,j+1} + Fw_{i-1,j-1} = RHS_{i,j}$$

For i=2, j=n_y-1

$$(C+H)w_{i,j} + Bw_{i+1,j} + Bw_{i-1,j} + Hw_{i+2,j} + Jw_{i,j+1} + Jw_{i,j-1} + Gw_{i,j-2}$$
$$+ Fw_{i+1,j+1} + Fw_{i+1,j-1} + Fw_{i-1,j+1} + Fw_{i-1,j-1} = RHS_{i,j}$$

For i=2, j=n_y

$$(C-G+H)w_{i,j} + Bw_{i+1,j} + Bw_{i-1,j} + Hw_{i+2,j} + Jw_{i,j-1} + Gw_{i,j-2}$$
$$+ Fw_{i+1,j-1} + Fw_{i-1,j-1} = RHS_{i,j}$$

For i=3.4..n_θ-2, j=1

$$\frac{C}{2}w_{i,j} + \frac{B}{2}w_{i+1,j} + \frac{B}{2}w_{i-1,j} + \frac{H}{2}w_{i+2,j} + \frac{H}{2}w_{i-2,j} + Jw_{i,j+1} + Gw_{i,j+2}$$
$$+ Fw_{i+1,j+1} + Fw_{i-1,j+1} = \frac{RHS_{i,j}}{2}$$

For i=n_θ-1, j=1

$$\frac{C}{2}w_{i,j} + \frac{B}{2}w_{i-1,j} + \frac{B}{2}w_{i+1,j} + \frac{H}{2}w_{i-2,j} + Jw_{i,j+1} + Gw_{i,j+2}$$
$$+ Fw_{i-1,j+1} + Fw_{i+1,j+1} = \frac{RHS_{i,j}}{2}$$

For i=n_θ-1, j=3.4...n_y-2

$$Cw_{i,j} + Bw_{i+1,j} + Bw_{i-1,j} + Hw_{i-2,j} + Jw_{i,j+1} + Jw_{i,j-1} + Gw_{i,j-2} + Gw_{i,j+2}$$
$$+ Fw_{i+1,j+1} + Fw_{i+1,j-1} + Fw_{i-1,j+1} + Fw_{i-1,j-1} = RHS_{i,j}$$

For i=n_θ, j=3...n_y-2

$$(C-H)w_{i,j} + Bw_{i-1,j} + Hw_{i-2,j} + Jw_{i,j+1} + Jw_{i,j-1} + Gw_{i,j-2} + Gw_{i,j+2}$$
$$+ Fw_{i-1,j+1} + Fw_{i-1,j-1} = RHS_{i,j}$$

For i=n_θ, j=n_y-1

$$(C-H)w_{i,j} + Bw_{i-1,j} + Hw_{i-2,j} + Jw_{i,j+1} + Jw_{i,j-1} + Gw_{i,j-2} + Fw_{i-1,j+1} + Fw_{i-1,j-1} = RHS_{i,j}$$

For i=n_θ, j=1

$$(\frac{C-H}{2})w_{i,j} + \frac{B}{2}w_{i-1,j} + \frac{H}{2}w_{i-2,j} + Jw_{i,j+1} + Gw_{i,j+2} + Fw_{i-1,j+1} = \frac{RHS_{i,j}}{2}$$

For i=n_θ-1, j=2

$$(C+G)w_{i,j} + Bw_{i-1,j} + Bw_{i-1,j} + Hw_{i-2,j} + Jw_{i,j+1} + Jw_{i,j-1} + Gw_{i,j+2} + Fw_{i-1,j+1} + Fw_{i-1,j-1} + Fw_{i+1,j+!} + Fw_{i+1,j-1} = RHS_{i,j}$$

For i=n_θ, j=2

$$(C+G-H)w_{i,j} + Bw_{i-1,j} + Hw_{i-2,j} + Jw_{i,j+1} + Jw_{i,j-1} + Gw_{i,j+2} + Fw_{i-1,j+1} + Fw_{i-1,j-1} = RHS_{i,j}$$

For i=n_θ, j=n_y

$$(C-G-H)w_{i,j} + Bw_{i-1,j} + Hw_{i-2,j} + Jw_{i,j-1} + Gw_{i,j-2} + Fw_{i-1,j-1} = RHS_{i,j}$$

For i=n_θ-1, j=n_y-1

$$Cw_{i,j} + Bw_{i+1,j} + Bw_{i-1,j} + Hw_{i-2,j} + Jw_{i,j+1} + Jw_{i,j-1} + Gw_{i,j-2} + Fw_{i+1,j+1} + Fw_{i+1,j-1} + Fw_{i-1,j+1} + Fw_{i-1,j-1} = RHS_{i,j}$$

For i=3...n_θ-2, j=2

$$(C+G)w_{i,j} + Bw_{i+1,j} + Bw_{i-1,j} + Hw_{i-2,j} + Hw_{i+2,j} + Jw_{i,j+1} + Jw_{i,j-1} + Gw_{i,j+2} + Fw_{i+1,j+1} + Fw_{i+1,j-1} + Fw_{i-1,j+1} + Fw_{i-1,j-1} = RHS_{i,j}$$

For i=3...n_θ-2, j=n_y-1

$$Cw_{i,j} + Bw_{i+1,j} + Bw_{i-1,j} + Hw_{i-2,j} + Hw_{i+2,j} + Jw_{i,j+1} + Jw_{i,j-1} + Gw_{i,j-2} + Fw_{i+1,j+1} + Fw_{i+1,j-1} + Fw_{i-1,j+1} + Fw_{i-1,j-1} = RHS_{i,j}$$

For i=3...n_θ-2, j=n_y

$$(C+G)w_{i,j} + Bw_{i+1,j} + Bw_{i-1,j} + Hw_{i-2,j} + Hw_{i+2,j} + Jw_{i,j-1} + Gw_{i,j+-2} + Fw_{i+1,j-1} + Fw_{i-1,j-1} = RHS_{i,j}$$

For i=n_θ-1, j=n_y

$$(C+G)w_{i,j} + Bw_{i+1,j} + Bw_{i-1,j} + Hw_{i-2,j} + Jw_{i,j-1} + Gw_{i,j-2} + Fw_{i+1,j-1} + Fw_{i-1,j-1} = RHS_{i,j}$$

The general equations for circumferential displacements (u1) are modified at the shell boundaries and the following equations are obtained for hinged supported shell.

For i=2, j=1

$$APU1_{(i,j)}u1_{(i,j)} + \left(ANU1_{(i,j)} + ASU1_{(i,j)}\right)u1_{(i,j+1)} + AEU1_{(i,j)}u1_{(i+1,j)} = FU1_{(i,j)}$$

For i=3.4…n_θ-1, j=1

$$APU1_{(i,j)}u1_{(i,j)} + \left(ANU1_{(i,j)} + ASU1_{(i,j)}\right)u1_{(i,j+1)} + AEU1_{(i,j)}u1_{(i+1,j)} + AWU1_{(i,j)}u1_{(i+1,j)} = FU1_{(i,j)}$$

For i=n_θ, j=1

$$APU1_{(i,j)}u1_{(i,j)} + \left(ANU1_{(i,j)} + ASU1_{(i,j)}\right)u1_{(i,j+1)} + AWU1_{(i,j)}u1_{(i+1,j)} = FU1_{(i,j)}$$

For i=2, j=2.3…..n_y-1

$$APU1_{(i,j)}u1_{(i,j)} + ANU1_{(i,j)}u1_{(i,j+1)} + ASU1_{(i,j)}u1_{(i,j-1)} + AEU1_{(i,j)}u1_{(i+1,j)} = FU1_{(i,j)}$$

For i=2, j=n_y

$$APU1_{(i,j)}u1_{(i,j)} + ASU1_{(i,j)}u1_{(i,j-1)} + AEU1_{(i,j)}u1_{(i+1,j)} = FU1_{(i,j)}$$

For i=3.4….n_θ-1 , j=2.3…..n_y-1

$$APU1_{(i,j)}u1_{(i,j)} + ANU1_{(i,j)}u1_{(i,j+1)} + ASU1_{(i,j)}u1_{(i,j-1)} + AWU1_{(i,j)}u1_{(i-1,j)} + AEU1_{(i,j)}u1_{(i+1,j)} = FU1_{(i,j)}$$

For i=3.4….n_θ-1, j=n_y

$$APU1_{(i,j)}u1_{(i,j)} + ASU1_{(i,j)}u1_{(i,j-1)} + AWU1_{(i,j)}u1_{(i-1,j)} + AEU1_{(i,j)}u1_{(i+1,j)} = FU1_{(i,j)}$$

For i=n_θ, j=2.3…..n_y-1

$$APU1_{(i,j)}u1_{(i,j)} + ANU1_{(i,j)}u1_{(i,j+1)} + ASU1_{(i,j)}u1_{(i,j-1)} + AWU1_{(i,j)}u1_{(i-1,j)} = FU1_{(i,j)}$$

For i=n_θ, j=n_y

$$APU1_{(i,j)}u1_{(i,j)} + ASU1_{(i,j)}u1_{(i,j-1)} + AWU1_{(i,j)}u1_{(i-1,j)} = FU1_{(i,j)}$$

The general equations for circumferential displacements (u2) are modified at the shell boundaries and the following equations are obtained for hinged supported shell.

For i=2, j=1

$$APU2_{(i,j)}u2_{(i,j)} + \left(ANU2_{(i,j)} + ASU2_{(i,j)}\right)u2_{(i,j+1)} + AEU2_{(i,j)}u2_{(i+1,j)} = FU2_{(i,j)}$$

For i=3.4….n_θ-1, j=1

$$APU2_{(i,j)}u2_{(i,j)} + \left(ANU2_{(i,j)} + ASU2_{(i,j)}\right)u2_{(i,j+1)} + AEU2_{(i,j)}u2_{(i+1,j)} + AWU2_{(i,j)}u2_{(i+1,j)} = FU2_{(i,j)}$$

For i=n_θ, j=1

$$APU2_{(i,j)}u2_{(i,j)} + \left(ANU2_{(i,j)} + ASU2_{(i,j)}\right)u2_{(i,j+1)} + AWU2_{(i,j)}u2_{(i+1,j)} = FU2_{(i,j)}$$

For i=2, j=2.3…..n_y-1

$$APU2_{(i,j)}u2_{(i,j)} + ANU2_{(i,j)}u2_{(i,j+1)} + ASU2_{(i,j)}u2_{(i,j-1)} + AEU2_{(i,j)}u2_{(i+1,j)} = FU2_{(i,j)}$$

For i=2, j=n_y

$$APU2_{(i,j)}u2_{(i,j)} + ASU2_{(i,j)}u2_{(i,j-1)} + AEU2_{(i,j)}u2_{(i+1,j)} = FU2_{(i,j)}$$

For i=3.4….n_θ-1 , j=2.3…..n_y-1

$$APU2_{(i,j)}u2_{(i,j)} + ANU2_{(i,j)}u2_{(i,j+1)} + ASU2_{(i,j)}u2_{(i,j-1)} + AWU2_{(i,j)}u2_{(i-1,j)} + AEU2_{(i,j)}u2_{(i+1,j)} = FU2_{(i,j)}$$

For i=3.4.…n_θ-1, j=n_y

$$APU2_{(i,j)}u2_{(i,j)} + ASU2_{(i,j)}u2_{(i,j-1)} + AWU2_{(i,j)}u2_{(i-1,j)} + AEU2_{(i,j)}u2_{(i+1,j)} = FU2_{(i,j)}$$

For i=n_θ, j=2.3.….n_y-1

$$APU2_{(i,j)}u2_{(i,j)} + ANU2_{(i,j)}u2_{(i,j+1)} + ASU2_{(i,j)}u2_{(i,j-1)} + AWU2_{(i,j)}u2_{(i-1,j)} = FU2_{(i,j)}$$

For i=n_θ, j=n_y

$$APU2_{(i,j)}u2_{(i,j)} + ASU2_{(i,j)}u2_{(i,j-1)} + AWU2_{(i,j)}u2_{(i-1,j)} = FU2_{(i,j)}$$

Modified axial displacements (v1) at the shell boundaries are obtained for hinged supported shell as shown below:

For i=1, j=2

$$APV1_{(i,j)}v1_{(i,j)} + ANV1_{(i,j)}v1_{(i,j+1)} + \left(AEV1_{(i,j)} + AWV1_{(i,j)}\right)v1_{(i+1,j)} = FV1_{(i,j)}$$

For i=2.3.….n_θ-1, j=2

$$APV1_{(i,j)}v1_{(i,j)} + ANV1_{(i,j)}v1_{(i,j+1)} + AWV1_{(i,j)}v1_{(i-1,j)} + AEV1_{(i,j)}v1_{(i+1,j)} = FV1_{(i,j)}$$

For i=n_θ, j=2

$$APV1_{(i,j)}v1_{(i,j)} + ANV1_{(i,j)}v1_{(i,j+1)} + AWV1_{(i,j)}v1_{(i-1,j)} = FV1_{(i,j)}$$

For i=1, j=3.4.….n_y-1

$$APV1_{(i,j)}v1_{(i,j)} + ASV1_{(i,j)}v1_{(i,j-1)} + ANV1_{(i,j)}v1_{(i,j+1)} + \left(AEV1_{(i,j)} + AWV1_{(i,j)}\right)v1_{(i+1,j)} = FV1_{(i,j)}$$

For i=1, =n_y

$$APV1_{(i,j)}v1_{(i,j)} + ASV1_{(i,j)}v1_{(i,j-1)} + \left(AEV1_{(i,j)} + AWV1_{(i,j)}\right)v1_{(i+1,j)} = FV1_{(i,j)}$$

For i=2.3.….n_θ-1, =3.4.….n_y-1

$$APV1_{(i,j)}v1_{(i,j)} + ASV1_{(i,j)}v1_{(i,j-1)} + ANV1_{(i,j)}v1_{(i,j+1)} + AWV1_{(i,j)}v1_{(i-1,j)} + AEV1_{(i,j)}v1_{(i+1,j)} = FV1_{(i,j)}$$

For i=2.3….n_θ-1, j=n_y

$$APV1_{(i,j)}v1_{(i,j)} + ASV1_{(i,j)}v1_{(i,j-1)} + AWV1_{(i,j)}v1_{(i-1,j)} + AEV1_{(i,j)}v1_{(i+1,j)} = FV1_{(i,j)}$$

For i=n_θ, j=3.4…..n_y-1

$$APV1_{(i,j)}v1_{(i,j)} + ASV1_{(i,j)}v1_{(i,j-1)} + ANV1_{(i,j)}v1_{(i,j+1)} + AWV1_{(i,j)}v1_{(i-1,j)} = FV1_{(i,j)}$$

For i=n_θ, j=n_y

$$APV1_{(i,j)}v1_{(i,j)} + ASV1_{(i,j)}v1_{(i,j-1)} + AWV1_{(i,j)}v1_{(i-1,j)} = FV1_{(i,j)}$$

Modified axial displacements (v2) at the shell boundaries are obtained for hinged supported shell as shown below:

For i=1, j=2

$$APV2_{(i,j)}v2_{(i,j)} + ANV2_{(i,j)}v2_{(i,j+1)} + \left(AEV2_{(i,j)} + AWV2_{(i,j)}\right)v2_{(i+1,j)} = FV2_{(i,j)}$$

For i=2.3….n_θ-1, j=2

$$APV2_{(i,j)}v2_{(i,j)} + ANV2_{(i,j)}v2_{(i,j+1)} + AWV2_{(i,j)}v2_{(i-1,j)} + AEV2_{(i,j)}v2_{(i+1,j)} = FV2_{(i,j)}$$

For i=n_θ, j=2

$$APV2_{(i,j)}v2_{(i,j)} + ANV2_{(i,j)}v2_{(i,j+1)} + AWV2_{(i,j)}v2_{(i-1,j)} = FV2_{(i,j)}$$

For i=1, j=3.4…..n_y-1

$$APV2_{(i,j)}v2_{(i,j)} + ASV2_{(i,j)}v2_{(i,j-1)} + ANV2_{(i,j)}v2_{(i,j+1)} + \left(AEV2_{(i,j)} + AWV2_{(i,j)}\right)v2_{(i+1,j)} = FV2_{(i,j)}$$

For i=1, =n_y

$$APV2_{(i,j)}v2_{(i,j)} + ASV2_{(i,j)}v2_{(i,j-1)} + \left(AEV2_{(i,j)} + AWV2_{(i,j)}\right)v2_{(i+1,j)} = FV2_{(i,j)}$$

For i=2.3….n_θ-1, =3.4…..n_y-1

$$APV2_{(i,j)}v2_{(i,j)} + ASV2_{(i,j)}v2_{(i,j-1)} + ANV2_{(i,j)}v2_{(i,j+1)} + AWV2_{(i,j)}v2_{(i-1,j)} + AEV2_{(i,j)}v2_{(i+1,j)} = FV2_{(i,j)}$$

For i=2.3….n_θ-1, j=n_y

$$APV2_{(i,j)}v2_{(i,j)} + ASV2_{(i,j)}v2_{(i,j-1)} + AWV2_{(i,j)}v2_{(i-1,j)} + AEV2_{(i,j)}v2_{(i+1,j)} = FV2_{(i,j)}$$

For i=n_θ, j=3.4…..n_y-1

$$APV2_{(i,j)}v2_{(i,j)} + ASV2_{(i,j)}v2_{(i,j-1)} + ANV2_{(i,j)}v2_{(i,j+1)} + AWV2_{(i,j)}v2_{(i-1,j)} = FV2_{(i,j)}$$

For i=n_θ, j=n_y

$$APV2_{(i,j)}v2_{(i,j)} + ASV2_{(i,j)}v2_{(i,j-1)} + AWV2_{(i,j)}v2_{(i-1,j)} = FV2_{(i,j)}$$

In order to verify the mathematical model for hinged supported cylindrical shell, results are compared with the results of finite element model. The three dimensional model is generated and solved with finite element package program ABAQUS. The dimensions and mechanical properties of the model is the same with that of the fixed supported cylindrical shell. Comparison of displacements and central stress obtained from current model and finite element model are presented in Figures 3.157 and 3.158. The difference between the deflections is 6.29 % and 6.88 % for central stress at most. Therefore, the model developed to analyze the nonlinear behavior of the laminated glass hinged cylindrical shell gives reliable results. The view of radial deflection contours obtained from ABAQUS is presented in Figure 3.159. Radial deflection takes its maximum value at the center of the unit.

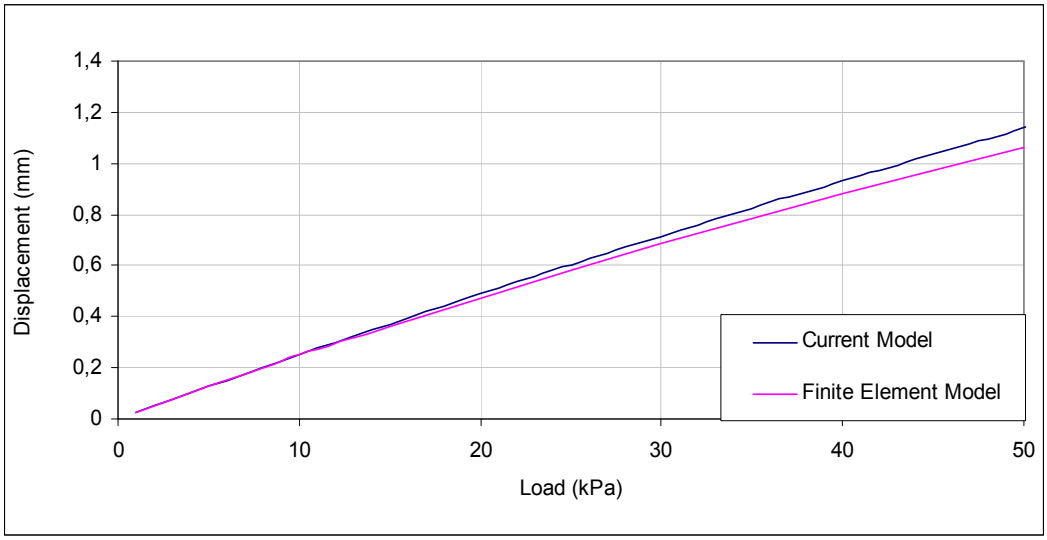

Figure 3.157 Central deflection values for hinged cylindrical shell

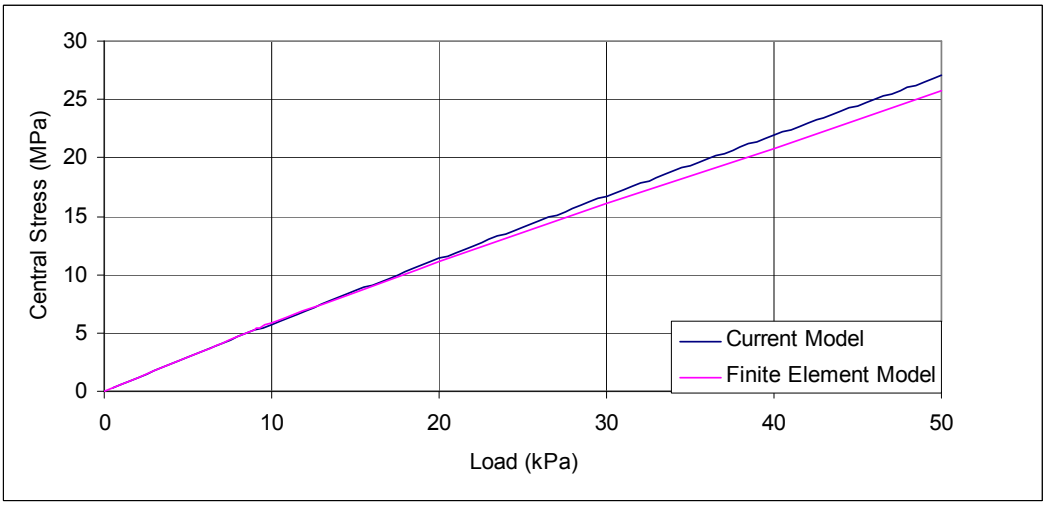

Figure 3.158 Central stress values for hinged cylindrical shell

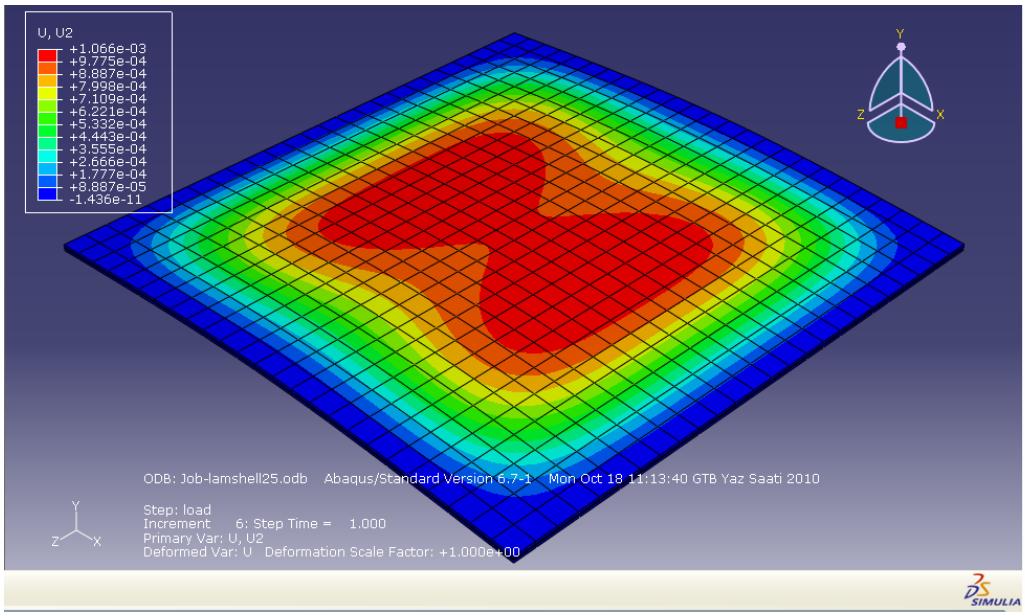

Figure 3.159 A view of radial deflection contour for hinged supported shell

Figures 3.160 and 3.161 show the comparison of linear and nonlinear approaches to predict the behavior of the cylindrical shell. Linear and nonlinear solution results are plotted as normalized deflection versus load in Figure 3.160. The level of nonlinearity may be defined as $\frac{w_{\max}}{h}$ ratio, where $w_{\max}$ is the deflection at the center of the shell, and h is the thickness of the single glass sheets. Separation between linear and nonlinear solutions starts when $\frac{w_{\max}}{h} > 0.15$. It can be said that nonlinear solution should be considered when the ratio of maximum deflection to thickness of a single glass beam is greater than 0.15. It is observed that this ratio (the level of nonlinearity) is about 0.8 for a load P=50 kPa in Figure 3.160. The central deflection obtained from linear approach is almost 1.25 times of the deflection obtained by nonlinear approach at load P=50 kPa. Figure 3.161 is plotted to observe stress versus load for linear and nonlinear behavior.

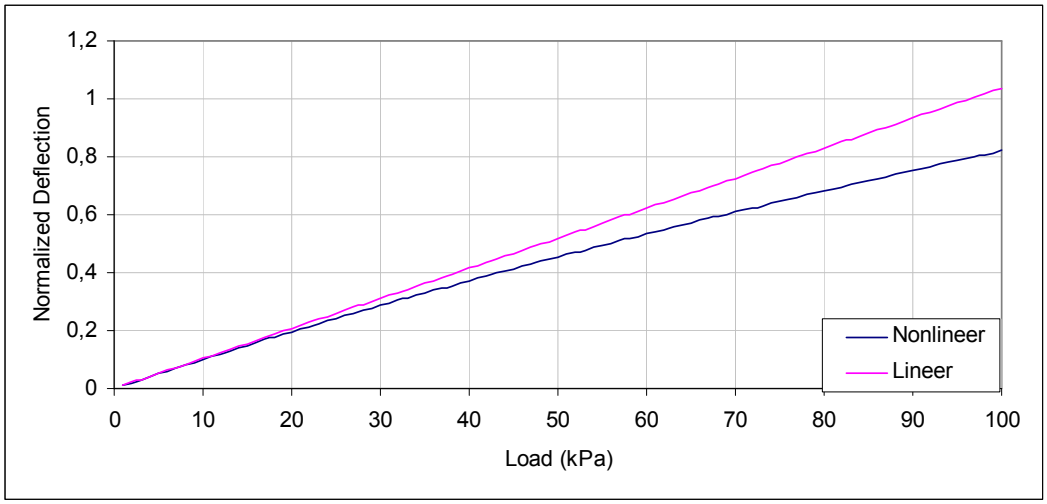

Figure 3.160 Normalized maximum deflection versus load for hinged supported shell

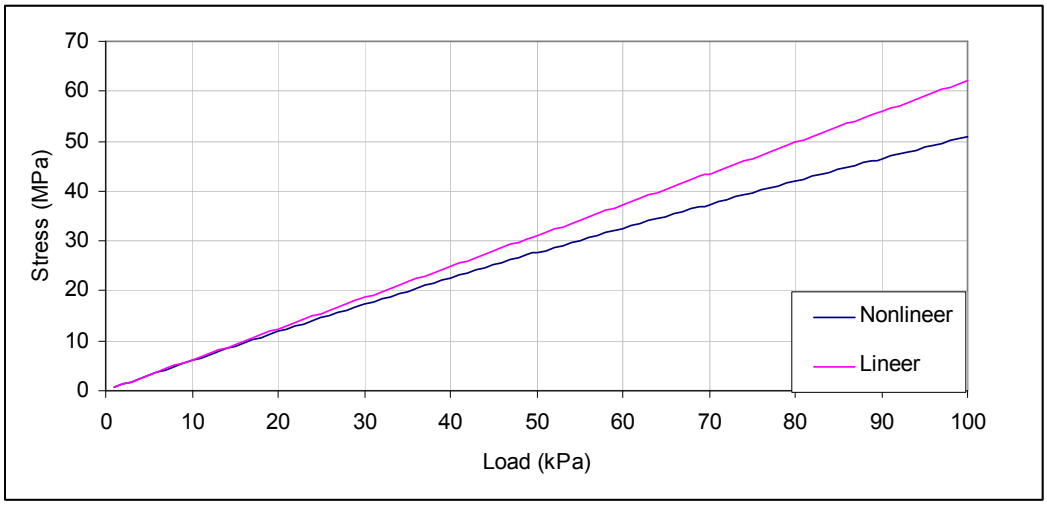

Figure 3.161 Stress versus load for hinged supported shell

Comparison of the behavior of monolithic, layered and laminated glass shells are given in Figures 3.162 and 3.163. For fixed supported shell unit the behavior of laminated glass unit is bounded by the behaviors of layered and monolithic glass units. While layered glass unit is found to be upper bound of laminated glass behavior, monolithic glass is found to be lower bound of laminated glass shell behavior. The behavior is different for hinged supported shell unit. For hinged supported shell unit the behavior of layered glass unit takes place between the behaviors of laminated and monolithic glass units. In contrary to the fixed supported

shell deflection and stress values of hinged supported monolithic glass unit is found to be higher than that of layered and laminated glass units. The same results are obtained by using finite element results.

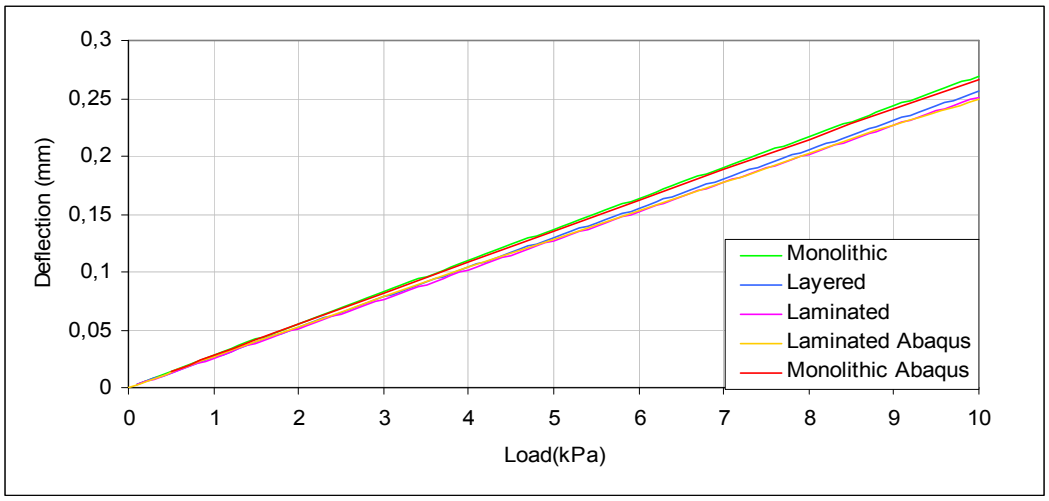

Figure 3.162 Comparison of maximum displacements of monolithic, laminated and layered glass units

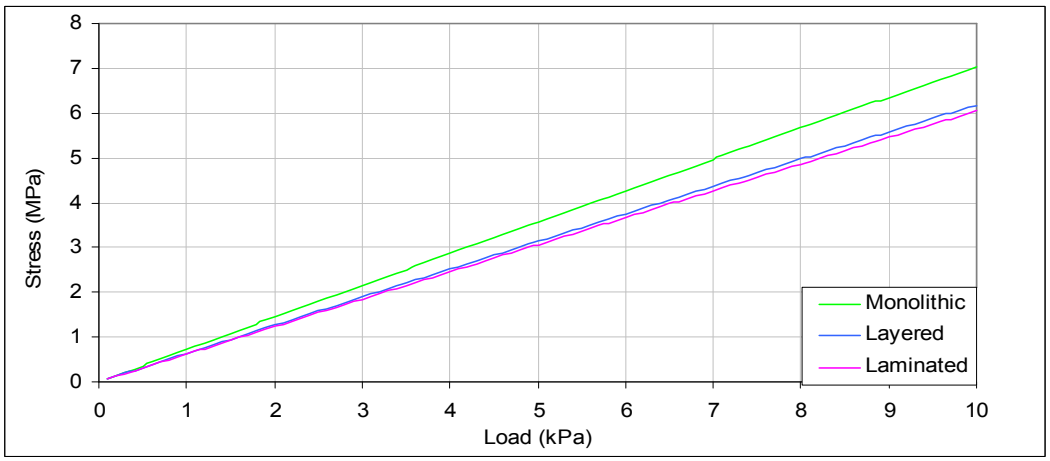

Figure 3.163 Comparison of maximum stress of monolithic, laminated and layered glass units

Figures 3.164 and 3.165 represent the circumferential deflection (u1 and u2) along the center line at y=0. Circumferential deflections are zero at the boundary and at $\theta=0$ and $\theta=\theta_1$ as we expected. Circumferential deflections in θ direction take their maximum values close to the midpoint of the quarter shell. There is a slight

difference between the circumferential deflections of the top and bottom glass sheets. Circumferential deflection of the top glass is larger than the bottom one. When the load is increased, deflection curves get closer to each other and the curvature of deflection lines increase. The ratio of maximum deflection value at 10 kPa to that at 5 kPa is nearly 2, while it is nearly 1 for 50 kPa and 45 kPa. The reason of this behavior is the nonlinearity of the shell unit. Radial deflections at the center of the shell unit along the θ direction for different load levels are illustrated in Figure 3.166. Radial displacements take their maximum value along the center line at θ=0 while they are zero at $\theta=\theta_1$. Because of the nonlinearity, radial deflections are getting closer to each other when the load is increased. Radial deflections of hinged supported shell are smaller than radial deflections of fixed supported shell.

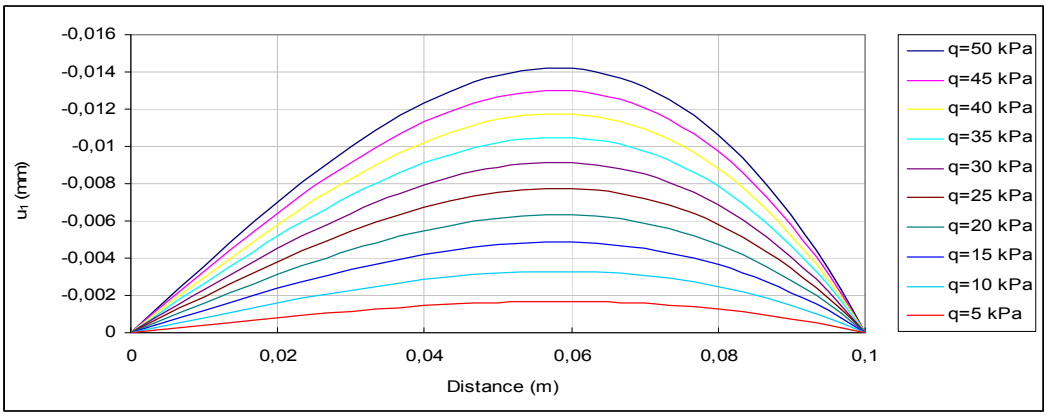

Figure 3.164 Circumferential displacement of the top glass unit along the center line at y=0

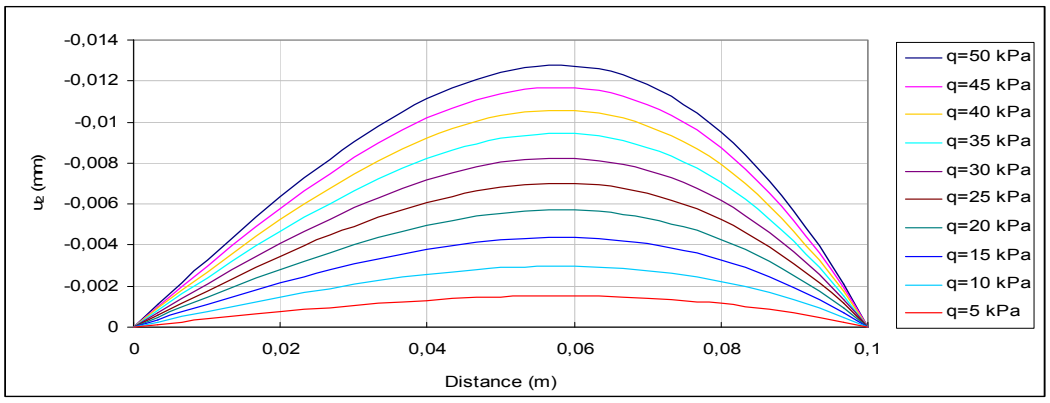

Figure 3.165 Circumferential displacement of the bottom glass unit along the center line at y=0

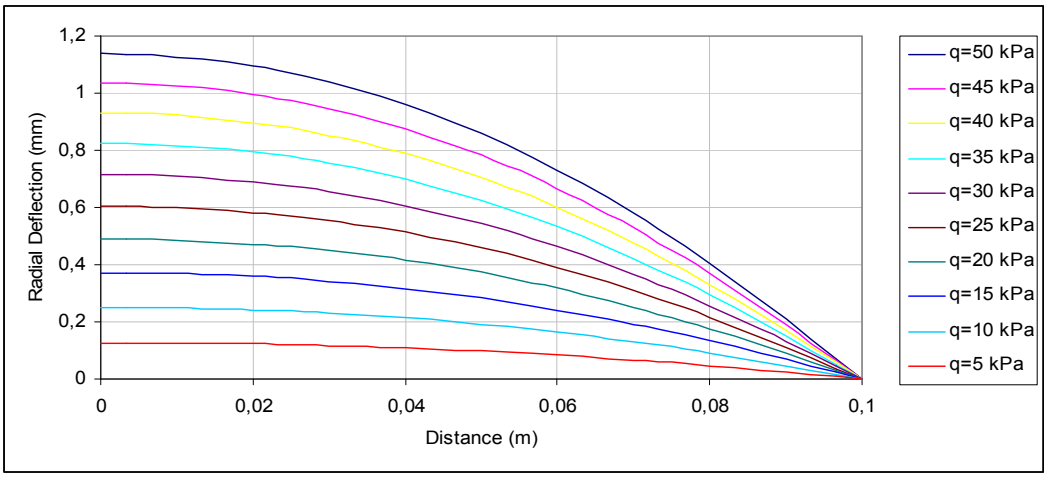

Figure 3.166 Radial deflection along the center line at y=0

Figures 3.167 and 3.168 are plotted to represent the axial deflections (v1 and v2) along the center line at θ=0 for top and bottom glass units, respectively. Axial deflections in y direction are zero at the boundary and at the center of the unit. While axial deflections at the top surface take both positive and negative values for loads under 25 kPa, they take only positive values for loads higher than 20 kPa. Axial deflections at the bottom surface take positive values. Axial deflections of the bottom glass are higher than axial deflections of top glass. Axial deflections, v1 and v2, for hinged supported shell take their maximum value at a point close to edge. Axial deflections of fixed supported shell unit are smaller than that of hinged supported shell. Unlike axial deflections of hinged supported shell, axial deflections of fixed supported shell change their sign at a point inside the domain for every load value and at top and bottom surface of the unit.

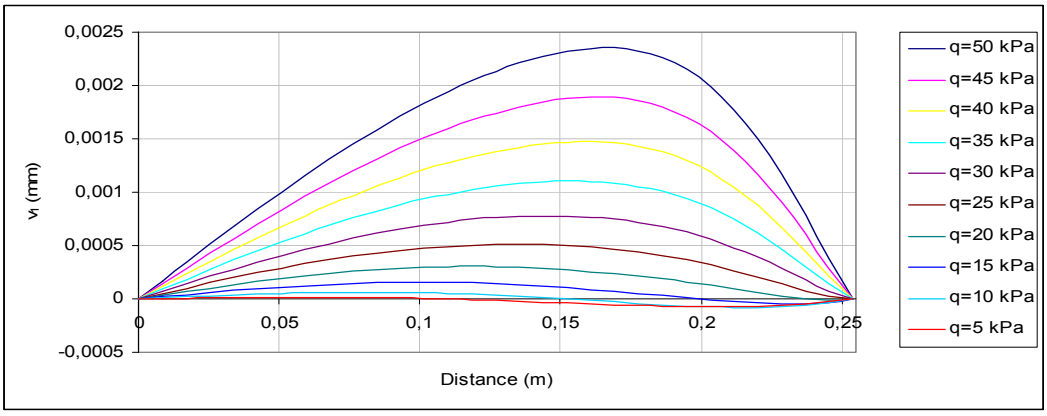

Figure 3.167 Axial displacement of the top glass unit along the center line at θ=0

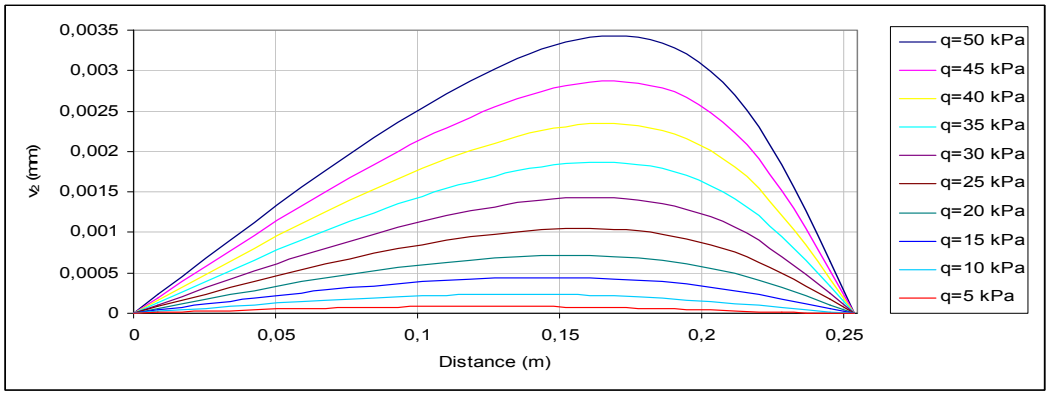

Figure 3.168 Axial displacement of the top glass unit at the center along the center line at θ=0

Figures 3.169-3.173 illustrate the radial, circumferential and axial displacements along the diagonal of the laminated glass shell unit. Radial displacements take their maximum value at the center of the unit and they are zero at $\theta=\theta_1$. Axial displacements are zero along the center line at θ=0 and $\theta=\theta_1$. The circumferential displacement (u1) of the top glass ply is larger than the circumferential displacement (u2) of the bottom glass ply as seen in Figures 3.168 and 3.169. In addition to the θ=0 and $\theta=\theta_1$ axial deflections (v1 and v2) are zero at a point in the domain as it is observable from Figures 3.172 and 3.173. The point shifts toward the corner of the unit while the load is increasing. Axial deflections (v1 and v2) are positive near the center they are negative near the edge for bottom and top glass sheets. The effect of geometric nonlinearity is observed since displacement curves for increasing load values are getting closer to each other.

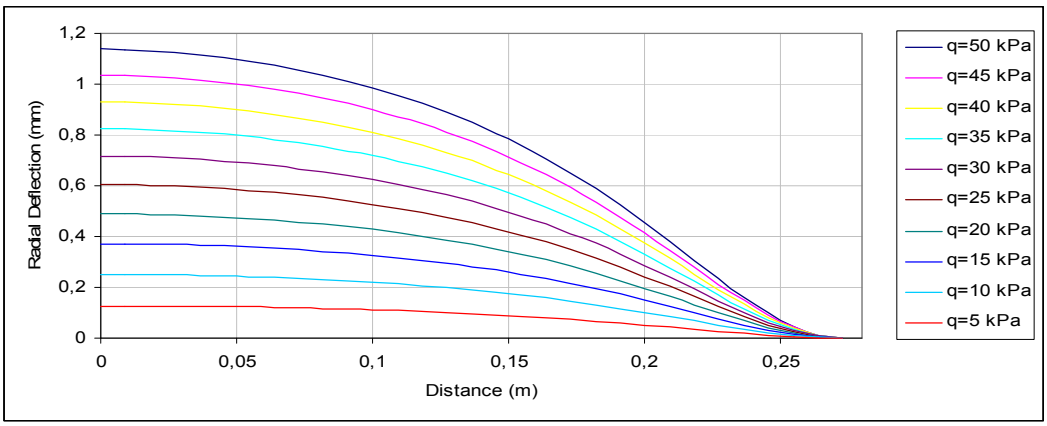

Figure 3.169 Radial displacement along the diagonal

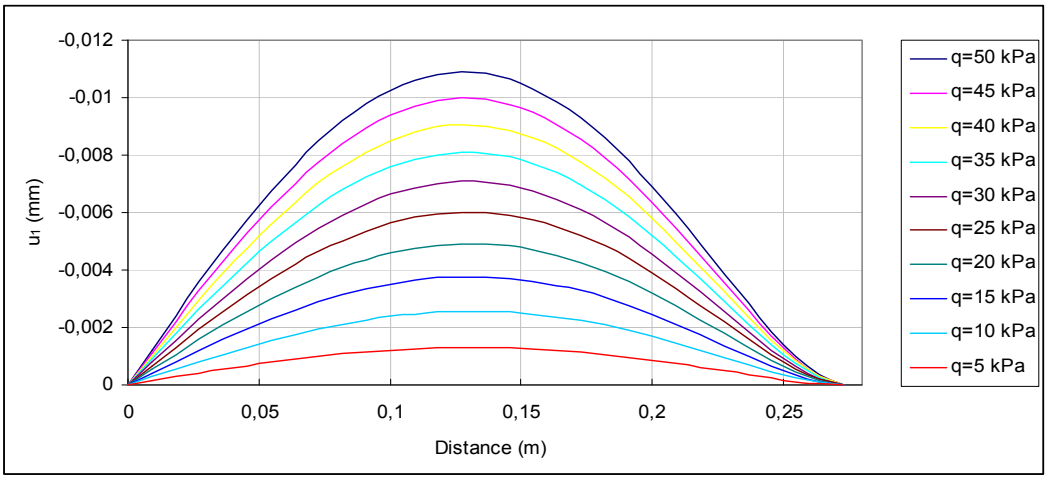

Figure 3.170 Circumferential displacement of the top glass shell along the diagonal

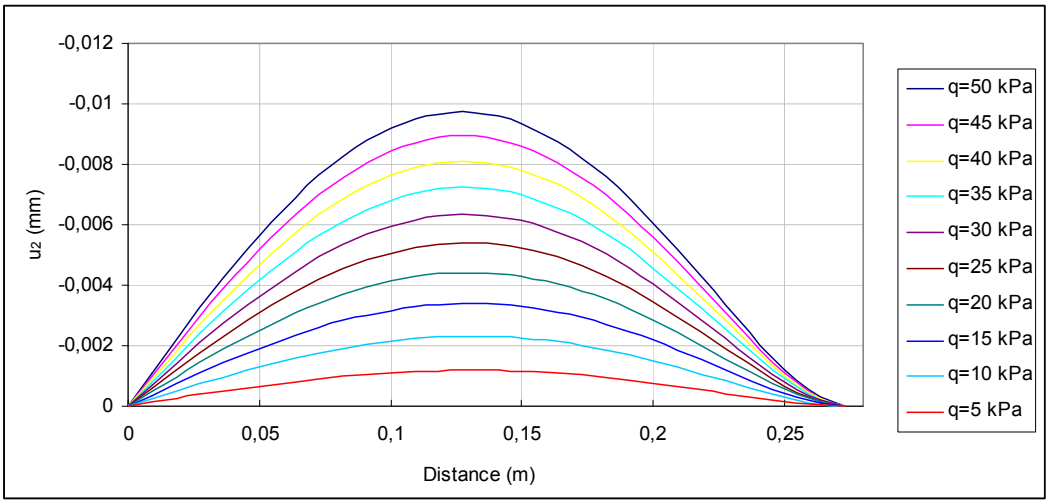

Figure 3.171 Circumferential displacement of the bottom glass shell along the diagonal

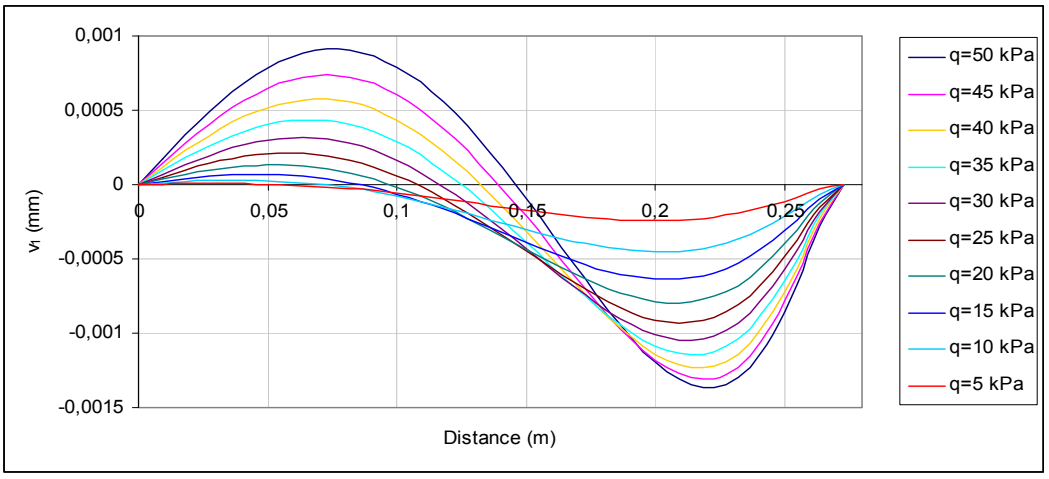

Figure 3.172 Axial displacement of the top glass shell along the diagonal

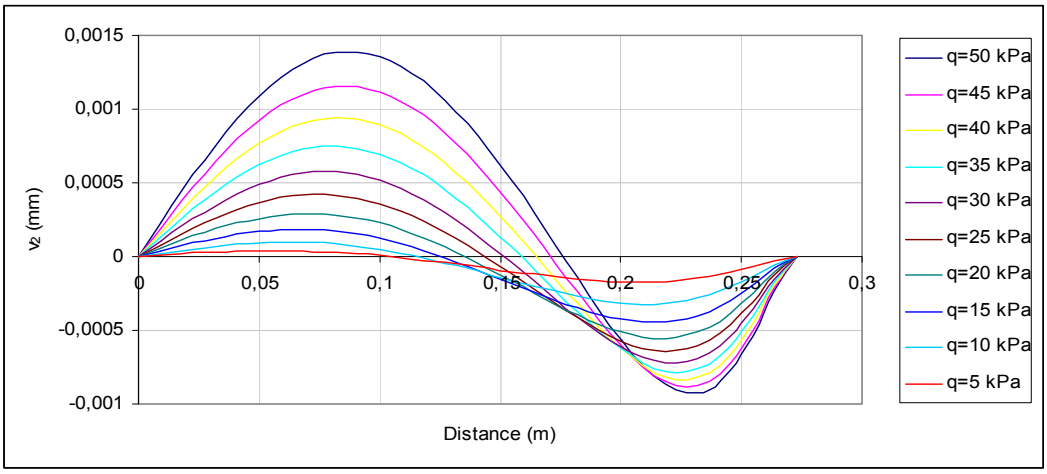

Figure 3.173 Axial displacement of the bottom glass shell along the diagonal

Maximum and minimum principal stress values are obtained by summing or subtracting the bending and membrane stresses. Figures 3.174 and 3.175 represent maximum and minimum principal stresses along the center line at y=0 on the top surface of the top glass unit for different load values, respectively. Maximum and minimum principal stresses from Figures 3.174 and 3.175 are observed as tension at the top surface of the top glass. Maximum principal stresses at the top surface take their maximum values close to the boundary of the unit but minimum principal stresses at top surface take their maximum values at the center of the unit. The value of maximum principal stress at top surface is 23 MPa for the applied 50 kPa load while it is 28 MPa for the bottom surface. Maximum and minimum principal stresses of bottom surface of bottom glass along the center line at y=0 are presented in Figures 3.176 and 3.177, respectively. Maximum and minimum principal stresses on the bottom surface of the bottom glass are tension along the line. Unlike maximum stresses on the top surface, maximum stresses on the bottom surface take their maximum value at the center of the shell. While maximum principal stresses of fixed supported shell are greater than that of hinged supported shell on the top surface, maximum principal stresses of fixed and hinged supported shell units are almost equal at bottom surface of the unit. Unlike principal stresses of hinged supported shell, principal stresses of fixed supported shell could be tension or compression at bottom surface of the unit.

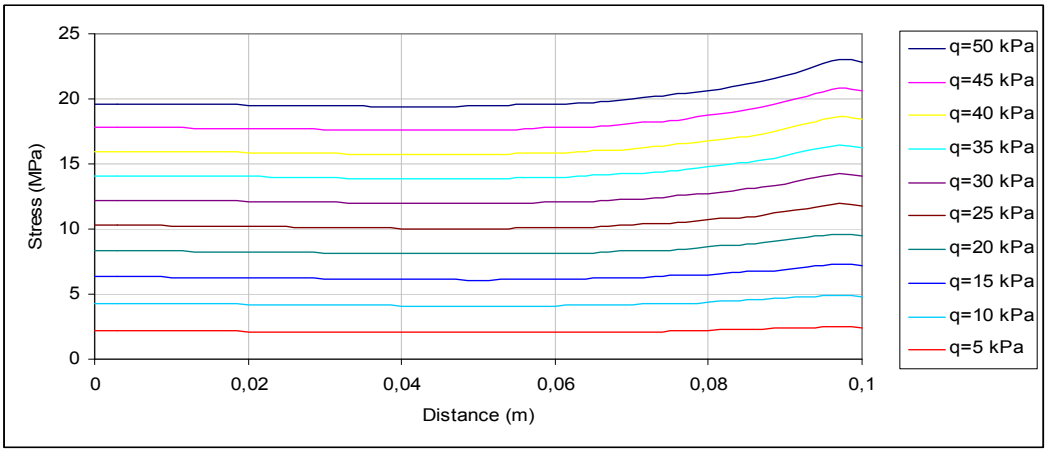

Figure 3.174 Maximum stresses at the top surface of the top glass along the θ direction of hinged supported shell

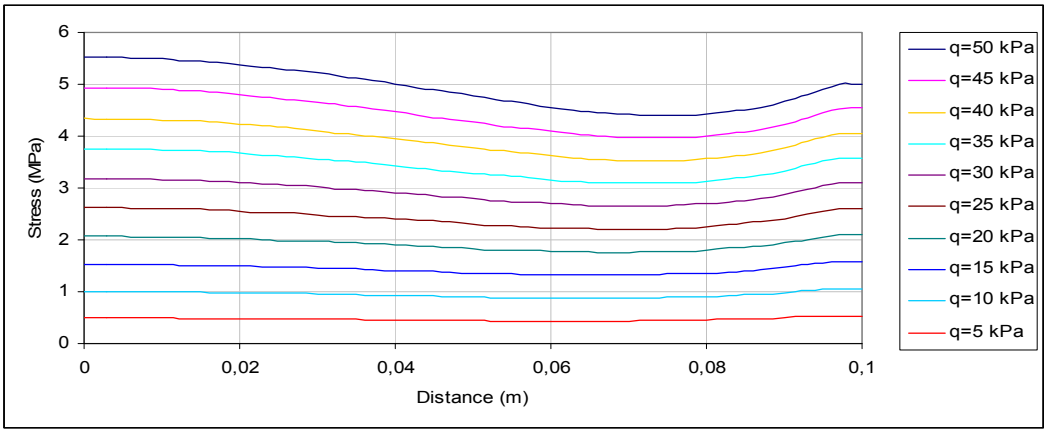

Figure 3.175 Minimum stresses at the top surface of the top glass along the θ direction of hinged supported shell

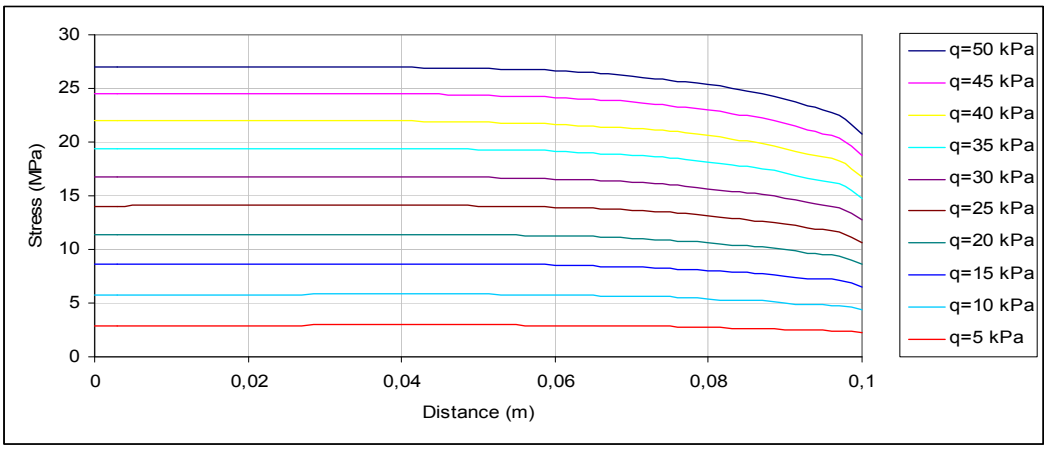

Figure 3.176 Maximum stresses at the bottom surface of the bottom glass along the θ direction of hinged supported shell

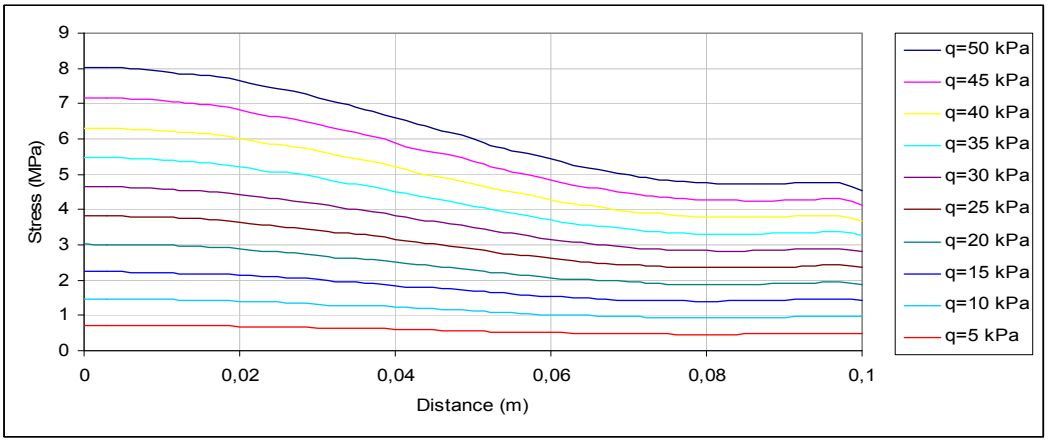

Figure 3.177 Minimum stresses at the bottom surface of the bottom glass along the θ direction of hinged supported shell

Figures 3.178-3.181 are plotted to observe the maximum and minimum principal stresses at the bottom surface of top glass shell andat the top surface of the bottom glass shell along the center line at y=0 for hinged supported laminated cylindrical shell. It is observed from Figures 3.178 and 3.180 that maximum principal stresses on the top surface of the bottom glass shell and bottom surface of the top glass shell are tension. While they take their maximum value at θ=0 for the bottom surface of the top glass shell, they take their maximum value at a point close to the edge at top surface of the bottom glass shell. The maximum principal stress at the bottom surface of the top glass shell is slightly higher than that top surface of the bottom glass shell. Minimum principal stresses at the top surface of the bottom glass shell and at the top surface of the bottom glass shell are illustrated in Figures 3.179 and 3.181, respectively. They take their maximum value along the center line at θ=0 of the unit. Minimum principal stresses at the bottom surface of the top glass shell are slightly higher than that of the top surface of the bottom glass shell.

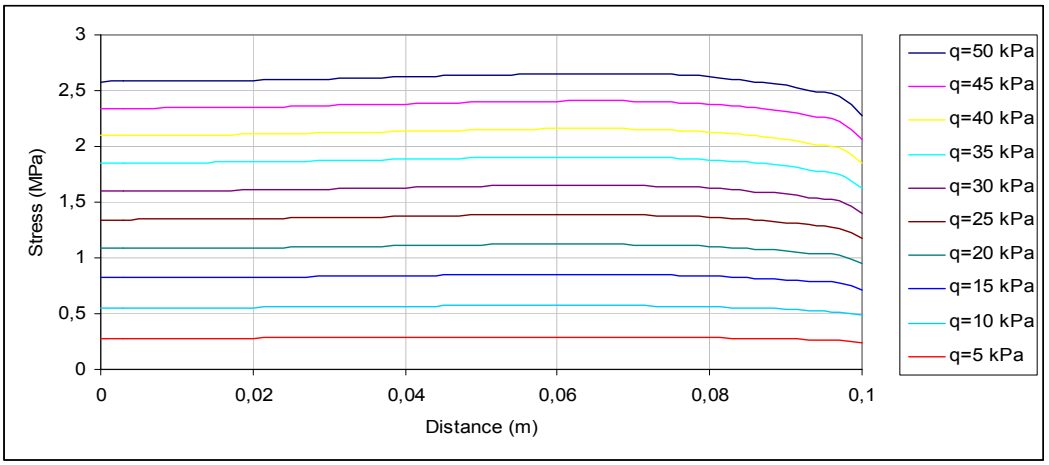

Figure 3.178 Maximum stresses at the bottom surface of the top glass shell along the centerline at y=0

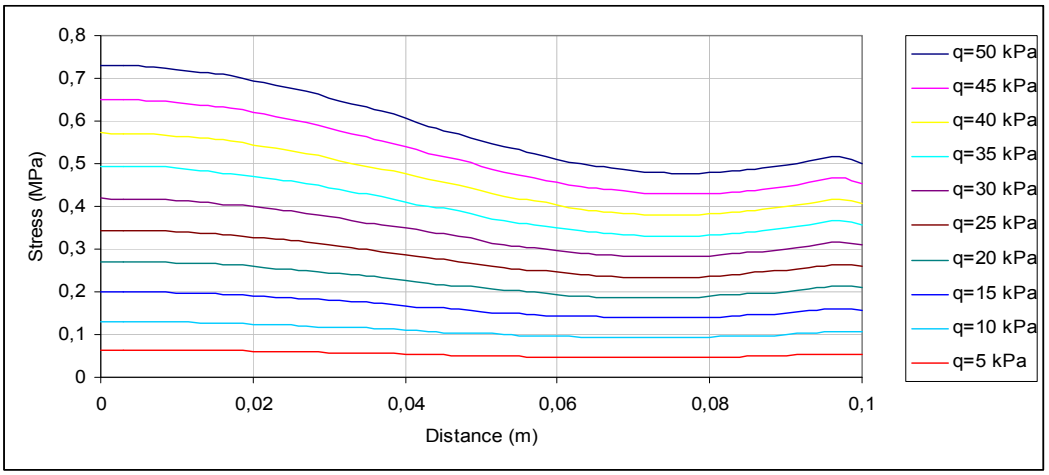

Figure 3.179 Minimum stresses at the bottom surface of the top glass shell along the centerline at y=0

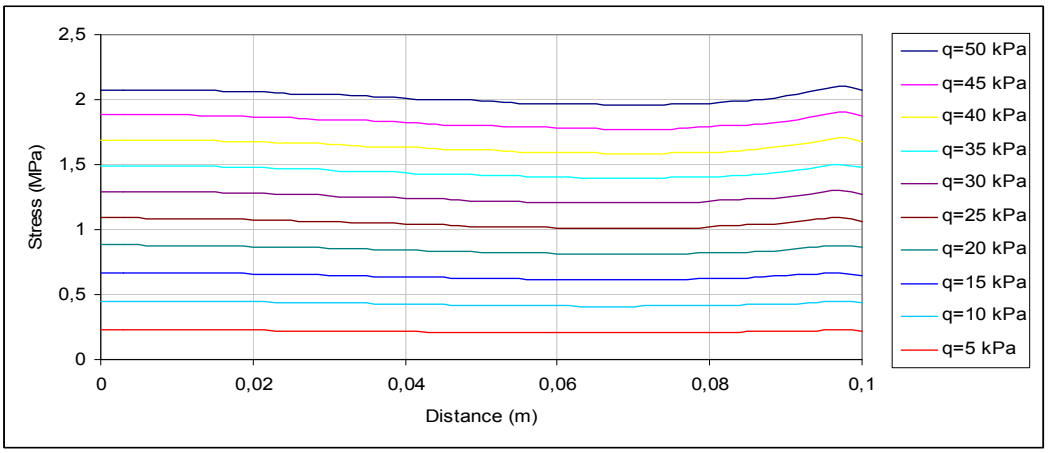

Figure 3.180 Maximum stresses at the top surface of the bottom glass shell along the centerline at y=0

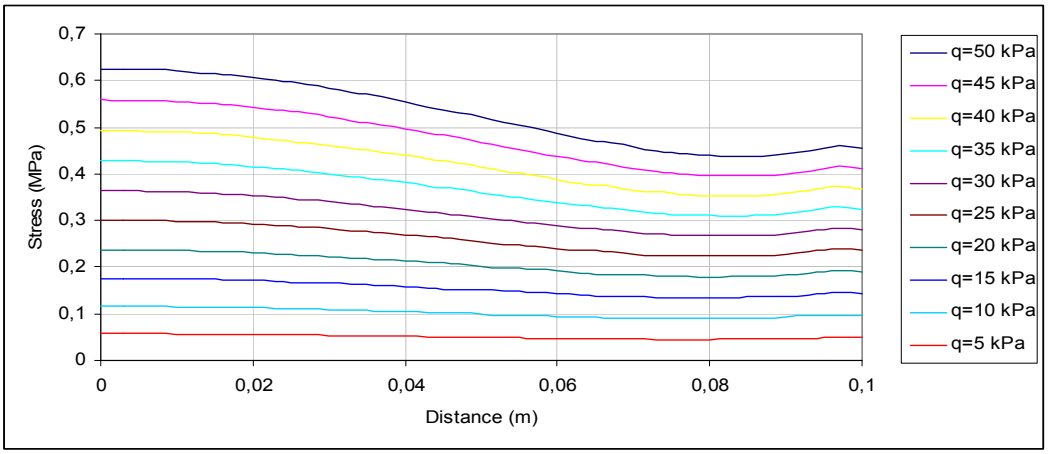

Figure 3.181 Minimum stresses at the top surface of the bottom glass shell along the centerline at y=0

Figures 3.182-3.185 are plotted to represent the maximum and minimum principal stresses at the top surface of top glass unit and bottom surface of the bottom glass unit along the center line at θ=0 . Maximum stress at the top and bottom surfaces of the shell is tension; they take their maximum value close to the midpoint of the line. Maximum stress lines at top surface of top ply are nearly straight till the half of the line. They take their minimum value 8 mm away from the boundary. Figure 3.181 illustrates how minimum principal stress changes along the center line at θ=0 on the top surface of the top glass shell. At the origin, they are tension and they change their sign at a point close to the middle of the line. Close to boundary of the unit they change their sign again and they become tension. Minimum principal stresses at the top surface take their maximum value as compression. Figures 3.186-3.189 show how maximum and minimum principal stresses change along the diagonal of the shell unit at top and bottom surfaces. Maximum principal stresses from Figures 3.186 and 3.188 are observed as tension at the top and bottom shell, but minimum principal stresses at the top and bottom shell from Figures 3.187 and 3.189 are observed as they change their sign. While minimum principal stresses at the top surface change their sign close to middle of diagonal length, minimum principal stresses at the bottom surface change their sign at a point close to the corner.

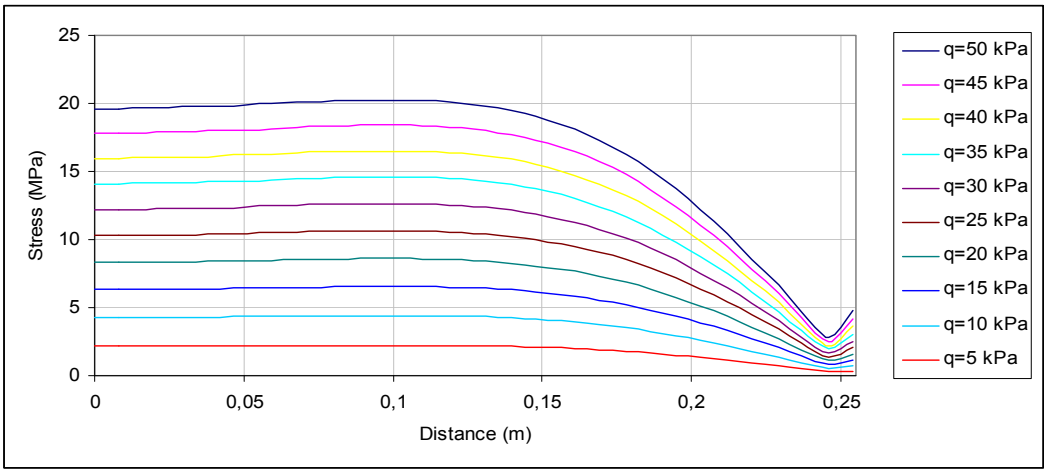

Figure 3.182 Maximum stresses at the top surface of the top glass along the center line at θ=0

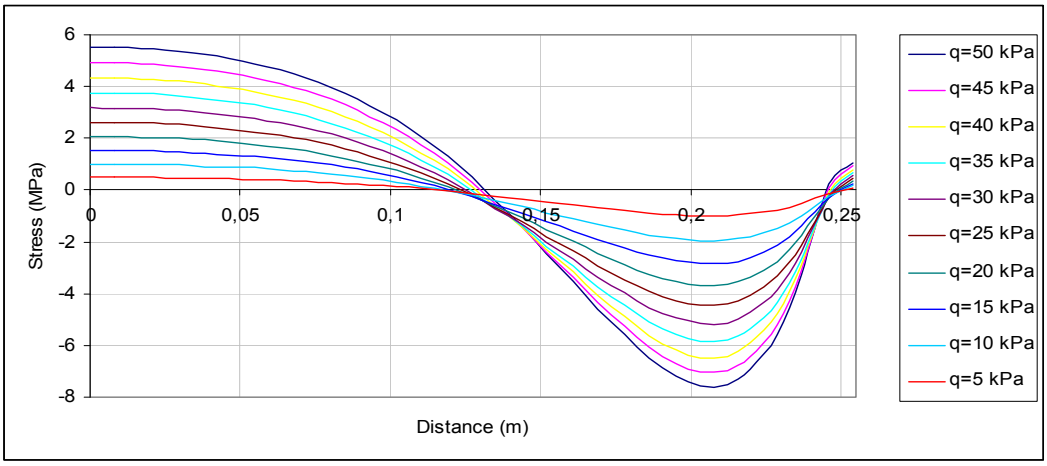

Figure 3.183 Minimum stresses at the top surface of the top glass along the center line at θ=0

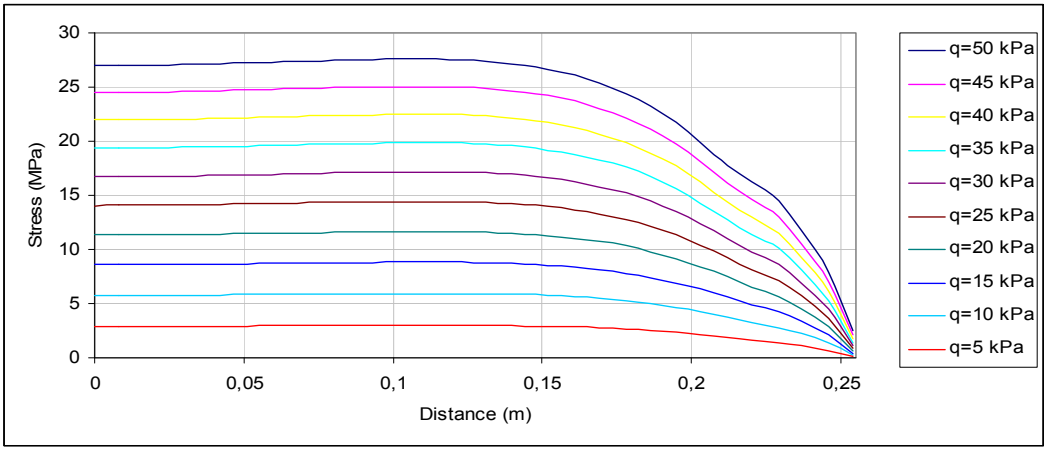

Figure 3.184 Maximum stresses at the bottom surface of the bottom glass along the center line at θ=0

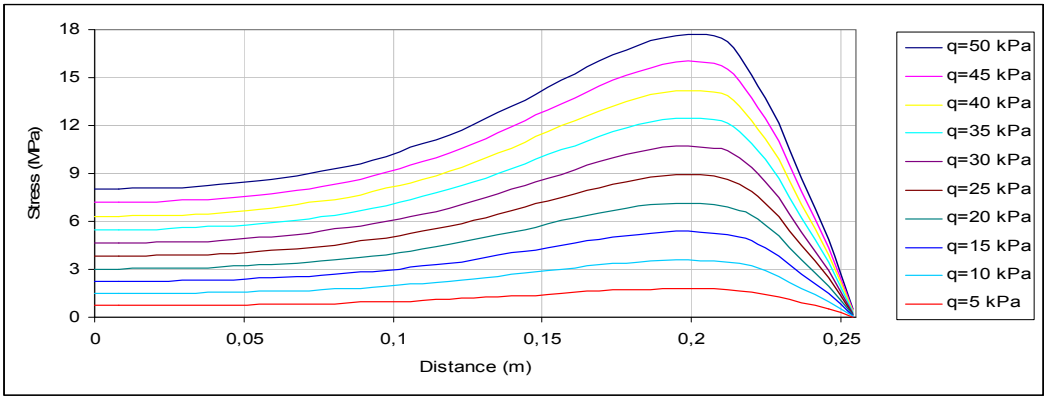

Figure 3.185 Minimum stresses at the bottom surface of the bottom glass along the center line at θ=0

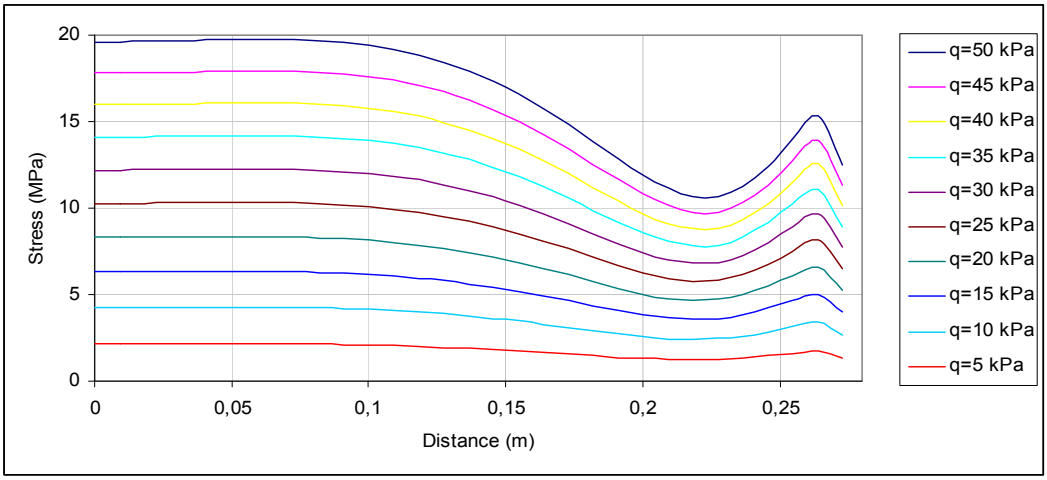

Figure 3.186 Maximum stresses at the top surface of the top glass shell along the diagonal

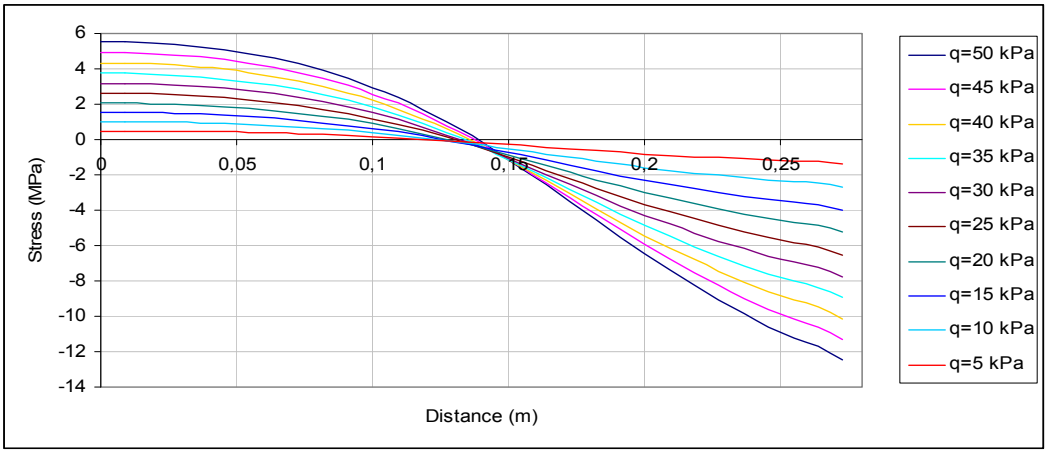

Figure 3.187 Minimum stresses at the top surface of the top glass shell along the diagonal

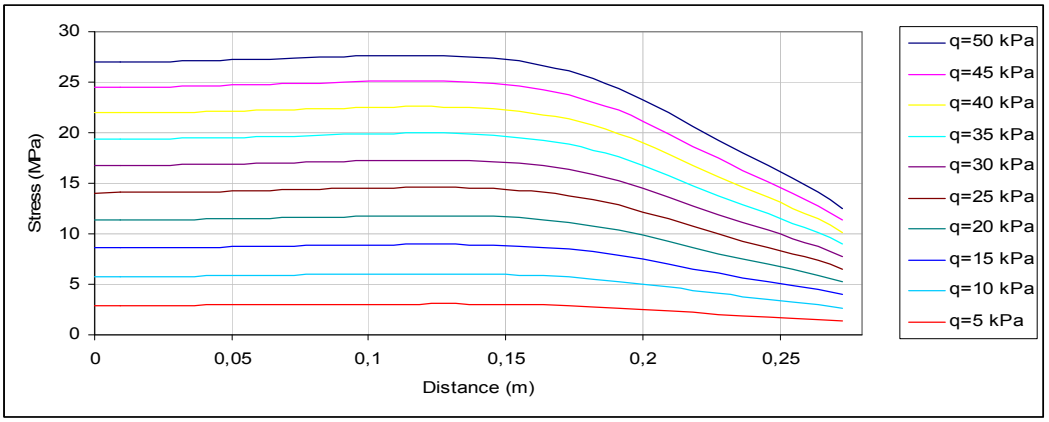

Figure 3.188 Maximum stresses at the bottom surface of the bottom glass shell along the diagonal

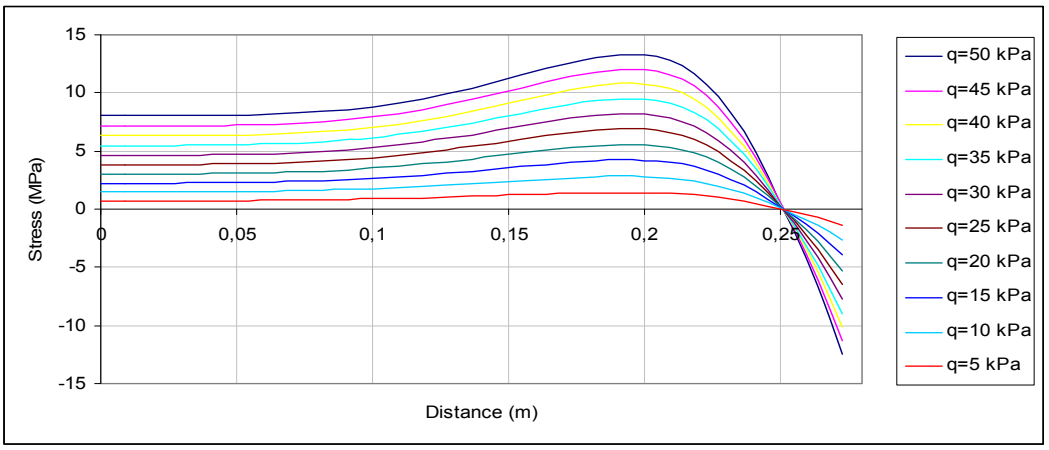

Figure 3.189 Minimum stresses at the bottom surface of bottom glass shell along the diagonal

Axial force on the two plies can be represented by the term Gbγ. Shear stress is contributed by the interlayer. Axial force is transmitted to top and bottom plies in opposite direction when shear strain is applied to the interlayer. Function of shear stress of PVB interlayer of the center of shell unit along the θ and y axis is plotted in Figures 3.190 and 3.191. For hinged supported shell, it is observed that shear stress is maximum at the supports and zero at the middle as is observable from these graphs. It is observed that shear stress at the upper support of shell unit is higher than the shear stress at the right support. Shear stress along the center line at θ=0 is zero because of the geometry of unit.

Coupled and bending stresses in θ and y direction for applied 10 kPa load are plotted in Figures 3.192 and 3.193 along the center line at y=0 and in Figures 3.194 and 3.195 along the center line at θ=0.

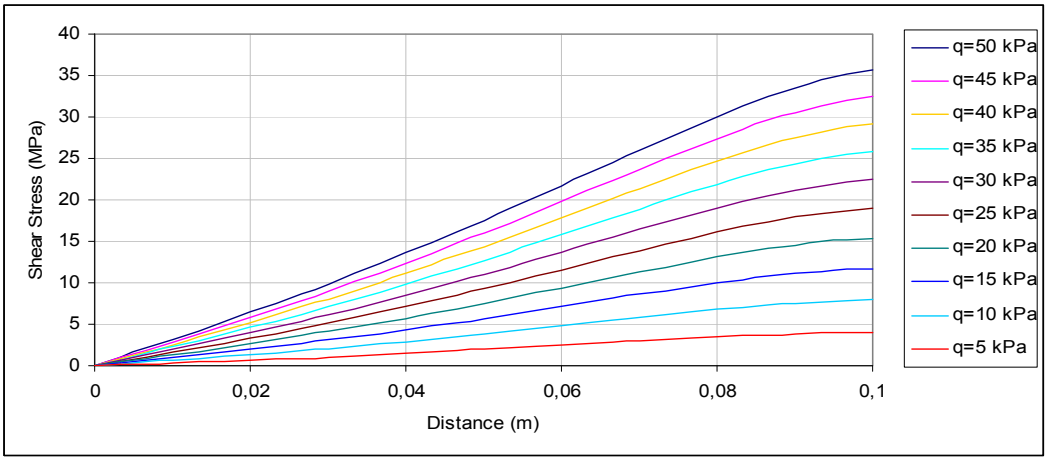

Figure 3.190 Shear stresses of the interlayer along the center line at y=0

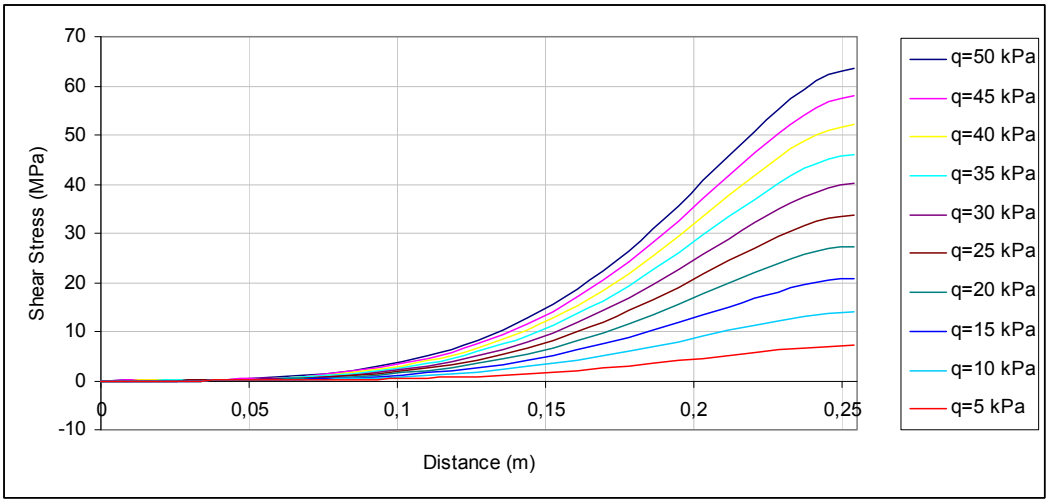

Figure 3.191 Shear stresses of the interlayer along along the center line at θ=0

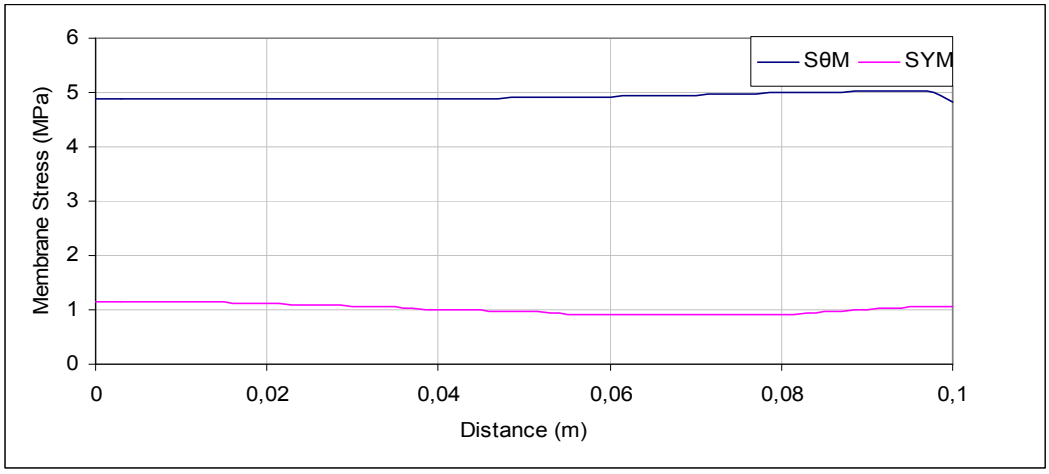

Figure 3.192 Membrane stresses along the center line at y=0 for 10 kPa

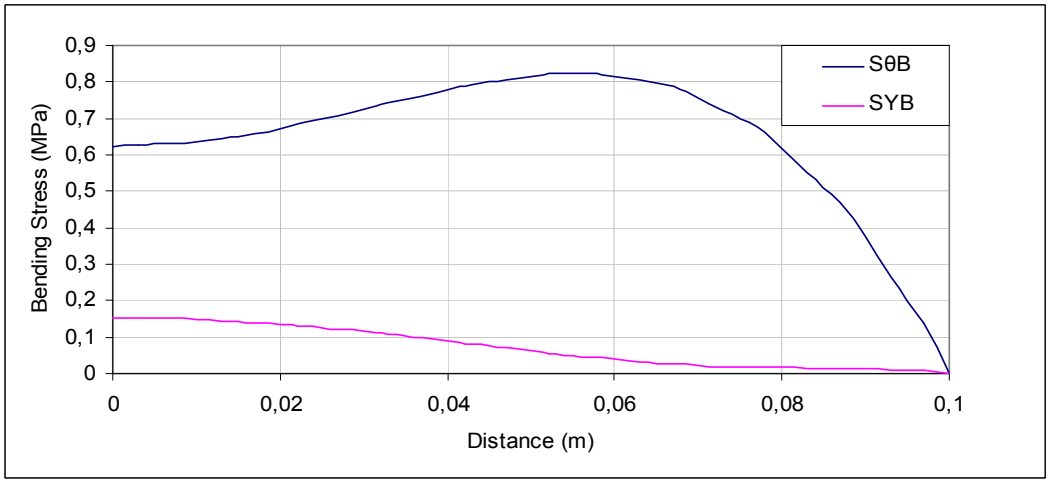

Figure 3.193 Bending stresses along the center line at y=0 for 10 kPa

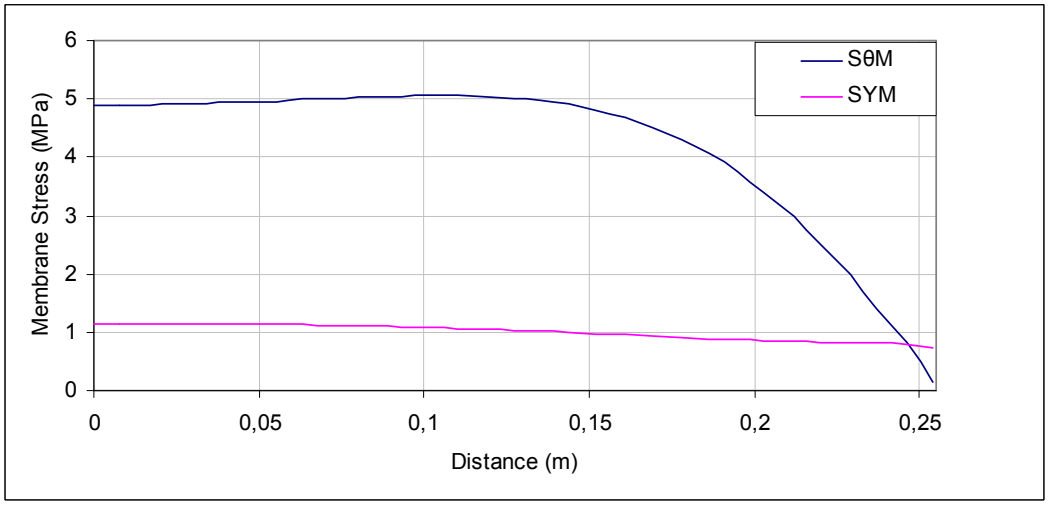

Figure 3.194 Membrane stresses along the center line at θ=0 for 10 kPa

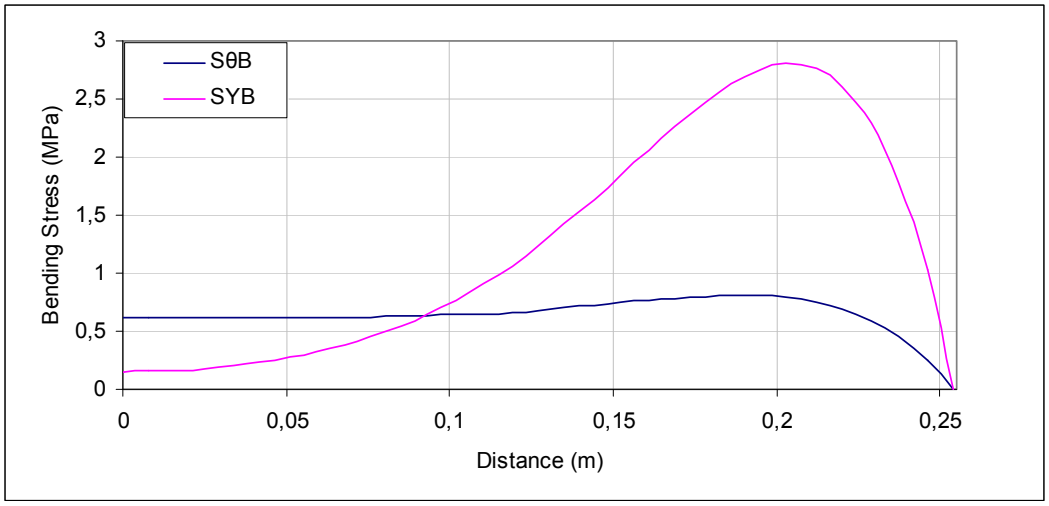

Figure 3.195 Bending stresses along the center line at θ=0 for 10 kPa

Strength factor value, which is calculated by dividing maximum principal stress of monolithic glass unit to maximum principal stress of laminated glass unit for hinged supported shell unit, varies between 0.859-0.863 as shown in Figure 3.196. Strength factor value gets smaller while the load is decreasing. It is observed that strength factor value of fixed supported shell is smaller than strength factor value of hinged supported shell. While strength factor value of fixed supported shell is between 1.03-1.07, it is between 1.15-1.16 for hinged supported shell unit.

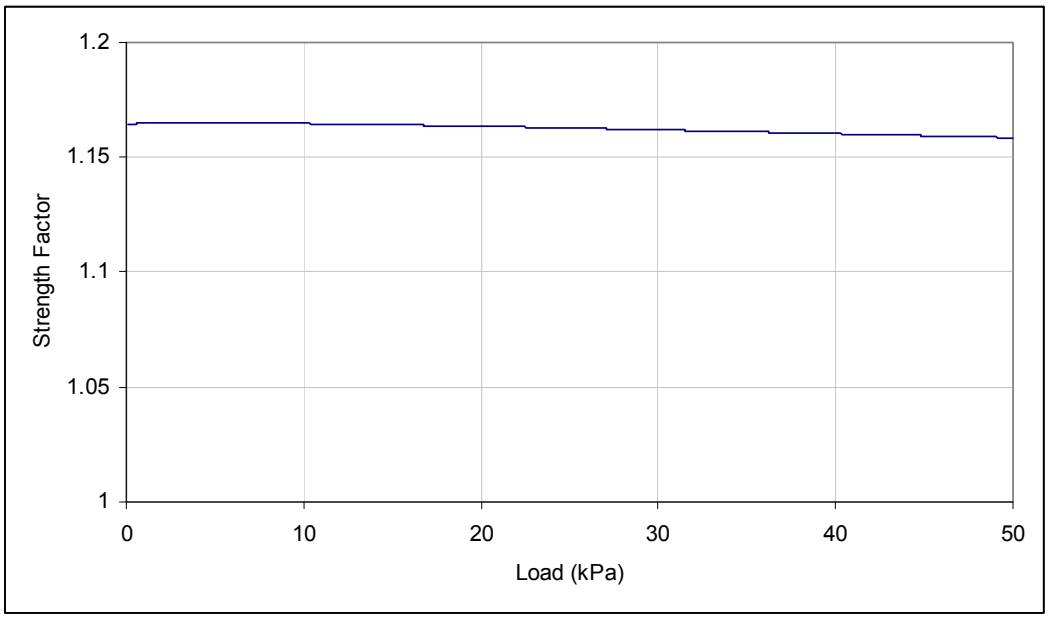

Figure 3.196 Strength factor versus load for hinged supported shell

Figures 3.197-3.201 are plotted in order to have detailed information about the contour of radial displacement for the quarter of the shell. Radial displacements are given for applied pressure q= 10, 20, 30, 40, 50 kPa. The radial deflections take their maximum value at the center of the unit.

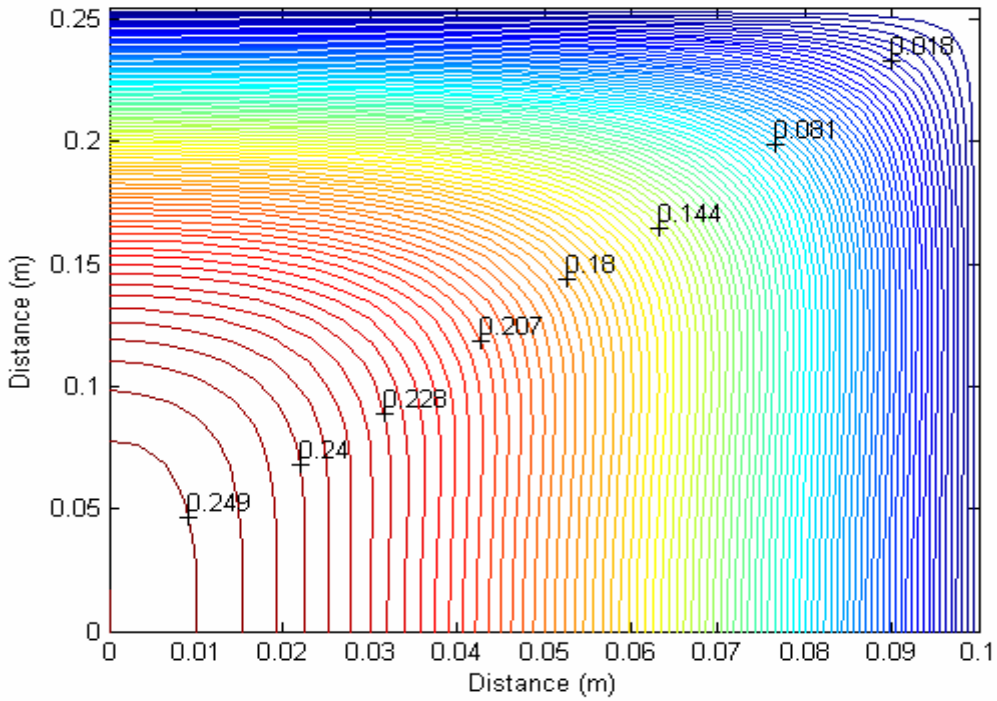

Figure 3.197 Contours of radial displacement (mm) for q=10 kPa

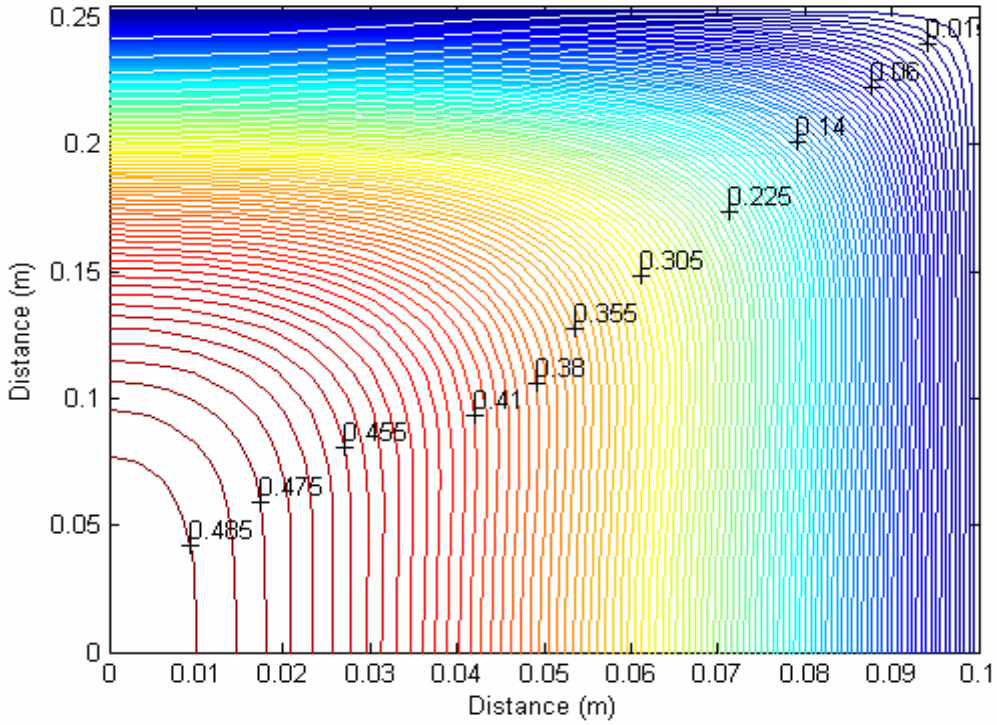

Figure 3.198 Contours of radial displacement (mm) for q=20 kPa

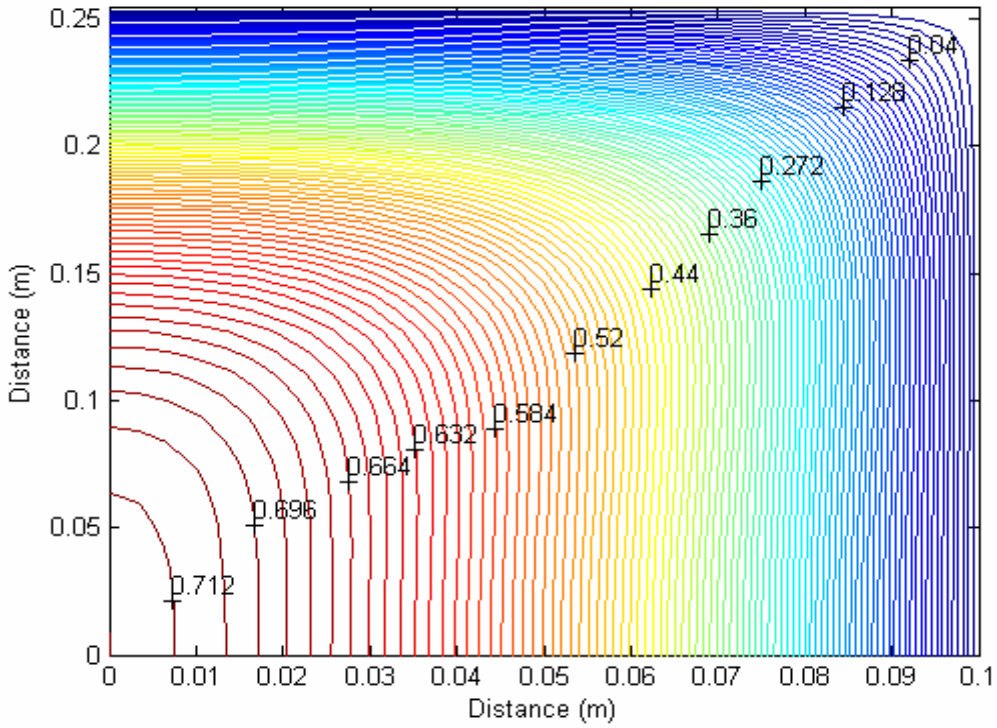

Figure 3.199 Contours of radial displacement (mm) for q=30 kPa

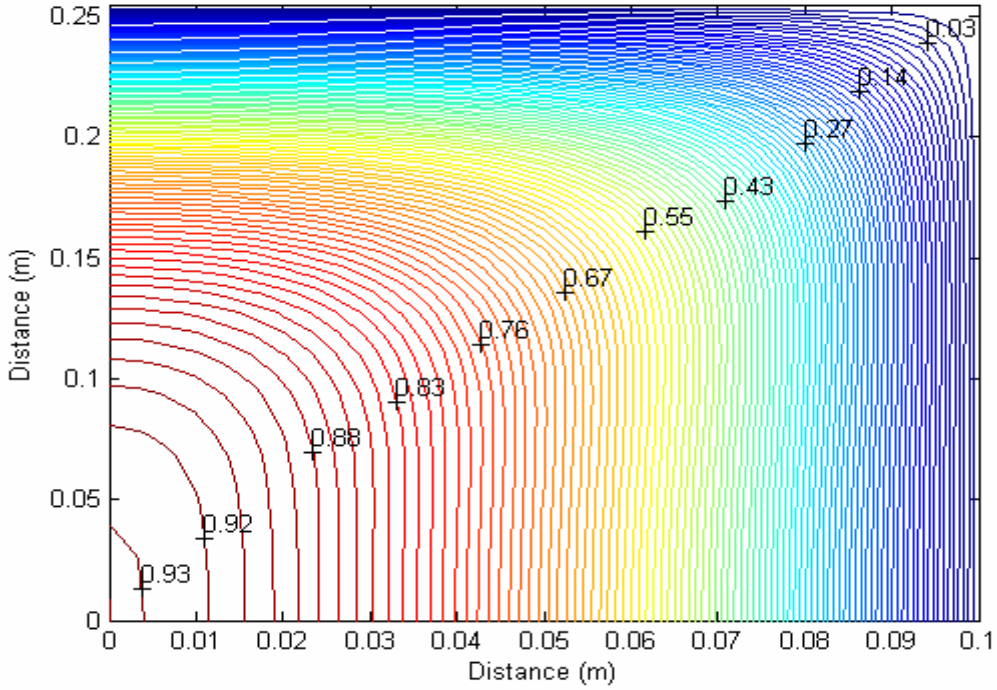

Figure 3.200 Contours of radial displacement (mm) for q=40 kPa

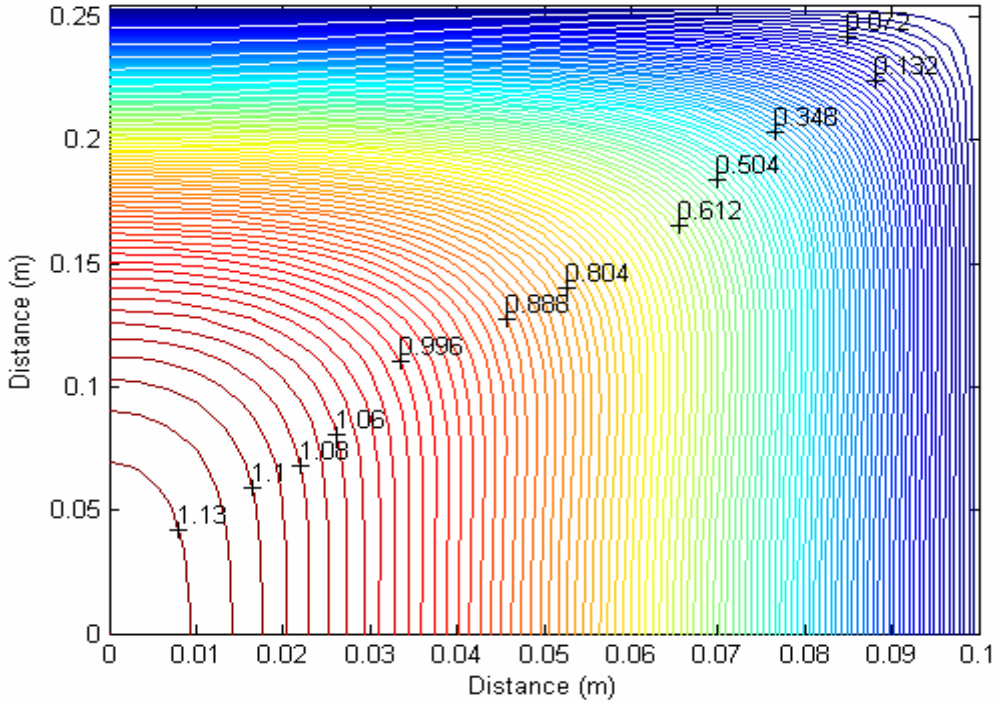

Figure 3.201 Contours of radial displacement (mm) for q=50 kPa

Fig 3.202-3.229 are plotted for the quarter of the laminated glass shell in order to have detailed information about the contour of maximum and minimum principal stress values at the top and bottom surfaces. Maximum principal stress contours are given for applied pressure q=10, 30, 40, 50, 70, 100 kPa in Figures 3.200-3.206 for the top of the unit and in Figures 3.209-3.215 for the bottom of the unit. Maximum principal stress on the top surface is at the right boundary of quarter shell. Maximum principal stress on the bottom surface of bottom glass is close to the center of the unit for small loads, but it moves toward the center of the unit horizontally. Maximum principal stress on the top surface and bottom surface of glass are tension at the shell surface as observed in Figures 3.202-3.215. Minimum principal stress contours for applied pressure are given at top and bottom surfaces in Figures 3.216-3.222 and Figures 3.223-3.229, respectively. Minimum principal stresses on the top and bottom surface could be tension or compression. The maximum value of minimum stress on the top surface is at the right boundary for pressures under 30 kPa. Then it moves to the center of the unit for loads greater than 30 kPa. The place of maximum value of minimum principal stresses move toward the left edge for higher load values. The minimum value of minimum principal stress at the bottom surface is at the corner of the unit.

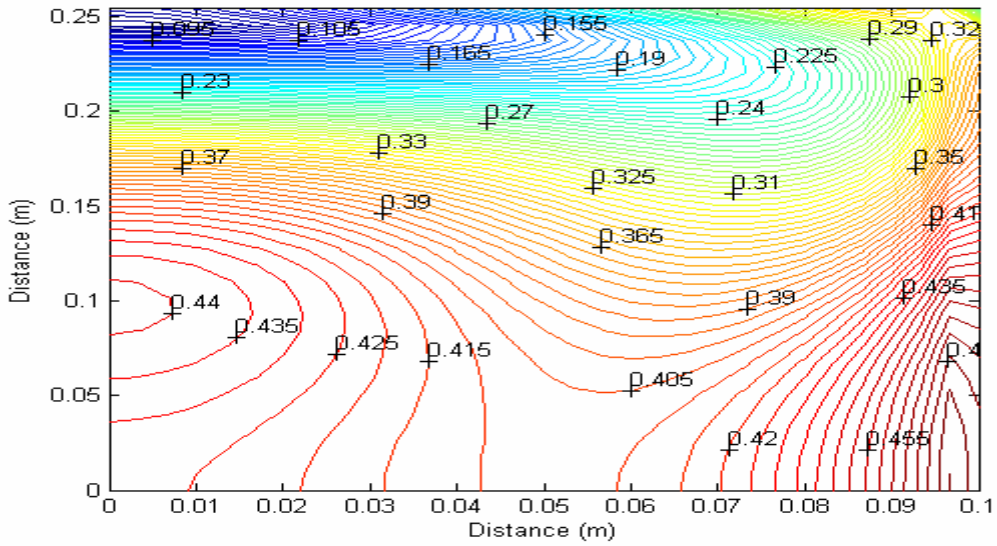

Figure 3.202 Contours of maximum principal stresses (*10^4 kPa) on the top surface of the top shell for q= 10 kPa

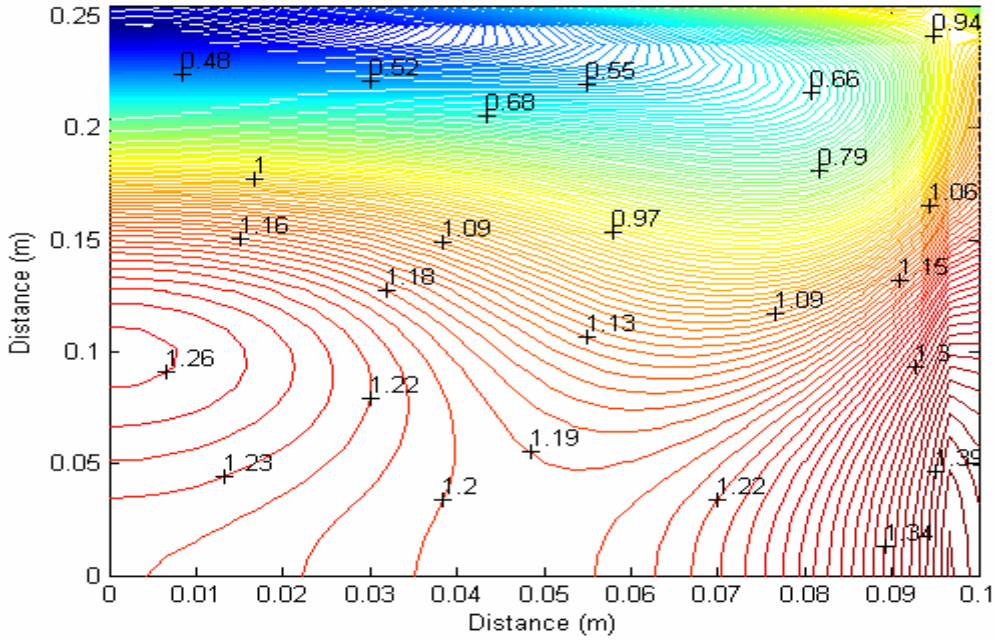

Figure 3.203 Contours of maximum principal stresses (*10^4 kPa) on the top surface of the top shell for q= 30 kPa

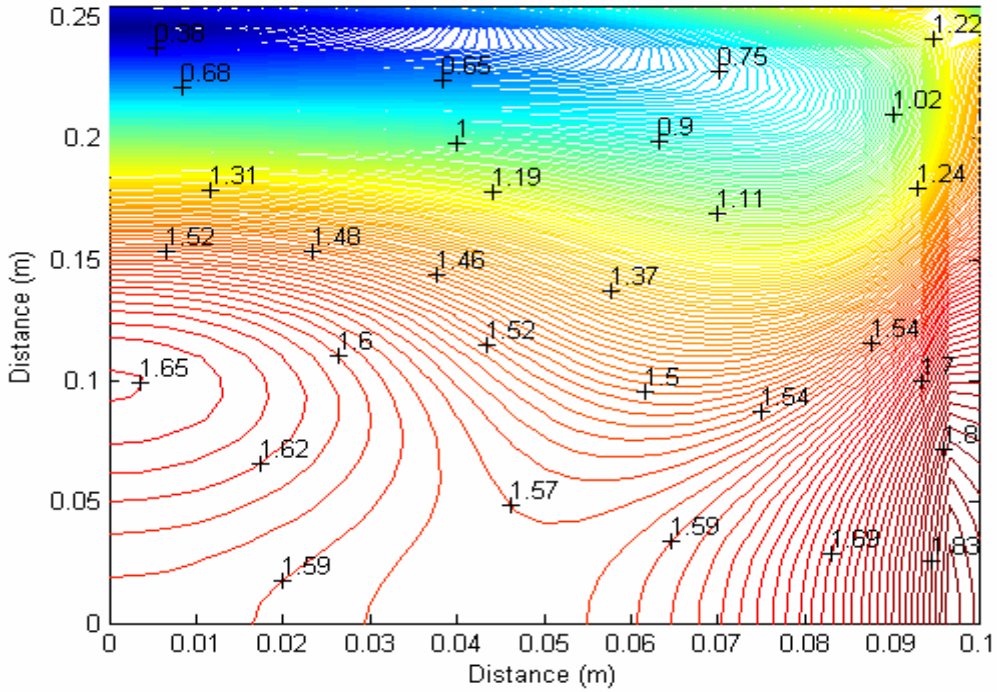

Figure 3.204 Contours of maximum principal stresses (*10^4 kPa) on the top surface of the top shell for q= 40 kPa

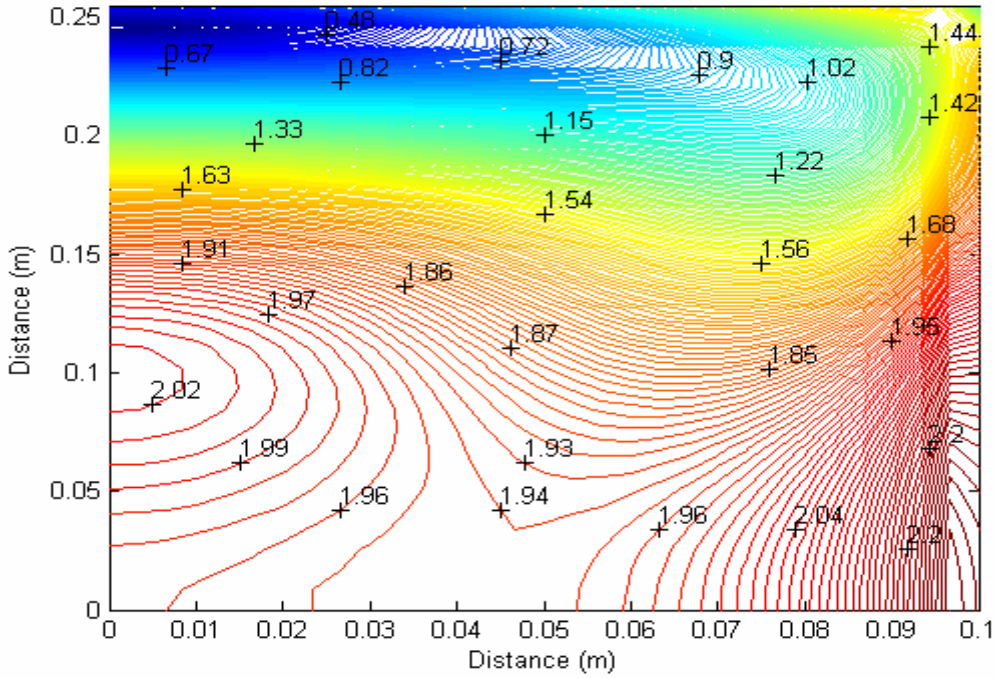

Figure 3.205 Contours of maximum principal stresses (*10^4 kPa) on the top surface of the top shell for q= 50 kPa

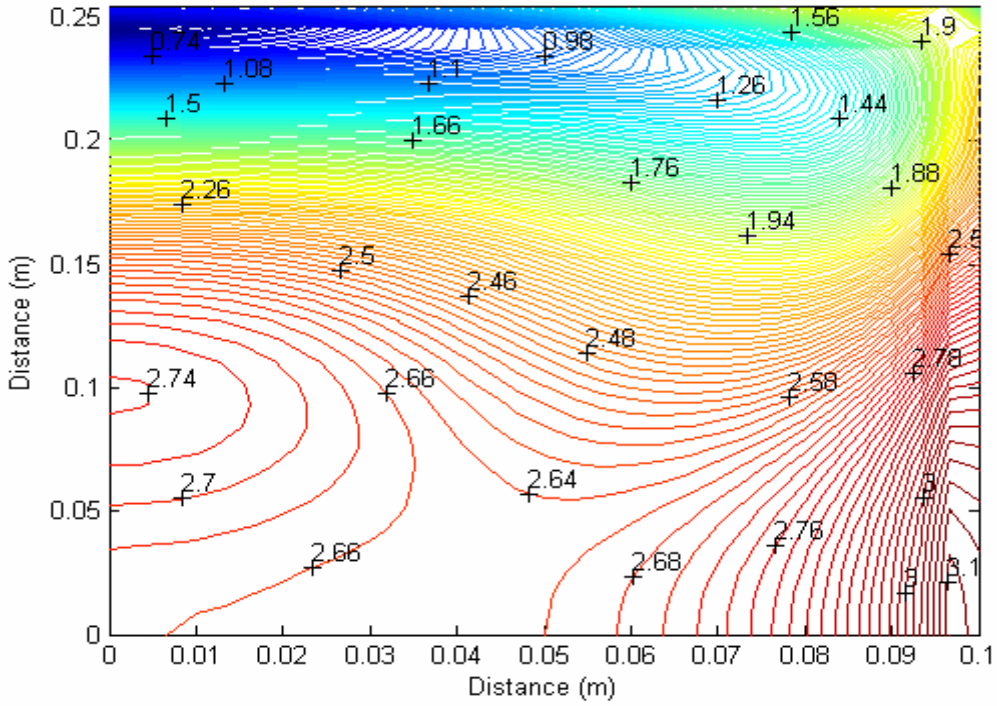

Figure 3.206 Contours of maximum principal stresses (*10^4 kPa) on the top surface of the top shell for q= 70 kPa

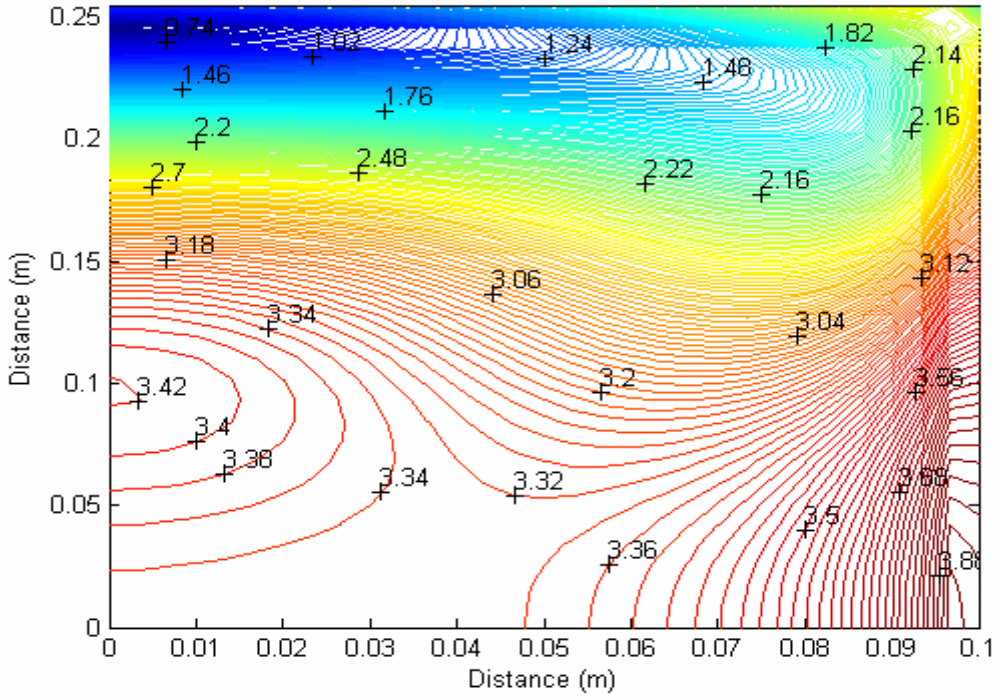

Figure 3.207 Contours of maximum principal stresses (*10^4 kPa) on the top surface of the top shell for q= 90 kPa

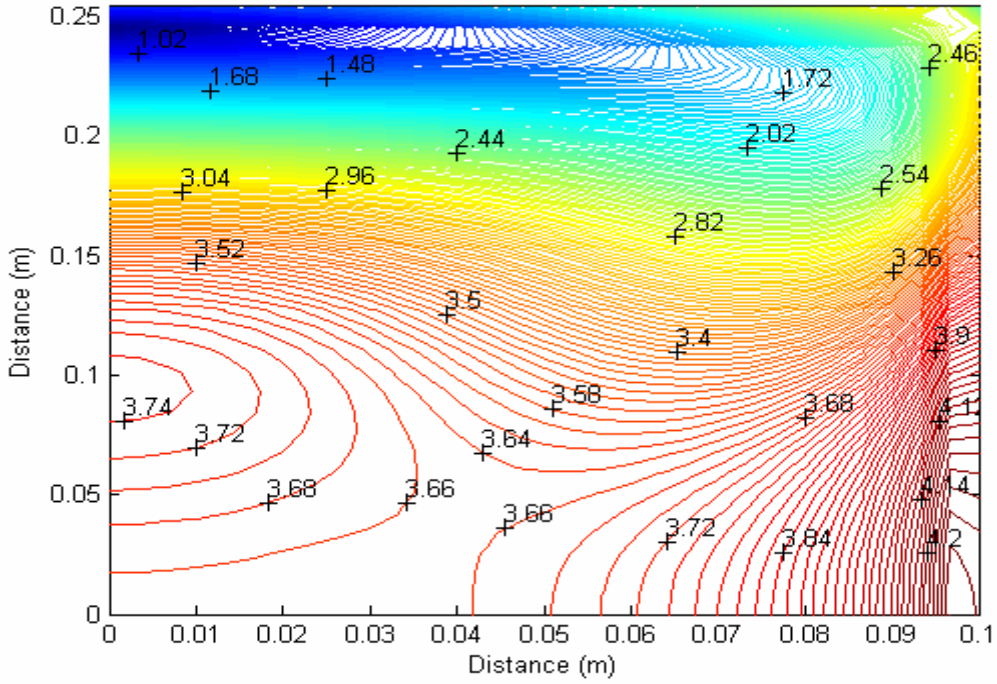

Figure 3.208 Contours of maximum principal stresses (*10^4 kPa) on the top surface of the top shell for q= 100 kPa

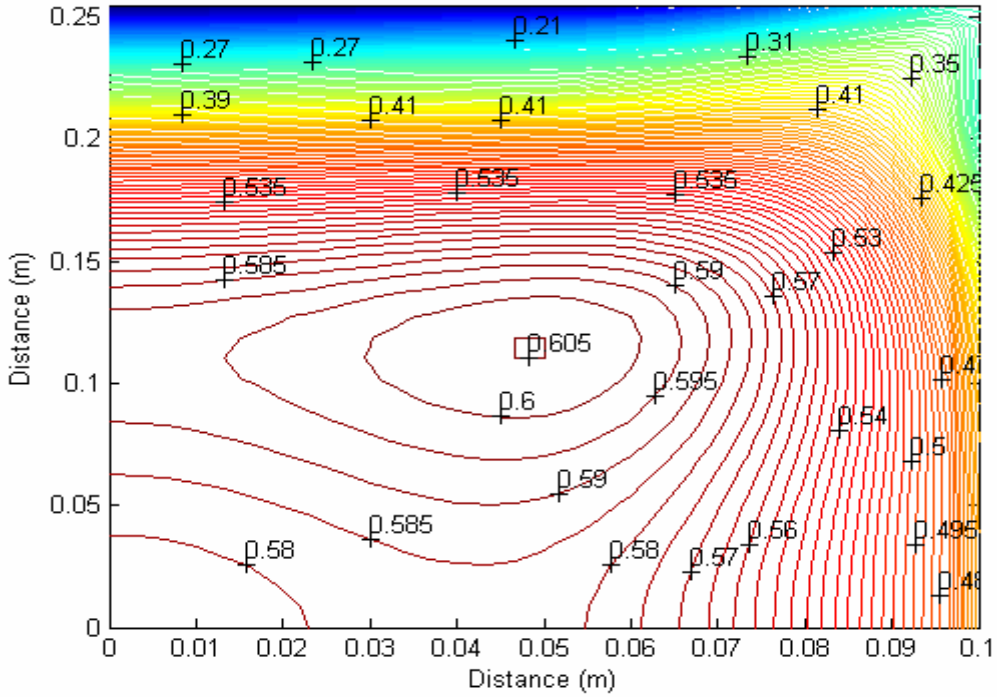

Figure 3.209 Contours of maximum principal stresses (*10^4 kPa) on the bottom surface of the bottom shell for q= 10 kPa

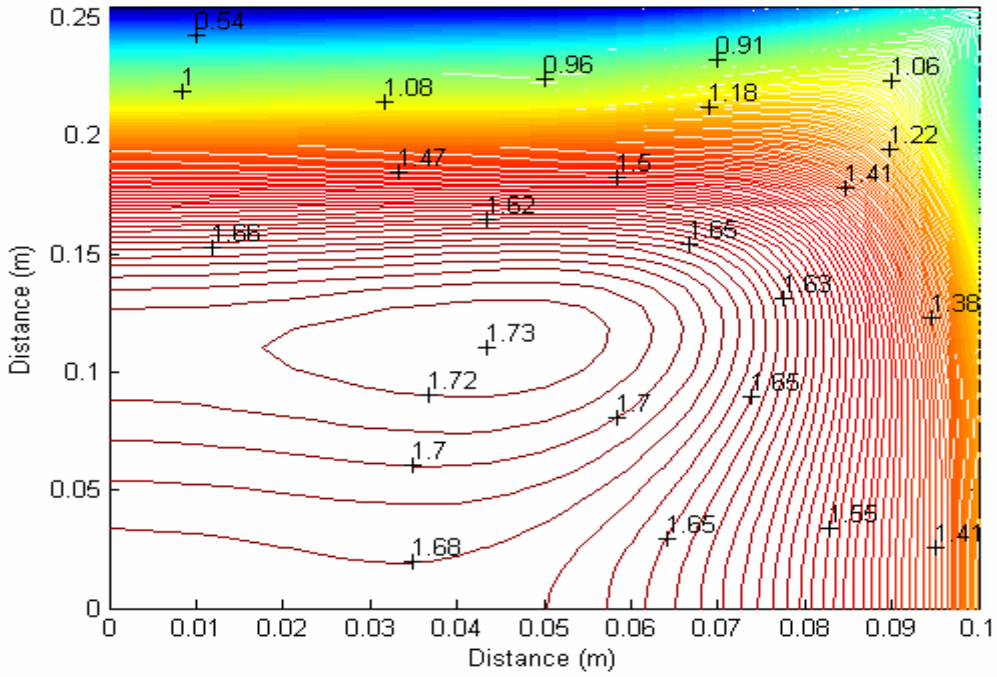

Figure 3.210 Contours of maximum principal stresses (*10^4 kPa) on the bottom surface of the bottom shell for q= 30 kPa

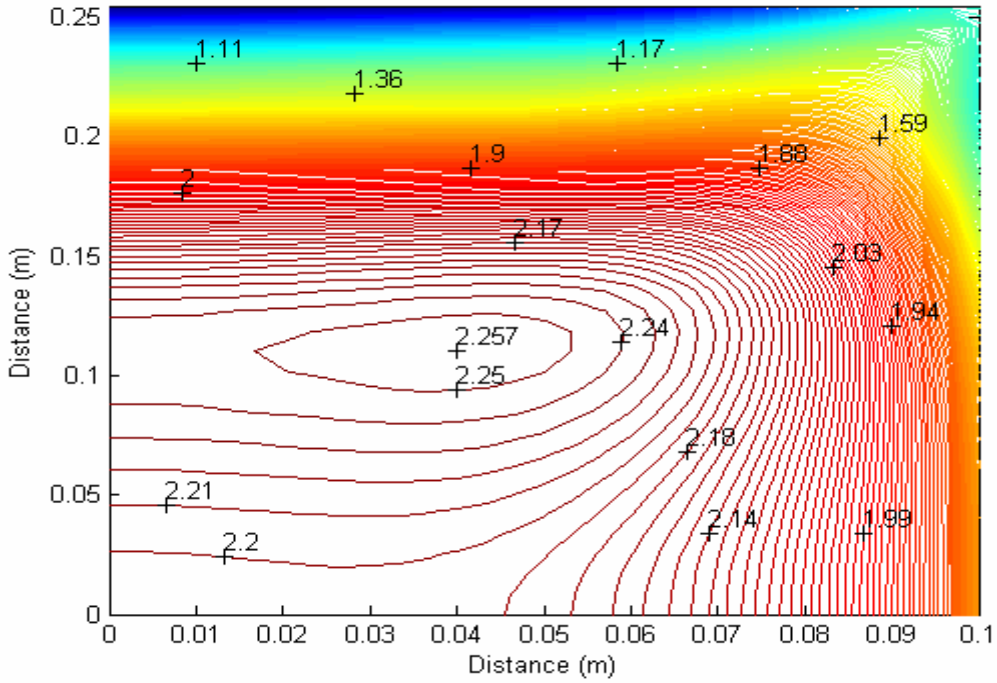

Figure 3.211 Contours of maximum principal stresses (*10^4 kPa) on the bottom surface of the bottom shell for q= 40 kPa

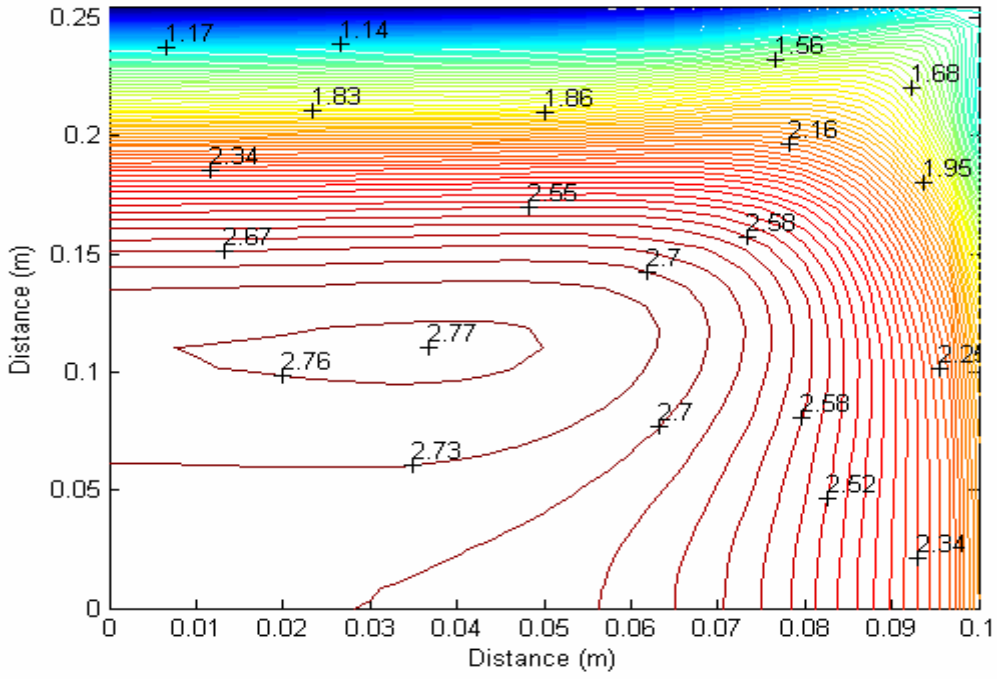

Figure 3.212 Contours of maximum principal stresses (*10^4 kPa) on the bottom surface of the bottom shell for q= 50 kPa

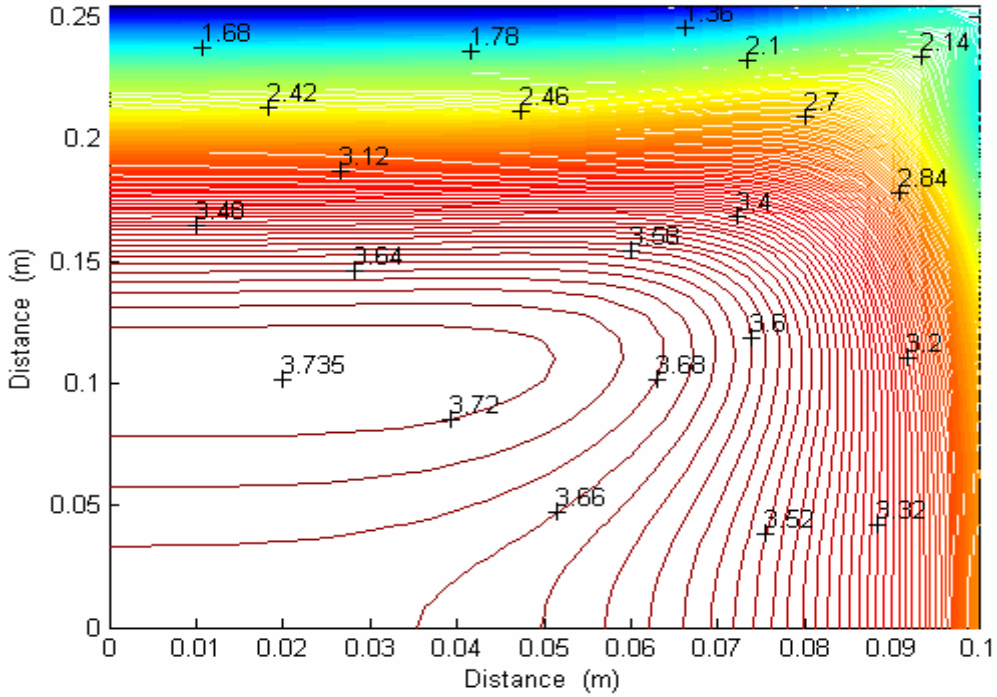

Figure 3.213 Contours of maximum principal stresses (*10^4 kPa) on the bottom surface of the bottom shell for q= 70 kPa

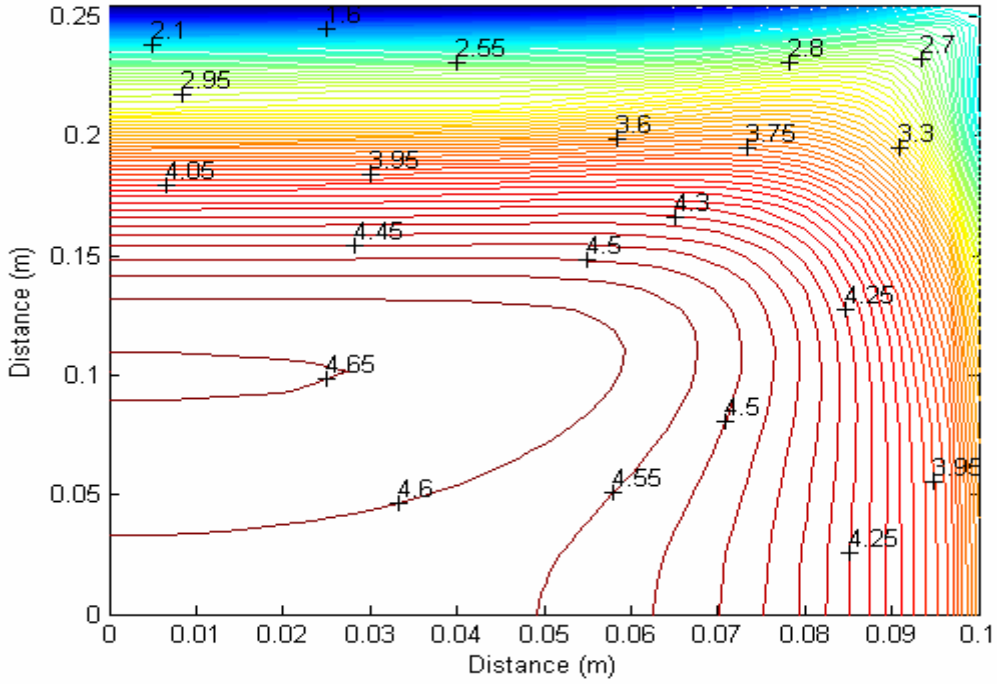

Figure 3.214 Contours of maximum principal stresses (*10^4 kPa) on the bottom surface of the bottom shell for q= 90 kPa

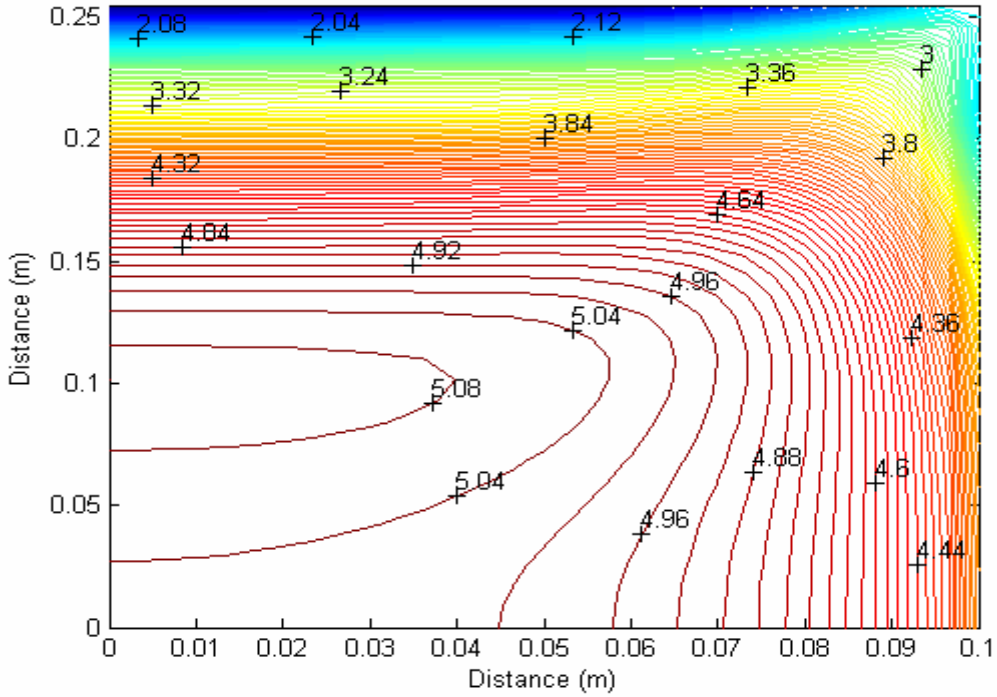

Figure 3.215 Contours of maximum principal stresses (*10^4 kPa) on the bottom surface of the bottom shell for q= 100 kPa

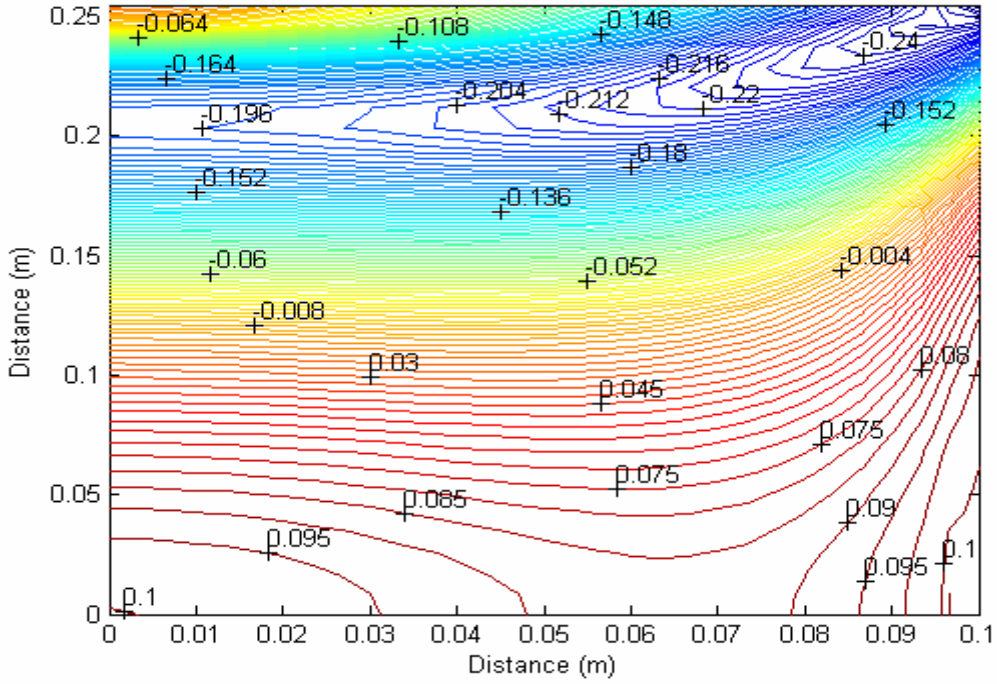

Figure 3.216 Contours of minimum principal stresses (*10^4 kPa) on the top surface of the top shell for q= 10 kPa

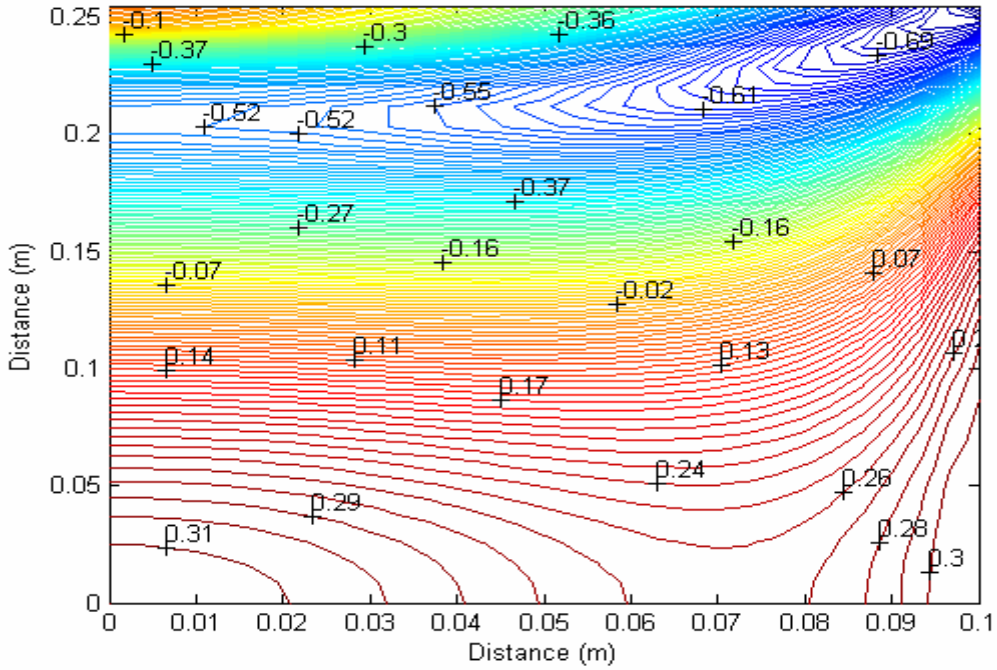

Figure 3.217 Contours of minimum principal stresses (*10^4 kPa) on the top surface of the top shell for q= 30 kPa

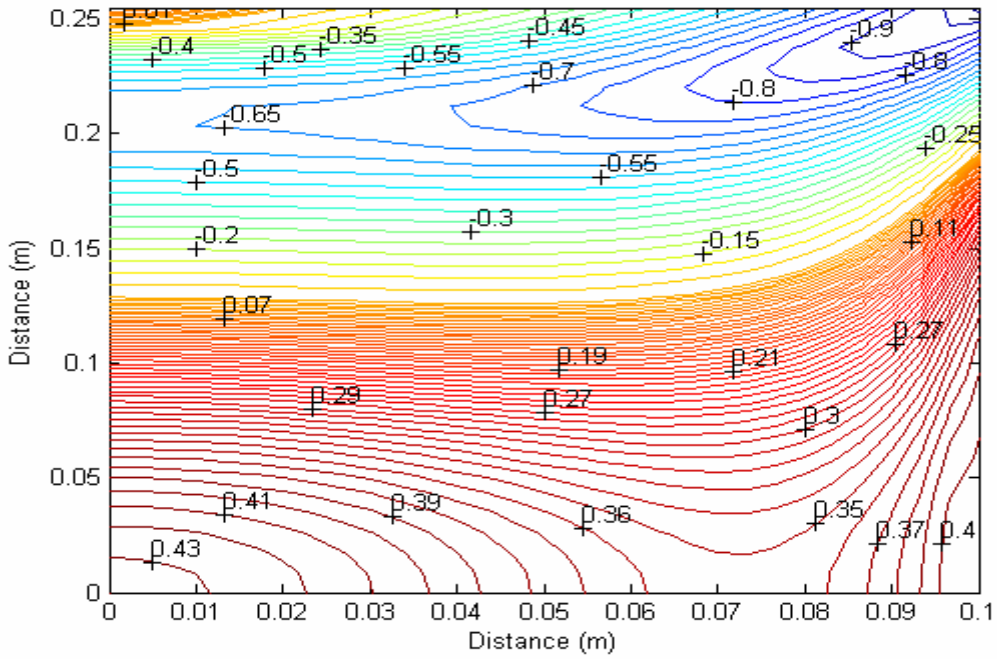

Figure 3.218 Contours of minimum principal stresses (*10^4 kPa) on the top surface of the top shell for q= 40 kPa

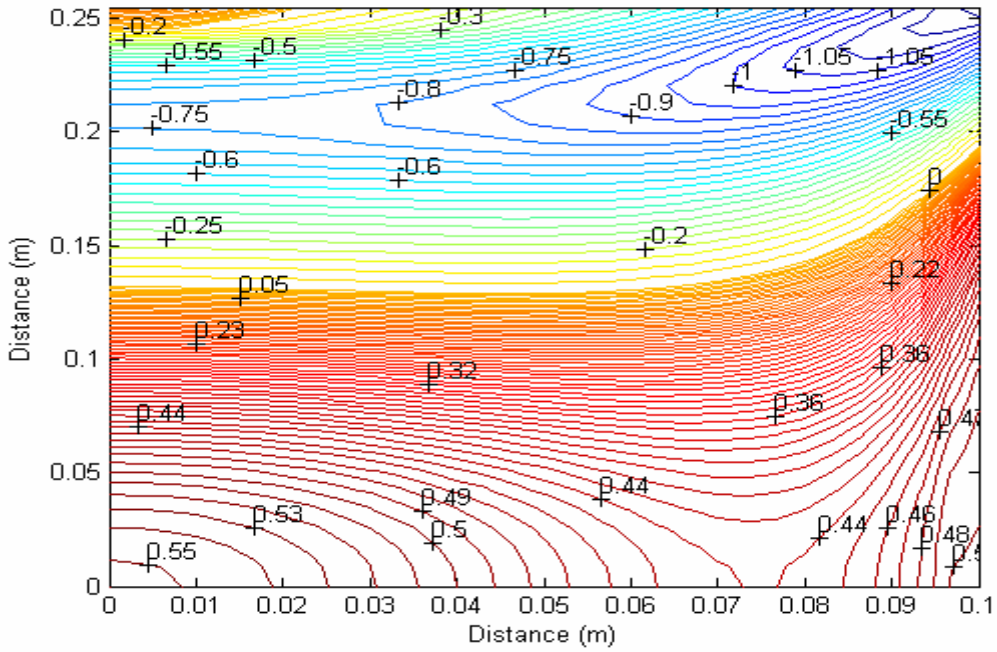

Figure 3.219 Contours of minimum principal stresses (*10^4 kPa) on the top surface of the top shell for q= 50 kPa

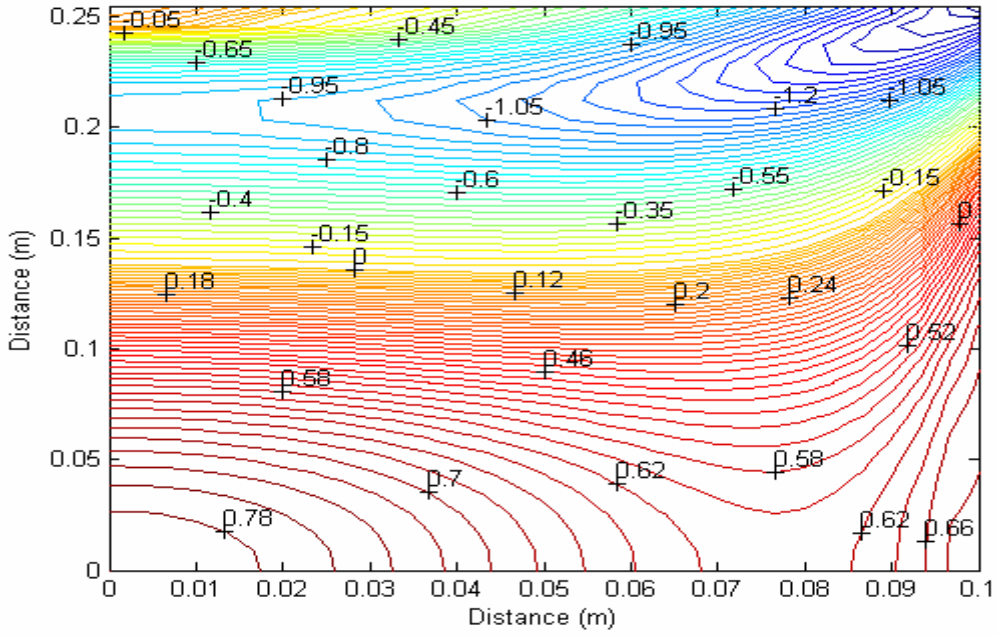

Figure 3.220 Contours of minimum principal stresses (*10^4 kPa) on the top surface of the top shell for q= 70 kPa

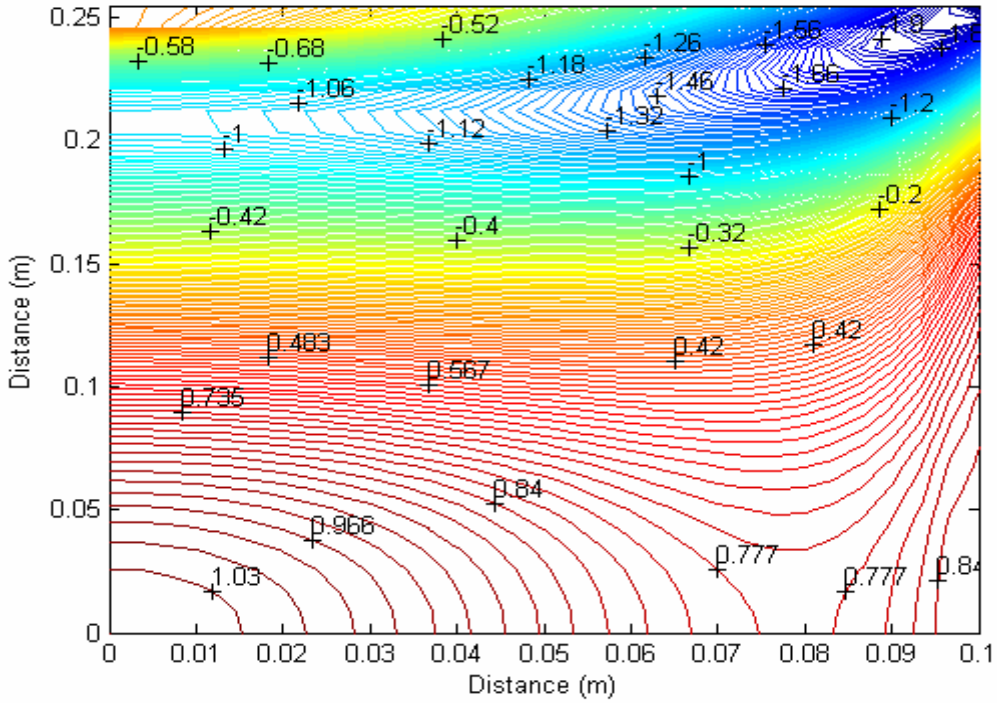

Figure 3.221 Contours of minimum principal stresses (*10^4 kPa) on the top surface of the top shell for q= 90 kPa

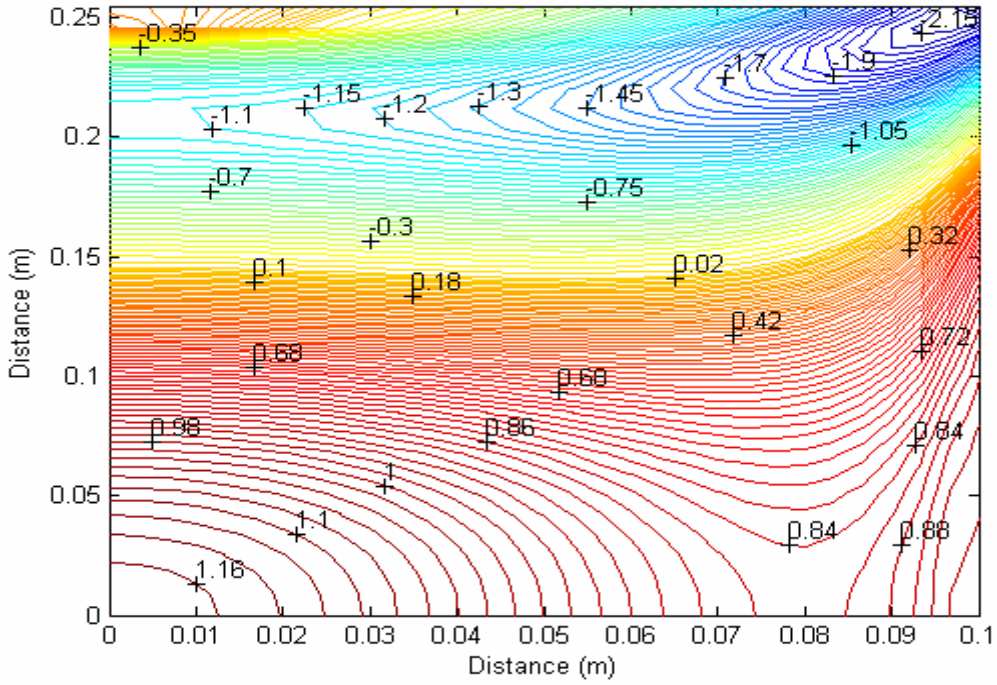

Figure 3.222 Contours of minimum principal stresses (*10^4 kPa) on the top surface of the top shell for q= 100 kPa

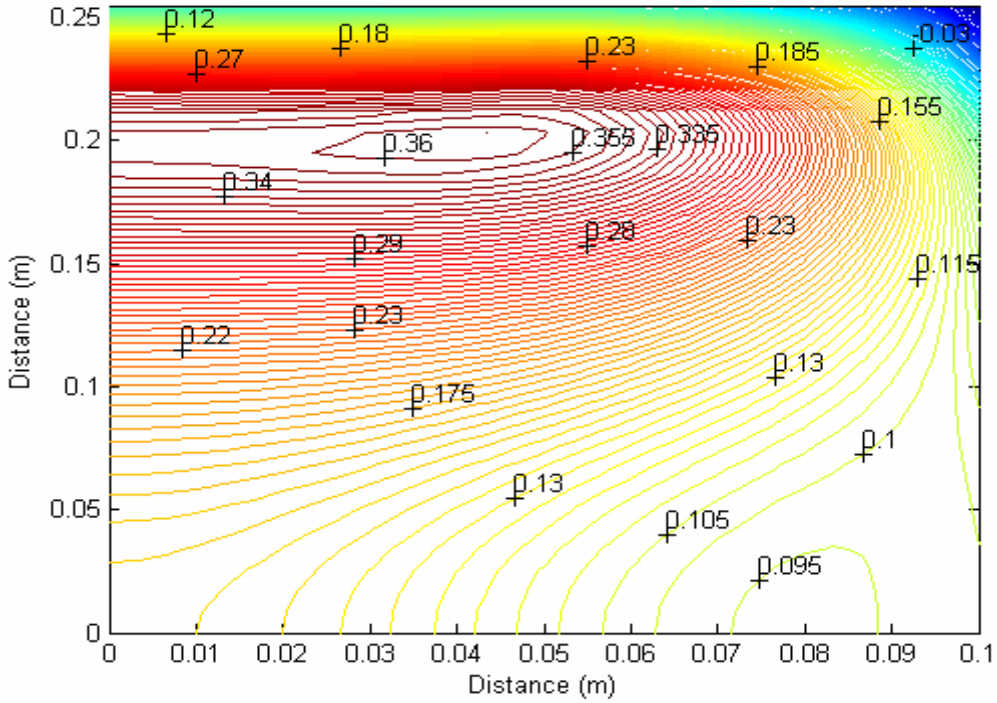

Figure 3.223 Contours of minimum principal stresses (*10^4 kPa) on the bottom surface of the bottom shell for q= 10 kPa

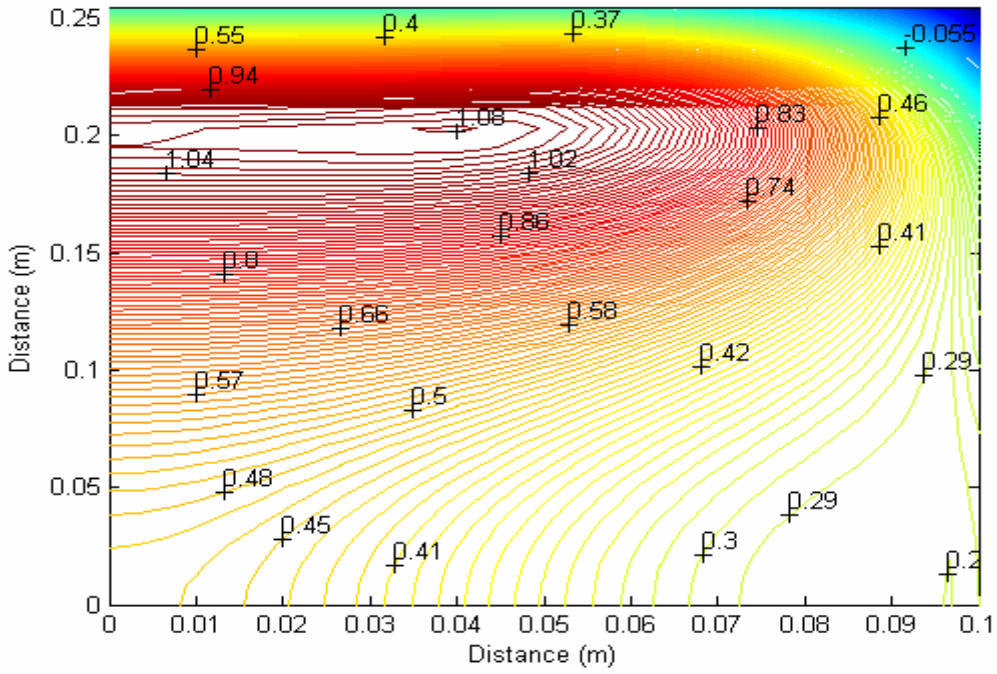

Figure 3.224 Contours of minimum principal stresses (*10^4 kPa) on the bottom surface of the bottom shell for q= 30 kPa

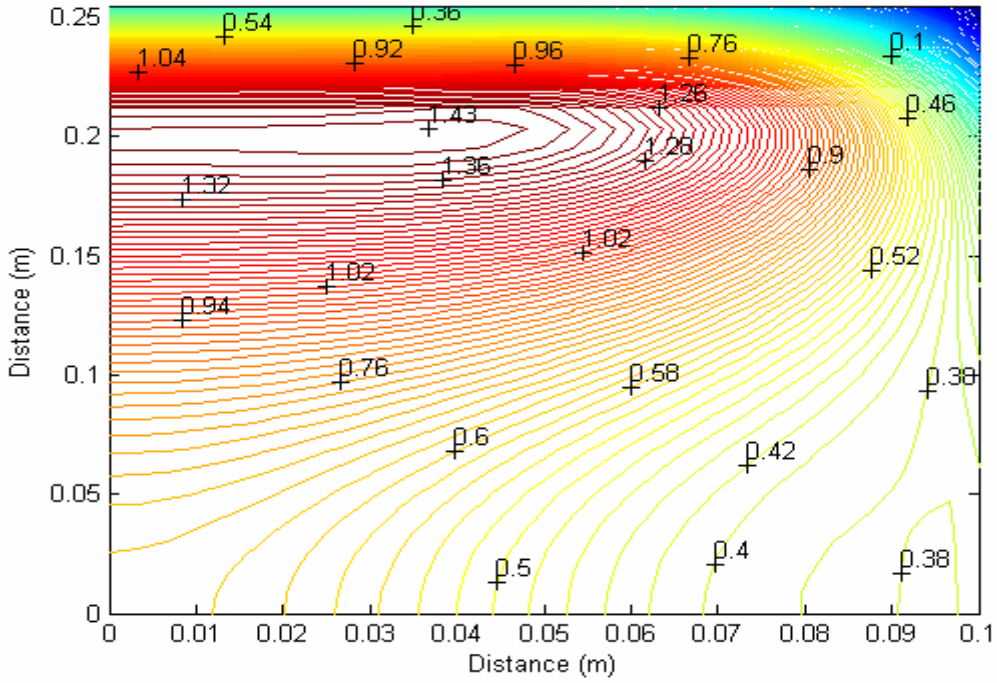

Figure 3.225 Contours of minimum principal stresses (*10^4 kPa) on the bottom surface of the bottom shell for q= 40 kPa

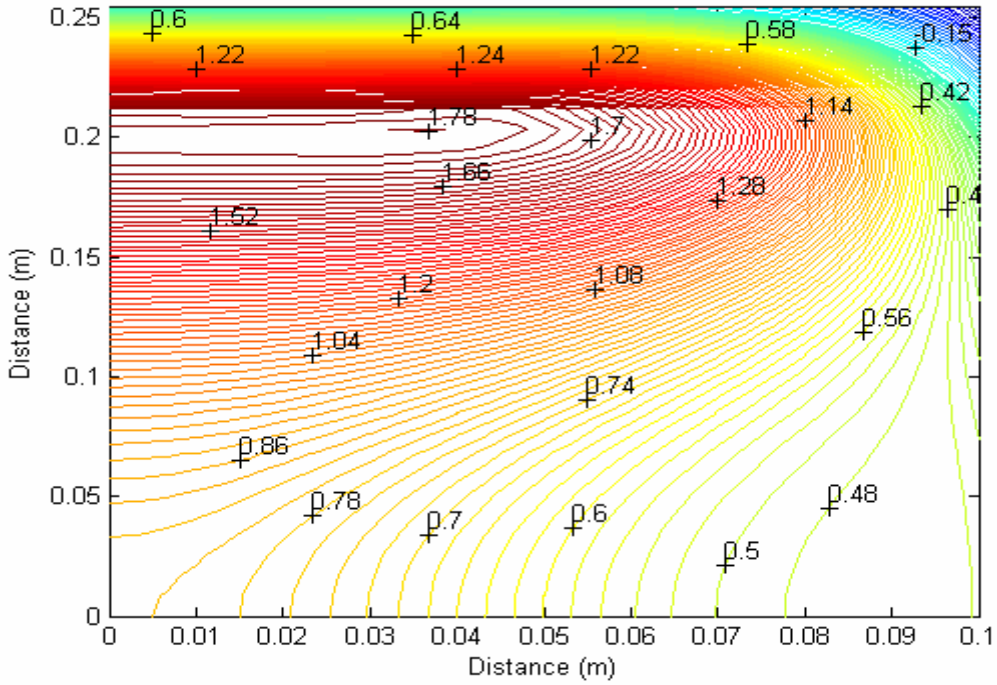

Figure 3.226 Contours of minimum principal stresses (*10^4 kPa) on the bottom surface of the bottom shell for q= 50 kPa

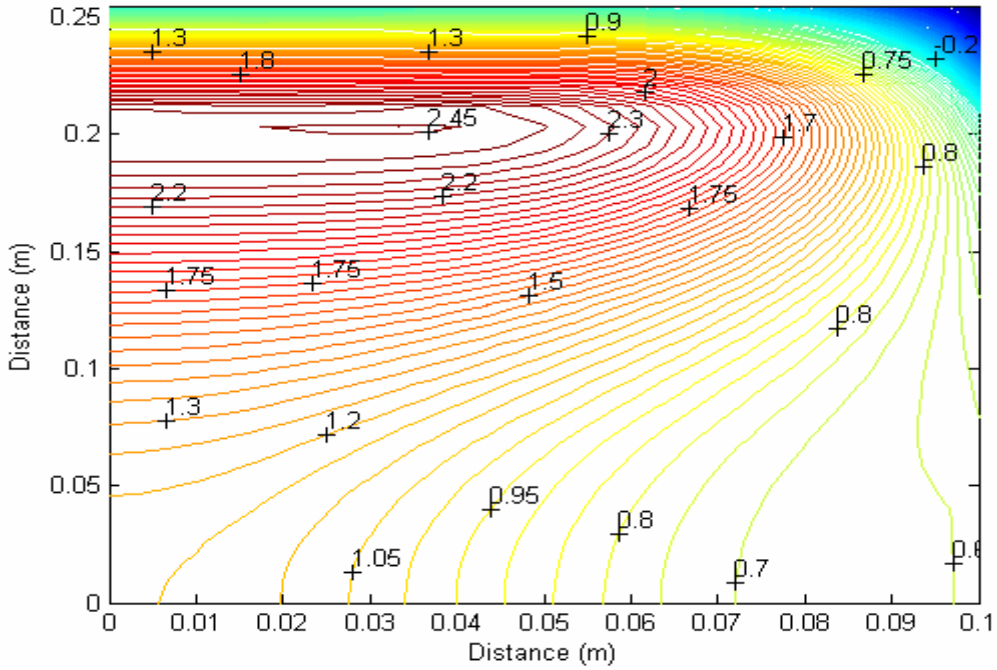

Figure 3.227 Contours of minimum principal stresses (*10^4 kPa) on the bottom surface of the bottom shell for q= 70 kPa

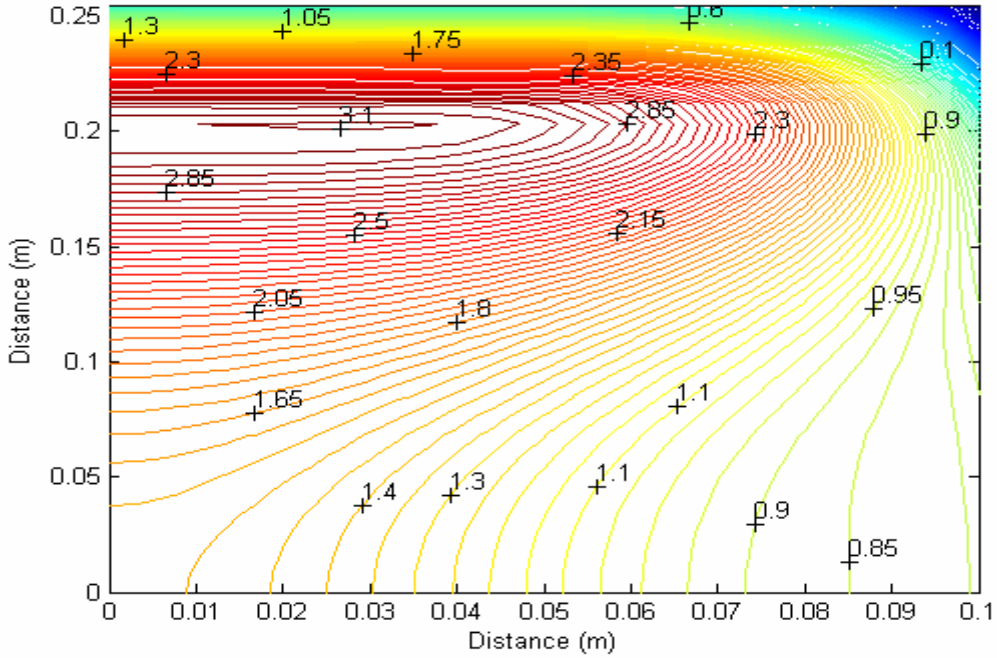

Figure 3.228 Contours of minimum principal stresses (*10^4 kPa) on the bottom surface of the bottom shell for q= 90 kPa

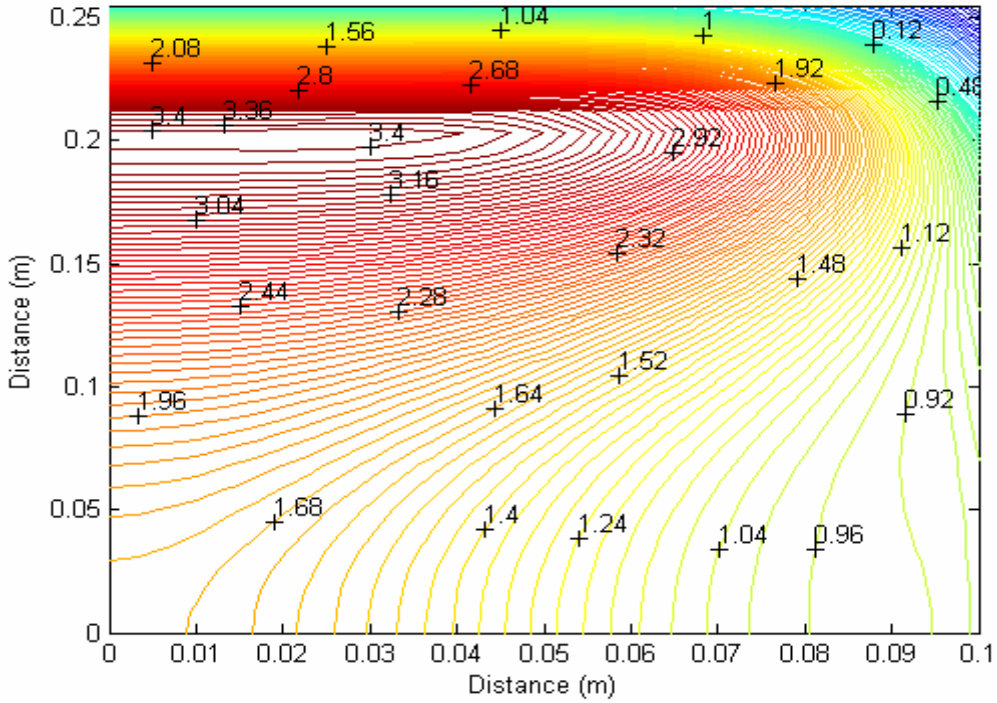

Figure 3.229 Contours of minimum principal stresses (*10^4 kPa) on the bottom surface of the bottom shell for q= 100 kPa

CHAPTER 4

SUMMARY AND CONCLUSIONS

In this study, analysis of laminated glass curved beam and shell units is carried out by using a mathematical model. Laminated glass units with two thin glass sheets and an interlayer PVB which connects them undergo very complex and highly nonlinear behavior under applied loads. Therefore, nonlinear theory has to be used for the true behavior of laminated units. Nonlinearity is due to the geometry of the unit that causes membrane stresses when the unit undergoes large deflection. The steps of the analysis go through the stages of writing total potential energy of laminated glass unit in terms of displacements, deriving the nonlinear governing differential equations using variational approach and minimum potential energy theorem, converting the nonlinear equations from continuous form to discrete form by using finite difference method and solving the equations by using special solvers that provide advantages in storage and computation time. For the circumferential displacements modified strongly implicit (MSI) procedure that provides substantial decrease in storage and computation time by storing only the finite difference coefficients is used. To overcome the convergence difficulties variable underrelaxation parameter is used for radial deflection w. Underrelaxation factor helps to generate a convergent sequence for the solution and to decrease the number of iterations to reach the solution. And also load needs to be applied in incremental steps for the convergent solution. From the results of the analysis, it is observed that nonlinear analysis is necessary for the true behavior of laminated glass curved beam and shell units.

Computer programs based on the derived formulation are developed for laminated glass curved beams and cylindrical shells. To verify the results of the developed

model for curved beams experimental results and finite element results are used. The finite element model is generated and solved by using finite element package program ABAQUS. Results of developed model reasonably agree with the finite element results and experimental results.

The developed models are capable of simulating layered and monolithic units in addition to the laminated units by equating shear modulus of interlayer to zero. To determine the strength of laminated glass curved beams and shells deflections, moments and stress functions of laminated glass unit are obtained. It is observed that the behavior of laminated glass curved beam units approach to the behavior of monolithic glass unit for high values of the interlayer shear modulus. The behavior of laminated glass arch is bounded by the behavior of monolithic and layered curved glass arches. However, these bounds are violated at some parts of the curved beam along its length, which is not the case in the behavior of straight beams. While the behavior of laminated glass unit is bonded by two limiting cases, which are monolithic and layered behavior, for the fixed supported cylindrical shell, the behavior of layered glass unit takes place between the behaviors of laminated and monolithic units for the hinged supported cylindrical shell unit. In contrary to the behavior of the fixed supported monolithic glass unit stress and deflection values of the hinged supported monolithic glass unit are found to be higher than that of layered and laminated glass units. These results are agree with the results obtained by using the finite element method. It is possible to conclude that the monolithic systems enter the nonlinear region later than the layered and laminated glass systems. For the laminated glass curved beams, the effect of PVB's shear modulus, the level of nonlinearity, displacement, moment and stress functions are investigated. To consider the effect of the boundary conditions to the behavior of the curved beam the model is solved for different boundary conditions. The comparison of results are given in figures. Nonlinearity level of simply supported beam is found to be higher than that of fixed supported beam. Strength factor, which is employed to adjust laminated strengths by using available design charts, is obtained for curved beams. It is observed that strength factor of the fixed supported laminated curved beam is

higher than that of the simply supported beam. While the strength factor of the simply supported curved beam is nearly 0.8, the strength factor of the fixed supported curved beam is nearly 0.7.

Because of high nonlinearity levels, double curvature is observed for laminated shells at high-pressure levels when applied towards to the top surface of the top glass shell. Stress and displacement contours are plotted for laminated shell unit. Because of nonlinearity it is observed form the figures that when the pressure is increasing, location of maximum principal stress changes. It immigrates towards the corner of laminated unit as the nonlinearity increases. To provide additional insight to the behavior of laminated glass curved beams and shells strength factor which is defined as the ratio of maximum principal stress in monolithic glass to the maximum principal tensile stress in laminated glass is analyzed. By adjusting strength factor, strength of laminated glass unit can be obtained by glass design charts, which are available for monolithic and annealed glasses. Strength factor for the fixed supported cylindrical glass shell is between 1.03-1.07, while it is between 1.15-1.16 for the hinged supported cylindrical glass shell.

4.1 Recommendations for future work

The present model may be modified for laminated glass shells, which have curvature in two directions. Experiments for the verification of developed model may be conducted. The effect of delamination in the laminated glass may be investigated. The effects of temperature, aspect ratio, interlayer thickness, glass thickness and applied loads on the behavior of laminated curved glass beams and shells may be studied. Dynamic model can be developed for the laminated glass curved beams and shells. The behavior of the laminated glass shells and curved beams under impact load may be analyzed for future studies.

REFERENCES

[1] Behr, R.A., Minor, J.E., Linden, M.P., Vallabhan, C.V.G. (1985). "*Laminated Glass units under uniform lateral pressure*." Journal of Structural Engineering, 111(5), 1037-1050.

[2] Behr, R.A., Linden, M.P., and Minor, J.E. (1986). "*Load duration and interlayer thickness effects on laminated glass.*" Journal of Structural Engineering, 112(6), 1441-53.

[3] Behr, R.A., Karson, M.J., and Minor, J.E. (1991). "*Reliability analysis of window glass failure pressure data*." Structural Safety, 11, 43-58.

[4] Behr, R.A., Minor, J.E., Norville, H.S. (1993). "*Structural behavior of architectural laminated glass."* Journal of Structural Engineering, 119(1), 202-222.

[5] Edel, M.T. (1997). "*The effect of temperature on the bending of laminated glass beams.*" M.S. Thesis, Texas A&M University, College Station, TX.

[6] Hildebrand, F.B. (1965). "*Methods of Applied Mechanics*." Prentice-Hall, Inc., Englewood Cliffs, N.J.

[7] Hooper, J.A. (1973). "*On the bending of architectural laminated glass.*" Int. J. Mech. Sci., 15, 309-323.

[8] Langhaar, H.L. (1962). "*Energy Methods in Applied Mechanics.*" John Wiley and Jones, Inc., New York.

[9] Linden, M.P., Minor, J.E., Behr, R.A., and Vallabhan, C.V.G. (1983). "*Evaluation of laterally loaded laminated glass by theory and experiment.*" Report, Glass Res. And Testing Lab., Texas Tech.

[10] Linden, M.P., Minor, J.E., and Vallabhan, C.V.G. (1984). "*Evaluation of laterally loaded laminated glass units by theory and experiment.*" Supplemental Report No. 1, Glass Res. And Testing Lab., Texas Tech.

[11] Minor, J.E., and Reznik, P.L. (1990). "*Failure strengths of laminated glass.*" Journal of Structural Enginering, 116(4), 1030-1039.

[12] Norville, H.S., King, K.W., Swofford J.L. (1998). "*Behavior and strength of laminated glass.*" Journal of Engineering Mechanics, 124(1), 46-53.

[13] Reddy, J.N. (1984). "*Energy and Variational Methods in Applied Mechanics.*" John Wiley and Jones, Inc., New York.

[14] Tuzcu, İ.E. (1998). "*Thickness and strength factor analyses of simply supported laminated glass units*." M.S. Thesis, Middle East Technical University, Ankara.

[15] Tezcan, S. (2001). "*Behavior of laminated glass beams*." M.S. Thesis, Middle East Technical University, Ankara.

[16] Vallabhan, C.V., Minor, J.E., Nagalla S.R. (1987). "*Stresses in layered glass units and monolithic glass plates.*" Journal of Structural Engineering, 113(1), 36-43.

[17] Vallabhan, C.V., Ramasamudra, M. (1991). "*Properties of PVB (Saflex) interlayer used in laminated glass*." Glass Res. And Testing Lab., Texas Tech.

[18] Vallabhan, C.V., Das, Y.C, Magdi, M., Asik, M., Bailey, J.R. (1993). "*Analysis of laminated glass units.*" Journal of Structural Engineering, 119(5), 1572-1585.

[19] Van Duser, A., Jagota, A., Bennison, S.J. (1999). "*Analysis of glass/polyvinyl butyral laminates subjected to uniform pressure.*" Journal of Engineering Mechanics, 125(4), 435-442.

[20] Magdi, M. (1990). "*Mathematical model for laminated window glass units*." M.S. Thesis, Texas Tech University , Lubbock.

[21] Vallabhan, C.V.G., Asik, M.Z. and Kandil, K. (1997) " *Analysis of structurally glazed systems*." Journal of Composite Structures 65(2), 231-239.

[22] Aşık, M.Z. and Vallabhan, C.V.G. (1997). "*On the Convergence of Nonlinear Plate Equations* ." Computers & Structures, 65 (2), 225-229 .

[23] Asik M.Z. (2003). "*Laminated Glass Plates: Revealing of Nonlinear Behavior*." Computers & Structures, 81 (28-29), 2659-2671.

[24] Asik M.Z., Tezcan S. (2005). " *A Mathematical Model for the Behavior of Laminated Glass Beams*." Computers & Structures, 83 (21-22), 1742-1753.

[25] Asik M.Z., Tezcan S. (2006) " *Laminated Glass Beams: Strength Factor and Temperature Effect.* " Computers & Structures, 84, (5-6), 364-373.

[26] Asik M.Z., Dural E. (2007). "*Effect of Support Conditions on the Vibration of the Laminated Composite Beams.* " Journal of Vibration and Control, 13, (9-10), 1361-1368.

[27] Uzhan T. (2010). "*Experimental Analysis of Curved Laminated Glass Beams.* " M.S. Thesis, Middle East Technical University, Ankara.

[28] Dawe D.J. (1974) "*Numerical studies using circular arch finite elements*" Computers and Structures, 4, 729-740.

[29] Rajasekaran S., Padmanabhan S. (1989). "*Equations of curved beams*", Journal of Engineering Mechanics, 115 (5), 1094-1111.

[30] Kang Y.J., You C.H., (1994) "*Thin walled curved beams. 1 Formulation of nonlinear equations.* " Journal of Engineering Mechanics, 120 (10), 2072-2100.

[31] Lin K.C., Heish C.M. (2007). "*The closed form general solutions of 2-D curved laminated glass beams of variable cross section*" Composite Structures, 79 (4) , 606-618.

[32] Schimmels S.A., Palazotto A.N. (1994). "*Nonlinear Geometric and Material Behavior of Shell Structures with Large Strains.*" Journal of Engineering Mechanics, 120(2), 320-345.

[33] Turkmen H.S. (1999). "*Structural Response of Cylindrically Curved Laminated Composite Shells Subjected to Blast Loading.*" Journal of Sound and Vibration, 249(4), 663-678.

[34] Aksogan O., Sofiyev A.H. (2002). "*The dynamic stability of a laminated truncated conical shell with variable elasticity moduli and densities subject to a time-dependent external pressure.*" The Journal of Strain Analysis for Engineering Design, 37 (3), 201-210.

[35] Ugural, A.C. (1999). "*Stresses in Plates and Shells*." McGraw- Hill.

[36] Timeshenko S., Krieger S.(1959) "*Theory of Plates and Shells*." McGraw- Hill.

[37] Palazotto A.N., Dennis S.T. (1992). "*Nonlinear Analysis of Shell Structures*." American Institute of Aeronautics and Astronautics.

[38] Palani G.S., Rajasekaran S. (1992). "*Finite element analysis of thin walled curved beams made of composites*" Journal of Structural Engineering, 118 (8), 2039-2062.

CURRICULUM VITAE

PERSONAL INFORMATION

Surname, Name: Dural, Ebru
Nationality: Turkish (TC)
Date and Place of Birth: 10 March 1979, Erzurum
Marital Status: Married
Phone: +90 312 210 44 57
Fax: +90 312 210 44 62
email: onlu@metu.edu.tr

EDUCATION

Degree	Institution	Year of Graduation
BS	Ataturk University Civil Engineering	2002
High School	Mehmet Akif Ersoy High School, Erzurum	1997

WORK EXPERIENCE

Year	Place	Enrollment
2002-Present	METU Department of Engineering Sciences	Research Assistant

PUBLICATIONS

1. Asik, M.Z., and Dural, E. (2006). "Effect of Support Conditions on the Vibration of the Laminated Composite Beams." Mathematical Methods in Engineering International Symposium.

2. Asik, M.Z., and Dural, E. (2006). "*A Mathematical Model for the Nonlinear Analysis of a Laminated Cylindrical Glass Shells.*" 7th World Congress on Computational Mechanics, Los Angeles, USA.

3. Asik, M.Z., Dural, E. and Bayar, G. (2007). "*Nonlinear Analysis of a Laminated Glass Arch*.", 3rd International Conference on Structural Engineering, Mechanics and Computation, Cape Town, South Africa.

4. Asik, M.Z., and Dural, E. (2008). "*A Computational Model For The Prediction Of The Nonlinear Behavior Of a Laminated Cylindrical Glass Shell.*", The 15th ICCES Conference, Hawai, USA.

5. Asik, M.Z., and Dural, E. (2008). "*Effect of Support Conditions on the Behavior of the Laminated Glass Arch.*", 8th World Congress on Computational Mechanics, 5th. European Congress on Computational Methods in Applied Sciences and Engineering, Venice, Italy.

6.Dural, E and Asik, M.Z. (2009). "*Kompozit Cam Eğrisel Kirişlerin Doğrusal Olmayan Davranışları.*" XVI. Ulusal Mekanik Kongresi, Kayseri, Turkey.

7. Asik, M.Z., and Dural, E. (2010). "*Nonlinear Analysis of a Laminated Cylindrical Glass Shell.*" The Ninth International Congress on Advances in Civil Engineering, Trabzon, Turkey.

8. Asik, M.Z., and Dural, E. (2006). "*Effect of Support Conditions on the Vibration of the Laminated Composite Beams.*" Journal of Vibration and Control September 2007 vol. 13 no. 9-10 1361-1368.

9. Asik, M.Z., Dural, E. , Uzhan, T. and Yetmez, M.(2010). "*Experimental and Mathematical Analysis of Curved Laminated Glass Beam."* International Conference on Theoretical, Applied, Computational and Experimental Mechanics , IIT Kharagpur, India

HOBBIES

Swimming, Reading, Computer Technologies, Movies, Music